

March 2019

## Understanding immunometabolic and suppressive factors that impact cancer development

Rebecca Swearingen Hesterberg  
*University of South Florida*, [becca.swearingen@gmail.com](mailto:becca.swearingen@gmail.com)

Follow this and additional works at: <https://digitalcommons.usf.edu/etd>



Part of the [Immunology and Infectious Disease Commons](#)

---

### Scholar Commons Citation

Hesterberg, Rebecca Swearingen, "Understanding immunometabolic and suppressive factors that impact cancer development" (2019). *USF Tampa Graduate Theses and Dissertations*.  
<https://digitalcommons.usf.edu/etd/8371>

This Dissertation is brought to you for free and open access by the USF Graduate Theses and Dissertations at Digital Commons @ University of South Florida. It has been accepted for inclusion in USF Tampa Graduate Theses and Dissertations by an authorized administrator of Digital Commons @ University of South Florida. For more information, please contact [digitalcommons@usf.edu](mailto:digitalcommons@usf.edu).

Understanding immunometabolic and suppressive factors that impact cancer development  
and progression

By:

Rebecca Swearingen Hesterberg

A dissertation submitted in partial fulfillment  
of requirements for the degree of  
Doctor of Philosophy  
Department of Cell Biology, Microbiology, and Molecular Biology  
College of Arts and Sciences  
University of South Florida

Major Professor: PK Epling-Burnette, PharmD., Ph.D.  
Committee: Daniel Abate-Daga, Ph.D.  
John L. Cleveland, Ph.D.  
Shari A. Pilon-Thomas, Ph.D.  
Sheng Wei, M.D.  
Daniel D. Billadeau, Ph.D.

Date of Approval: March 7, 2019

Keywords: anti-tumor immunity, immunometabolism, Cereblon, Polyamines, regulatory T cells

Copyright © 2019, Rebecca S Hesterberg

## DEDICATION

I dedicate this dissertation to...

...my husband, Stephen, who was with me when I decided to pursue research during our undergraduate studies, and who has shown unwavering support through the entirety of our time in Tampa. When we made the difficult decision to apply to and accept grad schools in Florida away from family and friends, your enthusiasm for our future served as my inspiration. I cannot fathom getting to this point in my career without your understanding, advice, and care. Living as two scientific minds under one roof has been the best adventure of my life and finding home and family with you has brought me immeasurable happiness. I love you.

...the Swearingens. Everyone I am lucky enough to be related to has been incredibly supportive, and I especially want to thank my parents, Jim and Tracy, and my sister, Jada. Since I was born, I was always told that I could do whatever I wanted to put my mind to. I have been lucky enough to have the perfect role models as parents, both of whom demonstrate that hard work can pay off. Mom, your powerful position in your career has always been an inspiration and your commitment to activities outside of work shows anyone can have everything with patience and dedication. Dad, watching you build your entrepreneurship as I was growing up taught me to follow my passions to success. Jada, thank you for always being a beam of positivity and goofiness. You all are the best.

...the Hesterbergs, Sally and Greg. The two of you have offered both cherished memories and ears for listening during both good and bad grad school times. Sally, your texts of support always brought a smile to my face, and Greg, thank you for always keeping me informed of the latest in popular science news.

...my friends, near and far. To my college friends, thank you for all the encouragement during grad school and for accepting this nerd into your life. To my running friends in Tampa, your agreement to run at 5am, train for marathons together, solve all the world's problems while running, and serve as each other's support kept me sane and grounded.



## ACKNOWLEDGEMENTS

I would like to first acknowledge my mentor, Dr. PK Epling-Burnette, whose research I became interested in while interviewing for the PhD program. Your mentorship has afforded opportunities both in the lab and outside that have been invaluable to my training. I feel incredibly fortunate to have worked in your lab during my graduate school career and I will always appreciate the time you took to teach immunology and train me in the techniques. I want to also thank the rest of the Burnette lab, both past and current members: Afua “Chu Chu” Akuffo, Aileen Alontaga, Ethan Arrington, Shiun Chang, Christelle Colin, Matt Beatty, Julia Billington, Chris Dukes, Aya Elmarsafawi, Bill Goodheart, Ying Han, Nathan Horvat, Adam Mailloux, Sharon McKnight, Cem Murdun, Jeff Painter, Xiao Tian, Lanzhu Yu. Whether we have actively worked on projects together or not, I have learned something from each of you.

I would like to thank Dr. John Cleveland for your time and your valuable input on my work. I would not be so thrilled to study polyamines without your enthusiasm and collaboration. I also thank the members of my committee, Dr. Daniel Abate-Daga, Dr. Shari Pilon-Thomas and Dr. Sheng Wei. Thank you for always giving me guidance and interesting questions to ponder. I am incredibly honored to have Dr. Daniel Billadeau from Mayo Clinic serve as the outside chair of my dissertation committee.

I want to thank all of our collaborators that have brought this work to what it is. I want to thank Dr. Dana Rollison for setting up such a wonderful team project. Those in her group have been fabulous to work with and I want to especially thank Rossybelle Amorrortu, Yayi Zhao, and Shalaka Hampras. I owe gratitude to the Cleveland lab members, too. Mario Fernandez and

Chunying Yang, thank you for your thoughts and hard work. I also want to acknowledge Nick Gimbrone for aiding in RNA-seq analysis and always being available to discuss polyamines.

I acknowledge the Moffitt core facilities, especially the flow cytometry, proteomics, chemical biology, bioinformatics, and genomics as well as the following members: Sean Yoder, Dr. John Koomen, Lancia Darville, Dr. Nick Lawrence, Dr. Harshani Lawrence, and Jodi Kroeger. I also want to thank comparative medicine and Kristen Spitler for all your help. The Southeast center for integrative metabolomics at UF and Tim Garrett at this core facility also helped a great deal in multiple aspects of our project. I want to mention the USF Health Lisa Muma Weitz Laboratory for Advanced Microscopy & Cell Imaging, too, for helping with transmission electron microscopy.

I lastly want to acknowledge the Cancer Biology PhD program for all of the help and opportunities over the years. Dr. Ken Wright, Cathy Gaffney and Janet Opel have all aided in my completion of the program. Thank you!

## TABLE OF CONTENTS

List of Tables .....	iv
List of Figures .....	v
Abstract .....	vii
Chapter One: Introduction .....	1
Introduction to T cell signaling .....	1
T cells and cancer .....	6
The role of CRBN in T cells .....	7
Polyamines in T cell activation .....	8
Anti-Tumor Immunity and Polyamines .....	10
Polyamines in autoimmune disease .....	12
Regulatory T cells and UV Radiation .....	13
Chapter Two: Cereblon Harnesses Myc-Dependent Bioenergetics and Anti-Tumor Activity of CD8 <sup>+</sup> T lymphocytes .....	16
Introduction .....	16
Results .....	16
CRBN is Dispensable for T cell Development but Represses T cell Activation .....	16
CRBN Controls the Bioenergetics of Activated T cells .....	21
CRBN Harnesses Arginine and Glutamine Metabolism and Controls the Expression of Myc in Activated CD8 <sup>+</sup> T cells .....	26
CRBN-Myc Circuit Controls CD8 <sup>+</sup> T cell Metabolism .....	30
CRBN Suppresses Extracellular Regulated (ERK) Signaling to Control Myc .....	35
<i>Crbn</i> Deficiency Augments T cell Activity in GVHD and Anti-Tumor Immune Responses and Myc Expression of CD8 <sup>+</sup> TIL .....	38
Discussion .....	43
Materials and Methods .....	46
Mouse Husbandry .....	46
Mouse Immune Cell Isolation .....	47
Mouse Polyclonal CD3 <sup>+</sup> and CD8 <sup>+</sup> T cell and OT-1 CD8 <sup>+</sup> T cell Activation .....	47
Human T cell Activation .....	47
Glucose Uptake and Flow Cytometry Analysis .....	48
Experimental Graft-Vs-Host (GVHD) Mouse Model .....	48
Metabolic Analysis .....	49
ATP, Hexokinase Enzymatic Assay and NAD/NADH .....	49
Amino Acid Uptake Assays .....	49
Quantitative PCR Analysis .....	49
Polyamine Extraction, LC/MS and Quantification .....	50
Gene Set Testing and Pathway Analyses .....	51

Transmission Electron Microscopy.....	52
Western Blot Analyses.....	52
Experimental Melanoma Mouse Model and ACT.....	53
Homeostatic Proliferation.....	53
Metabolomics Analysis.....	53
Compound Synthesis & Verification.....	55
Cytotoxicity Assays.....	56
Statistical Analysis.....	56
Critical Resources and Reagents.....	57
Chapter Three: The Role of Polyamines in Activated CD8 <sup>+</sup> T cells.....	62
Introduction.....	62
Results.....	62
Glutamine is a carbon source of polyamine biosynthesis in antigen-activated CD8 <sup>+</sup> T cells.....	62
Polyamine production is necessary for expression of T-box transcription factors involved in the CD8 effector phenotype and for viability.....	65
Polyamine production is necessary for activated CD8 <sup>+</sup> T cells to asymmetrically divide.....	67
Inhibition of polyamines decreases glycolysis and increases oxidative phosphorylation.....	71
Discussion.....	75
Methods.....	77
Mouse Husbandry.....	77
Isotope Analysis.....	77
Metabolic Analyses.....	78
Quantitative PCR Analysis.....	79
RNA-seq.....	79
Chapter Four: T-regulatory subpopulations associated with recent ultraviolet radiation exposure in a skin cancer screening cohort.....	81
Introduction.....	81
Results.....	81
Characterization of Tregs associated with UV exposure.....	81
Natural skin tone represents an effect modifier of the UVR and Treg association.....	88
Demographics are associated with Tregs.....	91
Recent UVR and Tregs are independently associated.....	93
Discussion.....	95
Methods.....	100
Study design and population.....	100
Spectrophotometer data collection.....	100
Blood collection and flow cytometry data acquisition and analysis.....	102
Statistical Methods.....	103
Chapter Five: Implications and Future Perspectives.....	105
References.....	109
Appendix A: Institutional Review Board Approval.....	126

Appendix B: Institutional Animal Care & Use Committee Approvals .....	128
Appendix C: Copyright Permissions of Previously Published Material .....	132

## LIST OF TABLES

Table 1:	Coinhibitory and Costimulatory receptors .....	5
Table 2:	Distribution of Immune Cells in <i>Crbn</i> <sup>-/-</sup> Mice .....	21
Table 3:	Statistical comparisons in reference to Figure 10 .....	35
Table 4:	Cereblon Genotyping Primers .....	46
Table 5:	RT-PCR Primer Sequences.....	50
Table 6:	Critical Reagents and Resources For Chapter Two .....	57
Table 7:	RT-PCR Primer Sequences.....	79
Table 8:	Circulating regulatory T (Treg) cell phenotypes and questionnaire factors .....	86
Table 9:	Circulating regulatory T (Treg) cell phenotypes and demographic characteristics .....	92
Table 10:	Circulating Group I-III regulatory T (Treg) cell phenotypes and demographic characteristics.....	93
Table 11:	Quartiles of circulating regulatory T (Treg) cell subpopulations and UV spectrophotometer readings among all 350 patients undergoing skin cancer screening.....	94
Table 12:	Quartiles of total Tregs, CLA+ and CCR4hi Tregs and UV spectrophotometer readings in all individuals and stratified by natural skin tone .....	95

## LIST OF FIGURES

Figure 1:	Proximal T cell signaling cascade .....	3
Figure 2:	Stimulatory and inhibitory molecules expressed on T cells .....	4
Figure 3:	Proposed mechanism for DFMO effects on the immune compartment in the tumor microenvironment.....	12
Figure 4:	Ablation of <i>Crbn</i> augments T Cell activation and function .....	19
Figure 5:	Deletion of <i>Crbn</i> increases effector function and long-lived memory .....	20
Figure 6:	Deletion of Cereblon does not significantly alter targets of IMiDs or mitochondria.....	24
Figure 7:	Cereblon loss augments energetics of activated T cells.....	25
Figure 8:	Activation of <i>Crbn</i> <sup>-/-</sup> T cells increases Myc-metabolism pathways.....	28
Figure 9:	<i>Crbn</i> harnesses arginine and glutamine metabolism and controls the expression of Myc in activated CD8 <sup>+</sup> T cells .....	29
Figure 10:	The phenotypes of activated <i>Crbn</i> <sup>-/-</sup> CD8 <sup>+</sup> T cells are Myc dependent.....	32
Figure 11:	Modulation of CRBN by IMiD compounds augments human CD8 <sup>+</sup> T Cell bioenergetics and Myc Expression.....	33
Figure 12:	Myc, 2-NBDG, CD98 and cell size of IMiD-treated activated human CD8 <sup>+</sup> T cells .....	34
Figure 13:	Myc expression elevation in activated <i>Crbn</i> <sup>-/-</sup> CD8 <sup>+</sup> T cells via ERK signaling .....	37
Figure 14:	<i>Crbn</i> <sup>-/-</sup> T cells have superior anti-tumor activity .....	41
Figure 15:	<i>Crbn</i> <sup>-/-</sup> T cells have increased function <i>in vivo</i> .....	42
Figure 16:	Synthesis of compounds CC-122 & MYCMI-6 .....	56
Figure 17:	Antigen activation of CD8 <sup>+</sup> T cells increases glutamine and arginine Metabolism .....	64
Figure 18:	Polyamines are primarily derived from glutamine .....	65

Figure 19:	Polyamine production blockade decreases T-bet-expressing cells and increases cell death .....	67
Figure 20:	Blocking polyamine biosynthesis alters asymmetric division.....	70
Figure 21:	Polyamine-driven asymmetric cell division is independent of hypusinated eIF5A .....	71
Figure 22:	RNA-seq analysis of DFMO-treated antigen activated CD8+ T cells .....	73
Figure 23:	DFMO treatment increases the spare-respiratory capacity of antigen activated CD8 <sup>+</sup> T cells.....	74
Figure 24:	Flow cytometry gating strategy for Treg cell analysis .....	84
Figure 25:	T cell populations in correlation with recent UV exposure among 350 individuals undergoing skin cancer screening.....	85
Figure 26:	Flow cytometry gating strategy controls in reference to Figure 24 .....	87
Figure 27:	Spearman rank correlation matrix for T cell populations among 350 skin cancer screening patients .....	88
Figure 28:	Effect modification by natural skin tone .....	90
Figure 29:	Spectrophotometer readings between forearm and forehead .....	101



## ABSTRACT

The immune system is responsible for surveillance against pathogens and malignancies and adoptive transfer of antigen-specific T is a powerful new cancer treatment option. There is a clinical need to understand more about the normal regulatory processes that prevent immunosurveillance and how to manipulate this for clinical benefit. This project aims to understand T cells from three different angles. First, the biological role of the negative regulator cereblon (CRBN) was investigated in CD8<sup>+</sup> T cells and my studies showed that higher levels of specific derivatives downstream of the amino acid glutamine may be beneficial to T cells in the immune microenvironment. Then, the functional role of these specific glutamine metabolites was studied in antigen-specific CD8<sup>+</sup> T cells. Finally, suppressive populations of regulatory T cells (Treg cells) were measured in patients at risk for skin cancer. Together, these results expanded our understanding of T cells in various facets of anti-tumor immunity and immune surveillance.

Immunomodulatory drugs (IMiDs) potentiate T cell effector functions through cereblon (CRBN), a substrate receptor of the DDB1-cullin-RING E3 ubiquitin ligase complex. However, the physiological roles of CRBN in T cells are unclear. Here, we report CRBN expression is regulated by T cell receptor (TCR) activation and harnesses metabolism of CD8<sup>+</sup> T cells. *Crbn* deficiency in CD8<sup>+</sup> T cells augments cellular metabolism manifest by elevated bioenergetics, with supraphysiological levels of polyamines secondary to enhanced glucose and amino acid transport, and increased expression of metabolic enzymes including ornithine decarboxylase. IMiD treatment similarly augments human CD8<sup>+</sup> T cell metabolism. Notably, control of metabolism by immunomodulatory drugs and *Crbn* deficiency is linked to increased and

sustained expression of the master metabolic regulator MYC. Finally, while *Crbn* deficient T cells exacerbate graft-versus-host disease *in vivo*, they endow tumor infiltrating lymphocytes with superior anti-tumor reactivity following adoptive transfer, revealing a new targetable pathway for adoptive T cell immunotherapy.

Polyamine biosynthesis is a well-conserved metabolic pathway that is increased upon activation in T cells, though the role that these metabolites serve in activated T cells has not been fully resolved. Novel implications for the role of polyamines in T cell metabolism and asymmetric cell division are presented here. First, it was found that antigen-activated CD8<sup>+</sup> T cells prefer glutamine for the carbon source of polyamines over arginine, which can also produce polyamines as a product of the urea cycle. We also report that glutamine-derived polyamines are necessary for increased glycolysis observed after T cell receptor activation and that biosynthetic blockade with pharmacological inhibitors of the rate limiting enzyme ornithine decarboxylase (OCD) increases the spare respiratory capacity of activated CD8<sup>+</sup> T cells. Further, polyamines act as a critical functional regulator for eukaryotic translation initiation factor 5A (eIF5a) through a process called hypusination. While hypusinated eIF5a is necessary for normal clonal expansion of antigen-activated CD8<sup>+</sup> T cells, it is not involved with the coupled distribution of CD8 and Myc proteins during asymmetric cell division suggesting that the role of polyamines in this process is independent of eIF5a. Together, these findings shed light on how polyamines control normal cellular functions of CD8<sup>+</sup> T cells.

Ultraviolet radiation (UVR) causing DNA damage is a well-documented risk factor for non-melanoma skin cancer (NMSC). Although poorly understood, UVR may also indirectly contribute to carcinogenesis by promoting immune evasion. We report the first epidemiological study designed to investigate the association between quantitative measures of UVR, obtained using a spectrophotometer, and circulating T regulatory (Treg) cells. In addition to total Treg cells, the proportion of functionally distinct Treg subsets defined by CD45RA and CD27 phenotypic markers, graded expression of FoxP3 and CD25, and those expressing cutaneous

lymphocyte-associated antigen (CLA) and the chemokine receptor CCR4 were enumerated in 350 individuals undergoing routine skin cancer screening exams and determined not to have prevalent skin cancer. No associations were identified for UVR exposure and the overall proportion of circulating Tregs. However, Treg subpopulations with an activation-associated phenotype, CD45RA<sup>+</sup>/CD27<sup>-</sup>, and those expressing cutaneous homing receptors were significantly and positively associated with UVR. These subpopulations of Treg cells also differed by age, sex, and race. After stratification by natural skin tone, and adjusting for age and sex, we found that spectrophotometer-based measures of UVR exposure but not self-reported measures of past sun exposure, were positively correlated with the highest levels of these Treg subpopulations, particularly among lighter skinned individuals. Findings from this large epidemiologic study highlight the diversity of human Treg cell subpopulations associated with UVR, and raise questions about the specific coordinated expression of CD45RA, CD27, CCR4, and CLA on Treg cells and the possibility that UVR contributes to NMSC carcinogenesis through Treg-mediated immune evasion.

Here, questions are addressed about fundamental aspects of T cell biology that includes their role in tumor immune surveillance, translational principles for the design and implementation of novel immunotherapies, and a comprehensive analysis of immunometabolism related to human and mouse experimental systems. Through interdisciplinary approaches, some of the questions about immunobiology and immunotherapy of cancer have been successfully addressed.

## CHAPTER ONE: INTRODUCTION

**A note to the reader:** portions of this chapter have been previously published in a review article in the journal *Medical Sciences*, Hesterberg et al. 2018<sup>1</sup> and in a research article in *Journal of Immunology*, Hesterberg et al. 2018<sup>2</sup>.

### Introduction to T cell signaling

T cell receptor (TCR) antigen activation is restricted by major histocompatibility cluster (MHC) and peptide recognition<sup>3</sup>. T cells lyse their targets (e.g., virally infected or malignant cells) through interaction of small peptide fragments bound in the groove of an MHC molecule, which strengthens selectivity for self over non-self and protects against autoimmunity<sup>3,4</sup>. Professional antigen-presenting cells (APCs) such as B-cells, macrophages and dendritic cells (DC) express both MHC class I and MHC class II for activating CD4<sup>+</sup> and CD8<sup>+</sup> T cells. Through receptor or phagocytosis-mediated antigen internalization, APCs process antigen into the correct fragment length for display by the MHC molecule for possible recognition by T cells<sup>5</sup>.

The TCR signaling complex engages numerous cascading molecular interactions largely mediated by phosphorylation, dephosphorylation or ubiquitinylation that result in cellular activation<sup>6</sup> (**Figure 1**). The TCR complex is composed of several protein that are necessary for survival and signaling including TCR $\alpha$  and TCR $\beta$  chains, the CD3 signaling molecules  $\delta/\epsilon$ , CD3 $\gamma/\epsilon$  and CD247 composed on the dimeric  $\zeta\zeta$ -chains or  $\zeta_n$ . The signaling cascade after TCR recognition of peptides and MHC molecules is complex and leads to effector responses. The initiating signal is generated by lymphocyte protein tyrosine kinase (Lck) and other Src family tyrosine kinases, including the zeta-chain associated protein kinase (Zap-70) that is recruited to the TCR/CD3 complex. Costimulation through leukocyte-associated antigen-1 (LFA1) which is

an integrin involved in T cell migration or CD28 interaction with CD80 (B7-1) or CD86 (B7-2) (see also **Figure 1**), activates the phosphorylation of the YXXM or YNPP signaling motifs<sup>7</sup> that regulates glucose metabolism. CD28 promotes stable recruitment of the adaptor protein Grb2/GADS along with Itk, Lck, and phosphatidylinositol 3 kinase (PI3K) heterodimer p85/p110 and SLP76. These interactions promote the activation of VAV-1, RasGRP, and the Ras/Raf/MEK/Erk pathway downstream of phosphorylated SLP-76 and Zap-70 modulating the TCR signal strength<sup>7</sup>. Finally, a complement of transcription factors nuclear factor of activated T cells (NFAT), cAMP response element-binding protein (CREB), Fox family transcription factor c-Fos, Jun (when in combination with c-Fos forms the AP-1 early response transcription factor complex), an NFκB family member c-Rel, and c-MYC (henceforth referred to as MYC) which coordinately regulate gene expression. Activation of CD28 leads to the phosphorylation of PI3K, phosphatidylinositol-3,4 bisphosphate (PIP2) and phosphoinositide-dependent kinase 1 (PDK1)<sup>8</sup>. These phosphorylation events integrate the TCR and CD28 signaling to induce the NFκB pathway including protein kinase C-theta (PKC-θ) and inhibit the ubiquitin ligase c-Cbl<sup>9</sup>. This ultimately leads to activation of the Bcl10, Malt1, Carma1 (CBM) complex that activates to IKKαβγ, NFκB, and REL<sup>10</sup>. In addition to PKC-θ, phosphorylation of AKT is critical for the regulation of mTORC1 and mTORC2 complexes of mTOR that bind GβL and Raptor or Rictor, respectively<sup>11,12</sup>. This is a critical step in MYC-dependent transcriptional regulation that stimulates dramatic changes in metabolism including glucose, amino acid, nucleotide and polyamine biosynthesis<sup>13,14</sup>.

Divalent cations such as calcium ( $\text{Ca}^{2+}$ ) are induced downstream of phospholipase Cγ1, PIP2, and inositol-1,4,5 triphosphate (IP3) which mobilize and release intracellular  $\text{Ca}^{2+}$  stores from the endoplasmic reticulum ( $\text{Ca}^{2+}$ -ER) a potential metabolic switch that can ultimately suppress intratumoral T cell functions<sup>15</sup>. Sustained signaling then promotes the influx of extracellular  $\text{Ca}^{2+}$  into the cells through calcium release-activated  $\text{Ca}^{2+}$  (CRAC) channels. Calcium-calmodulin interactions ( $\text{Ca}^{2+}$ /CaM) then activate the phosphatase calcineurin and

calcium/calmodulin-dependent protein kinase type IV calmodulin (CaMKIV), which dephosphorylates the cytoplasmic subunits of NFAT. This exposes a nuclear localization signal that results in nuclear transport and phosphorylation of CREB. This classical TCR signaling cascade leads to high rates of proliferation, cytotoxic function and cytokine production.

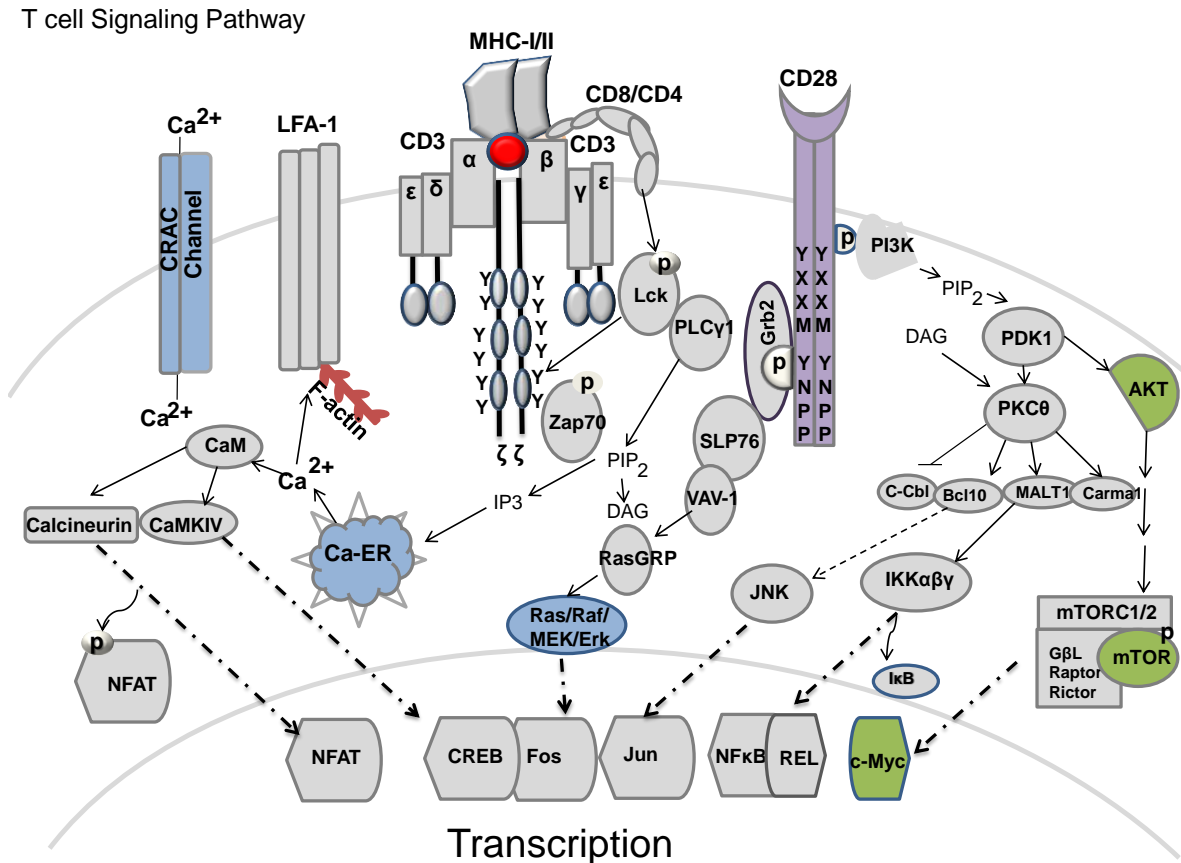


**Figure 1: Proximal T cell signaling cascade.** TCR proximal signaling pathways downstream of the TCR-APC signaling complex are responsible for the cascade of events leading to reprogramming and differentiation.

T cells express a host of receptors that act as co-stimulatory molecules or as co-inhibitors when interacting with various ligands on an antigen presenting cell (**Figure 2, Table 1**). These molecules promote or repress the functional outcomes of T cells such as cytotoxicity-associated granzyme B expression, cytokine release, and proliferation<sup>6,16-27</sup>. Co-stimulatory molecules on T cells were first identified through CD28, which is the founding member of the

immunoglobulin (Ig) family of costimulatory receptors. Additional receptors include those listed in **Table 1** and **Figure 2**.

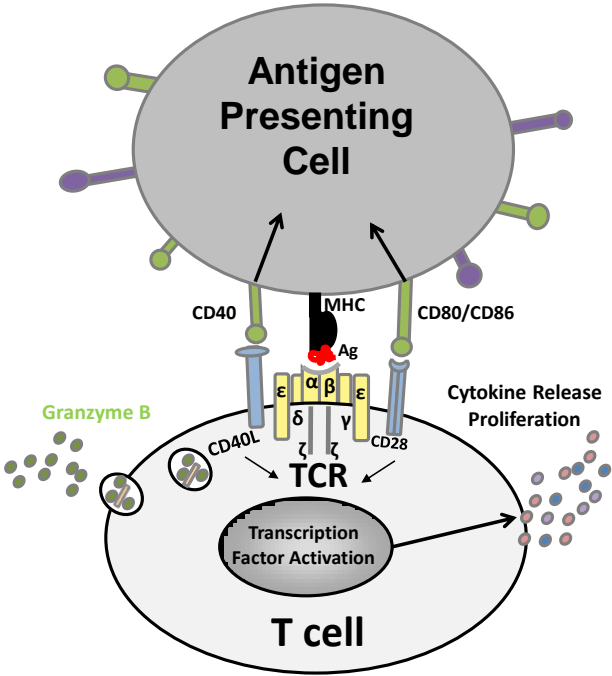


**Figure 2: Stimulatory and inhibitory molecules expressed on T cells.**

**Table 1: Coinhibitory and Costimulatory receptors**

<b>T Cell</b>	<b>Ligand or protein on Antigen Presenting Cell</b>	<b>Function</b>
CD28	CD80/CD86	costimulatory
CD40L	CD40	costimulatory
ICOS	ICOSL	Costimulatory, important for Th2 responses
CD27	CD70	Costimulatory, memory and activation
OX40	OC40L	Costimulatory, activation
LFA1	ICAM-1	Costimulatory, T cell migration
CD2	LFA3	Costimulatory, adhesion
HVEM	LIGHT, BTLA	Costimulatory
GITR	GITRL	Costimulatory
TIM1	TIM4	Costimulatory
Galectin 9	TIM3	Costimulatory
4-1BB	4-1BBL	Costimulatory
CTLA4	CD80, CD86	Coinhibitory
PD1	PDL1, PDL2	Coinhibitory
BTLA	HVEM	Coinhibitory
CD160	HVEM	Coinhibitory
Lag3	MHC Class II	Coinhibitory
Tim3	Galectin 9	Coinhibitory
TIGIT	CD155, CD112	Coinhibitory

T cell stimulation leads to dynamic changes in metabolic programming that are critical for the survival and homeostasis of the T cell compartment<sup>28</sup>. Similar to tumor cells, T cells must engage aerobic glycolysis and elevate oxidative phosphorylation (OXPHOS) to promote antigen-induced growth, proliferation and effector functions<sup>29</sup>. Accordingly, impaired metabolism caused by nutrient-poor environments leads to functional T cell exhaustion in chronic viral infections and tumors<sup>15,30</sup>. Furthermore, signaling invoked by immune checkpoint proteins, including PD-1<sup>31</sup>, CTLA-4<sup>32</sup>, Tim-3<sup>33</sup>, and lymphocyte-activation gene 3 (Lag3)<sup>34</sup>, suppress pathways involved in nutrient utilization, further driving T cell exhaustion. Thus, identifying T cell metabolic regulators, especially those targetable by small molecule agonists or inhibitors, is likely to have a dramatic impact on anti-tumor immunity, and on all forms of immunotherapy<sup>35</sup>.



## T cells and cancer

It is essential to maintain a balance between T cell promoting and T cell dampening signals, such as with the co-receptors. For example, over-activation can lead to autoimmune diseases driven by T cells and lack of T cell responses can lead to infections, cancer and other diseases. Cancer, in particular, can create a suite of signals that aid in escaping the immune system. Normally, cancer cells' genetic mutations could be recognized as foreign neo-antigens and over-expressed oncoproteins could increase antigenicity<sup>36</sup>. Further, danger-associated molecular patterns released by unhealthy cells, such as these cancer cells, cause dendritic cells or other antigen-presenting cells to recruit T cells into the tumor microenvironment for immune destruction<sup>37</sup>. This normal mechanism for malignant cells' destruction is not observed in the clinic given that cancers grow unfettered despite infiltrating T cells. There are several mechanisms of evasion from T cells, many of which occur through direct cell interactions between the malignant cells and T cells. For instance, cancer cells can down-regulate MHC, causing a lack of antigen presentation<sup>38</sup>. Finding mutated antigens can be difficult among all self-antigens that are not immune stimulatory<sup>39</sup>. Even if T cells recognize strongly-activating viral or neo-antigens, cancer cells can over-express ligands that bind to suppressive receptors such as PD-1 and CTLA4, effectively shutting off TCR signaling<sup>40</sup>.

There are also several mechanisms of T cell suppression in the tumor microenvironment that go beyond cell-cell interactions. First, malignant cells can recruit regulatory T cells (Tregs) that suppress effector T cell responses. These can be recruited by cytokines such as TGF $\beta$  or develop from conventional CD4<sup>+</sup> T cells by these same cytokines. Further, many of the repressive signals manifest in conventional CD4<sup>+</sup> and CD8<sup>+</sup> T cells can activate Treg cells. For example, PD-L1 causes CD4<sup>+</sup> T cells to differentiate into Treg cells and sustains Foxp3 expression, the transcription factor that denotes functional Treg cells<sup>41</sup>. Second, another suppressive cell population that is recruited and thrives in the cancer microenvironment is comprised of myeloid-derived suppressor cells (MDSCs). These cells can disable the TCR by

nitrosylation such that CD8<sup>+</sup> T cells can no longer respond to antigens<sup>42</sup>. MDSCs can also out-compete T cells for arginine and will release arginase, further depleting this amino acid essential for activated T cell survival<sup>43,44</sup>. Cancer cells also can create a hostile microenvironment for immune responses occur. Specifically, due to the Warburg effect where cancer cells have a preference for aerobic glycolysis over other metabolic pathways, there is a build-up of lactic acid that lowers the pH and inhibits T cell cytokine production<sup>45,46</sup>. Cancer cells can also out-compete T cells for nutrients necessary for activation<sup>46</sup>. For example, glucose deprivation caused by the elevated glycolytic rates of cancer cells can significantly impair T cell function<sup>15,47</sup>. Given that all these factors can occur at the same time within the tumor microenvironment, T cells become exhausted and suppressed before proper activation actually occurs.

### **The role of CRBN in T cells**

Cereblon (CRBN), first discovered through genetic linkage analysis in patients having a mild autosomal recessive non-syndromic intellectual disability, is the sole documented target of immunomodulatory drug (IMiD)-induced immune modulation, teratogenicity, and antineoplastic activity<sup>16,48</sup> in multiple myeloma<sup>49,50</sup>, B-cell malignancies<sup>51-53</sup> and deletion chromosome 5q myelodysplastic syndrome (del-5q MDS)<sup>54,55</sup>. From a historical perspective much like the mammalian target of rapamycin (mTOR), biological functions of CRBN are being revealed due to its prominent role in IMiD pharmacological responses. CRBN acts as the substrate recruiting module for the DNA damage-binding protein-1 (DDB1), Cullin 4 (Cul4A or B), and regulator of Cullins 1 (ROC1) E3 ubiquitin ligase complex<sup>56-58</sup>. Ligation to IMiD compounds modulates the specificity of the E3-ligase activity and directs the degradation of proteins involved in hematopoiesis, angiogenesis, and T cell and NK cell regulation<sup>52,59-61</sup>.

IMiD compound-induced, ubiquitin-dependent degradation of the lymphocyte transcriptional repressor Ikaros (encoded by *IKZF1*)<sup>62</sup>, its paralog Aiolos (encoded by *IKZF3*)<sup>63</sup>,

and casein kinase-1 $\alpha$  (CK1 $\alpha$ ), occurs following formation of an interaction interface comprised of a conserved  $\beta$ -hairpin-loop in these target proteins<sup>59,60,64</sup>. However, pharmacological effects of IMiD compounds on CRBN functions can also occur via non-proteasome means, where for example IMiD binding to CRBN displaces it from a complex with CD147 and the lactate transporter SLC16A1 (MCT1) in multiple myeloma cells, destabilizing this complex and leading to cancer cell death<sup>65</sup>. Interestingly, destabilization of the CD147/MCT1 core complex also occurs after CRBN genetic depletion revealing this as a ubiquitin-independent function.

Human and animal studies imply CRBN regulates two types of ion channel proteins involved in neuronal excitation, where a nonsense mutation (R419X) within the CRBN C-terminal domain is linked to a nonsyndromic mental retardation syndrome<sup>66</sup>. In other cell types CRBN appears to control metabolism, by directing degradation of glutamine synthetase (GS)<sup>67</sup> via interactions with acetylated lysines of GS that are triggered by high intracellular glutamine concentrations, and by suppressing the activity of the  $\alpha$ 1 subunit of AMP-activated protein kinase (AMPK  $\alpha$ 1)<sup>68</sup>, a regulator of energy homeostasis. Finally, CD4<sup>+</sup> T cells from mice lacking *Crbn* show increased IL-2 production following T cell receptor (TCR) stimulation, which has been attributed to the epigenetic regulation of the gene encoding the *Kcna3* voltage-activated potassium ion channel<sup>69</sup>. This is the basis for research in **Chapter Two**.

### **Polyamines in T cell activation**

Two of the amino acid precursors for ornithine, glutamine and arginine, are required for T cell activation<sup>70-72</sup> and metabolism of these molecules is increased downstream of TCR signaling events<sup>72</sup>, including mTOR, Myc and ERK/MAPK<sup>13,71</sup> that are linked through integrated signaling (**Figure 1**). Some studies have suggested that glycolysis is actually less important in some disease models compared to glutaminolysis<sup>73</sup>. Alloreactive TCR stimulation in the context of graft-versus-host disease (GVHD) was originally considered to be driven largely by glycolysis<sup>74-76</sup> until it was recently shown, using *in vivo* tracer studies, that glutamine is the

primary fuel source of alloreactive T cells in GVHD<sup>73,75</sup>. Furthermore, ODC enzymatic activity is significantly increased after T cell activation, suggesting that polyamines are produced downstream of either arginine or glutamine<sup>13,77,78</sup>.

Mass spectrometry-based global metabolomics and integrated transcriptome analysis has been used to map the changes in metabolic intermediates after TCR-stimulation<sup>44</sup>. Notably, proteins that regulate the arginine and proline pathways are enriched in TCR-stimulated CD4<sup>+</sup> T cells, and metabolic tracing studies have shown that TCR activation triggers flux of Arg into ornithine, putrescine, and agmatine, and more modest flux into spermidine and proline. Catabolism of Arg into polyamines in CD4<sup>+</sup> T cells is regulated by mitochondrial arginase-2 (ARG2) as arginase-1 is not expressed in these cells. Interestingly, dietary supplementation of Arg during T cell activation is associated with enhanced mitochondrial oxidative phosphorylation (OXPHOS) and mitochondrial spare respiratory capacity (SRC)<sup>28,79,80</sup>. Further the morphology and numbers of mitochondria are critical determinants for SRC and for a functional T cell memory response following secondary antigenic challenge<sup>28,79,80</sup>. Notably, *in vivo* Arg supplementation of transgenic mice bearing a TCR receptor that specifically recognizes the hemagglutinin antigen (HA 110–119 peptide) increases intracellular Arg levels and the survival of memory T cells<sup>44</sup>.

Glutamine is also required for long-term T cell responses *in vivo* and blocking the metabolism of this amino acid increases short-term effector function while inhibiting long-term responses<sup>72</sup>. Indeed, CD8<sup>+</sup> and Th1 CD4<sup>+</sup> T cells from mice lacking glutaminase, the enzyme responsible for the conversion of glutamine to glutamate, have increased expression of the effector phenotype transcription factor T-bet<sup>81,82</sup> and granzyme B. These glutaminase-lacking T cells fail to exert long-term responses *in vivo*, suggesting that glutamine is necessary for durable immunity. A metabolite of glutamine,  $\alpha$ -ketoglutarate, is also involved in chromatin accessibility of various regions of the genome, altering the expression of effector genes<sup>72</sup>.

Although it is evident that arginine and glutamine are involved in memory T cell development, chromatin accessibility and durable *in vivo* T cell immunity, a specific role for polyamines in CD8<sup>+</sup> T cell function has not been well-defined. Further, similar to phenotypes observed in other cell types, polyamines are required for T cell proliferation manifest after TCR stimulation<sup>13,83</sup>. Accordingly, although the mechanism(s) is unclear, polyamine depletion during initial T cell activation *in vitro* impairs cytotoxic function (CTL) against target cells<sup>84-89</sup>. This is the basis of investigation for **Chapter Three**.

### **Anti-Tumor Immunity and Polyamines**

Polyamines are essential components of T cell activation, where for example they are necessary for the effector functions and high rates of proliferation<sup>13,84-89</sup>. For example, several older *in vitro* studies suggest that blocking polyamine production with difluoromethylornithine (DFMO), an irreversible inhibitor of ODC1, suppresses cytotoxicity of activated CD8<sup>+</sup> T cells against alloantigens or tumor cells<sup>84-89</sup>. Surprisingly, several studies have demonstrated that ODC inhibition<sup>90-93</sup>, and/or treatment with polyamine transport inhibitors (PTIs), significantly reduces rates of tumor growth and that this is due to increase in anti-tumor immunity. Further, the anti-tumor response is linked to T cell anti-tumor activity, as the beneficial effects observed following treatment with ODC inhibitors and PTIs are reversed in *Rag*<sup>-/-</sup> mice lacking both T and B cells, and in athymic nude mice that lack only T cells consistent with activation of T cells after polyamine depletion in tumor models<sup>91,94</sup>. Moreover, polyamine inhibition increases CD8<sup>+</sup> T cell infiltration into the tumor bed<sup>91,94,95</sup>. Though CD8<sup>+</sup> T cells isolated from a similar B16F10 melanoma model lack cytotoxic functions *in vitro*<sup>93</sup>, it is clear that systemic polyamine inhibition of tumor-bearing mice can restore T cell anti-tumor immunity.

In the tumor microenvironment, MDSC, Treg and other cell populations suppress the immune response and contribute to tumor escape from immune surveillance<sup>42</sup>. These cells also use polyamines to invoke their suppressive activations and to support their metabolism. MDSCs

and other suppressive myeloid cells are evident in many infectious diseases, including leishmaniasis<sup>96</sup>, toxoplasmosis<sup>97</sup>, candidiasis<sup>98</sup>, and HIV-infected individuals<sup>99</sup>, and are significantly elevated in tumor-bearing animals<sup>100,101</sup>. Comparable suppressive cells have been identified in both mouse models and human cancers including melanoma, breast cancer, pancreatic, non-small cell lung and leukemia<sup>100</sup>.

Suppressive myeloid cells, specifically MDSCs, monocyte-derived M2 macrophages and some dendritic cells (DCs) are often present in high numbers in the tumor microenvironment. MDSCs retain the ability to produce NO and high levels of reactive oxygen species (ROS) leading to nitration of tyrosine residues of the TCR which disrupts its interaction with the peptide-MHC complex during antigen presentation<sup>5</sup> (**Figure 2**). MDSCs can also inhibit T cells by high rates of arginase, depleting arginine availability in the tumor microenvironment<sup>102</sup>, and DFMO treatment in mice with melanoma results in lower arginase activity specifically from MDSCs<sup>91</sup> (**Figure 3**).

Monocyte-derived macrophages can be polarized into M1 or M2 macrophages<sup>95,103,104</sup>. M2 macrophages do not make nitric oxide (NO), a major byproduct of M1 macrophages, and use arginase to hydrolyze imported arginine into ornithine and urea which depletes arginine in the tumor microenvironment, compromising intratumoral T cell functions and survival<sup>100,105,106</sup>. The suppressive functions of M2 macrophages relies on higher basal mitochondrial oxygen consumption rates driven by fatty acid oxidation (FAO)<sup>107</sup> and, accordingly, the development of M2 macrophages is blocked by inhibiting mitochondrial OXPHOS and FAO. Further, unlike M1 macrophages, M2 macrophages require glutaminolysis for proliferation and ODC inhibition through DFMO or polyamine transport inhibitor treatment of tumor-bearing mice significantly reduces intratumoral suppressive MDSCs<sup>91,94,95</sup> which should improve Arg availability for T cells that is necessary for their proliferation and persistence<sup>44,70,108,109</sup>. Polyamine inhibition also increases TNF $\alpha$  and IL-1 cytokine production by tumor infiltrating macrophages, suggesting reprogramming of macrophages into the M1 phenotype that augments presentation of tumor-

associated antigens, increases citrulline export and import, and further supports the TCA cycle via arginine-derived fumarate<sup>93,95</sup> (**Figure 3**). Recently, it has been shown that polyamines induce IDO1 expression in DCs through Src kinase and that results in a more immunosuppressive DC phenotype. Inhibition of ODC by DFMO reduces this signaling network and shifts DCs to a more immune stimulatory phenotype (**Figure 3**). Thus, it appears that although polyamines are required for normal CD8<sup>+</sup> T cell functions, the net effects of polyamine depletion on suppressive myeloid cells is to increase anti-tumor CD8<sup>+</sup> T cell activity by restoring a more conducive tumor microenvironment.

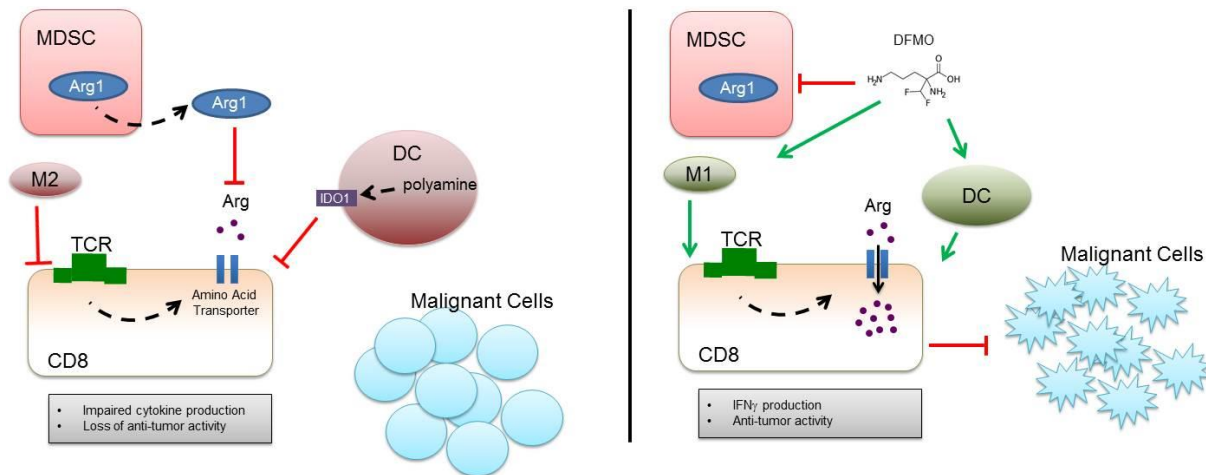


**Figure 3: Proposed mechanism for DFMO effects on the immune compartment in the tumor microenvironment.**

DFMO treatment inhibits MDSC arginase activity, IDO1 expression on DCs and M2 macrophages. These effects combined decrease MDSC suppressive activity and promote M1 macrophages and immunostimulatory DCs. This allows T cells to import more arginine, an amino acid transported at a higher rate downstream of the TCR. CD8<sup>+</sup> T cells can then produce more IFN $\gamma$  and enhance anti-tumor activity, leading to the apoptosis of malignant cells.

### Polyamines in autoimmune disease

Autoimmune diseases are provoked by abnormal, unchecked immune responses against normal host tissue, and are driven self-reactive TCRs and BCRs in the thymus and

bone marrow. Further, suppressive immune populations including MDSCs and regulatory T cells (Tregs), are necessary to establish peripheral tolerance against self-reactive effector T and B cells that escape negative selection<sup>110-112</sup>. Autoimmunity can arise in almost every peripheral tissue in the body, for example multiple sclerosis in the brain, thyroiditis and Graves's disease in the thyroid, rheumatoid arthritis and ankylosing spondylitis in the joints, psoriasis, eczema and scleroderma in the skin, diabetes in the pancreas, and celiac disease, ulcerative colitis, and Crohn's Disease that occur in the intestine. Interestingly, circulating polyamine levels are increased in patients with autoimmune diseases<sup>113,114</sup>. Further, polyamines have the ability to form nuclear aggregates<sup>115-117</sup> and it has been suggested that nuclear polyamine aggregates interact with DNA, RNA, or other macro-molecular structures to stabilize autoantigens. Strikingly, the most common autoimmune B-cell responses are generated to macromolecules such as double stranded DNA or single stranded DNA<sup>118,119</sup>. Abnormal polyamine levels have also been noted in systemic lupus erythematosus (SLE)<sup>120</sup>, and rheumatoid arthritis<sup>121</sup> that are characterized by anti-nuclear antibodies consistent with this hypothesis.

### **Regulatory T cells and UV Radiation**

Ultraviolet radiation (UVR) is an environmental factor that contributes to the development of non-melanoma skin cancer (NMSC), one of the most frequently diagnosed cancers in the United States<sup>122,123</sup>. The two most common types of NMSC, squamous cell carcinoma (SCC) and basal cell carcinoma (BCC), occur most often on areas of sun exposed skin<sup>123,124</sup>. UVR is involved in several stages of carcinogenesis<sup>122</sup>, including induction of DNA damage and possible immune suppression, enabling malignant cells to grow unchecked. Although the exact mechanism of the latter is not well understood, immune suppression associated with skin cancer is marked by both a reduction in conventional T cell functions<sup>125,126</sup> as a consequence of regulatory T (Treg) cells<sup>127</sup>.



Treg cells, which are characterized by the expression of the transcription factor FoxP3, CD4 and the IL-2 receptor  $\alpha$  chain (CD25), expand systemically and within various tumors where they uniformly have negative prognostic significance<sup>128-130</sup>. Differentiation markers on Tregs have been studied in humans with autoimmune disease, viral infection<sup>131-134</sup> and cancer, and include the protein tyrosine phosphatase (encoded by the *PTPRC* gene) CD45RA, CD62L (L-selectin) and CD27. While the coordinated differentiation of conventional T cells in humans, and of Tregs in mice, have been well delineated, the differentiation path for Tregs in humans is less well defined<sup>135</sup>. Both CD45RA and CD27, a co-stimulatory molecule involved in activation and memory development, can functionally distinguish Treg subsets<sup>17,136,137</sup>. All of these markers are expressed on naïve, resting T cells and medullary thymocytes but are downregulated after T cell receptor activation<sup>138</sup>. Patterns of chemokine receptors are also useful in distinguishing functional Treg populations that exhibit directional localization within inflammatory environments, including the skin<sup>139</sup>.

In mice, the frequency of neuropilin-1<sup>+</sup>, thymic-derived (i.e., natural) nTregs increased following exposure to low doses of UVB radiation<sup>140</sup>. UVR-induced expansion of Treg cells is mediated by antigen activation<sup>141</sup>, which, under specified conditions, enables their suppressive functions and triggers tissue-homing to the skin<sup>140,142,143</sup>. Antigen activation of Treg cells occurs through self-antigens and, in some tissues, the microbiome<sup>144</sup>. The coordination of UVR exposure and Treg expansion suggests that both may contribute to growth in keratinocyte carcinogenesis.

Functionally distinct Treg cell subpopulations characterized by specific phenotypic surface markers have been studied in various disease settings<sup>132,134,145</sup>. Thymic-derived Tregs expressing CD45RA, decline with age in mice<sup>146</sup>, during chronic viral infections<sup>134</sup>, and, following organ transplantation rejection<sup>132</sup>. We found previously that CD45RA<sup>+</sup>/CD27<sup>-</sup> Treg cells are expanded prior to disease progression and are specifically associated with poor survival in myelodysplastic syndrome (MDS)<sup>145</sup>. Although the CD45RA<sup>+</sup>/CD27<sup>-</sup> Treg subset is more

suppressive compared to CD45RA<sup>+</sup>/CD27<sup>+</sup> Treg subtypes on an individual cell basis, Treg population dynamics in the context of UVR, age, sex and race are poorly characterized<sup>135,145</sup>.

Epidemiological studies have reported associations between prevalence of chronic autoimmune diseases such as multiple sclerosis, lupus erythematosus, and rheumatoid arthritis, and distance from the equator, suggesting a role for UVR exposure in immune function<sup>147-150</sup>. Other studies using UVR as a treatment for multiple sclerosis and psoriasis have reported decreased immune function as a result of UVR photochemical therapy, primarily by inducing Treg cells within the lymph nodes followed by altering their skin migratory behavior<sup>151-153</sup>. Among psoriasis patients, circulating Treg cell populations increase following treatment with photochemical therapy, suggesting increases in immunosuppressive activity of Treg cells by UVR<sup>154</sup>. This is the basis for investigations in **Chapter Four**.

**CHAPTER TWO:**  
**CEREBLON HARNESSSES MYC-DEPENDENT BIOENERGETICS**  
**AND ANTI-TUMOR ACTIVITY OF CD8<sup>+</sup> T LYMPHOCYTES**

**Introduction**

Here, using a systems approach to study the physiological roles of Cereblon (CRBN), we report that CRBN expression is controlled by T cell receptor (TCR) signaling, that CRBN controls the master T cell metabolic regulator c-Myc (*Myc*)<sup>13</sup>, and that deficiency or inhibition of CRBN invokes a unique T cell metabolic program that overcomes barriers to anti-tumor T cell immunity, illuminating a new immunotherapeutically tractable pathway that could be exploited in adoptive T cell therapy.

**Results**

**CRBN is Dispensable for T cell Development but Represses T cell Activation**

CRBN expression levels initially decrease following TCR stimulation at both the mRNA and protein level in mouse (**Figure 4A and B**) and human CD8<sup>+</sup> T cells (**Figure 5A**), and then increase to levels higher than those found in unstimulated cells, consistent with a function for CRBN in harnessing T cell activation. To test this hypothesis, we assessed the roles of CRBN in controlling T cell functions in *Crbn* deficient mice<sup>155</sup>, where *Crbn* deletion was achieved by Cre recombinase-mediated excision of *Crbn* exons 3 and 4 after mating with CAG-Cre-expressing transgenic deleter mice that excised the gene from all tissues (*Crbn*<sup>-/-</sup>) (**Figure 5B**). Consistent with previous reports of mice with a similar global deletion of *Crbn*<sup>69</sup>, normal basal serum levels of the cytokines IFN $\gamma$ , IL-2 and TNF $\alpha$  (**Figure 5C**), as well as CD4<sup>+</sup> and CD8<sup>+</sup> T cell populations,

are equally distributed in *Crbn*<sup>-/-</sup> and *Crbn*<sup>+/+</sup> littermates (**Figure 5D**), which have similar proportions of CD69<sup>+</sup> and CD25<sup>+</sup> T cells in the spleen, lymph node, peripheral blood and bone marrow (**Table 2**). The distribution of naïve, long-term memory, and effector memory T cells was also comparable in 3-month old *Crbn*<sup>-/-</sup> and *Crbn*<sup>+/+</sup> littermates (Table S1), and the numbers of thymocytes, and thymic subpopulations, were similar in *Crbn*<sup>-/-</sup> and *Crbn*<sup>+/+</sup> mice (**Table 2**). Finally, *Crbn* deficiency had no impact on B cell, NK1.1<sup>+</sup> NK cells, or Treg numbers (**Table 2**).

Homeostatic responses within the T cell compartment were then assessed by evaluating age-associated T cell phenotypes. Proportions of activated CD44<sup>+</sup>CD8<sup>+</sup> (**Figure 5E**) and CD44<sup>+</sup>CD4<sup>+</sup> T cells (**Figure 5F**) were similar in *Crbn*<sup>-/-</sup> and *Crbn*<sup>+/+</sup> mice with both groups showing the expected age-dependent increase in CD44 positive cells that are induced through homeostatic turnover<sup>156,157</sup>. Notably, however, age-associated changes in the memory CD8<sup>+</sup> T cell compartment were significantly different in *Crbn*<sup>-/-</sup> mice with the preservation of long-lived CD44<sup>+</sup>/CD127<sup>+</sup>/KLRG1<sup>-</sup> CD8<sup>+</sup> cells (**Figure 5G**) and corresponding reductions in the CD44<sup>+</sup>/CD127<sup>-</sup>/KLRG1<sup>+</sup> (**Figure 5H**) short-lived memory cells<sup>158</sup> suggesting that *Crbn* deficiency may regulate CD8<sup>+</sup> memory T cell fate.

To assess possible effects of the *Crbn* deficiency on T cell activation, *Crbn*<sup>-/-</sup> and *Crbn*<sup>+/+</sup> T cells were stimulated with anti-CD3ε with or without anti-CD28 costimulation. Notably, activated *Crbn*<sup>-/-</sup> T cells produce significantly increased levels of IL-2 and IFNγ versus *Crbn*<sup>+/+</sup> T cells even without CD28 costimulation (**Figure 4C-D**), as well as elevated secreted levels of TNFα (**Figure 4E**), IL-17 (**Figure 4F**) and IL-10 (**Figure 5I**) and have significantly increased *Irfng* mRNA with suboptimal anti-CD3ε (3 μg/mL) (**Figure 4G**). Finally, there were marked increases in the number of proliferating CD4<sup>+</sup> and CD8<sup>+</sup> *Crbn*<sup>-/-</sup> T cells, based on the division index (**Figure 4H**). As a similar proportion of *Crbn*<sup>-/-</sup> cells enter cell division as *Crbn*<sup>+/+</sup> cells (*i.e.*, the percent of T cells that divide, **Figure 4H**), this suggests *Crbn* deficiency regulates fitness and/or persistence of T cells rather than entry into the cell cycle and impacts both cell populations. Previous analysis of *Crbn* deficient mice indicated that epigenetic up-regulation of *Kcna3* that

encodes the voltage-gated potassium channel protein Kv1.3 is mechanistically linked to hyperactive response in CD4<sup>+</sup> T cells <sup>69</sup>, and Kv1.3 is essential for T cell proliferation <sup>159</sup>. Although activated *Crbn*<sup>-/-</sup> CD4<sup>+</sup> T cells express higher levels of *Kcna3* transcripts<sup>69</sup>, we found no differences in *Kcna3* mRNA levels in purified *Crbn*<sup>+/+</sup> versus *Crbn*<sup>-/-</sup> CD8<sup>+</sup> T cells stimulated under suboptimal anti-CD3ε conditions, and minimal changes in *Kcna3* expression were observed following anti-CD3ε/anti-CD28-induced activation of either *Crbn*<sup>+/+</sup> or *Crbn*<sup>-/-</sup> CD8<sup>+</sup> T cells (**Figure 4I**, **Figure 5J**). Thus, other mechanisms likely account for the hyperproliferative phenotype of *Crbn*<sup>-/-</sup> CD8<sup>+</sup> T cells.

Given normal serum cytokines and a lack of evidence of spontaneous T cell activation in *Crbn*-deficient mice, we reasoned CRBN functions to harness responses provoked by TCR engagement. To test this notion, TCR signal strength, spontaneous activation, and persistence was evaluated in antigen-activated *Crbn*<sup>-/-</sup> CD8<sup>+</sup> T cells, which were generated by crossing *Crbn*<sup>-/-</sup> mice to ovalbumin (OVA) peptide TCR-transgenic-(Tg) mice (OT1) <sup>160</sup>. As expected, 96% of CD8<sup>+</sup> splenocytes from *Crbn*<sup>-/-</sup>;OT-1 mice displayed TCR reactivity to the H-2K<sup>b</sup> OVA tetramer (**Figure 5K**). Splenocytes were stimulated with the immunodominant high affinity SIINFEKL peptide (N4), as well as with a variant OVA peptide with intermediate affinity (SAINFEKL, A2) that provokes negative selection of immature T cells, or with a very low affinity OVA peptide (SIIGFEKL, G4) for the OT1 TCR <sup>161</sup>. OT1;*Crbn*<sup>-/-</sup> T cells displayed increased proliferation in response to increasing doses of N4 and A2 peptides compared to wild type OT1 T cells, but did not respond to the G4 peptide (**Figure 4J**) or to the OT1-irrelevant melanoma peptide antigen tyrosinase-related protein 2 (Trp2, SVDFFWL (**Figure 5L**)). Although OT1 and OT1;*Crbn*<sup>-/-</sup> T cells expressed comparable levels of CD69 in response to the N4 and A2 peptides immediately after activation, prolonged expression of CD69 (**Figure 4K**) independent of exogenous IL-2 (**Figure 5L**) was manifest in OT1;*Crbn*<sup>-/-</sup> T cells. Thus, CRBN controls the persistence of activated T cells after antigen stimulation, but does not lower the threshold of activation or confer responses to an irrelevant antigen.

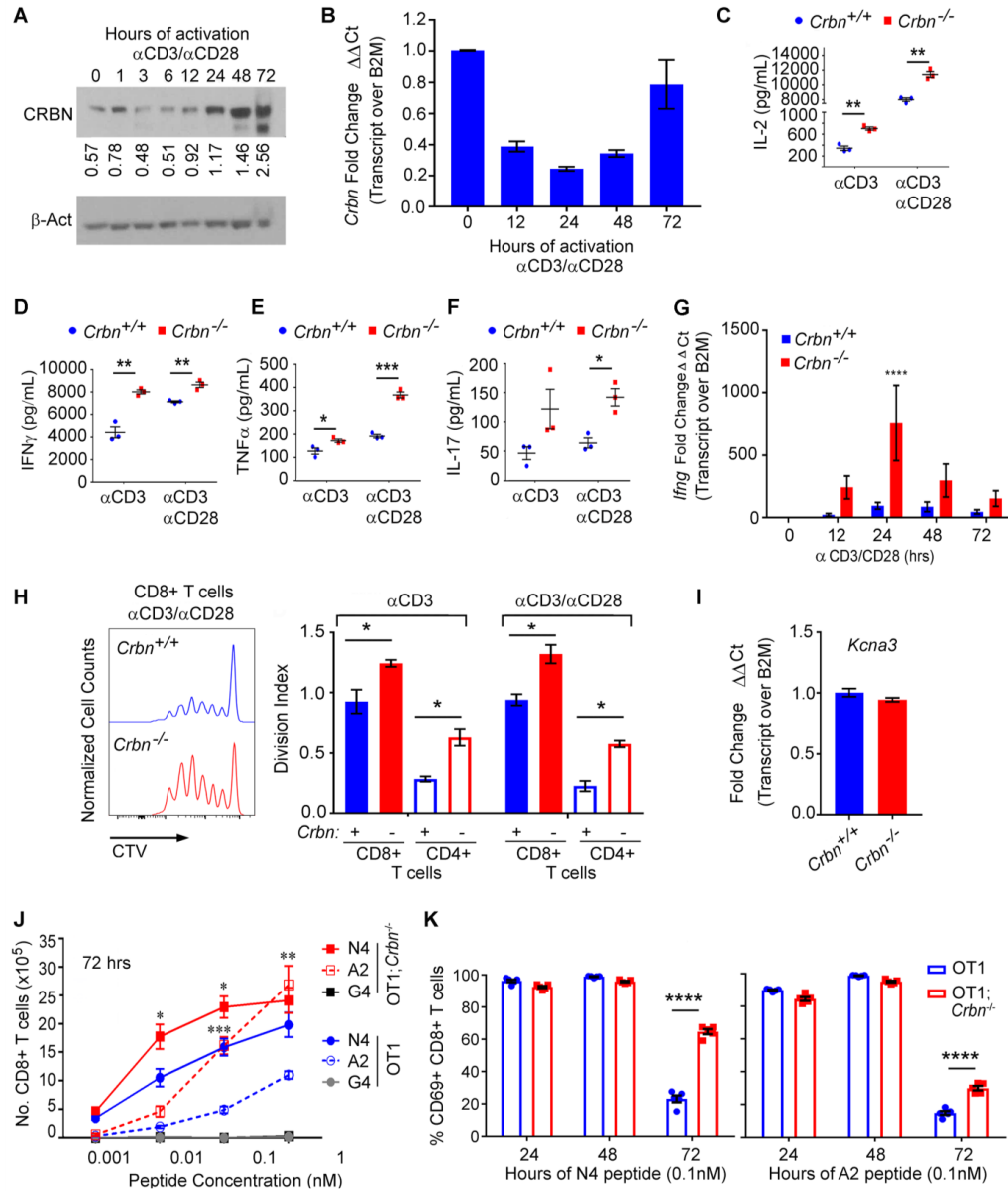


**Figure 4: Ablation of *Crbn* Augments T Cell Activation and Function.** CRBN protein (A) and mRNA (B) expression in 3  $\mu$ g/mL anti-CD3/anti-CD28 activated mouse CD3<sup>+</sup> T cells over time; densitometry calculations of CRBN normalized to  $\beta$ -actin are displayed below the lanes; (C-F) Production of IL-2 (C) IFN $\gamma$  (D) TNF $\alpha$  (E), and IL-17 (F) after 72 hr activation in *Crbn*<sup>+/+</sup> and *Crbn*<sup>-/-</sup> T cells following stimulation with anti-CD3 +/- anti-CD28; (G) Fold change in expression of *Ifng* relative to *B2M* in *Crbn*<sup>+/+</sup> and *Crbn*<sup>-/-</sup> T cells following stimulation with anti-CD3 +/- anti-CD28 for 12, 24, 48, and 72 hrs; (H) *Crbn*<sup>+/+</sup> and *Crbn*<sup>-/-</sup> CD8<sup>+</sup> T cell proliferation after 72 hr of anti-CD3 +/- anti-CD28 stimulation as measured by Cell Trace Violet (CTV) and quantified by division index (mean number divisions per cell); (I) *Kcna3* mRNA levels in purified CD8<sup>+</sup> T cells after activation with anti-CD3+anti-CD28; (J) Total number of OT1 and OT1;*Crbn*<sup>-/-</sup> T cells at 72 hr in response to SIINFEKL peptide (N4), S<sub>A</sub>INFEKL (A2), and SIIGFEKL (G4) as determined by cell counting with trypan blue dye and flow cytometry for percent viable CD8<sup>+</sup> T cells; (K) CD69 expression in OT1 and OT1;*Crbn*<sup>-/-</sup> T cells after 72 hr of culture with 0.1 nM N4 or A2 peptide. \*p<0.05, \*\*p<0.01, \*\*\*p<0.001, \*\*\*\*p<0.0001

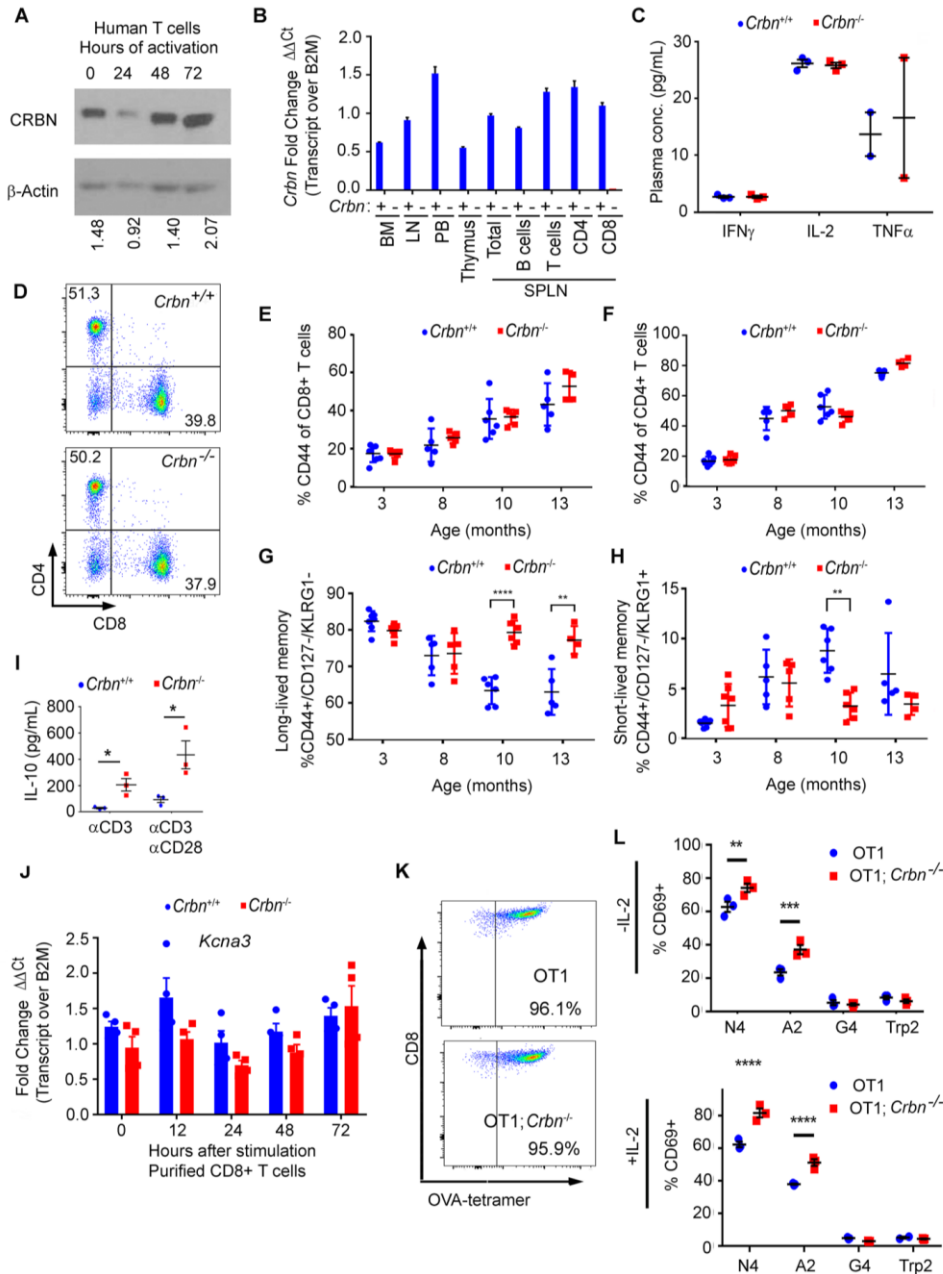


**Figure 5: Deletion of *Crbn* increases effector function and long-lived memory.** (A) Expression of CRBN protein in human T cells after activation with anti-CD3 $\epsilon$  + anti-CD28; (B) *Crbn* mRNA levels in the indicated immune tissues or in isolated B cells, T cells, CD4<sup>+</sup> T cells, CD8<sup>+</sup> T cells derived from spleen of *Crbn*<sup>+/+</sup> (+), *Crbn*<sup>-/-</sup> (-) mice, normalized to Tata binding protein (*Tbp*); (C) Levels of IFN $\gamma$ , IL-2 and TNF $\alpha$  in plasma of *Crbn*<sup>+/+</sup> and *Crbn*<sup>-/-</sup> mice; (D) Percent CD4<sup>+</sup> and CD8<sup>+</sup> T cells among total CD3<sup>+</sup> splenocytes in 3 month old *Crbn*<sup>+/+</sup> and *Crbn*<sup>-/-</sup> mice; (E-F) CD44 expression on (E) CD8 and (F) CD4 T cells in aging *Crbn*<sup>+/+</sup> and *Crbn*<sup>-/-</sup> mice. (G-H) Percent of cells defined in (E) CD127<sup>+</sup>KLRG1<sup>lo</sup> (G) and CD127<sup>+</sup>KLRG1<sup>hi</sup> (H) among CD44<sup>+</sup>CD8<sup>+</sup> T cells; (I) Secretion of IL-10 from plasma defined in Figure 1C-D, F-G; (J) *Kcna3* mRNA levels after activation with 3  $\mu$ g/ml plate-bound anti-CD3+anti-CD28; (K) OVA-reacting tetramer positive CD8<sup>+</sup> splenocytes from OT1 and OT1;*Crbn*<sup>-/-</sup> mice; (L) CD69 expression after 72 hr of OT1 and OT1;*Crbn*<sup>-/-</sup> splenocytes cultured with 0.1 nM of the indicated peptide with and without 10 ng/mL IL-2.

**Table 2: Distribution of Immune Cells in *Crbn*<sup>-/-</sup> Mice.**

Population name	<i>Crbn</i> <sup>+/+</sup>		<i>Crbn</i> <sup>-/-</sup>		P-value
	Mean (SD)	n	Mean (SD)	n	
<b>Thymic Populations</b>					
• CD4+ (SP)	16.5 (4.6)	11	14.7 (4.5)	9	0.39
• CD8+ (SP)	5.4 (2.6)	11	4.7 (2.3)	9	0.52
• CD4+/CD8+ (DP)	65.1 (14.2)	11	63.1 (13.7)	9	0.77
• CD4-/CD8- (DN)	13.0 (7.2)	11	14.6 (9.2)	9	0.69
• DN1	10.2 (2.5)	11	11.8 (3.0)	9	0.25
• DN2	7.9 (5.1)	11	6.3 (4.9)	9	0.51
• DN3	51.0 (12.9)	11	53.1 (13.4)	9	0.74
• DN4	31.0 (6.9)	11	28.9 (6.4)	9	0.51
<b>Splenic Lymphocytes</b>					
• B220+ CD3- B cell	32.8 (8.5)	11	33.5 (16.5)	11	0.90
• B220- CD3+ T cells	45.9 (6.7)	11	36.4 (7.1)	11	<b>0.004</b>
• B220-CD3-NK1.1+ NK cells	18.8 (6.2)	11	19.4 (10.9)	11	0.87
• CD3+CD8+ T cells	25.7 (5.1)	11	29.7 (8.9)	11	0.21
• CD3+CD4+ T cells	62.3 (15.8)	11	65.4 (10.2)	11	0.58
• CD3+CD4+CD25+Foxp3+ T reg cells	9.7 (0.7)	3	10.8 (4.9)	3	0.71
• CD3+CD4+CD69+ T cells	6.0 (1.7)	11	5.1 (0.9)	11	0.17
• CD3+CD8+CD69+ T cells	4.6 (0.8)	11	3.8 (1.0)	11	<b>0.06</b>
• CD3+CD4+CD25+ T cells	4.2 (0.7)	11	4.7 (0.9)	11	0.09
• CD3+CD8+CD25+ T cells	0.5 (0.6)	11	0.7 (0.8)	11	0.55
<b>Lymph Node Lymphocytes</b>					
• B220- CD3+ T cells	77.9 (6.9)	11	77.4 (6.9)	11	0.85
• B220-CD3-NK1.1+ NK cells	22.8 (18.1)	11	27.7 (15.8)	11	0.50
• CD3+CD8+ T cells	32.8 (10.5)	11	36.0 (11.8)	11	0.51
• CD3+CD4+ T cells	65.7 (10.2)	11	62.3 (11.6)	11	0.47
• CD3+CD4+CD25+Foxp3+ Treg cells (n=3)	10.5 (0.8)	11	10.3 (0.7)	3	0.72
• CD3+CD4+CD69+ T cells	6.6 (0.8)	11	6.9 (0.7)	11	0.35
• CD3+CD8+CD69+ T cells	4.6 (0.9)	11	5.0 (1.0)	11	0.41
• CD3+CD4+CD25+ T cells	4.0 (1.0)	11	4.8 (1.2)	11	0.11
• CD3+CD8+CD25+ T cells	0.5 (0.5)	11	0.5 (0.3)	11	0.93
<b>Splenic Memory Populations</b>					
CD3+CD4+CD44-CD127-KLRG1- T cells	70.8 (4.0)	7	69.4 (5.1)	7	0.56
CD3+CD4+CD44+CD127-KLRG1- T cells	11.4 (2.3)	7	11.0 (1.4)	7	0.72
CD3+CD4+CD44+CD127-KLRG1+ T cells	0.2 (0.1)	7	0.2 (0.1)	7	0.23
CD3+CD8+CD44-CD127-KLRG1- T cells	74.8 (3.2)	7	75.6 (2.9)	7	0.63
CD3+CD8+CD44+CD127-KLRG1- T cells	14.4 (3.9)	7	13.9 (1.6)	7	0.73
CD3+CD8+CD44+CD127-KLRG1+ T cells	0.3 (0.1)	7	0.6 (0.4)	7	0.08

### CRBN Controls the Bioenergetics of Activated T cells

To assess if the hyperactivated state of *Crbn*<sup>-/-</sup> T cells was associated with changes in the expression of the IMiD targets Ikaros, CK1 $\alpha$  or IRF-4<sup>52,57,64,162</sup>, western blot analyses of activated *Crbn*<sup>+/+</sup> and *Crbn*<sup>-/-</sup> T cells was performed. While IRF-4 was robustly induced following anti-CD3 $\epsilon$ /anti-CD28 stimulation, the expression of Ikaros, CK1 $\alpha$  or IRF-4 was not dependent on *Crbn* status (**Figure 6A**). To gain additional insights into the hyperactivated state manifest in .



*Crbn*<sup>-/-</sup> T cells, expression profiling of naïve versus anti-CD3ε/anti-CD28-activated *Crbn*<sup>+/+</sup> and *Crbn*<sup>-/-</sup> T cells was performed. These analyses revealed activated *Crbn*<sup>-/-</sup> T cells expressed 816 unique genes versus activated *Crbn*<sup>+/+</sup> T cells (**Figure 6B-D**); in contrast, nominal changes in gene expression were observed in naïve *Crbn*<sup>-/-</sup> and *Crbn*<sup>+/+</sup> T cells (**Figure 6B**). Gene set enrichment analysis (GSEA) of genes uniquely changed in activated *Crbn*<sup>-/-</sup> T cells revealed that unique transcripts were highly enriched in metabolic and mitochondrial processes (**Figure 7A**). In accord with these findings, activated *Crbn*<sup>-/-</sup> CD8<sup>+</sup> T cells had higher basal rates of glycolysis and respiration than activated *Crbn*<sup>+/+</sup> CD8<sup>+</sup> T cells, based on their extracellular acidification rates (ECAR) and O<sub>2</sub> consumption rates (OCR) (**Figure 7B-C, E-F**). Finally, the overall reduction in OCR observed following oligomycin treatment indicates mitochondrial ATP production is elevated in *Crbn*<sup>-/-</sup> CD8<sup>+</sup> T cells in comparison to *Crbn*<sup>+/+</sup> CD8<sup>+</sup> T cells (**Figure 7E**).

Costimulation with CD28 or other costimulatory molecules is normally required to induce changes in T cell metabolism, and this prevents anergy<sup>163</sup>. However, increases in basal ECAR and OCR were also evident in polyclonal *Crbn*<sup>-/-</sup> CD8<sup>+</sup> T cells stimulated with anti-CD3ε alone (**Figure 7C, F**). Further, increases in bioenergetics were manifest in polyclonal *Crbn*<sup>-/-</sup> CD8<sup>+</sup> T cells activated with anti-CD3ε/anti-CD28 (**Figure 7C, F**) and in OT1;*Crbn*<sup>-/-</sup> CD8<sup>+</sup> T cells stimulated with high-affinity peptides versus *Crbn*<sup>+/+</sup> CD8<sup>+</sup> T cells (**Figure 7D, G**). Moreover, activated CD8<sup>+</sup> *Crbn*<sup>-/-</sup> T cells display significant increases in glucose uptake (evident by uptake of the fluorescent glucose analog 2-NBDG, **Figure 7H-I**), marked increases in hexokinase (HK) activity (**Figure 7J**) and a higher NAD<sup>+</sup>/NADH ratio (**Figure 7K**), which is consistent with robust respiration and glycolytic rates<sup>164</sup>. Intracellular ATP levels were, however, comparable in *Crbn*<sup>-/-</sup> and *Crbn*<sup>+/+</sup> T cells suggesting that increased generation and utilization of ATP is proportional in *Crbn*<sup>-/-</sup> CD8<sup>+</sup> T cells (**Figure 7L**). Finally, co-treatment with 2-deoxyglucose (2-DG, which blocks glycolysis) or oligomycin (which suppresses mitochondrial ATPase) abolished or impaired the proliferative advantage of activated *Crbn*<sup>-/-</sup> T cells (**Figure 7M-N**), respectively. Thus, glycolysis

is required for the robust metabolic phenotype of *Crbn*<sup>-/-</sup> CD8<sup>+</sup> T cells and increased OXPHOS also contributes to their superior proliferative response.

In addition to increases in basal levels of OXPHOS (**Figure 7E-G**), there was a trend toward higher spare respiratory capacity (SRC) in anti-CD3 $\epsilon$ /anti-CD28 stimulated *Crbn*<sup>-/-</sup> T cells (**Figure 7E, 6E**). SRC is important for memory T cell (T<sub>M</sub>) differentiation and mitochondrial remodeling appears to instruct T cell metabolic programming, where T<sub>M</sub> manifest fused mitochondria<sup>28</sup>. Mitochondrial biomass, as assessed by MitoTracker Green staining, was not significantly increased in activated *Crbn*<sup>-/-</sup> CD8<sup>+</sup> T cells (**Figure 6F**). By electron microscopy some changes in mitochondria were evident in activated *Crbn*<sup>-/-</sup> CD8<sup>+</sup> T cells, where there were significant increases in the number of mitochondria (**Figure 6G-H**) during T cell activation. However, there were no significant increases in mitochondrial length (**Figure 6I**), or in total intracellular or mitochondrial ROS (**Figure 6J**), which could reflect increases in glutathione metabolism manifest in activated *Crbn*<sup>-/-</sup> CD8<sup>+</sup> T cells (see below, **Figure 8B**). In contrast, *Crbn* deficiency was associated with the expression of classic markers of effector CD8<sup>+</sup> T cells (T<sub>E</sub>), where there were significant increases in the levels of mRNAs encoding Tbet (T-box 21, *Tbx21*), *Eomes*, granzyme B (*Gzmb*), and perforin (*Prf1*) after activation (**Figure 7O-R**). Thus, *Crbn* deficiency promotes differentiation towards a hyperactive effector CD8<sup>+</sup> T cell fate following TCR stimulation.

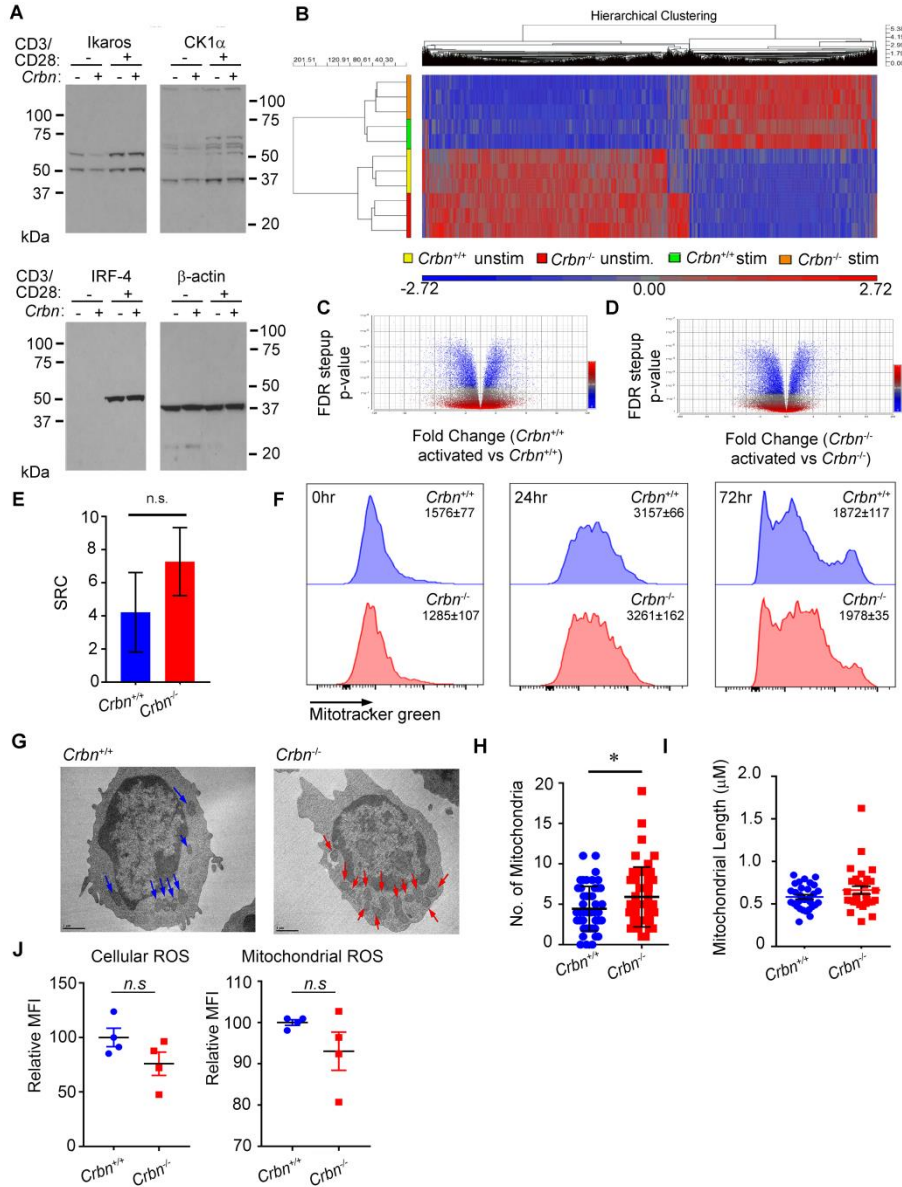


**Figure 6: Deletion of Cereblon does not significantly alter targets of IMiDs or mitochondria** (A) Immunoblot for proteins that have been described as targets of CRBN in the context of IMiD compound treatment. *Crbn*<sup>+/+</sup> and *Crbn*<sup>-/-</sup> T cells were activated with 5  $\mu$ g/mL anti-CD3 $\epsilon$  and 1  $\mu$ g/mL anti-CD28 or were left unstimulated; (B) Unsupervised clustering of transcripts from unactivated (naïve) and 12 hr anti-CD3 $\epsilon$ /anti-CD28 activated *Crbn*<sup>+/+</sup> and *Crbn*<sup>-/-</sup> purified T cells (naïve *Crbn*<sup>+/+</sup>, *n*=3; naïve *Crbn*<sup>-/-</sup>, *n*=2; activated *Crbn*<sup>+/+</sup>, *n*=3; and activated *Crbn*<sup>-/-</sup>, *n*=3); (C-D) Volcano plots showing activation-induced mRNA fold change unique to *Crbn*<sup>+/+</sup> T cells (C) and *Crbn*<sup>-/-</sup> T cells (D); (E) Spare respiratory capacity (SRC) of 24 hr activated *Crbn*<sup>+/+</sup> and *Crbn*<sup>-/-</sup> CD8<sup>+</sup> T cells, calculated from Figure 6E; (F) Mitotracker Green staining of naïve and 24- and 72-hr activated *Crbn*<sup>+/+</sup> and *Crbn*<sup>-/-</sup> CD8<sup>+</sup> T cells; representative of 3 independent experiments; (G-I) Transmission electron microscopy of *Crbn*<sup>+/+</sup> and *Crbn*<sup>-/-</sup> CD8<sup>+</sup> T cells 24 hr after activation; (H) Number of mitochondria; (I) average mitochondrial length; (J) Intracellular ROS and mitochondrial ROS levels in *Crbn*<sup>+/+</sup> and *Crbn*<sup>-/-</sup> CD8<sup>+</sup> T cells after 24 hr of activation. \**p*<0.05, \*\**p*<0.01, \*\*\**p*<0.001, \*\*\*\**p*<0.0001

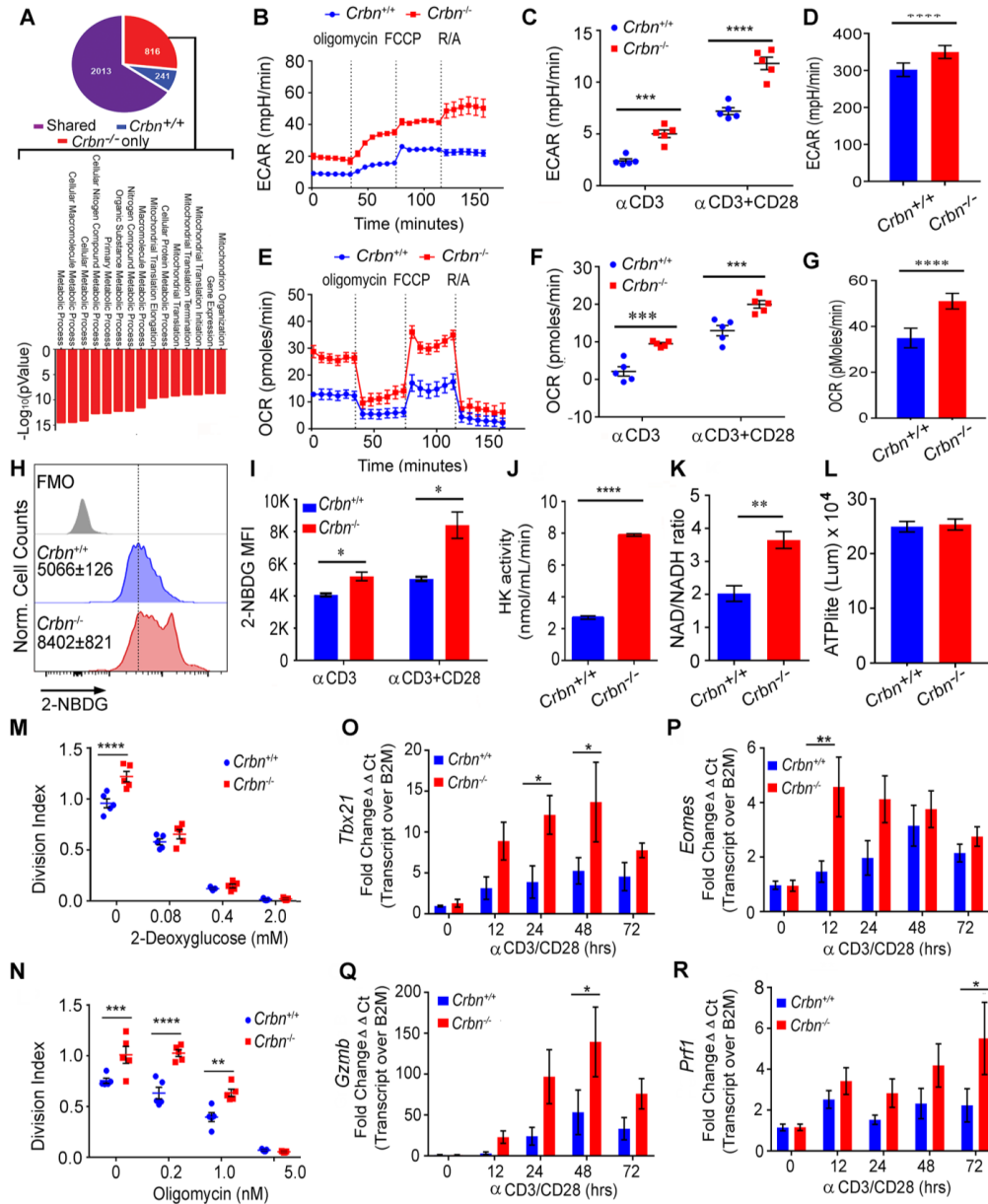


**Figure 7: Cereblon Loss Augments Energetics of Activated T cells.** (A) Transcriptional changes after anti-CD3 and anti-CD28 stimulation of *Crbn*<sup>+/+</sup> T cells, *Crbn*<sup>-/-</sup> T cells, or both (Shared), and analysis of those pathways that only change in *Crbn*<sup>-/-</sup> T cells; (B-D) Extracellular acidification rates of activated *Crbn*<sup>+/+</sup> and *Crbn*<sup>-/-</sup> CD8<sup>+</sup> T cells (B-C) or N4 peptide-stimulated OT1 versus OT1;*Crbn*<sup>-/-</sup> (D); (E-G) Oxygen consumption rates of activated *Crbn*<sup>+/+</sup> and *Crbn*<sup>-/-</sup> CD8<sup>+</sup> T cells (E-F) or N4 peptide-stimulated OT1 versus OT1;*Crbn*<sup>-/-</sup> (G); (H-I) Glucose uptake of activated *Crbn*<sup>+/+</sup> and *Crbn*<sup>-/-</sup> CD8<sup>+</sup> T cells with anti-CD3 +/- anti-CD28 as measured by the fluorescent glucose analog, 2-NBDG mean fluorescent intensity (MFI); (J) Hexokinase activity of activated *Crbn*<sup>+/+</sup> and *Crbn*<sup>-/-</sup> CD8<sup>+</sup> T cells; (K) NAD<sup>+</sup>/NADH ratio of activated *Crbn*<sup>+/+</sup> and *Crbn*<sup>-/-</sup> CD8<sup>+</sup> T cells; (L) ATP production of activated *Crbn*<sup>+/+</sup> and *Crbn*<sup>-/-</sup> CD8<sup>+</sup> T cells; (M-N) *Crbn*<sup>+/+</sup> and *Crbn*<sup>-/-</sup> CD8<sup>+</sup> T cell proliferation after 72 hr of anti-CD3 + anti-CD28 stimulation with 2-DG (K) or oligomycin (L) treatment; (O-R) *Crbn*<sup>+/+</sup> and *Crbn*<sup>-/-</sup> CD8<sup>+</sup> T cell qRT-PCR analysis of Tbet (*Tbx21*) (O), *Eomes* (P), Granzyme B (*Gzmb*) (Q) and Perforin (*Prf1*) (R) mRNA levels at times indicated after activation with anti-CD3 and anti-CD28. \*p<0.05, \*\*p<0.01, \*\*\*p<0.001, \*\*\*\*p<0.0001

## **Crbn Harnesses Arginine and Glutamine Metabolism and Controls the Expression of Myc in Activated CD8<sup>+</sup> T cells**

To assess mechanisms that account for the superior metabolic phenotype of *Crbn*<sup>-/-</sup> CD8<sup>+</sup> T cells, global metabolomic profiling was performed by liquid chromatography-mass spectrometry in positive and negative ionization modes. MZmine (freeware) was used to identify and align features, and gap filling was performed to fill in features missed in the first alignment. Identified features of *Crbn*<sup>+/+</sup> and *Crbn*<sup>-/-</sup> CD8<sup>+</sup> T cells were then defined by principal component analysis (PCA) and those with a 2-fold or greater change and p-values  $\leq 0.1$  were analyzed for pathway over-representation (**Figure 8A-C**). Pathway enrichment analysis of differentially expressed metabolites revealed a highly significant involvement of the “Arginine/Proline” pathway (**Figure 8A-B**, FDR 0.006,  $-\log(p)$  9.47). A heatmap of these differentially expressed metabolites revealed anti-CD3 $\epsilon$ /anti-CD28 activated *Crbn*<sup>-/-</sup> CD8<sup>+</sup> T cells have increased utilization of glutamine, arginine and ornithine and that these cells accumulate high levels of downstream metabolites, including proline and the polyamines putrescine, spermidine and spermine (**Figure 9A-C**).

Both L-arginine (L-Arg) and L-glutamine (L-Gln) can serve as the carbon and nitrogen units for polyamine biosynthesis<sup>165</sup>. *Slc7a1* encoding the L-Arg transporter CAT-1<sup>166</sup>, and the *Slc38a1* (SNAT1) and *Slc38a2* (SNAT2) glutamine transporters<sup>167</sup>, are required to sustain glutaminolysis in T cells<sup>13</sup>. Notably, activated *Crbn*<sup>-/-</sup> CD8<sup>+</sup> T cells express elevated levels of all three of these transporters (**Figure 8D-F, 9B**). Moreover, elevated expression of mRNAs encoding enzymes that catabolize ornithine or direct polyamine biosynthesis, specifically *Odc1*, *Oat*, *Srm* and *Sms*, confirmed that this pathway is amplified in activated *Crbn*<sup>-/-</sup> versus *Crbn*<sup>+/+</sup> CD8<sup>+</sup> T cells (**Figure 8G-J, 9B**). Further, uptake studies of U-<sup>14</sup>C-labeled L-Arg and L-Gln confirmed transport of both amino acids is enhanced in activated *Crbn*<sup>-/-</sup> CD8<sup>+</sup> T cells (**Figure 9D-E**) and targeted LC-MS/MS analyses established activated *Crbn*<sup>-/-</sup> T cells have supra-physiological intracellular levels of putrescine, spermidine and spermine (**Figure 9F-H**). Finally,

the hyper-proliferative state of activated *Crbn*<sup>-/-</sup> CD8<sup>+</sup> T cells required increases in polyamines, as this was abolished by treatment with alpha-difluoromethylornithine (DFMO), an irreversible inhibitor of ODC<sup>168</sup> (**Figure 9I**).

Myc is a master regulator of metabolic transcription programs<sup>169</sup>, and in particular coordinately regulates polyamine metabolism<sup>170</sup> through the transcriptional regulation of *Odc1* (**Figure 9B**). Further, in activated T cells Myc control includes the induction of transporters and enzymes that direct glutamine catabolism and flux into polyamines<sup>13,165,170</sup>. Given the metabolic phenotypes and augmented glutamine flux into polyamines in activated *Crbn*<sup>-/-</sup> CD8<sup>+</sup> T cells, we subjected differentially expressed genes (**Figure 7A**) to GSEA for transcriptional drivers linked to differentially-expressed transcripts. These analyses revealed highly significant pathway enrichment in Myc, Max and Myc/Max-regulated genes (**Figure 8K-M**), suggesting metabolic and gene expression changes in activated *Crbn*<sup>-/-</sup> T cells are Myc driven. Consistent with this hypothesis, there were significant increases and sustained levels of MYC protein in CD3<sup>+</sup> *Crbn*<sup>-/-</sup> versus CD3<sup>+</sup> *Crbn*<sup>+/+</sup> T cells, and of *Myc* mRNA in activated *Crbn*<sup>-/-</sup> versus *Crbn*<sup>+/+</sup> CD8<sup>+</sup> T cells (**Figure 9J** and **9K**, respectively). Finally, the kinetics of the induction of *Myc* mRNA following CD8<sup>+</sup> T cell activation paralleled the suppression of *Crbn* transcripts (**Figure 8N**), and supporting the notion that CRBN normally harnesses MYC expression, and MYC-driven phenotypes, in antigen-activated T cells.

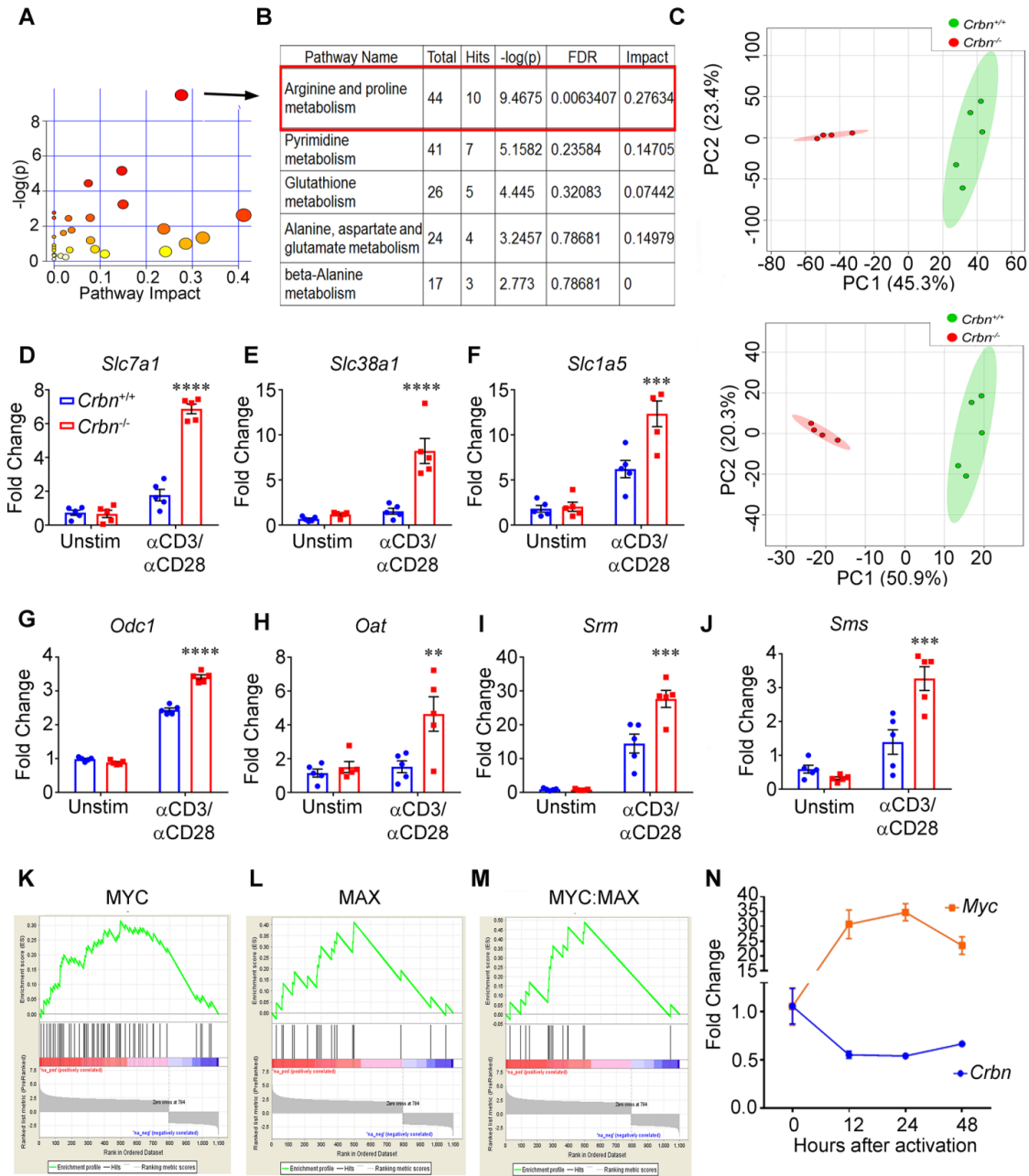


**Figure 8: Activation of *Crbn*<sup>-/-</sup> T cells increases Myc-metabolism pathways.** (A-C) Metabolomics analysis of *Crbn*<sup>+/+</sup> and *Crbn*<sup>-/-</sup> CD8<sup>+</sup> T cells 24 hr after activation; (A-B) Pathway analysis of metabolite abundance; (C) Principle component analysis of metabolites measured in positive mode (*top*) and negative mode (*bottom*); (D-J) qRT-PCR analysis of the expression of the indicated amino acid transporters and enzymes relevant to glutamine, arginine and polyamine metabolism in *Crbn*<sup>+/+</sup> and *Crbn*<sup>-/-</sup> T cells without activation or following 24 hr stimulation with anti-CD3ε and anti-CD28; representative of 2-3 independent experiments; (K-M) Transcription factor drivers found by GSEA of the changes in activated *Crbn*<sup>-/-</sup> T cells shown in Figure 7A; (N) *Myc* and *Crbn* mRNA levels were determined in parallel at the indicated intervals in wild type CD8<sup>+</sup> T cells stimulated with anti-CD3ε and anti-CD28. \*\*p<0.01, \*\*\*p<0.001, \*\*\*\*p<0.0001



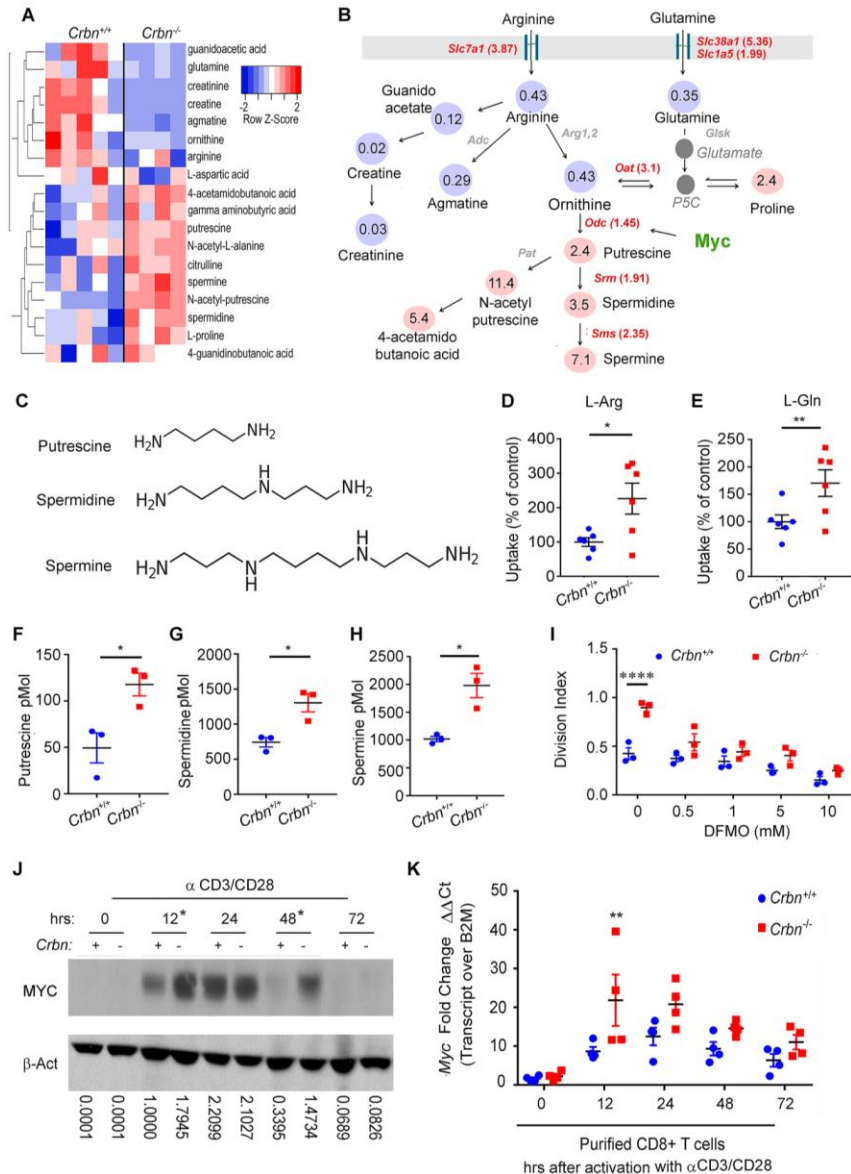


**Figure 9: Crbn Harnesses Arginine and Glutamine Metabolism and Controls the Expression of Myc in Activated CD8<sup>+</sup> T cells.** (A-B) Metabolomic analysis of 24hr-activated *Crbn*<sup>+/+</sup> and *Crbn*<sup>-/-</sup> CD8<sup>+</sup> T cells by LC-MS/MS. (A) Heat map of metabolites that are significantly different and (B) average fold change in the arginine, glutamine, and proline metabolites; blue indicates downregulated metabolites in the pathway, pink denotes increased metabolites in the pathway. mRNA expression for enzymes and transporters for each reaction are shown with fold change indicated. All enzymes and transporters were upregulated by the fold indicated in *Crbn*<sup>-/-</sup> CD8<sup>+</sup> T cells; (C) Structure of the polyamines putrescine, spermidine and spermine; (D-E) Uptake of L-Arginine and L-Glutamine by *Crbn*<sup>+/+</sup> and *Crbn*<sup>-/-</sup> CD8<sup>+</sup> T cells after 24 hr of anti-CD3 and anti-CD28 activation; (F-H) Intracellular putrescine, spermidine and spermine levels measured by LC-MS/MS of activated *Crbn*<sup>+/+</sup> and *Crbn*<sup>-/-</sup> CD8<sup>+</sup> T cells; (I) *Crbn*<sup>+/+</sup> and *Crbn*<sup>-/-</sup> CD8<sup>+</sup> T cell proliferation after 72 hr of anti-CD3 + anti-CD28 stimulation with DFMO treatment; (J) MYC protein levels in activated *Crbn*<sup>+/+</sup> and *Crbn*<sup>-/-</sup> T cells (denoted + and -) were determined by Western blot analysis at the indicated intervals following stimulation with anti-CD3 + anti-CD28; (K) *Myc* mRNA levels in *Crbn*<sup>+/+</sup> and *Crbn*<sup>-/-</sup> CD8<sup>+</sup> T cells following activation by anti-CD3+anti-CD28 for the number of hours indicated. \*p<0.05, \*\*p<0.01, \*\*\*\*p<0.0001



### **Crbn-Myc Circuit Controls CD8<sup>+</sup> T cell Metabolism**

Consistent with the findings of increased Myc expression, other Myc-driven responses, including increases in cell size<sup>13,14</sup> and in the expression of the Myc target CD98<sup>171</sup>, were also manifest in activated *Crbn*<sup>-/-</sup> CD8<sup>+</sup> T cells (**Figure 10A-C**). A series of inhibitors have been identified that block Myc:Max heterodimerization with excellent selectivity and potency (**Figure 10D-E**). Co-treatment of activated CD8<sup>+</sup> T cells with 10074-G5, an inhibitor of Myc:Max dimerization<sup>172</sup>, suppressed the expression of the Myc transcription target *Odc1*. Additional Myc:Max dimerization disruptors, MYCMI-11 and MYCMI-6<sup>173</sup>, were tested in independent assays. MYCMI-11 was obtained from the National Institutes of Health, and the synthesis of MYCMI-6 was derived internally based on previously published structures as detailed in supplemental methods<sup>173</sup>. As expected, disruption of the Myc-Max bHLHZip interaction by these drugs blocked the expression of *Odc1* in *Crbn*<sup>-/-</sup> T cells (**Figure 10F**). Interestingly, the effector gene signature of *Crbn*<sup>-/-</sup> T cells, including *Tbx21*, *EOMES*, *Gzmb* and *Ifng*, was also decreased in a dose-dependent manner with co-treatment of 10074-G5 (**Figure 10G**) or by co-treatment with MYCMI11 or MYCMI6 (**Figure 10H**). Thus, the metabolic and T<sub>E</sub> signature of activated *Crbn*<sup>-/-</sup> CD8<sup>+</sup>T cells is Myc dependent.

IMiD-directed proteasomal degradation of Ikaros and Aiolos in multiple myeloma or lymphoma cells has been linked to subsequent suppression of Myc, and this appears to contribute to tumor cell death<sup>59,174</sup>. Treatment of human CD8<sup>+</sup> T cells with the potent IMiD CC-122 (avadomide) significantly increased IFN $\gamma$  secretion especially in cells stimulated with low levels of anti-CD3 $\epsilon$  and anti-CD28 (**Figure 11A**). To test if a CRBN-MYC circuit was also manifest in human T cells, activated human CD4<sup>+</sup> and CD8<sup>+</sup> T cells from healthy donors were treated with the IMiD compounds lenalidomide, pomalidomide and CC-122. Notably, MYC protein levels, as measured by mean fluorescence intensity (MFI) (**Figure 11B**), were increased by treatment with all three IMiDs, and this effect was more profound in activated CD8<sup>+</sup> versus CD4<sup>+</sup> T cells. Further, CD98 expression, uptake of the glucose analog 2-NBDG, OCR, ECAR

and cell size were also augmented in activated human CD8<sup>+</sup> T cells by treatment with IMiDs (**Figure 11C-G, 12A-C, Table 3**). Finally, effects of IMiD treatment on 2-NDBG uptake and cell size were effectively blocked by co-treatment of activated human CD8<sup>+</sup> T cells with the Myc/Max inhibitor 10074-G5 (**Figure 11F-5G, Table 3**). Thus, IMiD compound modulation of CRBN function also drives a superior MYC-dependent metabolic circuit in activated human CD8<sup>+</sup> T cells.

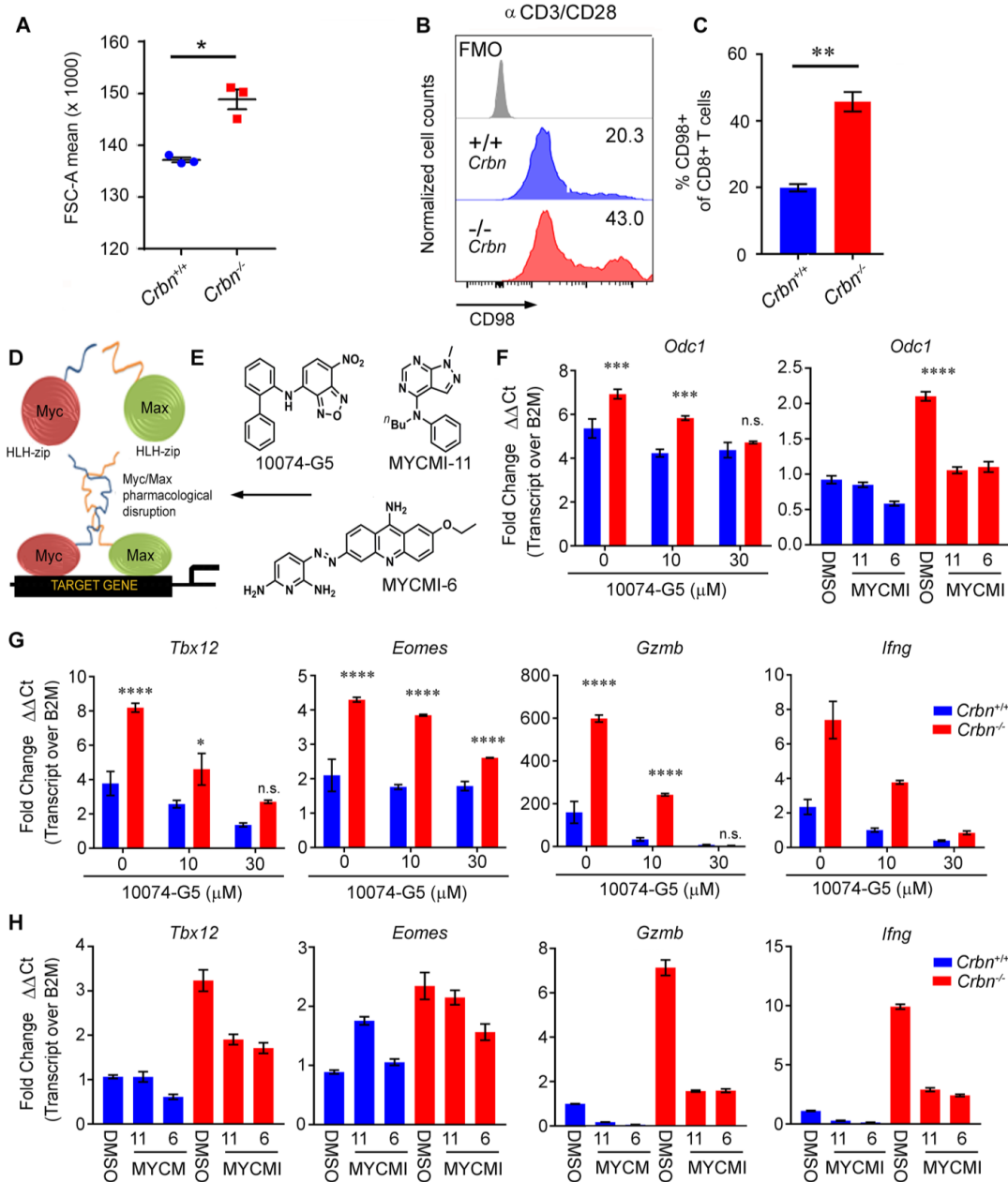


**Figure 10: The Phenotypes of Activated *Crbn*<sup>-/-</sup> CD8<sup>+</sup> T cells Are Myc Dependent.** (A) Cell size (Forward scatter cell-area mean x 1000) of *Crbn*<sup>+/+</sup> and *Crbn*<sup>-/-</sup> CD8<sup>+</sup> T cells after anti-CD3 and anti-CD28 stimulation (72 hr); (B-C) Flow histograms for expression of CD98 in *Crbn*<sup>+/+</sup> and *Crbn*<sup>-/-</sup> CD8<sup>+</sup> T cells after anti-CD3 and anti-CD28 stimulation for 24 hr; (D) Mechanism of Myc/Max disruptors; (E) Chemical structures of Myc inhibitors used for analyses; (F-G) mRNA levels of (F) *Odc1* and (G) *Tbet* (*Tbx21*), *EOMES*, *Granzyme B* (*Gzmb*), and *Ifng* in *Crbn*<sup>+/+</sup> and *Crbn*<sup>-/-</sup> CD8<sup>+</sup> T cells after anti-CD3 + anti-CD28 activation for 24 hr with the indicated doses of 10074-G5; (H) mRNA levels of *Tbet* (*Tbx21*), *EOMES*, *Granzyme B* (*Gzmb*), and *Ifng* in *Crbn*<sup>+/+</sup> and *Crbn*<sup>-/-</sup> CD8<sup>+</sup> T cells after anti-CD3 + anti-CD28 activation for 24 hr with 30μM MYCMI-11 or MYCI-6. \*p<0.05, \*\*p<0.01, \*\*\*\*p<0.0001

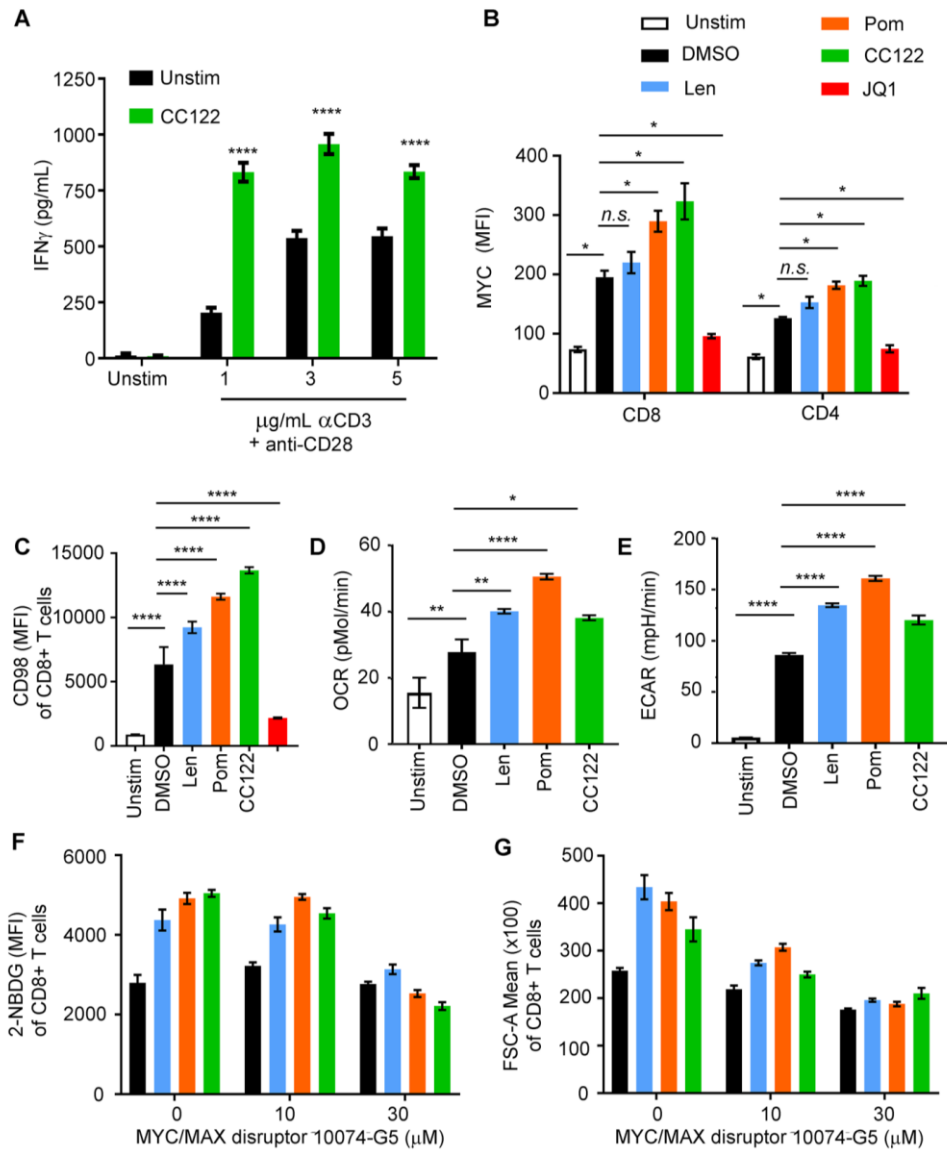


**Figure 11: Modulation of CRBN by IMiD Compounds Augments Human CD8<sup>+</sup> T Cell Bioenergetics and MYC Expression.** (A) Secretion of IFN $\gamma$  in unstimulated (unstim) and CC122 treated cells stimulated with increasing doses of anti-CD3 (1,3,and 5)  $\mu$ g/mL plus constant levels of anti-CD28 for 72 hr; (B) MYC protein levels in unstimulated and anti-CD3 + anti-CD28 activated human CD8<sup>+</sup> T cells treated with IMiD compounds for 5 days as detected by flow cytometry. IMiDs were tested at 10  $\mu$ M and include lenalidomide (Len), Pomalidomide (Pom), avadomide (CC122); (C) CD98 surface expression in activated human CD8<sup>+</sup> T cells treated with IMiD compounds for 5 days; (D-E) O<sub>2</sub> consumption rates (OCR) and extracellular acidification rate (ECAR) after drug treatment; (F-G) Glucose uptake (F) and cell size (G) of activated (treated with anti-CD3 + anti-CD28) human CD8<sup>+</sup> T cells treated with IMiDs +/- the MYC/MAX dimerization inhibitor 10074-G4, as measured by the fluorescent glucose analog 2-NBDG (mean fluorescent intensity, MFI) (F) and FSC-A (G). For statistical comparisons see Table 2. \* $p < 0.05$ , \*\* $p < 0.01$ , \*\*\* $p < 0.001$ , \*\*\*\* $p < 0.0001$

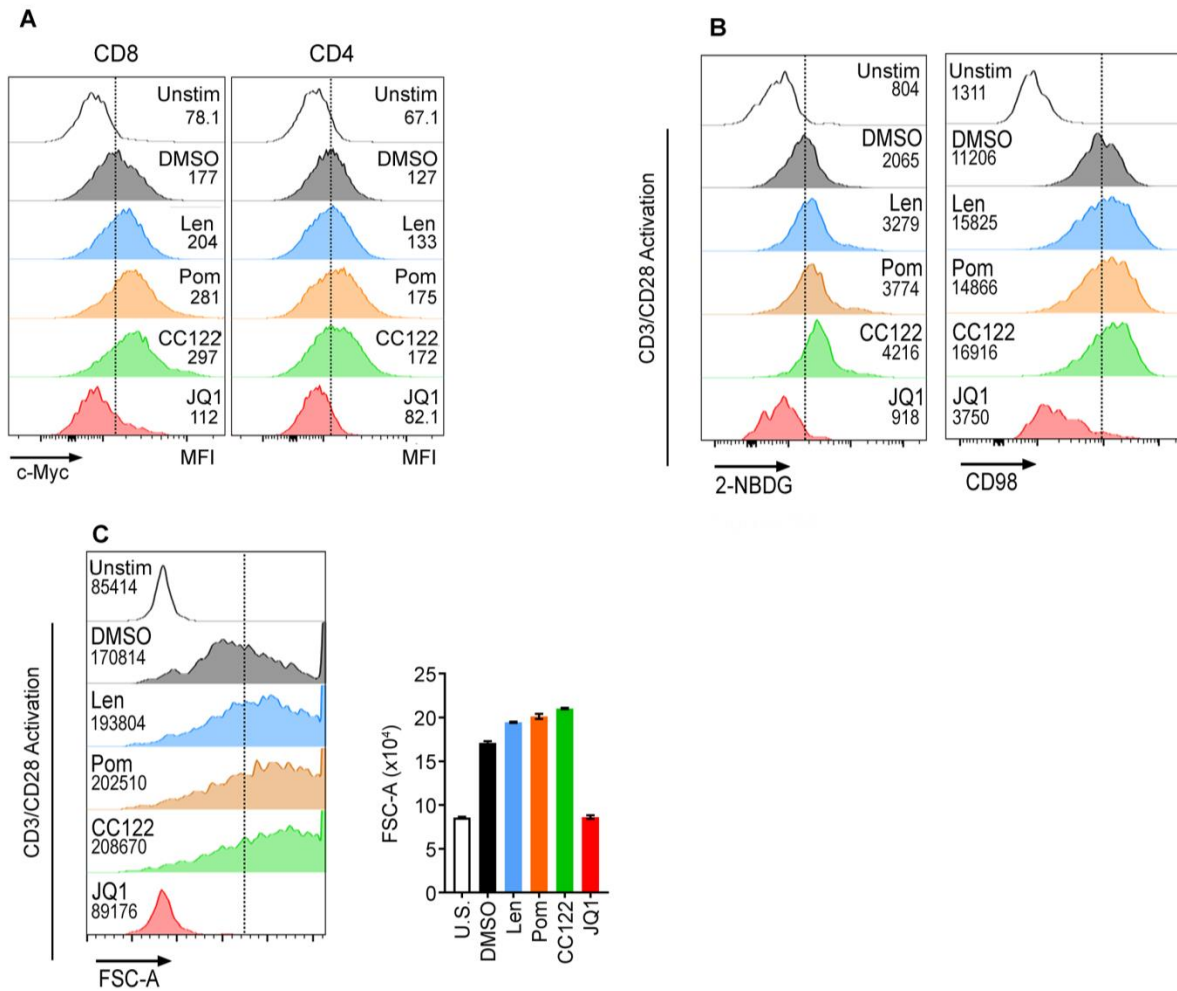


**Figure 12: Myc, 2-NBDG, CD98 and cell size of IMiD-treated activated human CD8<sup>+</sup> T cells.** (A-C) Glucose uptake, represented by 2-NBDG levels (A), CD98 expression (B), and cell size (C) as measured by forward scatter area (FSC-A), of human CD8<sup>+</sup> T cells activated for 5 days with anti-CD3 and anti-CD28 and treated with the indicated IMiD compounds or the JQ1 inhibitor (as a control, as JQ1 blocks *MYC* transcription). Data shown are representative of 2-3 healthy donors; numbers indicate MFI of peak shown in histograms.

**Table 3: Statistical comparisons in reference to Figure 11**

Function	Population	Comparison	Sample size	P-value	Summary
Myc (MFI)	CD8 <sup>+</sup> T-cells	Unstimulated vs stimulated (DMSO)	3	0.0150	*
		DMSO vs Len	3	0.1874	n.s.
		DMSO vs Pom	3	0.0156	*
		DMSO vs CC122	3	0.0286	*
		DMSO vs JQ1 (for antibody staining specificity)	3	0.0301	*
	CD4 <sup>+</sup> T-cells	Unstimulated vs stimulated (DMSO)	3	0.0241	*
		DMSO vs Len	3	0.1974	n.s.
		DMSO vs Pom	3	0.0241	*
		DMSO vs CC122	3	0.0563	*
		DMSO vs JQ1 (for antibody staining specificity)	3	0.0450	*
CD98 (MFI)	CD8 <sup>+</sup> T-cells	Unstimulated vs stimulated (DMSO)	5 technical	0.0001	****
		DMSO vs Len	5 technical	0.0001	****
		DMSO vs Pom	5 technical	0.0001	****
		DMSO vs CC122	5 technical	0.0001	****
		DMSO vs JQ1 (control for pathway specificity)	5 technical	0.0001	****
Basal OCR (pMol/min)	CD8 <sup>+</sup> T-cells	Unstimulated vs stimulated (DMSO)	6 technical	0.0091	**
		DMSO vs Len	6 technical	0.0036	**
		DMSO vs Pom	6 technical	0.0001	****
		DMSO vs CC122	6 technical	0.0153	*
Basal ECAR (mpH//min)	CD8 <sup>+</sup> T-cells	Unstimulated vs stimulated (DMSO)	6 technical	0.0001	****
		DMSO vs Len	6 technical	0.0001	****
		DMSO vs Pom	6 technical	0.0001	****
		DMSO vs CC122	6 technical	0.0001	****
Glucose uptake (2-NBDG, MFI)	CD8 <sup>+</sup> T-cells	DMSO vs Len	3 technical	<0.0001	*****
		DMSO vs Pom	3 technical	<0.0001	*****
		DMSO vs CC122	3 technical	<0.0001	*****
	CD8 <sup>+</sup> T-cells 10074-G5 10 $\mu$ M	DMSO vs DMSO+10074-G5 (impact of Myc suppression on activated human T-cells)	3 technical	0.5891	n.s.
		Len vs Len+10074-G5	3 technical	>0.9999	n.s.
		Pom vs Pom+ 10074-G5	3 technical	>0.9999	n.s.
		CC122 vs CC122+10074-G5	3 technical	0.3599	n.s.
	CD8 <sup>+</sup> T-cells 10074-G5 30 $\mu$ M	DMSO vs DMSO+10074-G5	3 technical	>0.9999	n.s.
		Len vs Len+10074-G5	3 technical	<0.0001	*****
		Pom vs Pom+ 10074-G5	3 technical	<0.0001	*****
FCS-A Mean (x100)	CD8 <sup>+</sup> T-cells	Unstimulated vs stimulated (not shown)	3 technical		
		DMSO vs Len	3 technical	<0.0001	*****
		DMSO vs Pom	3 technical	<0.0001	*****
	CD8 <sup>+</sup> T-cells treated with 10074-G5 10 $\mu$ M	DMSO vs CC122	3 technical	0.0034	**
		DMSO vs DMSO+10074-G5	3 technical	0.5987	n.s.
		Len vs Len+10074-G5 10 $\mu$ M	3 technical	<0.0001	*****
		Pom vs Pom+ 10074-G5 10 $\mu$ M	3 technical	0.0010	**
	CD8 <sup>+</sup> T-cells treated with 10074-G5 30 $\mu$ M	CC122 vs CC122+10074-G5 10 $\mu$ M	3 technical	0.0012	**
		DMSO vs DMSO+10074-G5	3 technical	0.0066	**
		Len vs Len+10074-G5	3 technical	<0.0001	*****
	Pom vs Pom+ 10074-G5	3 technical	<0.0001	*****	
	CC122 vs CC122+10074-G5	3 technical	<0.0001	*****	

### CRBN Suppresses Extracellular Regulated Kinase (ERK) Signaling to Control MYC

MYC is a potent regulator of cell proliferation and its precise control is critical for maintaining normal functions and preventing oncogenic transformation. While *Crbr*<sup>-/-</sup> T cells

have increased levels of Myc, restorative processes suppress Myc in the post-activation period. Myc expression is controlled by several prominent signaling events downstream of TCR activation and co-activating signals<sup>175</sup>. In T cells, Myc mRNA levels are controlled by the Ca<sup>2+</sup>-activated transcription factors Fos/Jun (AP-1)<sup>175,176</sup> that are also regulated by ERK1/2 signaling. Notably suboptimally activated *Crbn*<sup>-/-</sup> T cells had significantly higher levels of both total and phosphorylated ERK1/2 than *Crbn*<sup>+/+</sup> T cells (**Figure 13A**), suggesting that increased ERK1/2 signaling may be involved in the differential regulation of Myc. Indeed, treatment with the selective MEK inhibitor PD98059 effectively suppressed levels of total and phospho-ERK1/2 in activated *Crbn*<sup>-/-</sup> T cells and completely suppressed Myc protein levels in these cells (**Figure 13A**). Strikingly, suppression of ERK1/2 signaling also completely abolished the increases in Myc mRNA manifest in activated *Crbn*<sup>-/-</sup> T cells (**Figure 13B**). Finally, MEK inhibition also suppressed the increased expression of the Myc-dependent (see **Figure 10G-H**) effector genes *Tbx21*, *Eomes*, *Gzmb* and *Ifng* in activated *Crbn*<sup>-/-</sup> T cells (**Figure 13C-F**), as well as that of the Myc target *Odc1* (**Figure 13G**). Collectively, these findings indicate that a Crbn-MEK-ERK1/2 signaling circuit controls the expression of Myc, and Myc-driven phenotypes, in activated T cells.

Following TCR engagement, the activity of several ion channels is induced, including both K<sup>+</sup> and Ca<sup>2+</sup> channel proteins, which accumulate at the immunological synapse to generate intracellular signals<sup>159</sup>. As Ca<sup>2+</sup> signaling activates AP-1 (Fos/Jun) complexes, and as Fos/Jun activity is induced by ERK1/2 signaling, we also assessed effects of the *Crbn* deficiency on TCR-mediated Ca<sup>2+</sup> flux. Purified CD8<sup>+</sup> T cells from *Crbn*<sup>-/-</sup> and *Crbn*<sup>+/+</sup> mice were stimulated with suboptimal levels of anti-CD3ε and anti-CD28 and were treated with thapsigargin (an irreversible endoplasmic reticulum [ER] Ca<sup>2+</sup> adenosine triphosphatase-ATPase inhibitor), which reduces luminal ER Ca<sup>2+</sup> stores and stimulates flux of Ca<sup>2+</sup> into the cell via CRAC (Ca<sup>2+</sup>-release activating Ca<sup>2+</sup>) channel activation<sup>177</sup>. Interestingly, thapsigargin-induced Ca<sup>2+</sup> influx was significantly elevated in *Crbn*<sup>-/-</sup> versus *Crbn*<sup>+/+</sup> CD8<sup>+</sup> T cells (**Figure 13H**) and in response to treatment with the Ca<sup>2+</sup> ionophore ionomycin (**Figure 13I**), suggesting a contribution of

increased intracellular  $Ca^{2+}$  in the enhanced signaling manifest in  $Crbn^{-/-}$  CD8<sup>+</sup> T cells. Finally, consistent with increased levels of cytosolic  $Ca^{2+}$ , expression of the  $Ca^{2+}$ -responsive Nur77/Nr4a1 orphan steroid receptor,<sup>178</sup> was significantly elevated in activated  $Crbn^{-/-}$  versus  $Crbn^{+/+}$  CD8<sup>+</sup> T cells (**Figure 13J**).

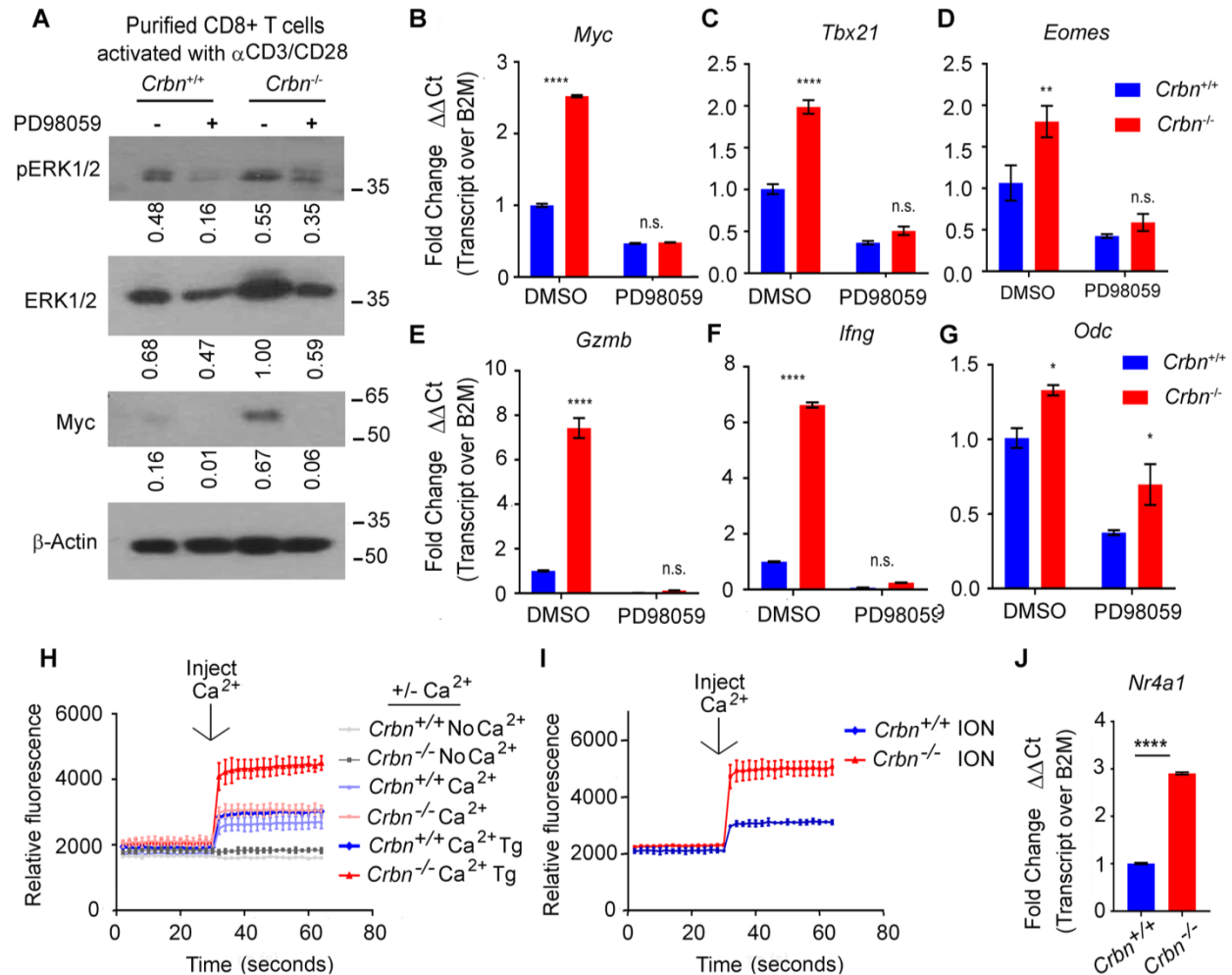


**Figure 13: Myc Expression Elevation in Activated  $Crbn^{-/-}$  CD8<sup>+</sup> T cells via ERK signaling.**

(A) Myc, ERK and pERK protein expression by Western blotting in  $Crbn^{+/+}$  and  $Crbn^{-/-}$  CD8<sup>+</sup> T cells with and without 25  $\mu$ M PD98059 24hr after activation with anti-CD3 and anti-CD28; (B-G)  $Crbn^{+/+}$  and  $Crbn^{-/-}$  CD8<sup>+</sup> T cell qRT-PCR analysis of Myc (*c-Myc*) (C) and Tbet (*Tbx21*) (D) *Eomes* (E), *Odc* (F), Granzyme B (*Gzmb*) (G), and *Ifng* (H) mRNA with 25  $\mu$ M PD98059 24hr after activation with anti-CD3 and anti-CD28 in  $Crbn^{+/+}$  and  $Crbn^{-/-}$  CD8<sup>+</sup> T cells; (H-I) Calcium flux in  $Crbn^{+/+}$  and  $Crbn^{-/-}$  CD8<sup>+</sup> T cells that have been after 24 hr of anti-CD3+anti-CD28 stimulation; final concentrations after injections were as follows: 0.5 mM calcium, 10  $\mu$ M Thapsigargin (Tg), 1  $\mu$ g/mL ionomycin (ION); (J) *Nr4a1* mRNA levels in  $Crbn^{+/+}$  and  $Crbn^{-/-}$  CD8<sup>+</sup> T cells activated for 24 hr with anti-CD3 + anti-CD28. \* $p < 0.05$ , \*\* $p < 0.01$ , \*\*\*\* $p < 0.0001$



## ***Crbn* Deficiency Augments T Cell Activity in GVHD and Anti-Tumor Immune Responses, and Myc Expression of CD8<sup>+</sup> TIL**

To assess the effects of *Crbn* deficiency on polyclonal T cell activation *in vivo* to allo-antigens, a lethal graft-versus-host disease (GVHD) model was employed, where lethally irradiated MHC-mismatched Balb/C (H2<sup>d</sup>) recipients are reconstituted with donor-derived (H2<sup>b</sup>) CD3-depleted bone marrow<sup>179</sup>. This is a clinically relevant problem, as toxicity is observed in multiple myeloma patients receiving IMiDs after allogeneic hematopoietic cell transplantation<sup>180</sup> and AP-1-mediated Myc expression is controls T cell metabolism in patients after stem cell transplants<sup>181</sup>. After randomization, equal numbers of affinity purified H2<sup>b</sup> C57Bl/6 *Crbn*<sup>+/+</sup> and *Crbn*<sup>-/-</sup> T cells were transferred into lethally irradiated H2<sup>d</sup> Balb/c mice. Notably, recipients receiving *Crbn*<sup>-/-</sup> T cells displayed a rapid loss in body weight and quickly succumbed to GVHD (**Figure 14A**, p=0.017) versus recipients receiving *Crbn*<sup>+/+</sup> T cells. Histopathological analyses of skin, small intestine and liver (**Figure 15A**) showed pathology consistent with GVHD<sup>179</sup>. Finally, there were significantly higher percentages of splenic CD4<sup>+</sup> and CD8<sup>+</sup> effector T cells expressing IFN $\gamma$  in mice receiving *Crbn*<sup>-/-</sup> T cells 14-days post-transplant (**Figure 14B**), yet *Crbn*<sup>-/-</sup> and *Crbn*<sup>+/+</sup> donor cells expressed similar levels of the pro-inflammatory cytokines IL-17 (**Figure 15B**) and IL-5 (**Figure 15C**), which can provoke tissue toxicity.

The effects of *Crbn* deficiency on lymphopenia-associated proliferation and memory conversion through self-antigen engagement were then assessed<sup>156</sup>. T cells from *Crbn*<sup>+/+</sup> and *Crbn*<sup>-/-</sup> littermates were adoptively transferred into sublethally-irradiated syngeneic mice. Although age-related differences in homeostatic populations were evident in these mice (**Figure 5G-H**), the division index of both CD4<sup>+</sup> and CD8<sup>+</sup> T cells, and splenocyte numbers, were equally distributed among mice receiving *Crbn*<sup>+/+</sup> versus *Crbn*<sup>-/-</sup> T cells (**Figure 15D-F**). Moreover, naïve T cells that proliferated in response to acute, transient lymphopenia acquired the characteristic conversion to a memory-like T cell phenotype<sup>156</sup> (**Figure 15G-H**). Thus, *Crbn* is dispensable for

T cell development, but regulates the magnitude of the T cell response following TCR engagement.

Tumoricidal effector functions of tumor infiltrating lymphocytes (TIL) are restricted by low metabolic resources, including arginine<sup>44</sup>, glutamine<sup>182</sup> and glucose that are utilized by the tumor<sup>183</sup>, suppressive myeloid populations (MDSCs and suppressive DCs)<sup>184,185</sup>, and by the prominent expression of inhibitory checkpoint proteins such as PD-1<sup>31</sup>. Given their metabolic phenotypes and their superior activity in the GVHD model, we hypothesized *Crbn*<sup>-/-</sup> T cells might display superior anti-tumor activity. To test if this was manifest in an adoptive cell therapy (ACT) scenario, adoptive transfer studies were performed with purified CD8<sup>+</sup> T cells from *Crbn*<sup>-/-</sup> versus *Crbn*<sup>+/+</sup> mice in randomized, sublethally irradiated B16 melanoma-bearing mice that were administered with exogenous IL-2 to support T cell expansion. Importantly, these studies demonstrated that recipients adoptively transferred with *Crbn*<sup>-/-</sup> CD8<sup>+</sup> T cells had significant delays in B16 tumor growth compared to recipients receiving *Crbn*<sup>+/+</sup> CD8<sup>+</sup> T cells (**Figure 14C**). Thus, *Crbn* deficient CD8<sup>+</sup> T cells have superior anti-tumor activity.

These findings suggested that *Crbn*-deficient mice should be inherently more resistant to tumor growth following transplant. To test this, B16 (B16F10) melanoma tumors were injected subcutaneously into *Crbn*<sup>+/+</sup> and *Crbn*<sup>-/-</sup> mice and their tumor growth was monitored. Notably, tumor progression was significantly suppressed in *Crbn*<sup>-/-</sup> recipient mice (**Figure 14D-E**). Characterization of immune cells revealed that the percentage of CD45<sup>+</sup> hematopoietic cells, the numbers of CD3<sup>+</sup> T cells and Tregs, and the distribution of CD4<sup>+</sup> and CD8<sup>+</sup> T cells were similar in the tumors and spleens of both cohorts (**Figure 14F, 15I-J**). However, activated populations of CD8<sup>+</sup> T cells, including CD44<sup>+</sup> and PD-1<sup>+</sup> cells, were selectively and significantly increased (by 2-3 fold) in the TIL from tumors of *Crbn*<sup>-/-</sup> versus *Crbn*<sup>+/+</sup> recipient mice (**Figure 14G**). Interestingly, the T cell exhaustion markers LAG3 and KLRG1 were similar the intratumoral T cells of the two cohorts (**Figure 14G, 15K**), suggesting the expanded T cell

population was activated but avoided the exhausted phenotype characteristic of PD-1-expressing TIL<sup>34,186</sup>.

PD-1 receptor engagement normally blocks glucose uptake<sup>31</sup>. Notably, *Crbn*<sup>-/-</sup> CD8<sup>+</sup> TIL have a significantly higher representation of PD-1<sup>+</sup> 2-NBDG<sup>hi</sup> cells, indicating these TIL have a superior metabolic phenotype and are resistant to the effects of PD-1 ligation (**Figure 14H**). To determine if TIL manifest in the tumors of *Crbn*<sup>-/-</sup> recipient mice are more reactive to tumor-associated peptides, tetrameric proteins were used to detect the melanoma-associated Trp2 antigen expressed in B16 melanoma<sup>187</sup>. Within the CD44<sup>+</sup> population, *Crbn*<sup>-/-</sup> recipient mice had 2-fold more CD44<sup>+</sup>Trp2<sup>+</sup>CD8<sup>+</sup> TIL than the TIL of *Crbn*<sup>+/+</sup> recipient mice (**Figure 14I**). Further, quite strikingly, Myc protein levels were 5-fold higher in *Crbn*<sup>-/-</sup> versus *Crbn*<sup>+/+</sup> CD44<sup>+</sup>Trp2<sup>+</sup>CD8<sup>+</sup> TIL (**Figure 14J**).

Consistent with the superior anti-tumor reactivity of *Crbn*<sup>-/-</sup> TIL, granzyme B levels were elevated in the CD8<sup>+</sup> TIL of *Crbn*<sup>-/-</sup> versus *Crbn*<sup>+/+</sup> B16 melanoma-bearing recipient mice (**Figure 14K**). Finally, OT1;*Crbn*<sup>-/-</sup> CD8<sup>+</sup> T cells displayed superior cytotoxic activity against OVA-expressing B16 tumor cells versus OT1;*Crbn*<sup>+/+</sup> CD8<sup>+</sup> T cells (**Figure 15L**).

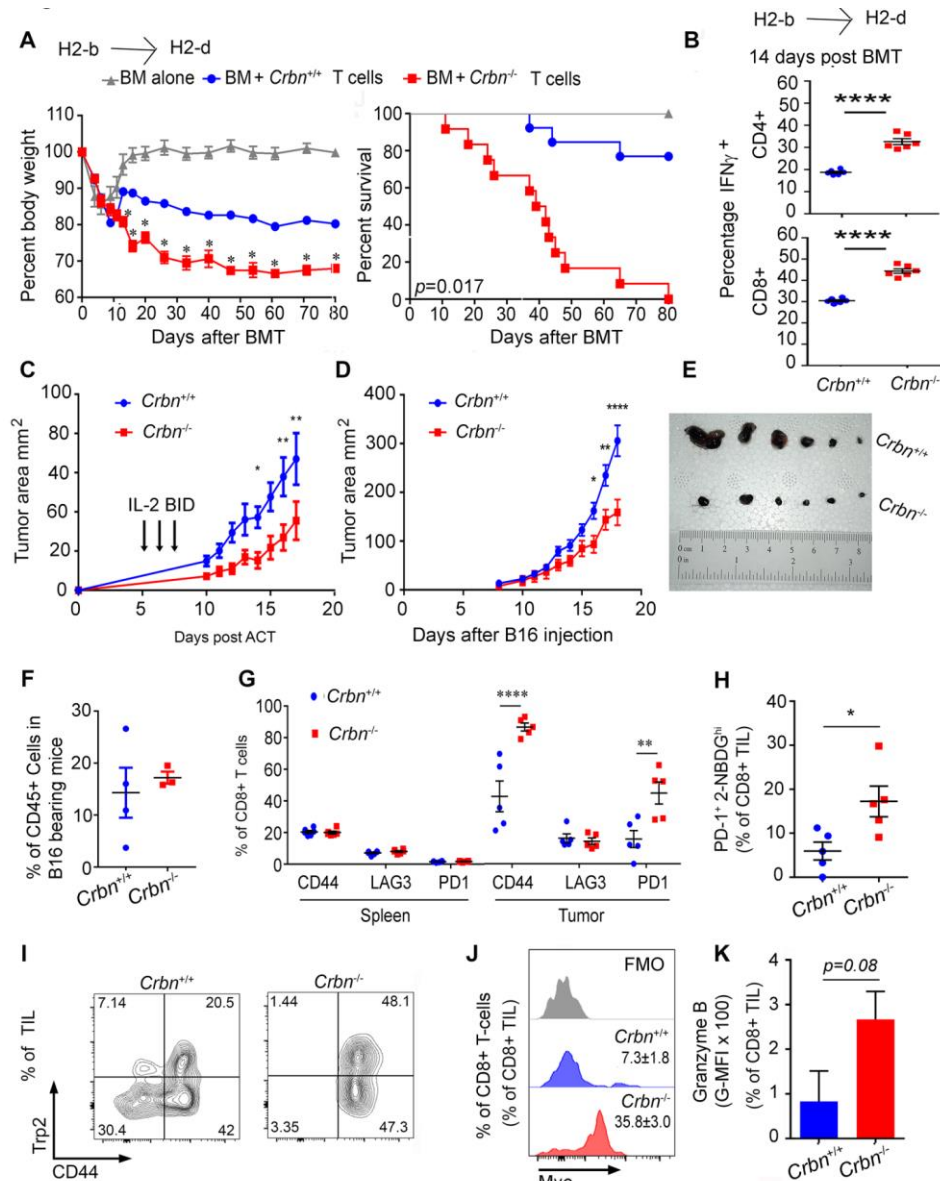


**Figure 14: *Crbn*<sup>-/-</sup> T cells Have Superior Anti-Tumor Activity.** (A) Effects of graft-versus-host-disease (GVHD) model of Balb/C mice receiving C57Bl/6 T cell-depleted bone marrow with and without *Crbn*<sup>+/+</sup> or *Crbn*<sup>-/-</sup> T cells (H2<sup>b</sup>) after lethal body irradiation; percent body weight and survival of Balb/C H2<sup>d</sup> recipient mice was monitored at the indicated intervals; (B) Percent IFN $\gamma$  producing cells from donor *Crbn*<sup>+/+</sup> or *Crbn*<sup>-/-</sup> CD8<sup>+</sup> T cells derived from the GVHD model following re-stimulation with PMA and ionomycin *ex vivo* on day 14 post-transplant; (C) B16 tumor area in CD45.1<sup>+</sup> *Crbn*<sup>+/+</sup> mice randomized to receive *Crbn*<sup>+/+</sup> or *Crbn*<sup>-/-</sup> T cells and IL-2 treatment 3 days after tumor inoculation; (D-E) B16 tumor area over time (D) or at day 14 after tumor inoculation subcutaneously (E) in *Crbn*<sup>+/+</sup> and *Crbn*<sup>-/-</sup> recipient mice; (F) CD45<sup>+</sup> cell populations in tumors from the animals noted in (D) and (E); (G) PD-1, Lag3, and CD44 cell surface expression in CD8<sup>+</sup> cell populations in the spleens and tumors from the animals noted in (D) and (E); (H) PD-1 expression and 2-NBDG uptake in *Crbn*<sup>+/+</sup> and *Crbn*<sup>-/-</sup> CD8<sup>+</sup> TIL; (I) Expression of CD44 and reactivity to Trp2 peptide in *Crbn*<sup>+/+</sup> and *Crbn*<sup>-/-</sup> CD8<sup>+</sup> TIL; (J) Intracellular Myc expression as measured by flow cytometry in *Crbn*<sup>+/+</sup> and *Crbn*<sup>-/-</sup> CD8<sup>+</sup> TIL; (K) Expression of Granzyme B in the indicated TIL. \* $p<0.05$ , \*\* $p<0.01$ , \*\*\* $p<0.001$ , \*\*\*\* $p<0.0001$

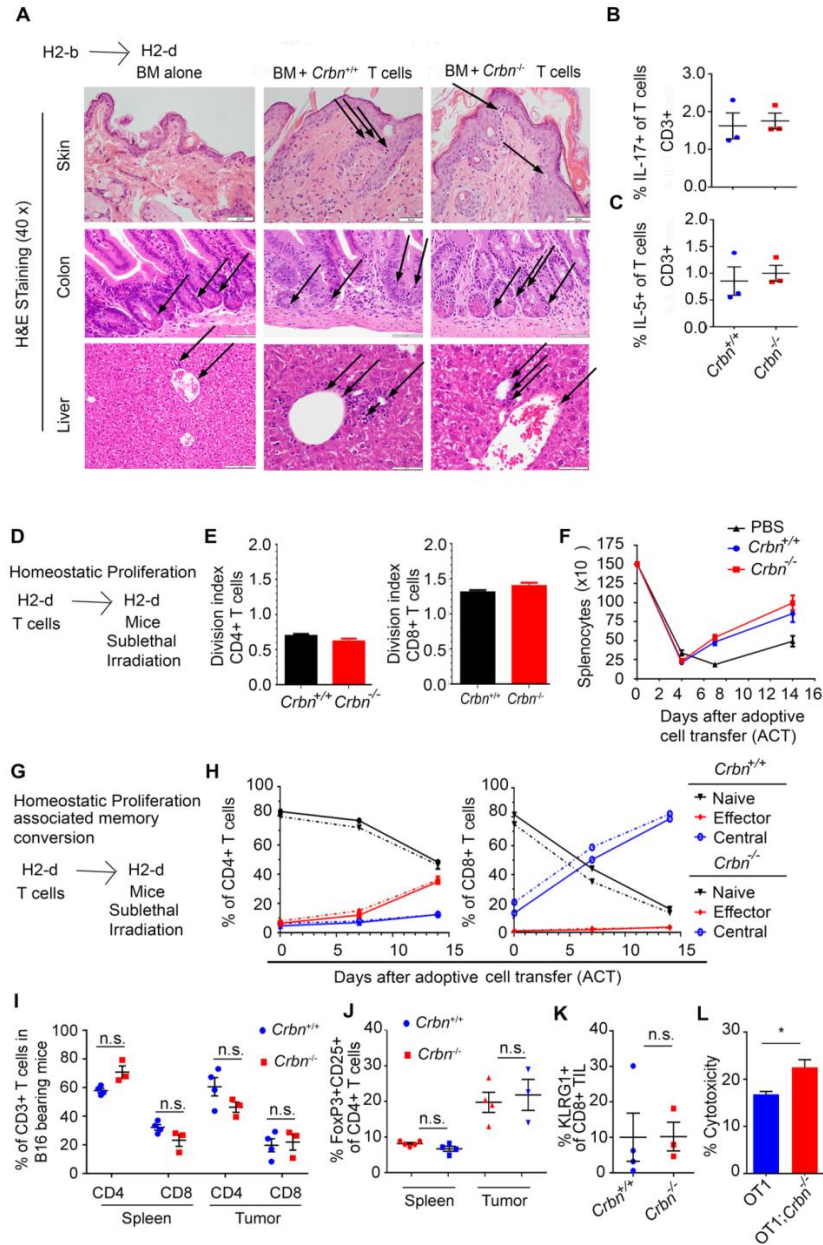


**Figure 15: *Crbn*<sup>-/-</sup> T cells have increased function *in vivo*.** (A-B) in reference to Figure 14A-B; (A) H&E of skin, colon and liver from mice in the GVHD model. Arrows indicate immune infiltrates and areas of pathology; (B-C) Percent IL-17 and IL-5 producing T cells from donor *Crbn*<sup>+/+</sup> and *Crbn*<sup>-/-</sup> following re-stimulation with PMA and ionomycin *ex vivo* on day 14 post-transplant; (C) *Crbn*<sup>+/+</sup> and *Crbn*<sup>-/-</sup> CD45.2<sup>+</sup> T cells were adoptively transferred into sublethally-irradiated CD45.1 mice; (D) Schematic of experimental setup; (E) Average number of divisions of the adoptively transferred CD4<sup>+</sup> (left) and CD8<sup>+</sup> (right) T cells as determined by CellTrace Violet dilution; (F) Number of splenocytes after adoptive cell transfer over time; (G) Schematic of experimental setup; (H) Percent of naïve (CD44<sup>Neg</sup>CD62L<sup>+</sup>), Effector (CD44<sup>+</sup>CD62L<sup>Neg</sup>), and Central Memory (CM, CD44<sup>+</sup>CD62L<sup>+</sup>) of CD4<sup>+</sup> T cells and CD8<sup>+</sup> T cells from animals noted in Figure 15D-F; (I-J) CD4<sup>+</sup> and CD8<sup>+</sup> cell populations and Treg cells (J) in the spleens and tumors from the animals noted in Figure 14D-E; (K) KLRG1<sup>+</sup> cells % of CD8<sup>+</sup> TIL from animals noted in Figure 14D-E; (L) OT1 and OT1;*Crbn*<sup>-/-</sup> T cells % cytotoxicity of OVA-expressing B16 cells.

## Discussion

Here we show that targeting CRBN in activated mouse and human CD8<sup>+</sup> T cells, either via genetic means or through small molecule treatment, generates a robust metabolic, hyperactive CD8<sup>+</sup> T<sub>E</sub> phenotype that has enhanced activity in models of GVHD and anti-tumor adoptive cell therapy. The latter findings are particularly exciting, as multiple mechanisms suppress the metabolism of intratumoral T cells<sup>30,44</sup>, including nutrient sequestration by metabolically active tumor cells<sup>44,188</sup>, cancer-associated stroma<sup>189</sup>, MDSCs<sup>5,190</sup>, tolerogenic macrophages and DCs<sup>185,191</sup>. Suppressive myeloid cells in particular act as metabolic sinks for L-Arg and L-tryptophan (L-Trp), which are directly incorporated into proteins, or in the case of L-Trp, acts as a substrate for indoleamine 2,3-dioxygenase 1 (IDO1)<sup>192,193</sup> that stimulates CD4<sup>+</sup>CD25<sup>+</sup>Foxp3<sup>+</sup> Tregs<sup>194</sup>. Further, L-Arg depletion triggers downregulation of the TCRζ chain<sup>191</sup>, and high levels of nitric oxide generated by MDSCs nitrosylate the TCR-CD8 complex to induce antigen-specific CD8<sup>+</sup> T cell tolerance in tumors<sup>5</sup>.

Quite strikingly, CRBN is revealed to harness CD8<sup>+</sup> T cell metabolism via control of MEK/ERK signaling leading to Myc, a master regulator of T cell activation<sup>13</sup> and of asymmetric division of T cells into effector versus memory cell fates<sup>14</sup>. Notably, Green and colleagues have shown that Myc augments metabolism and enables the proliferation and persistence of CD4<sup>+</sup> and CD8<sup>+</sup> T cells via transcriptional reprogramming that includes induction of enzymes directing glycolysis, glutaminolysis and polyamine biosynthesis<sup>13</sup>. Consistent with high Myc activity, *Crbn*-deficient activated mouse CD8<sup>+</sup> T cells, and human CD8<sup>+</sup> T cells treated with IMiD compounds, exhibit higher levels of Myc and enhanced nutrient uptake, NAD<sup>+</sup>/NADH ratios, glycolytic rates, and basal and reserve capacity for OXPHOS. Further, Myc function is required to sustain the hypermetabolic phenotype of activated mouse and human CD8<sup>+</sup> T cells, as these are cancelled by treatment with validated inhibitors of Myc:Max function. Thus, a CRBN-MYC circuit controls the magnitude and persistence of antigen-specific activation of CD8<sup>+</sup> T cells, and drives a hyperactive T<sub>E</sub> cell fate that has superior anti-tumor activity.

MYC expression is controlled by several means, including mRNA decay<sup>195</sup>, ubiquitin-mediated protein turnover<sup>196</sup>, miRNA and lncRNA regulation<sup>197-199</sup>, transcription<sup>200</sup> and translation<sup>201</sup>. Thus, the control of *Myc* mRNA and protein levels in activated T cells, and by CRBN in this context, is likely complex. Accordingly, it was important to elucidate the mechanisms that augment *Myc* expression in *Crbn*<sup>-/-</sup> CD8<sup>+</sup> T cells. What is known is that there is both an increase in transcription initiation and repression of a block in transcriptional elongation associated with *Myc* mRNA induction<sup>175</sup>. Furthermore, translational regulation of MYC includes a polyamine-directed pathway<sup>202</sup>, which we have shown is highly elevated in *Crbn*-deficient T cells that rely on polyamine biosynthesis to sustain their hyperactive phenotype. Here we show that a primary regulator of *Myc* mRNA and protein expression is MEK/ERK signaling. Precisely how CRBN harnesses ERK1/2 signaling is not yet clear, though we postulate this may involve TCR-mediated activation of PLC $\gamma$ 1, that generates diacylglycerol to promotes Ras-ERK signaling<sup>203</sup>, as well as inositol 1,4,5-trisphosphate (IP<sub>3</sub>) that activates calcium signaling<sup>159</sup>, which we show is also up-regulated in *Crbn*<sup>-/-</sup> CD8<sup>+</sup> T cells. *Crbn*<sup>-/-</sup> T cells display increased Ca<sup>2+</sup> flux after directly triggering CRAC channel activation with thapsigargin treatment and by ionomycin-mediated activation of IP<sub>3</sub><sup>159,204</sup> suggesting CRBN may directly regulate Ca<sup>2+</sup> channel activity to enable sustained Ca<sup>2+</sup> influx in these cells. Interestingly, rat CRBN overexpression suppresses neuron excitation by trapping the BK<sub>ca</sub>-associated Slo1 protein in the endoplasmic reticulum (ER) which prevents the maturation and surface assembly of the functional Ca<sup>2+</sup> channel<sup>205</sup>. Alternatively, it is possible that MEK/ERK signaling is somehow linked to CRBN-directed control of the CD147/MCT1 lactate transporter complex that is disrupted by loss of *Crbn* or by treatment with IMiDs<sup>65</sup>.

Our findings that equal numbers of Tregs and conventional T cells are present in tumor-bearing *Crbn*<sup>-/-</sup> and *Crbn*<sup>+/+</sup> mice argues for intrinsic roles for CRBN in intratumoral effector T cells. In addition to nutrient competition, the engagement of multiple checkpoint proteins in TIL<sup>31,32,34,186</sup> blocks uptake and metabolism of glucose and amino acids, by inhibiting PI3K/AKT-

mediated activation of mTOR<sup>33</sup>. Therefore, differential early activation signals in *Crbn*<sup>-/-</sup> and *Crbn*<sup>+/+</sup> CD8<sup>+</sup> T cells may be critical to fine-tune the distal events that control the duration of the immune response and metabolic fitness. Checkpoint blockade therapy in particular relies on the induction of Tbet-associated chromatin remodeling of lineage-selective gene loci to control the effector phenotype of both CD4<sup>+</sup> and CD8<sup>+</sup> T cells<sup>81,206,207</sup>. Notably, *Tbx21* expression is increased 7-12 fold in activated *Crbn*<sup>-/-</sup> CD8<sup>+</sup> T cells, consistent with their cytokine production, gene signature, and metabolic phenotypes. Further, although Tbet is generally associated with rapid turnover via apoptosis, the balanced expression of Tbet and Eomes as manifest in activated *Crbn*<sup>-/-</sup> CD8<sup>+</sup> T cells has been associated with survival and memory formation in the context of chronic viral infection<sup>208</sup>.

Other than nutrient supplementation<sup>109</sup>, which highly likely also fuels cancer cells and/or expands immunosuppressive cell populations, there are no identified targets or strategies that can selectively enhance the metabolic activity of cytotoxic T cells within the tumor microenvironment. Thus, our findings that targeting CRBN can augment the activity of T cells in ACT could have far reaching clinical applications. Furthermore, this work also implicates that control of effector T cell metabolism may ameliorate GVHD in the clinic. Indeed, Ca<sup>2+</sup> mobilization<sup>209</sup> and CD98 signaling<sup>171</sup>, control by the PD-1/PD-L1 axis<sup>210</sup>, and anaplerosis of alloreactive T cells<sup>73</sup> have all been implicated in GVHD severity, and all three of these responses appear harnessed by CRBN.

Virtually all anti-cancer therapeutic T cell modalities face the hurdle of inactivation via exhaustion<sup>29,211</sup>. Our findings of a CRBN-MEK/ERK-MYC circuit (**Figure 13**) that augments, sustains and drives an antigen-specific T cell phenotype support the notion that this barrier can be overcome by pharmacologic or genetic targeting of human CRBN, and that this represents an attractive accessory to other immune cell therapies, including TIL therapy or chimeric antigen receptor T cell (CAR-T) therapy. Consistent with this notion, Myc is a Yamanaka stem cell factor<sup>212</sup> and when overexpressed in T cells along with other cooperating stem cell factors, Myc



can fully revive terminally differentiated CD8<sup>+</sup> T cells and maintain antigen specificity<sup>213</sup>. Stemness in T cells has been hypothesized to have therapeutic potential for immunotherapy to preserve the persistence of the cells *in vivo*<sup>214</sup>. Notably, the accumulation of long-lived memory cells in aged *Crbn*<sup>-/-</sup> mice also implicates *Crbn* in the control of memory differentiation. Consistent with the findings presented herein, we have previously shown that IMiD treatment reverses tolerance in T cells from MDS patients<sup>215</sup> that display T cell incompetence due to exhaustion<sup>53,215-219</sup>, which is caused by the accumulation of MDSC<sup>184,220,221</sup>, the expansion of suppressive macrophages and DCs<sup>222</sup>, excessive inflammatory cytokine production, the expansion of Tregs<sup>184</sup>, and telomere repair defects<sup>223</sup>. The fact that IMiD compounds are capable of revitalizing T cell responses in MDS suggest that this drug class offers promise as an adjuvant for immunotherapeutic modalities in many cancer types.

## Materials and Methods

### Mouse Husbandry

Germline *Crbn* heterozygous mice (*Crbn*<sup>+/-</sup>)<sup>155</sup> were obtained from from Dr. Anjali Rajadhyaksha (Cornell University). Mice were genotyped according to previously established methods and genotypes were confirmed by genomic PCR and western blots (**Figure 3**). OT1 transgenic mice<sup>160</sup> were bred to *Crbn*<sup>-/-</sup> mice for two generations to create OT1;*Crbn*<sup>-/-</sup> mice. C57BL/6 and littermates of *Crbn*<sup>-/-</sup> mice were used as *Crbn*<sup>+/+</sup> controls. Mice were genotyped using methods described by Jackson Lab (<https://www.jax.org/jax-mice-and-services>) and all genotyping primers can be found in **Table 4**. Stocks were maintained and bred at the H. Lee Moffitt Cancer Center and Research Institute under approved protocols by the Institutional Animal Care and Use Committee.

**Table 4: Cereblon Genotyping Primers**

Mouse strain	Primer	Sequence 5'-3'
<i>Crbn</i> <sup>-/-</sup>	<i>Loxf</i> (Wild-type forward primer)	AGGAGCACTGAACGGCTTACAG
<i>Crbn</i> <sup>-/-</sup>	<i>f</i> (knockout forward primer)	TTGTTTCAGAACTGCTGGGATGTG
<i>Crbn</i> <sup>-/-</sup>	<i>LoxR</i> (common reverse primer)	CGCATGCTGACTGATCACAGC

### **Mouse Immune Cell Isolation**

Spleens were isolated from euthanized *Crbn*<sup>+/+</sup> and *Crbn*<sup>-/-</sup> mice and processed into single cell suspension. Splenocytes were further processed by adding RBC lysis buffer for 1 minute. Pan CD3<sup>+</sup> T cells, CD8<sup>+</sup> T cells, CD4<sup>+</sup> T cells, and B cells were isolated from 6-8 week *Crbn*<sup>+/+</sup> and *Crbn*<sup>-/-</sup> splenocytes by immunomagnetic negative selection.

### **Mouse Polyclonal CD3<sup>+</sup> and CD8<sup>+</sup> T cell and Ot-1 CD8<sup>+</sup> T cell Activation**

For flow-based assays, RT-PCR, Seahorse analyses, cytokine analysis and metabolomics, 96-well round bottom plates were coated with 0.1-10 µg/mL anti-CD3ε in 100 µL PBS overnight at 4°C or for 90 min at 37°C. *Crbn*<sup>+/+</sup> and *Crbn*<sup>-/-</sup> T cells were plated in equal numbers (2x10<sup>5</sup> per well) with and without anti-CD28. For cytokine analyses, supernatants were harvested at 48 hr for IL-2 and IL-17 and at 72 hr for TNFα, IFNγ, IL-10, and IL-4. Cytokines were quantified from standard curves by enzyme-linked immunosorbent assay (ELISA) according to the manufacturer's protocols. For western blot analysis, 12-well plates were coated with 5µg/mL anti-CD3ε and 2x10<sup>6</sup> T cells per well were plated with 1µg/mL anti-CD28. For OT1 and OT1;*Crbn*<sup>-/-</sup> activation, whole splenocytes were plated at 10<sup>6</sup> per well in a 24-well plate and activated with 0.001-1nM N4, A2, G4, or Trp2 and 10ng/mL IL-2 (unless indicated otherwise). All T cell experiments were conducted in RPMI supplemented with FBS, Penicillin, Streptomycin, Gentamicin, non-essential amino acids, sodium pyruvate and beta-mercaptoethanol.

### **Human T cell Activation**

Healthy donor buffy coats were obtained from OneBlood (Tampa, Florida) and were diluted 1:4 in PBS. T cells were isolated as per manufacturer's protocol (RosetteSep Human T cell enrichment Cocktail Kit) and frozen at -80°C in 90% FBS and 10% DMSO before use. 96-well round bottom plates were coated with 5µg/mL anti-CD3 in 100µL PBS 90 minutes at 37°C and placed in 4°C before use. T cells were plated at 2x10<sup>5</sup> per well with 1µg/mL anti-CD28. T

cells were treated with 10 $\mu$ M lenalidomide, pomalidomide, CC122 or JQ1 for 5 days. All T cells were analyzed for flow-based assays. For Seahorse assays, CD4<sup>+</sup> T cells were removed by immunomagnetic selection (CD4 microbeads) prior to analysis.

### **Glucose Uptake and Flow Cytometry Analysis**

Antibodies and Trp2 tetramer were added at 0.2  $\mu$ g per 10<sup>6</sup> cells in 100- $\mu$ L volume FACs buffer (PBS with 2 mM EDTA, 1% FBS and 1% BSA) for 20-30 min at 4°C. The OVA tetramer was used for staining of OT1 and OT1;*Crbn*<sup>-/-</sup> splenocytes by adding 1.5- $\mu$ L of the tetramer to 10<sup>6</sup> cells in 100- $\mu$ L FACs buffer for 20 min at room temperature prior to antibody staining. Viability was determined by staining cells with Zombie Near IR dye, Ghost Dye 780 or Live/Dead Yellow for fixed cells, or with 7AAD and DAPI for fresh isolated cells. Proliferation of *Crbn*<sup>+/+</sup> and *Crbn*<sup>-/-</sup> T cells by dye dilution was determined by staining cells with 5-10  $\mu$ M CellTrace Violet for 10 min at 37°C in PBS prior to activation. Glucose uptake was analyzed by staining cells with 10  $\mu$ M 2-(N-(7-Nitrobenz-2-oxa-1,3-diazol-4-yl)Amino)-2-Deoxyglucose (2-NBDG) in PBS for 30-60 minutes at 37°C degrees. MitoTracker staining was analyzed by staining cells with 50 nM MitoTracker Green in PBS for 30 min at 37°C degrees. All data collection was performed on an LSRII or FACS Canto II (BD Biosciences) and analysis was performed on Flowjo software.

### **Experimental Graft-Vs-Host (GVHD) Mouse Model**

To induce GVHD, we performed the major histocompatibility complex (MHC)-mismatched C57BL/6 to BALB/cJ bone marrow transplant model as described Valenzuela, et al.<sup>179</sup>. Polyclonal *Crbn*<sup>-/-</sup> and *Crbn*<sup>+/+</sup> T cells (C57BL/6) were purified to 95% purity using the negative selection according to manufacturer's instructions (EasySep Mouse T cell isolation kit). BALB/c mice were lethally irradiated with 800-900 cGy and injected with 5x10<sup>6</sup> CD3-depleted *Crbn*<sup>+/+</sup> bone marrow cells with and without 10<sup>6</sup> T cells from either *Crbn*<sup>+/+</sup> and *Crbn*<sup>-/-</sup> mice via tail vein 24 hr after irradiation. Weight was measured at the indicated intervals (**Figure 14**). To measure function of donor T cells after disease onset, splenocytes were harvested 14 days after

transplant and re-stimulated with PMA, ionomycin, and 1  $\mu$ L/mL Brefeldin A. Cells were fixed and stained for analysis of intracellular IFN $\gamma$  and IL-17 using protocols and antibodies from BD Biosciences.

### **Metabolic Analyses**

Seahorse metabolic assays were conducted using activated *Crbn*<sup>+/+</sup> and *Crbn*<sup>-/-</sup> CD8<sup>+</sup> T cells or drug-treated human CD8<sup>+</sup> T cells were plated in Seahorse base medium supplemented with 6 mM glucose and 1 mM glutamine at 10<sup>5</sup> T cells per well in a 96-well Seahorse plate. Mitochondrial stress tests were used as per manufacturer's protocol. Extracellular acidification and oxygen consumption rates were analyzed using Wave Software.

### **ATP, Hexokinase Enzymatic Assay And NAD/NADH**

*Crbn*<sup>+/+</sup> and *Crbn*<sup>-/-</sup> CD8<sup>+</sup> T cells were activated for 24 hr with anti-CD3 $\epsilon$  and anti-CD28 (ATP & NAD/NADH) or 48 hr (HK activity). Analysis was performed as per manufacturer's protocol.

### **Amino Acid Uptake Assays**

Arginine and glutamine uptake assays were performed using *Crbn*<sup>+/+</sup> and *Crbn*<sup>-/-</sup> CD8<sup>+</sup> T cells that were activated for 24 hr and 3x10<sup>6</sup> per mouse were suspended in 1x PBS with Ca<sup>2+</sup> and Mg<sup>2+</sup>/0.1% Glucose. 0.2  $\mu$ Ci of the indicated amino acid was added and incubated at room temperature for 20 min. To stop the reaction, cells were spiked with 1x cold PBS. Cells were then washed twice with ice cold 1x PBS and subsequently lysed with 0.1% NaOH. The lysate was mixed with scintillation buffer and counts were determined with a TriCarb 2810 TR liquid scintillation analyzer (PerkerElmer).

### **Quantitative PCR Analysis**

Cells pellets were kept in Buffer RLT and at -80°C until RNA isolation. RNA was isolated as following manufacturer's protocol (Qiagen) and kept at -20°C until quantification. RNA was converted into cDNA as per manufacturer's protocol (Bio-Rad) and 1-2 ng were used to quantify the expression of the following genes: *c-Myc* and *Crbn* by Taqman; *Gzmb*, *Pfr1*, *Tbx21*,

*EOMES*, *Slc7a1*, *Slc38a1*, *Slc1a5*, *Odc1*, *Oat*, *Srm*, and *Sms* by Sybr Green; *B2M* by Taqman and Sybr Green. Sybr green probe sequences are listed in **Table 5**.

**Table 5: RT-PCR Primer Sequences**

Gene	Sequence 5'-3'
<i>Slc7a1</i> Forward	TGGTCTTGTGCTTCATCGTG
<i>Slc7a1</i> Reverse	GACACCAGAGAATCCAAAGGG
<i>Slc38a1</i> Forward	TTACCAACCATCGCCTTC
<i>Slc38a1</i> Reverse	ATGAGAATGTGCGCTGTG
<i>Slc38a2</i> Forward	GGTATCTGAACGGTGACTATCTG
<i>Slc38a2</i> Reverse	TCTGCGGTGCTATTGAATGC
<i>Granzyme B</i> Forward	TGCTGCTAAAGCTGAAGAGTAAG
<i>Granzyme B</i> Reverse	CGTGTTTGAGTATTTGCCATTG
<i>T-bet</i> Forward	CCTGGACCCAACCTGTCAACT
<i>T-bet</i> Reverse	AACTGTGTTCCCGAGGTGTC
<i>Eomes</i> Forward	TACGGCCAGGGTTCTCCGCTCTAC
<i>Eomes</i> Reverse	GGGCCGGTTGCACAGGTAGACGTG
<i>Perforin</i> Forward	GCAGCTGAGAAGACCTATCAGGAC
<i>Perforin</i> Reverse	TCTGAGCGCCTTTTTGAAGTC
<i>B2M</i> Forward	TTTGGTGCTTGTCTCACTGA
<i>B2M</i> Reverse	CAGTATGTTCCGGCTTCCCATTG
<i>Odc1</i> Forward	GACGAGTTTGACTGCCACATC
<i>Odc1</i> Reverse	CGCAACATAGAACGCATCCTT
<i>Oat</i> Forward	GGAGTCCACACCTCAGTCG
<i>Oat</i> Reverse	CCACATCCCACATATAAATGCCT
<i>Srm</i> Forward	ACATCCTCGTCTTCCGCAGTA
<i>Srm</i> Reverse	GGCAGGTTGGCGATCATCT
<i>Sms</i> Forward	CACAGCACGCTCGACTTCAA
<i>Sms</i> Reverse	TGCCATTCTTGTTCTGTGAAGTT

### Polyamine Extraction, LC/MS And Quantitation

*Extraction.* Cell pellets ( $1 \times 10^6$  T cells per replicate,  $n = 3$ ) were spiked with 5  $\mu$ L of internal standard solution containing 1  $\mu$ g/mL of  $^{13}\text{C}_4$ -putrescine,  $^{13}\text{C}_5$ -ornithine, 1,1,2,2,3,3,4,4-D<sub>8</sub>-N-(3-Aminopropyl) Butane-1,4-Diamine:3HCl (D<sub>8</sub>-spermidine), and 1,1,2,2,3,3,4,4-D<sub>8</sub>-N,N'-Bis(3-Aminopropyl)-1,4-Butanediamine:4HCl (D<sub>8</sub>-spermine). An aliquot (200- $\mu$ L) of HPLC grade methanol heated to 80°C was added to each sample, vortexed and incubated for 5 min at 80°C. Samples were centrifuged at 16,200 x  $g$  for 15 min at 4°C. The extraction process was repeated using 100- $\mu$ L of hot methanol at 80°C. The supernatants containing metabolites from both extractions were pooled and dried in a vacuum centrifuge (Savant SC210A, ThermoFisher Scientific). Samples were resuspended in 50- $\mu$ L of HPLC grade water.

*Liquid Chromatography-Selected Ion Monitoring.* Metabolomics was performed on an ultra-performance liquid chromatography (UPLC model U3000, Dionex) interfaced with an

electrospray Q Exactive HF mass spectrometer (ThermoFisher Scientific) using full MS and selected ion monitoring (LC-SIM) for quantification of each target. The following solvent system is used: solvent A is 100% HPLC grade water (Burdick & Jackson, Honeywell) containing 0.05% Heptafluorobutyric acid, and solvent B is aqueous 90% acetonitrile with 0.1% formic acid. For each sample, a 10- $\mu$ l aliquot of the metabolite mixture was loaded onto an Accucore reverse phase C18 column (27826-153030, 2.1 mm x 100 mm, 2.6  $\mu$ m particle size, ThermoFisher Scientific). A gradient of 20% B to 80% B was applied over 6 min with a flow rate of 0.350 mL/min followed by re-equilibration over 3 min, for a total of 9 min for the LC experiment. Mass spectrometry instrument parameters for SIM on the Q Exactive HF included the following: resolution 70,000; isolation window width 1.0  $m/z$  and isolation offset 0.2  $m/z$ ; AGC target 2e5; maximum IT 100 ms; an inclusion list containing the  $m/z$  for each metabolite, its respective stable isotope standard (SIS) and a scheduled time window for metabolite elution.

*Data Analysis for Metabolite Quantification.* Xcalibur Quan Browser (version 3.0.63, ThermoFisher Scientific, San Jose, CA) was used for data analysis. Metabolite amounts (pmol) were calculated using the peak area ratio of each molecule to its respective.

### **Gene Set Testing and Pathway Analyses**

Unactivated and 12 hr post-activated (5  $\mu$ g/mL anti-CD3, 1  $\mu$ g/mL anti-CD28) T cells from *Crbn*<sup>+/+</sup> and *Crbn*<sup>-/-</sup> mice were lysed and total RNA extracted using the iPrep Trizol Plus RNA kit. One hundred nanograms of total RNA was amplified and labeled with biotin using the Ambion Message Amp Premier RNA Amplification Kit following the manufacturer's protocol initially described by Van Gelder, et al. <sup>224</sup>. Hybridization with the biotin-labeled RNA, staining, and scanning of the chips on the GeneChip GCS3000 scanner followed the prescribed procedure outlined in the Affymetrix technical manual and has been previously described <sup>225</sup>. The oligonucleotide probe arrays used were the Mouse Genome 430 2.0 Arrays, which contain over 45,000 probe sets representing over 34,000 transcripts. The array output files were visually inspected for hybridization artifacts and then analyzed using Affymetrix Expression Console v

1.4 using the MAS 5.0 algorithm, scaling probe sets to an average intensity of 500. Pre-processing and normalization was then performed using Partek microarray data analysis software. Raw intensity files were processed using robust multi-array average (RMA). Principle Component Analysis and unsupervised hierarchical clustering were performed. Statistical analysis was performed using two-way ANOVA. Gene lists with 2-fold differential expression and  $FDR \leq 0.05$  between the unactivated and activated state in *Crbn*<sup>+/+</sup> and *Crbn*<sup>-/-</sup> T cells were compared. Gene Ontology (GO) analysis was performed on genes differentially expressed only in *Crbn*<sup>-/-</sup> T cells following activation using MetaCore by GeneGo. The microarray data have been deposited to the Gene Expression Omnibus database under accession number GSE81725.

### **Transmission Electron Microscopy**

Pellets from unstimulated and 24 hr stimulated T cells were fixed immediately in cacodylate buffer (pH 7.4-7.5) with 2% glutaraldehyde overnight, and resuspended in 1% osmium tetroxide. Samples were dehydrated step-wise (50%, 70%, 95%, 100%) in increasing concentrations of alcohol followed by step-wise (2:1, 1:1, 1:2, 0:1 alcohol to resin) infiltration of resin. Resin blocks were cut on a microtome and images were acquired on a JEOL 1400 transmission electron microscope. Number of mitochondria and average mitochondrial length was determined by visual inspection using Adobe Photoshop.

### **Western Blot Analyses**

T cells were lysed in RIPA lysis buffer supplemented with protease (Roche Pharmaceuticals, Pleasanton, CA) and phosphatase (Sigma-Aldrich) inhibitors. 30-40  $\mu$ g protein was separated by SDS-PAGE on 4-12% gradient Bis-Tris gels using Novex Protein Separation System (Thermo Fisher Scientific). Antibodies used are indicated in the Key Resources Table. Densitometry was performed on 600 dpi greyscale images using ImageJ software (<http://imagej.nih.gov/ij/>) and values were normalized to  $\beta$ -Actin.

## **Experimental Melanoma Mouse Model and Act**

Mice were injected with  $1 \times 10^5$  B16 melanoma cells subcutaneously on the left flank. Tumors were measured every 2-3 days by taking two perpendicular measurements and volume was calculated by the equation “ $a \times b^2 \times 0.52$ ” where a is the longest measurement and b is the perpendicular measurement. Mice were euthanized when tumors ulcerated or the longest side exceeded 20 mm. Some cohorts of mice were euthanized early (day 10-14) for TIL analysis by flow cytometry. Tumors for this analysis were processed into single cell suspension and agitated for 30 min in complete RPMI (noted above) supplemented with Collagenase I, Collagenase IV, Hyaluronidase, and DNase I. Populations of T cells from spleens and tumors were stained as described and immediately analyzed. For adoptive cell transfer, CD45.1 mice were sublethally irradiated 3 days after initial tumor inoculation at 600rad and  $2 \times 10^6$  T cells were injected via tail vein. Mice were then treated with 250,000 I.U. IL-2 (R&D Systems) via intraperitoneal injections twice daily for 3 days (6 total doses).

## **Homeostatic Proliferation**

CD45.1 mice were sublethally irradiated at 600rad and  $2 \times 10^5$  CellTrace Violet-labeled *Crbn*<sup>+/+</sup> and *Crbn*<sup>-/-</sup> T cells were injected via tail vein. Average number of divisions (division index) and memory populations were analyzed among spleen populations on day 7 after adoptive cell transfer.

## **Metabolomics Analysis**

*Sample preparation.* Samples were thawed on ice then centrifuged at 20,000 x g for 5 minutes at 4 °C to pellet the cells. Supernatants were discarded and the pellets were washed with 1 mL of 40 mM ammonium formate. The samples were mixed on a vortex and then centrifuged at 20,000 x g for 5 minutes at 4 °C and supernatants were discarded. The wash step was performed 2 more times. To each sample, 50  $\mu$ L of 5 mM ammonium acetate and 10-20 pieces of 0.7 mm zirconia beads were added. Homogenization was done on a Bead Beater (BioSpec, Bartlesville, OK) at 1800 rpm for 30 seconds. Samples were incubated at 4°C for 30



min. Protein concentrations were determined using Qubit Protein Assay kit. Prior to extraction, samples were normalized to 300 µg/mL or to the lowest protein concentration by diluting to 50 µL with 5 mM ammonium acetate. Each sample received 10 µL of internal standards solution, containing creatine-D3 H<sub>2</sub>O, L-Leucine-D10, L-tryptophan-2,3,3-D3, Citric acid 13C6, L-tyrosine Ring 13C6, L-tryptophan 13C11, L-leucine 13C6, L-phenylalanine Ring-13C6, N-BOC-L-tert-leucine, and N-BOC-L-aspartic acid. Samples were extracted by protein precipitation using 1 mL ice-cold 80% methanol/20% water and mixed on the Bead Beater (BioSpec Products) at 1,800 rpm for 30 seconds. Further protein precipitation was allowed by incubating the samples at 4 °C for 30 minutes. Samples were centrifuged at 20,000 x g for 5 minutes at 4 °C to pellet the protein. An aliquot of the supernatant (1 mL) was transferred from each sample into clean tube and dried under a gentle stream of nitrogen at 30°C. Dried extracts were re-suspended with 30 µL reconstitution solution consisting of injection standards in 0.1% formic acid in water containing 6 µg/mL of Boc-L-tyrosine, Boc-L-tryptophan, and Boc-D-phenylalanine. Resuspension was allowed at 4°C for 10 -15 minutes; then, samples were centrifuged at 20,000 x g for 5 minutes at 4°C. Supernatants were collected into clean LC-vials for LC-MS metabolomics analysis.

*LC-MS.* Global metabolomics profiling was performed on a Thermo Q-Exactive Orbitrap mass spectrometer with Dionex UHPLC and autosampler. All samples were analyzed with positive and negative heated electrospray ionization with a mass resolution of 35,000 at m/z 200 as separate injections. Sheath gas and auxiliary gas flow rates were set at 50 and 10, respectively, with auxiliary gas temperature of 350°C. Spray voltage was set to 3.0 kV and capillary temperature to 325°C. Mass range was from m/z 70 to 1000 with MS acquisition for 17.5 minutes. Separation was achieved on an ACE 18-PFP 100 x 2.1 mm, 2 µm column (MAC-MOD Analytical, Chadds Ford, PA) with mobile phase A as 0.1% formic acid in water and mobile phase B as acetonitrile. The flow rate was 350 µL/min with a column temperature of 25°C. Total LC run time was 20.5 minutes. The initial condition of 100% A at 0.35 mL/min was

held for 3 minutes then a linear gradient from 0-80% B for 10 min. To wash the column, 80% B was held for 3 min before going back to 0% B. For each sample, 4  $\mu$ L was injected for negative ion analysis and 2  $\mu$ L for positive ions.

*Data processing.* Data from positive and negative ion modes were processed separately. LC-MS files were first converted to open-format files (i.e. MzXML) using MSConvert (Proteowizard 3.0.10095). MZmine 2.23 was used to identify features, deisotope peaks, align features and perform gap filling to fill in any features that may have been missed in the first alignment algorithm<sup>226</sup>. All adducts and complexes were identified and removed from the data set prior to statistical analysis.

Statistical analyses were performed separately on the positive and negative ion data including both previously identified and unknown metabolites. Metaboanalyst 3.0<sup>227</sup> was used for statistical analysis using unpaired peak intensity tables in column format exported from MZmine. Data integrity, missing data estimation, and data filtering were first performed on the data set. Normalization of the samples to allow adjustment of differences among the samples was performed using normalization by sum (i.e. total ion signal). Log transformation and autoscaling were selected. Univariate analysis by ANOVA was performed. Chemometric analysis including Principal Component Analysis (PCA) and Partial Least Squares-Discriminant Analysis (PLS-DA) were conducted. Unsupervised clustering with visualization in a heat map was also done on the data set.

### **Compound Synthesis & Verification**

CC-122 and MYCMI-6 compounds were synthesized in collaboration with the Moffitt Chemical Biology Core. Steps for synthesis of these two drugs are displayed in **Figure 16**. Both compounds' purities were checked by NMR and HPLC.

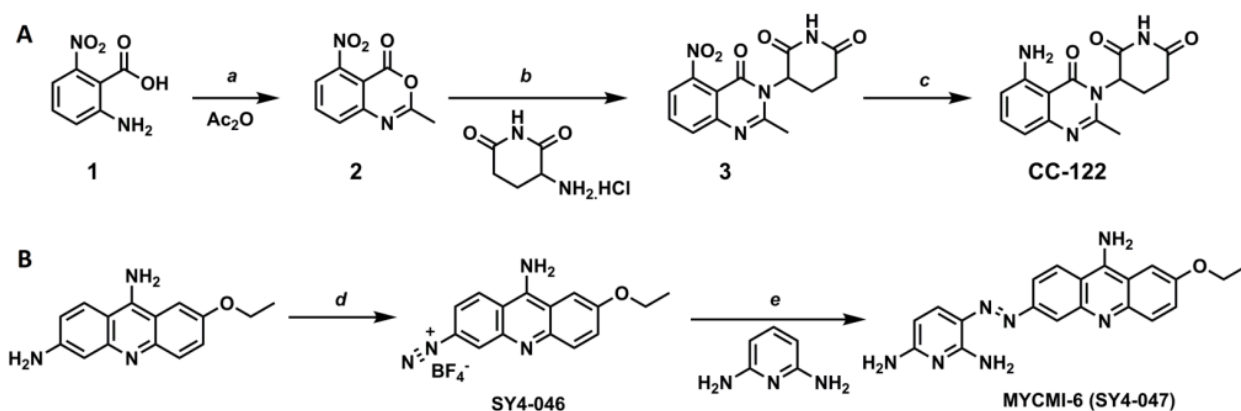


### Figure 16: Synthesis of compounds CC-122 & MYCMI-6

(A) Synthesis of CC-122; *Reagents and conditions.* (a) 200 °C, 30 min, 85%; (b) Pyridine, 140 °C, 18 h, 23%; (c) Pd(OH)<sub>2</sub>, H<sub>2</sub> (balloon), DMF, rt, 12 h, 51%; **B: Synthesis of MYCMI-6;** *Reagents and conditions.* (d) NaNO<sub>2</sub>, HCl, 0 °C; 2. HBF<sub>4</sub>; (e) 1. 2N HCl; 2. NaOAc.

### Cytotoxicity Assays

B16-OVA target cells (gift from Dr. S Pilon-Thomas) were treated with 10ng/mL of IFN $\gamma$  for 2 hours at 37°C and re-plated in a flat-bottom 96-well plate. Activated OT1 and OT1;*Crbr*<sup>-/-</sup> were then added at a 5:1 T cell to target ratio for 6 hours. LDH release in the media as per manufacturer's protocol and percent of target cells lysed was determined by the following equation:

$$\frac{\text{Experimental LDH} - \text{T cell spontaneous LDH} - \text{B16OVA spontaneous LDH}}{\text{B16OVA total LDH} - \text{B16OVA spontaneous LDH}} \times 100$$

### Statistical Analysis

P values were determined using GraphPad Prism Software (GraphPad Software, Inc, La Jolla, CA) by Student's t test, Mantel-Cox Log-rank test, or two-way ANOVA as listed in figure legend. Equal variance is assumed between groups. All data represented as mean with error bars representing  $\pm$  standard error. Number of animals in each group is listed in figure legends for experiments entailing biological replicates. Technical replicate experiments are

representative of 2-3 independent experiments and contain 3-6 replicates. Group sizes were based on prior experience with similar studies.

### Critical Resources and Reagents

Critical assays, reagents, and mice purchased from commercial sources or received from academic sources are listed in **Table 6**.

**Table 6: Critical Reagents and Resources For Chapter Two**

REAGENT or RESOURCE	SOURCE	IDENTIFIER
<b>Antibodies</b>		
CRBN	Abcam	#ab139408
c-Myc	Cell Signaling Technology	#5605
IKZF1	Cell Signaling Technology	#5443
CK1 $\alpha$	Cell Signaling Technology	#2655
IRF4	Cell Signaling Technology	#4948
Monoclonal Anti-Actin antibody produced in mouse	Sigma	#A4700
CD3e Monoclonal Antibody (145-2C11), Functional Grade	ThermoFisher	#16-0031-81
CD28 Monoclonal Antibody (37.51), Functional Grade	ThermoFisher	#16-0281-81
CD3 Monoclonal Antibody (HIT3a), Functional Grade	ThermoFisher	#16-0039-81
CD28 Monoclonal Antibody (CD28.2), Functional Grade	ThermoFisher	#16-0289-85
CD69-PE-CF594	BD Biosciences	Clone: H1.2F3
CD3, mouse, multiple fluorochromes used	Biolegend, BD Biosciences or Tonbo	Clone: 17A2
CD3-APC, human	Tonbo	Clone: UCHT1
B220, mouse, multiple fluorochromes used	BD Biosciences or Biolegend	Clone: RA3-6B2
CD19,mouse, multiple fluorochromes used	Biolegend or Invitrogen	Clone: 6D5
NK1.1, mouse	BD Biosciences	Clone: PK136
CD8 $\alpha$ , mouse, multiple fluorochromes used	Biolegend, Tonbo or BD	Clone:53-6.7 or 2.43
CD4, mouse, multiple fluorochromes used	Biolegend, BD Biosciences or Tonbo	Clone: GK1.4 or RM4-5
CD25-APC, mouse	Tonbo	Clone: PC61.5
V $\alpha$ 2-PE, mouse	eBioscience	Clone: B20.1
V $\beta$ 5-FITC, mouse	eBioscience	Clone: MR9-4
CD98-PE, mouse	Biolegend	Clone: RL388
CD98-PE, human	BD Biosciences	Clone: UM7F8
CD44-BV510	Biolegend	Clone: IM7
CD127-PE-Cy7, mouse	Biolegend	Clone: A7R34
KLRG1-BV421, mouse	Biolegend	Clone: 2F1/KLRG1
IFN $\gamma$	BD Biosciences	Clone: XMG1.2

**Table 6 (Continued)**

IL-17A	BD Biosciences	Clone: TC11-18H10.1
IL-5	BD Biosciences	Clone: TRFK5
c-Myc, human/mouse, multiple colors used	Cell Signaling Technology	Clone:D84C12
Foxp3, multiple fluorochromes used	eBioscience	Clone: FJK-16s
PD1-PE	Tonbo	Clone: J43.1
B-actin	Sigma	#A3854-200
<b>Biological Samples</b>		
Human PBMCs	One Blood, St Petersburg, FL	N/A
<b>Chemicals, Peptides, and Recombinant Proteins</b>		
OVA (257-264)	Anaspec	#AS-60193-1
OVA-A2 Peptide, SAINFEKL, OVA (257-264) Variant	Anaspec	#AS-64383
OVA-G4 Peptide, SIIGFEKL, OVA (257-264) Variant	Anaspec	#AS-64384
TRP - 2 (180 - 188)	Anaspec	#AS-61058
Recombinant Murine IL-2	Peptotech	#212-12
Recombinant Murine IFN $\gamma$	Peptotech	#315-05
2-Deoxy-D-glucose	Sigma	#D8375
Oligomycin A	Sigma	#75351
$^{13}\text{C}_4$ -putrescine	Cambridge Isotope Labs	# CLM-6574
$^{13}\text{C}_5$ -ornithine	Cambridge Isotope Labs	#CLM-4724
1,1,2,2,3,3,4,4-D $_8$ -N-(3-Aminopropyl) Butane-1,4-Diamine:3HCL	Cambridge Isotope Labs	#DLM-9262
1,1,2,2,3,3,4,4-D $_8$ -N,N'-Bis(3-Aminopropyl)-1,4-Butanediamine:4HCL	Cambridge Isotope Labs	#DLM-9262
HPLC Grade Water	Honeywell Chemicals	#AH3654
HPLC Grade Methanol	Honeywell Chemicals	#AH2304
HPLC Grade Acetonitrile	Honeywell Chemicals	#AH0154
Formic Acid	Thermo Fisher	#PI28905
Accucore C18 Column 150 x 3.0 mm, 2.6 $\mu\text{m}$	Thermo Fisher	#27826-153030
Ionomycin	Thermo Fisher	#I24222
Fluo4AM	Thermo Fisher	#F14217
Heptafluorobutyric acid	ProteoChem	#LC6206
Hyaluronidase V	Sigma	#H6254
Collagenase type I	Sigma	#SCR103
Collagenase type IV	Sigma	#C5138
DNase I	Sigma	#DN25
JQ-1	Sigma	#SML0974
10074-G5	Sigma	#G3798
RIPA buffer	Sigma	#R0278
Recombinant Mouse IL-2 Protein	R&D Systems	#402
L-TYROSINE (RING- $^{13}\text{C}_6$ , 99%)	Cambridge Isotope Labs	#CLM-1542
L-TRYPTOPHAN ( $^{13}\text{C}_{11}$ , 99%)	Cambridge Isotope Labs	#CLM-4290-H-PK
L-LEUCINE ( $^{13}\text{C}_6$ , 99%)	Cambridge Isotope Labs	#CLM-2262-H-PK

**Table 6 (Continued)**

L-PHENYLALANINE (RING- <sup>13</sup> C <sub>6</sub> , 99%)	Cambridge Isotope Labs	#CLM-1055-0
N-BOC-L-tert-Leucine, 98%	Acros Organics	#368010010
N-BOC-L-Aspartic acid, 99%	Acros Organics	#303210010
BOC-L-Tyrosine, 99+%	Acros Organics	#275700050
Nalpha-BOC-L-Tryptophane, 97%	Acros Organics	#275690050
BOC-D-Phenylalanine, 99+%	Acros Organics	#275740050
Calcium Chloride	Sigma	#C4901
Creatine-d <sub>3</sub> H <sub>2</sub> O (methyl-d <sub>3</sub> )	CDN isotopes	#D-1972
D-Leucine-d <sub>10</sub>	CDN isotopes	#D-5607
L-Tryptophan-2,3,3-d <sub>3</sub>	CDN isotopes	#D-7419
Water with 0.1% Formic Acid (v/v), Optima™ LC/MS Grade	Fisher Scientific	#LS1184
Citric acid ( <sup>13</sup> C <sub>6</sub> , 99%)	Cambridge Isotope Labs	#CLM-9021
GLUTAMINE, L-[14C(U)]	American Radiolabeled Chemicals	#ARC0196-50
Arginine L-[14C(U)]	Perkin Elmer	#NEC267E050UC
<b>Critical Commercial Assays</b>		
IFN gamma Mouse ELISA Kit	ThermoFisher	#KMC4022
Seahorse XF Cell Mito Stress Test Kit	Agilent	#103015-100
Mouse IL-2 Recombinant Protein, eBioscience	Invitrogen	#14-8021-64
Mouse IL-17 Quantikine ELISA Kit	R&D systems	#M1700
Mouse IL-10 Quantikine ELISA Kit	R&D systems	#M1000B
Mouse TNF-alpha Quantikine ELISA Kit	R&D systems	#MTA00B
Mouse IFN-gamma Quantikine ELISA Kit	R&D systems	#MIF00
Mouse IL-4 Quantikine ELISA Kit	R&D systems	#M4000B
Pierce™ LDH Cytotoxicity Assay Kit	Thermo Fisher	#88953
Hexokinase Activity Assay Kit (Colorimetric)	Abcam	#ab136957
NAD/NADH-Glo™ Assay	Promega	#G9071
GeneChip™ Mouse Genome 430 2.0 Array	Thermo Fisher	#900495
Qubit Protein Assay Kit	Thermo Fisher	#Q33211
MessageAmp™ Premier RNA Amplification Kit	Thermo Fisher	#AM1792
ATPlite Luminescence Assay System, 300 Assay Kit	Perkin Elmer	#6016943
<b>Deposited Data</b>		
Microarray data	Gene Expression Omnibus	GSE81725
<b>Experimental Models: Cell Lines</b>		
B16-F10	ATCC	#CRL-6475
B16-OVA	N/A	
<b>Experimental Models: Organisms/Strains</b>		
C57Bl6	Jackson	#000664
CD45.1	Jackson	#002014
OT1	Jackson	#003831
BALB/cJ	Jackson	#000651
<i>Crbn</i> <sup>-/-</sup>		N/A
<b>Oligonucleotides</b>		

**Table 6 (Continued)**

Mm00487804_m1 Myc	ThermoFisher	#4331182
Mm01182414_m1 Crbn	ThermoFisher	#4351372
Mm00437762_m1 B2m	ThermoFisher	#4331182
Mm00446971_m1 Tbp	ThermoFisher	#4331182
RT-PCR Primers (Supplemental Table)	IDT	N/A
Genotyping primers (Supplemental Table)	IDT	N/A
<b>Software and Algorithms</b>		
Graphpad V7	GraphPad Software	
Flowjo V10	BD	
Metaboanalyst 4.0	<a href="http://www.metaboanalyst.ca/">http://www.metaboanalyst.ca/</a>	
Xcalibur Quan Browser	Thermo Fisher	
Partek	Partek, Inc.	
Gene Go	Thomson Reuters	
ImageJ	<a href="http://imagej.nih.gov/ij/">http://imagej.nih.gov/ij/</a>	
MZmine	<a href="http://mzmine.github.io/">http://mzmine.github.io/</a>	
MSConvert	<a href="http://proteowizard.sourceforge.net/">http://proteowizard.sourceforge.net/</a>	
Wave version 2.6	Agilent Technologies	
<b>Other</b>		
Pan T cell Isolation Kit II, mouse	Miltenyi	#130-095-130
CD8a+ T cell Isolation Kit, mouse	Miltenyi	#130-104-075
CD4+ T cell Isolation Kit, mouse	Miltenyi	#130-104-454
B cell Isolation Kit, mouse	Miltenyi	#130-090-862
CD3e Microbead Kit, mouse	Miltenyi	#130-094-973
EasySep™ Mouse T Cell Isolation Kit	Stemcell	#19851
RosetteSep Human T cell Enrichment Cocktail	Stemcell	#15061
CD4 Microbeads, human	Miltenyi	#130-045-101
Leukocyte Activation Cocktail, with BD GolgiPlug™	BD Biosciences	#550583
CellTrace Violet	Molecular Probes	#C34557
iTAgiTAG Tetramer/PE – H-2 Kb OVA (SIINFEKL)	MBL	#T0300
2-NBDG (2-(N-(7-Nitrobenz-2-oxa-1,3-diazol-4-yl)Amino)-2-Deoxyglucose)	Molecular Probes	#N13195
Zombie NIR	Biolegend	# 423105
Ghost Dye Red 780	Tonbo	#13-0865-T500
MitoTracker Green	Thermo Fisher	# M7514
7-AAD	BD Biosciences	#559925
DAPI (4',6-Diamidino-2-Phenylindole, Dihydrochloride)	Thermo Fisher	#D1306
Live/Dead Yellow	Molecular Probes	
CD3 Microbead Kit	Miltenyi	#130-094-973
Power SYBR™ Green PCR Master Mix	Thermo Fisher	#4367659
Taqman Universal PCR Master Mix	Thermo Fisher	#4304437
iPrep™ Trizol™ Plus RNA Kit	Thermo Fisher	#IS10007
eBioscience™ Foxp3 / Transcription Factor Staining Buffer Set	Thermo Fisher	#00-5523-00
iScript™ Reverse Transcription Supermix for RT-qPCR	Bio-Rad	#1708841
RNeasy Plus Mini Kit	Qiagen	#74134

**Table 6 (Continued)**

RPMI Media	Thermo Fisher	#11875
Zirconia Beads	Biospec Products	#11079107zx
iTAg Tetramer/APC - H-2 Kb TRP2 (SVYDFFVWL)	MBL	#T03015



## CHAPTER THREE: THE ROLE OF POLYAMINES IN ACTIVATED CD8<sup>+</sup> T CELLS

### Introduction

It remains to be determined what role polyamines serve in CD8<sup>+</sup> T cells aside from a well-defined role in proliferation<sup>13</sup>. Here, we report how polyamines are generated in activated CD8<sup>+</sup> T cells, and using DFMO to block polyamine production, we demonstrate that this pathway controls glycolysis, IFN $\gamma$  production, and is necessary for asymmetric division.

### Results

#### **Glutamine is carbon source of polyamine biosynthesis in antigen-activated CD8<sup>+</sup>**

#### **T cells**

The OT-1 mouse model with defined specificity for the OVA-derived peptide, SIINFEKL (N4), is a useful model to investigate pathways involved in the antigen activation of CD8<sup>+</sup> T cell. SIINFEKL peptide treatment for 24 hours activates oxygen consumption and extracellular acidification of OT-1 CD8<sup>+</sup> T cells relative to treatment with the tyrosinase-related protein 2 (Trp2) used as a non-activating peptide control (**Figure 17A-B**). Broad expression of amino acid transporters is evident within 24 hours in activated versus non-activated OT-1 cells (**Figure 17C**). These transporters include the general glutamine transporter, *SLC1A5*, the arginine cation transporter, *SLC7A1*, other cationic family members, the large subunit of the neutral amino acid transporter CD98, *SLC3A2*, and two glutamine transporters relevant to T cell biology, *SLC38A1* and *SLC38A2*, suggesting that these cells can actively transport many amino acids including glutamine and arginine. Both arginine and glutamine can serve as carbon

sources in the biosynthesis of polyamines, and the influx of both  $^{14}\text{C}$ -L-Arg and  $^{14}\text{C}$ -L-Gln is specifically induced after stimulation with the N4 versus Trp2 peptide (**Figure 17D**). To determine if polyamine levels and the polyamine biosynthetic pathway is relevant after antigen activation, we studied the expression of *Odc* mRNA and enzyme function, *Oat*, *Aldh18a1*, *Srm*, and *Sms* enzymes in OT-1 cells receiving N4 and Trp2 treatment (as shown in **Figure 17E-G**) and indicated schematically in **Figure 17F**. Notably, all of these enzymes were increased in activated OT-1 CD8<sup>+</sup> T cells.

Given that both arginine and glutamine uptake is significantly increased with TCR stimulation, activated CD8<sup>+</sup> T cells were labeled with  $^{13}\text{C}$ -arginine or  $^{13}\text{C}$ -glutamine to fully label the intracellular arginine and glutamine pools (**Figure 18A-C**). Activated CD8<sup>+</sup> T cells labeled with  $^{13}\text{C}$ -glutamine had significantly higher incorporation of carbons into ornithine, putrescine, spermidine, and spermine compared to pools labeled from  $^{13}\text{C}$ -arginine (**Figure 18D**) despite the higher levels of arginine uptake (**Figure 18D**) in activated T cells. This suggests that polyamine pools may be primarily derived from the precursor glutamine. Indeed, overall intracellular levels of  $^{13}\text{C}$ -glutamine were significantly decreased compared to  $^{13}\text{C}$ -arginine, suggesting that glutamine may be more actively metabolized following activation (**Figure 18E**). To confirm that polyamines are derived from glutamine, activated CD8<sup>+</sup> T cells were cultured with the glutamine antagonist, 6-Diaza-5-oxo-L-norleucine (DON) to block glutaminase activity. Intracellular ornithine and polyamines were decreased by treatment with DON (**Figure 18F**), confirming that glutamine contributes to polyamine biosynthesis in antigen-activated CD8<sup>+</sup> T cells.

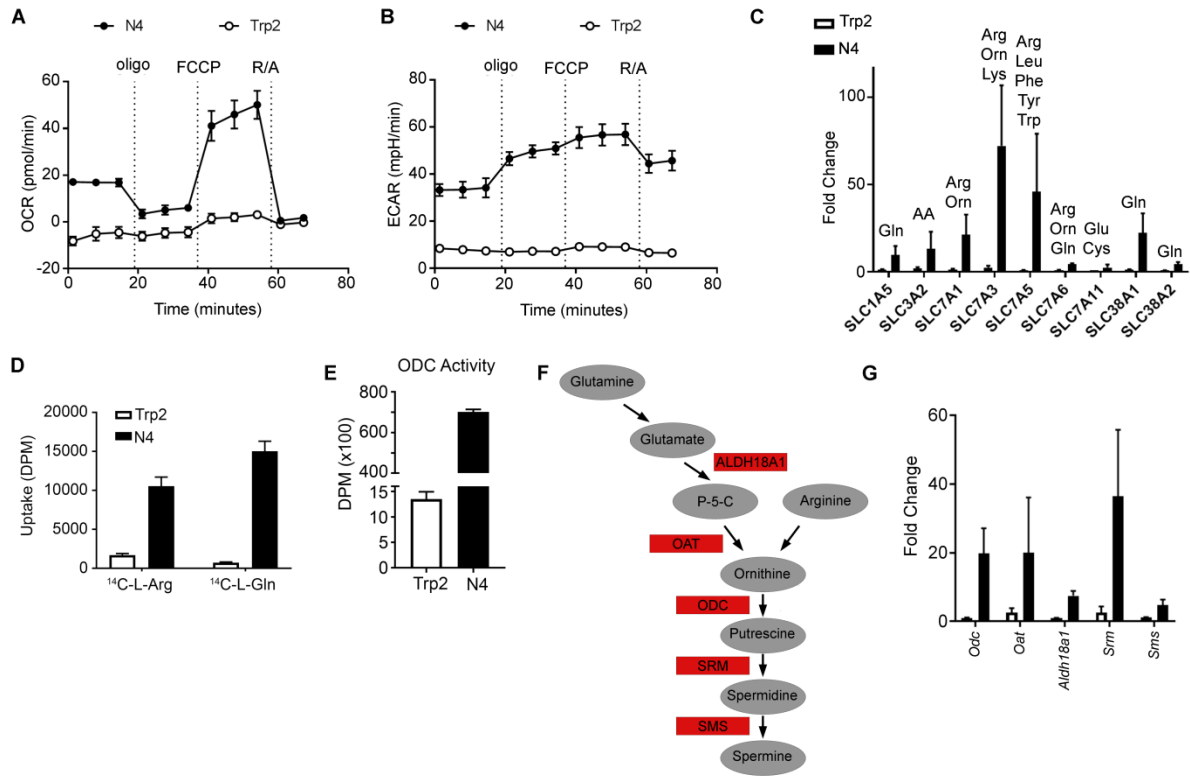


**Figure 17: Antigen activation of CD8<sup>+</sup> T cells increases glutamine and arginine metabolism.** (A-B) Oxygen consumption (OCR) and extracellular acidification (ECAR) rates of OT-1 CD8<sup>+</sup> T cells activated with N4 or Trp2 peptides for 24 hours; (C) RT-PCR for amino acid transporters; (D) Uptake of  $^{14}\text{C}$ -Arginine and  $^{14}\text{C}$ -Glutamine; (E) Relative ornithine decarboxylase; (F) RT-PCR for enzymes in the ODC & polyamine pathway

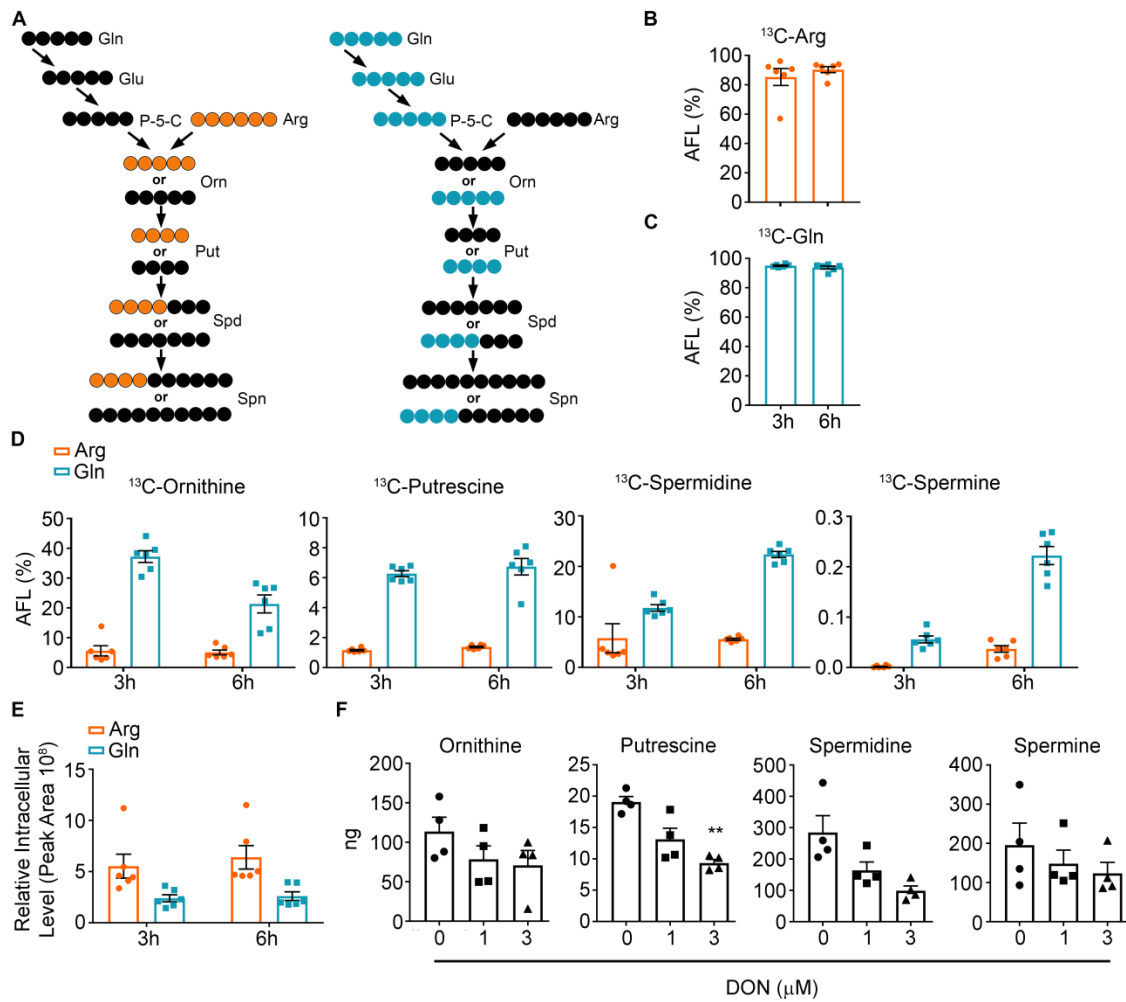


**Figure 18: Polyamines are primarily derived from glutamine.** (A) Isotope labeling strategy for fully-labeled arginine (orange) and glutamine (blue). Colored dots represent  $^{13}\text{C}$  molecules measured against fully black molecules to calculate apparent fractional labeling (AFL); (B-C) Percent of  $^{13}\text{C}$ -Arginine and  $^{13}\text{C}$ -Glutamine among total arginine and glutamine; (D) Percent  $^{13}\text{C}$ -Ornithine,  $^{13}\text{C}$ -Putrescine,  $^{13}\text{C}$ -Spermidine and  $^{13}\text{C}$ -Spermine among total of these molecules; (E) Total intracellular glutamine and arginine levels; (F) Total intracellular ornithine and polyamine levels with and without DON treatment during activation.

### **Polyamine production is necessary for expression of T-box transcription factors involved in the $\text{CD8}^+$ effector phenotype and for viability**

Given the significant increase in polyamine production after TCR activation, the role of polyamines in the phenotype of activated  $\text{CD8}^+$  T cells was next assessed with the ODC inhibitor, difluoromethylornithine (DFMO) (**Figure 19A**) that blocks the rate-limiting step of polyamine biosynthesis<sup>168</sup>. Expression of early activation markers, CD69 and CD25, were not

altered by DFMO treatment (**Figure 19B**), demonstrating that ODC blockade does not impact the TCR activation signaling cascade that leads to the expression of early activation antigens (as detailed in the **Introduction**). The *Tbx21* gene, encoding the transcription factor T-bet, and the gene eomesodermin (*Eomes*) are critical regulators of CD8<sup>+</sup> T cell function and differentiation<sup>81,82,228</sup> and differentially regulate short-and long-lived memory precursor populations<sup>229,230</sup>. Titrating down T-bet expression, especially relative to Eomes, has been associated with shorter-lived cells because Eomes can induce CD122 (IL-2R $\beta$  chain) that is responsible for IL-15 signaling, a cytokine that drives CD8<sup>+</sup> T cell memory<sup>231</sup>. In addition to effector and memory differentiation, T-bet and EOMES are differentially associated with T cell exhaustion during viral infection and during cancer immunotherapy. A T-bet<sup>dim</sup>Eomes<sup>hi</sup> expression profile has been linked to better long-term viral control during chronic human immunodeficiency virus infection<sup>232</sup> but higher T-bet-expressing CD8<sup>+</sup> T cells is associated with effector functions of tumor infiltrating cells<sup>233</sup>. Treatment with DFMO decreases the proportion of T-bet expressing CD8<sup>+</sup> T cells post-activation but does not change the expression of Eomes (**Figure 19C-D**), suggesting that polyamine blockade could increase long-term T-bet<sup>dim</sup>Eomes<sup>hi</sup> memory populations. Treatment with DFMO during TCR activation, however, reduces cellular viability (**Figure 19E**) and eventually leads to activation of caspase 3/7 expression (**Figure 19EF**), suggesting that cell death by reduced polyamine production leads to the enrichment of Tbet<sup>dim</sup>Eomes<sup>hi</sup> CD8<sup>+</sup> T cells.

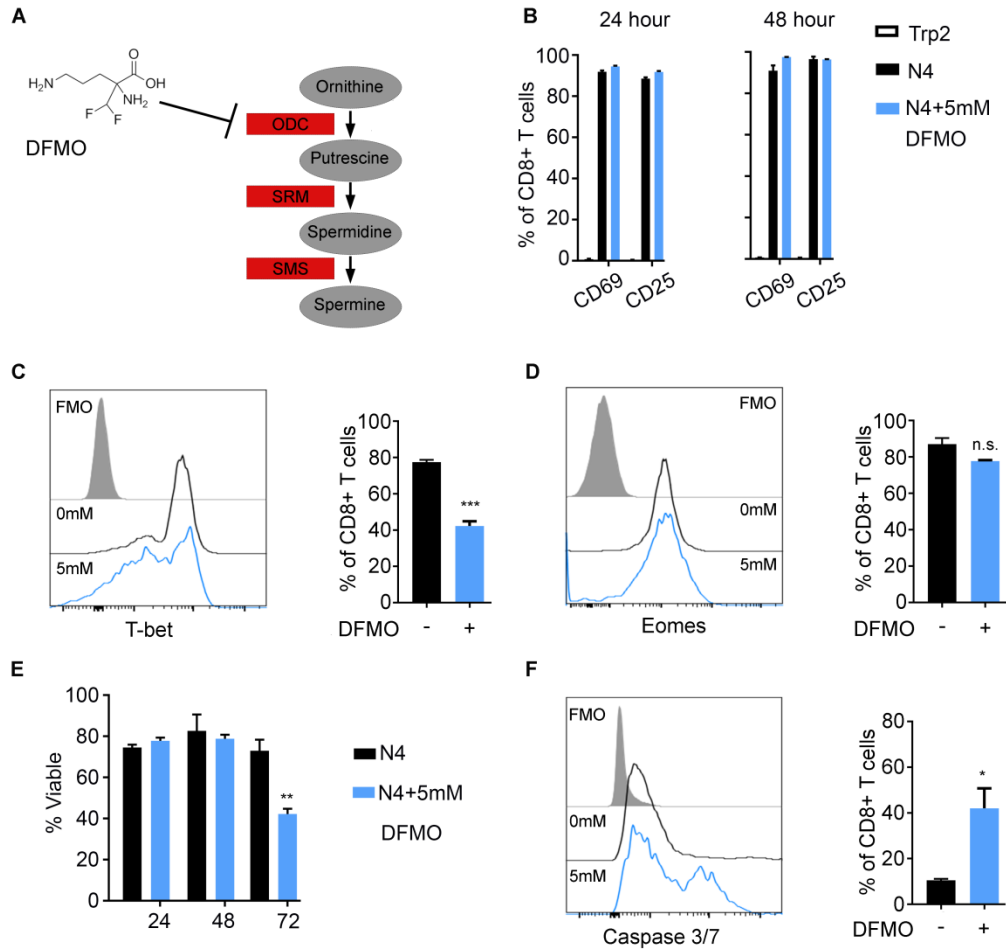


**Figure 19: Polyamine Production blockade decreases T-bet-expressing cells but increases cell death.** (A) DFMO is an irreversible inhibitor of ornithine decarboxylase (ODC); (B) Cell surface expression for activation markers CD25 and CD69 after 24-48 hours exposure of DFMO; (C-D) Percent of CD8<sup>+</sup> T cells expressing transcription factors T-bet and Eomes after 72 hour activation with and without DFMO; (E) Percent of viable cells over time during activation with and without DFMO; (F) Percent of CD8<sup>+</sup> T cells with high Caspase 3/7 activity after 72 hours of DFMO treatment during activation. \* $p < 0.05$ , \*\* $p < 0.01$ , \*\*\* $p < 0.001$

### Polyamine production is necessary for activated CD8<sup>+</sup> T cells to asymmetrically divide

Consistent with other studies using ODC<sup>13</sup> blockade, DFMO-treated CD8<sup>+</sup> T cells displayed a reduced cell trace violet dilution (**Figure 20A**). Interestingly, this occurs without impacting S-phase transition as the entire population progresses through the first round of division. The cell proliferation arrest was reversed by putrescine indicating that the impact of DFMO is caused by the specific depletion of this metabolite. During early rounds of division

following TCR stimulation, activated CD8<sup>+</sup> T cells undergo a unique process known as asymmetric cell division (ACD). Differential expression of CD8 on the cell surface and differential expression of the transcription factor Myc are hallmarks of this phenotype<sup>14</sup>. Specifically, CD8<sup>lo</sup>/Myc<sup>lo</sup> CD8<sup>+</sup> T cells have decreased glycolytic rates relative to CD8<sup>hi</sup>/Myc<sup>hi</sup> T cells and exhibit a propensity to form long-term anti-viral immunity *in vivo* in chronic infections<sup>14,234</sup>. Evidence suggests that glutaminolysis regulates Myc distribution relative to CD8 cell surface expression<sup>14</sup>. Given that we have shown that glutamine is the preferred carbon source of polyamine production (**Figure 18E-G**), we reasoned that polyamines may be involved in the ACD process. To more efficiently study this process, polyclonal T cells were derived from the Myc-eGFP reporter mice in which enhanced GFP is inserted into exon 2 creating an N-terminal EGFP/Myc protein<sup>235</sup>, and were activated with anti-CD3 and anti-CD28 +/- DFMO. CD8 populations were defined within the first round of division using dilution of CellTrace Violet and staining with CD8 (**Figure 20B**). DFMO treatment reduced CD8 cell surface expression during the first round of division (**Figure 20B**) compared to control treated cells, which resulted in an enrichment of CD8<sup>lo</sup> T cells and a decrease in the CD8<sup>hi</sup> population (**Figure 20C**).

The master metabolic regulator Myc is distributed with CD8 cell surface expression during ACD, such that within the first round of division, CD8<sup>hi</sup> cells express higher Myc protein and CD8<sup>lo</sup> cells express lower Myc protein<sup>14</sup>. Interestingly, Myc is a transcriptional activator of *Odc* mRNA<sup>236</sup> and there is a positive feed-back loop where polyamines regulate the translation of Myc protein<sup>202,237</sup>. DFMO treatment suppressed the average Myc-GFP protein expression in all activated CD8<sup>+</sup> T cells (**Figure 20D**) consistent to an accumulation of CD8<sup>lo</sup>/Myc<sup>lo</sup> cells in the first round of division. DFMO-treated CD8<sup>+</sup> T cells were then divided into CD8<sup>hi</sup> and CD8<sup>lo</sup> cells. Notably, Myc protein expression was decreased in both populations (**Figure 20E**), demonstrating that polyamines are required for the distribution of Myc during ACD.

Polyamines control protein translation through the hypusination pathway in which the aminobutyl group of spermidine is transferred as hypusine to eukaryotic translation initiation

factor 5A (eIF5A) and becomes hydroxylated to become the active form, hypusinated eIF5A<sup>165</sup> (**Figure 21A**). Hypusinated eIF5A broadly impacts protein translation as an elongation factor, and the enzymes that direct hypusination of eIF5A are increased in antigen-activated CD8<sup>+</sup> T cells (**Figure 21B**). The activation of eIF5A can be inhibited by the spermidine mimetic GC7, which blocks the enzyme responsible for transferring the aminobutyl group to eIF5A (**Figure 21A**). Similar to treatment of activated CD8<sup>+</sup> T cells with DFMO, targeting the hypusination pathway significantly decreased proliferation in response to TCR stimulation (**Figure 21C**). First-generation CD8<sup>+</sup> T cells treated with GC7, however, had no major alterations in CD8<sup>hi</sup> and CD8<sup>lo</sup> populations (**Figure 21D-E**). Indeed, first generation CD8<sup>+</sup> T cells treated with GC7 had normal distribution of Myc in addition to the normal distribution of CD8 (**Figure 21F**). Moreover, GC7 maintained the positive relationship between CD8 and Myc that is disrupted by DFMO (**Figure 21G-I**). These results suggest that putrescine plays a critical, previously unidentified role, in differentially distributing Myc and CD8 during ACD independent of other polyamines such as spermidine which is involved in controlling hypusination of eIF5A. Moreover, this suggests that DFMO treatment and blockade in polyamine production with PTIs may alter the memory T cell response during viral infection or cancer immunotherapy.



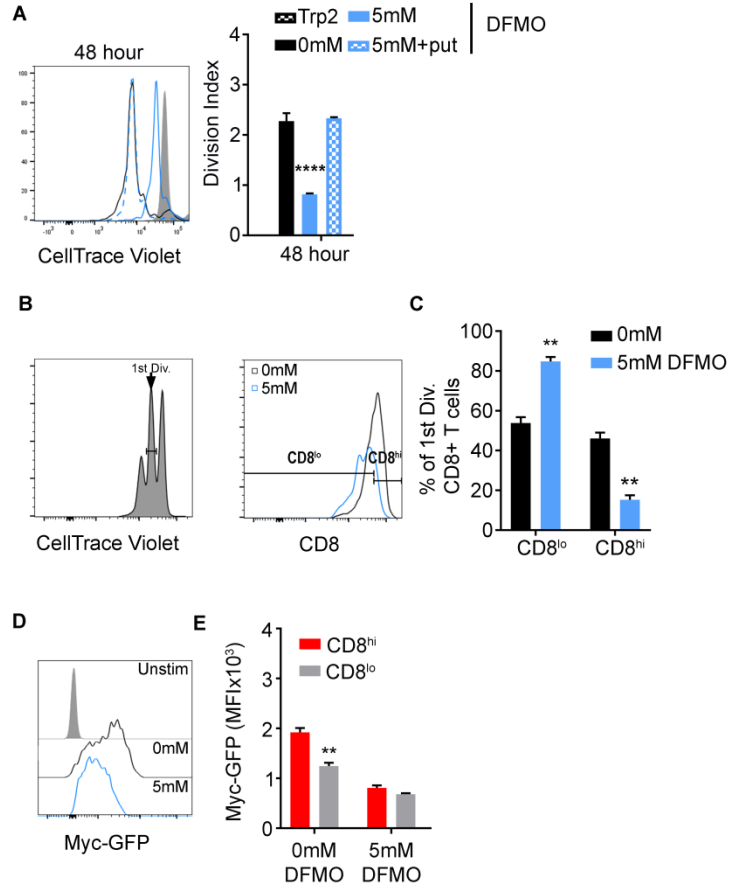


**Figure 20: Blocking polyamine biosynthesis alters asymmetric division.** (A) Average number of divisions (division index) after 48 hours of antigen activation with and without DFMO and the addition of 500  $\mu$ M putrescine; (B) Gating strategy to analyze asymmetric cell division; (C) Percent of CD8<sup>hi</sup> and CD8<sup>lo</sup> CD8<sup>+</sup> T cells within the first round of division after 48 hours of DFMO treatment; (D) Total Myc-GFP expression among all CD8<sup>+</sup> T cells; (E) Myc-GFP geometric mean fluorescent intensity (MFI) in first round of division CD8<sup>hi</sup> and CD8<sup>lo</sup> populations. \*\* $p < 0.01$ , \*\*\*\* $p < 0.0001$

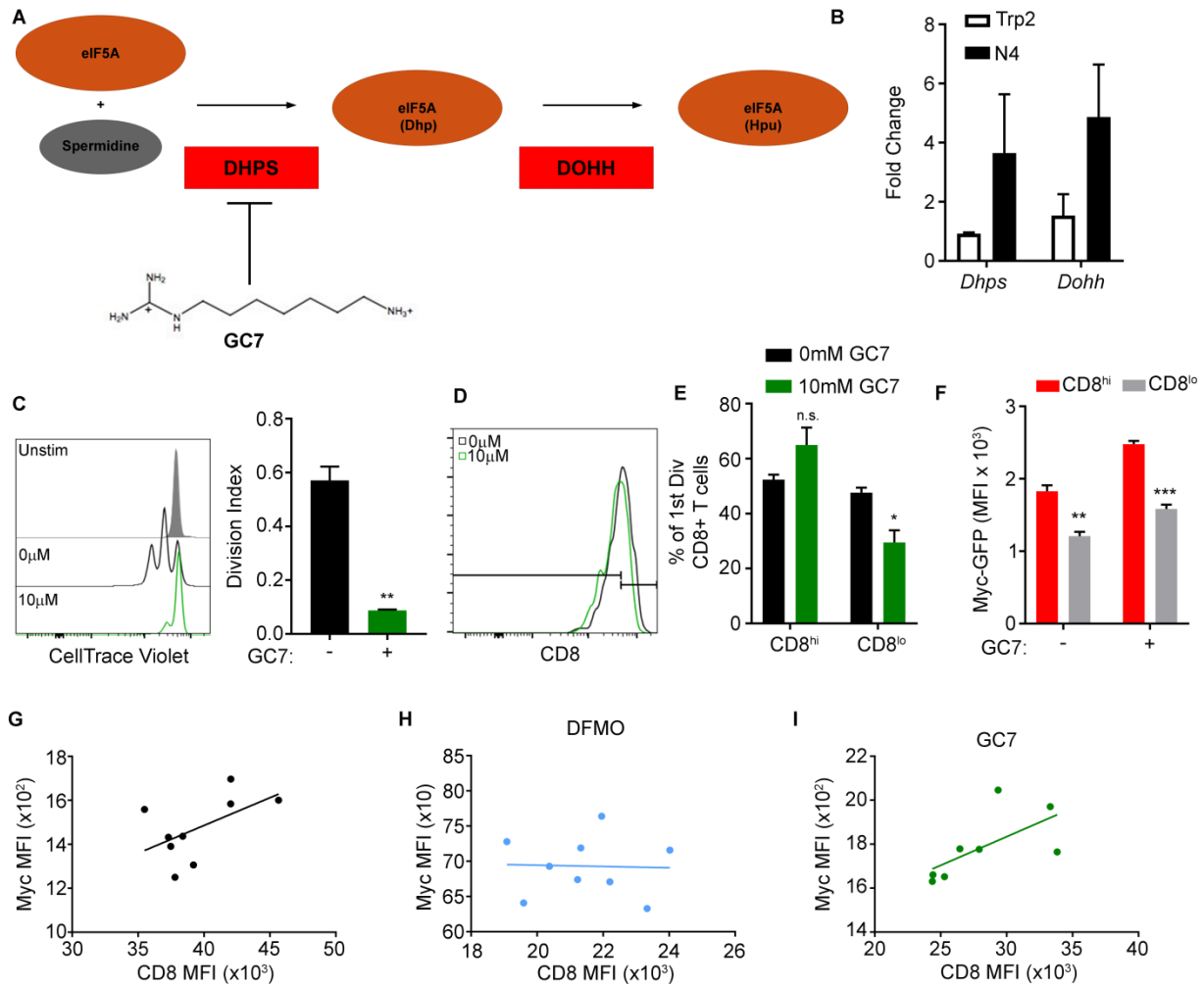


**Figure 21: Polyamine-driven asymmetric cell division is independent of hypusinated eIF5A.** (A) Hypusination pathway in which spermidine is used to create dehypusinated eIF5A to eventually become the activated hypusinated eIF5A; (B) mRNA expression of enzymes in the hypusination pathway after antigen activation; (C) CellTrace Violet histogram (left) and average number of divisions (right) after 48 hours of anti-CD3 and anti-CD28 activation; (D-E) CD8<sup>hi</sup> and CD8<sup>lo</sup> populations among the first round of division for CD8<sup>+</sup> T cells activated for 48 hours; (F) Myc-GFP geometric mean fluorescent intensity (MFI) in first round of division CD8<sup>hi</sup> and CD8<sup>lo</sup> populations; (G-I) MFI of CD8 versus MFI of Myc within the first round of division. \*p<0.05, \*\*p<0.01, \*\*\*p<0.001

### Inhibition of polyamines decreases glycolysis and increases oxidative phosphorylation

To further elucidate which signaling pathways are altered by polyamines, DFMO-treated activated CD8<sup>+</sup> T cells were subjected to RNA-seq analysis. These results revealed that

polyamine blockade significantly alters the expression of many genes (**Figure 22A**). Transcripts were further analyzed using previously-defined KEGG pathways. Both glycolysis and fatty acid metabolism pathways are significantly decreased by DFMO treatment (**Figure 22B**,  $p=0.016$  &  $0.001$  respectively). Interestingly, we found that cysteine and methionine metabolism and oxidative phosphorylation (OxPhos) were increased in DFMO-treated T cells, though OxPhos was not significant (**Figure 22B**,  $p=0.011$  &  $0.194$  respectively).

Metabolic changes in activated T cells have downstream effects on effector function so global metabolomic profiling of DFMO-treated CD8<sup>+</sup> T cells was conducted by LC/MS (as described in **Chapter Two**). Several metabolites were changed after DFMO treatment including both amino acids and glycolytic intermediates (**Figure 23A**). Reductions in glycolysis were confirmed by the Seahorse SF analyzer where glycolytic rates were suppressed by DFMO treatment (**Figure 23B**), consistent with the RNA-seq data. Conversely, the mitochondrial stress test demonstrated that basal oxygen consumption rates were minimally affected by DFMO treatment, and that these drug-treated cells have significantly increased spare respiratory capacity (SRC) after FCCP (**Figure 23C**). Consistent with higher mitochondrial respiration, an increase in mitochondrial biomass was observed through mitotracker green staining (**Figure 23D**).

Next, a modified Seahorse mitochondrial stress test was performed on DFMO-treated OT-1 CD8<sup>+</sup> T cells (**Supplemental Figure 23E-H**) to acutely suppress glycolysis, glutaminolysis and fatty acid oxidation in order to define the fuel source contributing to the increased levels of SRC. Interestingly, acutely blocking glycolysis by injecting 2-deoxyglucose (2-DG) decreased the SRC of DFMO-treated CD8<sup>+</sup> T cells as well as severely decreasing ATP production (**Figure 23H-J**). This suggests that glucose transport and utilization accounts for the increase in SRC in DFMO-treated cells. The acute blockade of glutaminolysis by DON also decreased SRC without impacting ATP production (**Figure 23G, I-J**). Further, blocking Cpt1a and fatty acid oxidation by etomoxir had no effect on oxygen consumption or ATP production by CD8<sup>+</sup> T cell

with and without DFMO treatment (**Figure 23F, I-J**). Therefore, glucose and glutamine fuel the enhanced SRC of DFMO-treated antigen-activated CD8<sup>+</sup> T cells.

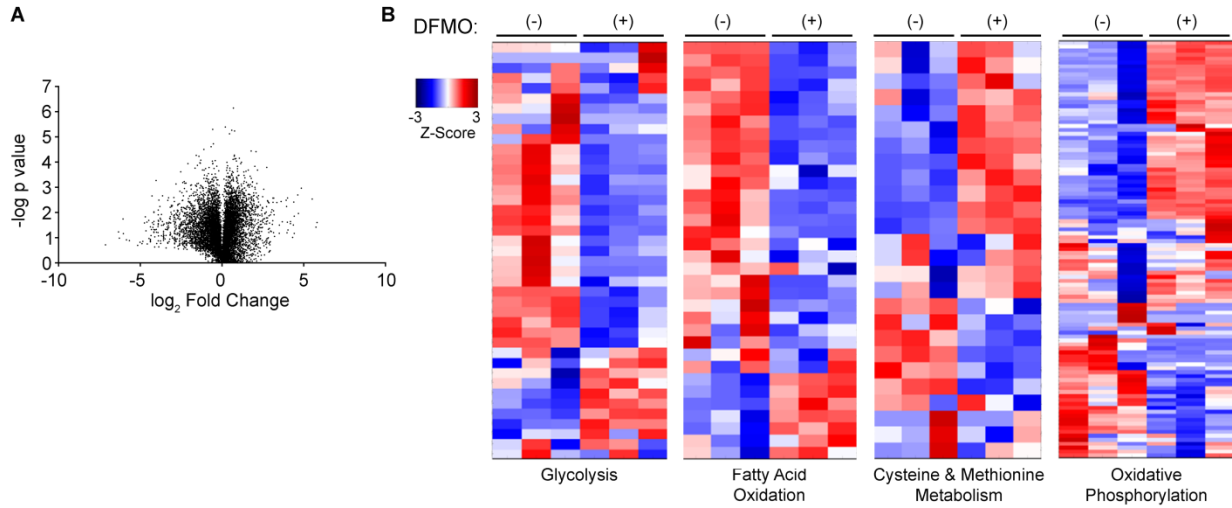


**Figure 22: RNA-seq analysis of DFMO-treated CD8<sup>+</sup> T cells activated for 48 hours.** (A) Fold change in transcription after 48 hours of DFMO treatment as well as p values of individual T tests; (B) Unsupervised clustering of transcriptional changes with and without DFMO treatment in KEGG-defined pathways: glycolysis, fatty acid oxidation, cysteine & methionine metabolism and oxidative phosphorylation.

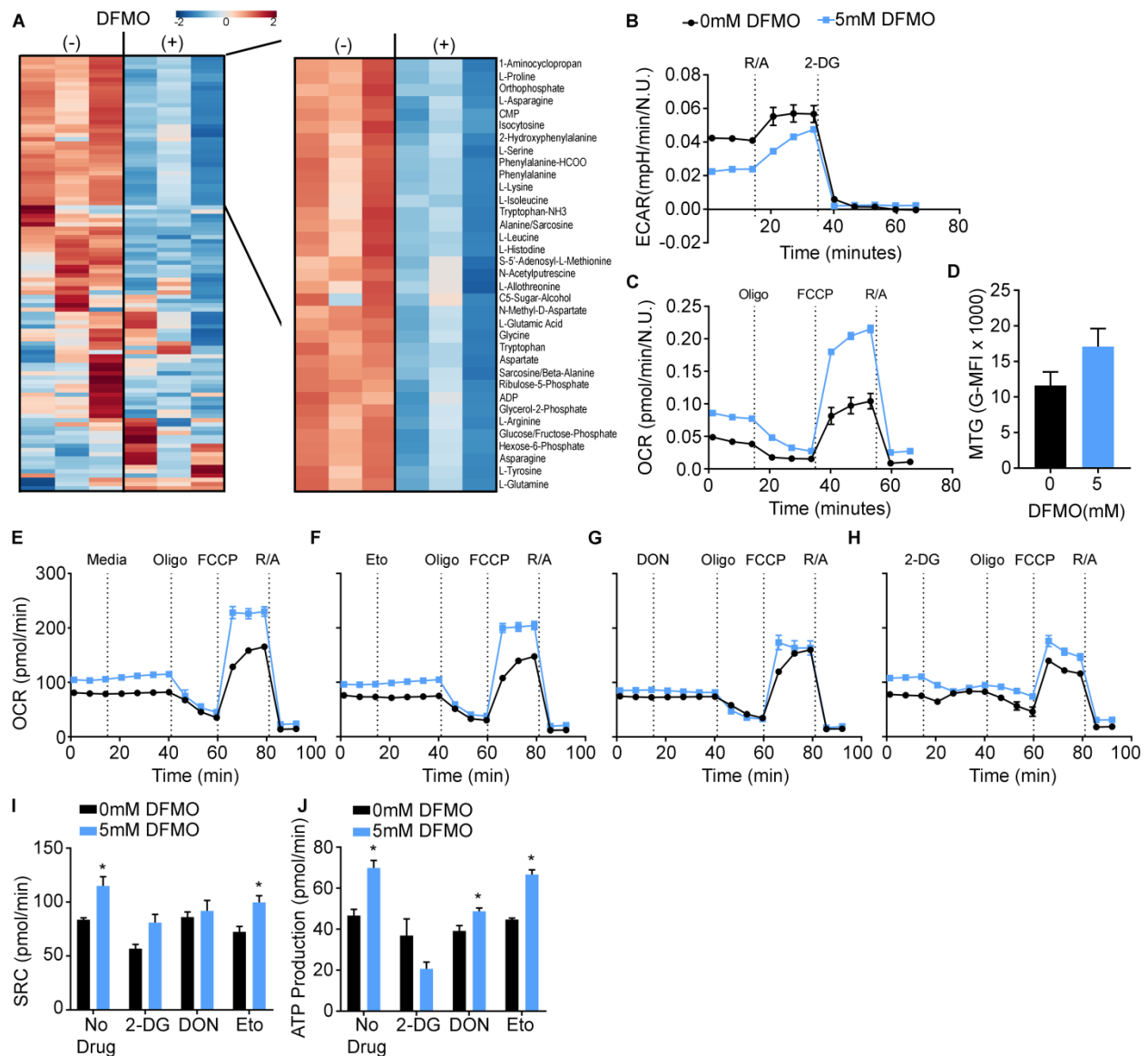


**Figure 23: DFMO treatment increases the spare-respiratory capacity of antigen activated CD8<sup>+</sup> T cells.** (A) Unsupervised clustering of annotated metabolites from a global metabolomics screening of CD8<sup>+</sup> T cells activated and treated with and without DFMO for 48 hours; (B-C) Seahorse analysis of extracellular acidification (ECAR) and oxygen consumption (OCR) using the glycolysis rate assay and mitochondrial stress test (MST); (D) Intracellular mitochondrial biomass as measured by the G-MFI of MitoTracker Green; (E-H) Oxygen consumption rates measured by a modified MST in which etomoxir, DON, 2-DG or Seahorse Media were injected prior to running the normal MST. (I) Spare respiratory capacity and ATP production as measured by oxygen consumption demonstrated in E-H. \*p<0.05

## Discussion

Here we demonstrate that TCR-specific stimulation increases intracellular polyamine levels, largely driven by the metabolism of glutamine rather than arginine. Blocking polyamine production profoundly alters gene expression and metabolic rates of activated CD8<sup>+</sup> T cells and revealed that polyamines play an important role in Myc and CD8 distribution during asymmetric division. The relative distribution of T-bet and Eomes following DFMO treatment also suggests that the T-box transcription factor balance is tipped toward Eomes. It is still unclear, however, if balanced T-bet and Eomes expression dictates the ultimate fate of activated CD8<sup>+</sup> T cells although T-bet deficiency favors the generation of central rather than short-lived effector cells.

Interestingly, our studies demonstrate that putrescine to play a specific and possibly critical role in asymmetric division. Specifically, DFMO treatment not only increased CD8<sup>lo</sup> T cells, but also disrupted the distribution of Myc and CD8 expression during asymmetric cell division, leading to **(Figure 20B-E, 21G-H)** higher percentages of CD8<sup>lo</sup>Myc<sup>lo</sup> cells which appears critical for CD8<sup>+</sup> T cell fate during chronic viral infection and possibly during anti-tumor immunity. Similar to DFMO-treated cells, previous studies have demonstrated CD8<sup>lo</sup>/Myc<sup>lo</sup> T cells have increased oxygen consumption and lower extracellular acidification compared to CD8<sup>hi</sup>Myc<sup>hi</sup>.

ACD directs T cell fate. Isolation and adoptive cell transfer of CD8<sup>lo</sup>/Myc<sup>lo</sup> cells isolated during the first round of division display significantly better recall responses *in vivo* after vaccination but poor initial viral clearance<sup>14</sup>. Given that DFMO treatment induces CD8<sup>lo</sup>Myc<sup>lo</sup> dominance during the first round of division, polyamine blockade could result in more CD8<sup>+</sup> T cell recall following vaccination. Investigating the role of polyamine production in this setting is important for understanding the role of polyamine metabolism in CD8<sup>+</sup> T cell differentiation and immunotherapy. For instance, during TIL or CAR-T cell production, the use of DFMO may

dampen T cell expansion but lead to more persistent memory cells *in vivo*, which has been identified as a key barrier to successful CAR-T<sup>238,239</sup>.

It is notable that glutamine is the primary source of CD8<sup>+</sup> T cells' polyamine production after TCR stimulation (**Figure 18E**). Arginine-derived ornithine has been demonstrated in activated CD4<sup>+</sup> T cells, but a competitive isotope tracer experiment like the one presented here has not been previously published<sup>44</sup>. Glutamine is an amino acid frequently found in low abundance in the tumor microenvironment. Therefore activated CD8<sup>+</sup> T cells' in the tumor microenvironment may have reduced polyamine levels. Many cancer cells increase amino acid metabolism and accumulate or secrete high levels of polyamines in the extracellular milieu<sup>240</sup>. Since putrescine has the ability to reverse the proliferative block induced by DFMO on CD8<sup>+</sup> T cells (**Figure 19A**), it is possible that activated CD8<sup>+</sup> T cells may transport excess polyamines to bypass ODC inhibition. Future studies are required to define the intracellular polyamine levels in CD8<sup>+</sup> T cells in the tumor setting and to define their polyamine transport capability. Polyamine transport suppression may decrease intracellular polyamine availability and suppress proliferation.

Metabolomics analysis showed lower glycolytic intermediates following DFMO treatment in OT-1 T cells (**Figure 23A**), concordant with a reduced extracellular acidification rate and reduced expression of the glycolytic enzymes (**Figure 23B, 22B**). The significant alterations in gene expression were not due to altered levels of TCR signaling since normal CD69 and CD25 cell surface expression were observed (**Figure 18B**). Normally, increases in glycolysis occurs after TCR stimulation, and this increases the rate at which pyruvate is converted into lactate over the rate that pyruvate is oxidized and shuttled into the mitochondria for use in the TCA cycle<sup>13,80,241-243</sup>. Despite these findings, acute inhibition of glycolysis by 2-DG severely decreased the spare respiratory capacity of DFMO-treated activated CD8<sup>+</sup> T cells (**Figure 23G, I-J**), suggesting some dependence on the glycolysis. However, 2-DG also inhibits the TCA cycle and its intermediates<sup>244</sup>, and thus it is plausible that DFMO augments the TCA cycle in CD8+ T

cells, allowing higher ATP production from pyruvate. Intracellular glutamine could also be converted into more alpha-ketoglutarate to fuel the TCA cycle in the presence of DFMO, given that one direction for glutamine to be metabolized is blocked. Further studies using isotopically labeled glutamine and glucose would confirm the effects of polyamine production on the TCA cycle. The preference for OxPhos observed after DFMO treatment is also consistent with an abundance of CD8<sup>lo</sup>/Myc<sup>lo</sup> populations during ACD.

Collectively, we have identified a crucial metabolic pathway in CD8<sup>+</sup> T cells, where suppression of polyamine biosynthesis alters proliferation, T-bet and Eomes expression and stimulates mitochondrial SRC and OxPhos. Thus, manipulating the polyamine pathway may be useful in the setting of immunotherapy. Future studies are required to assess the impact of polyamines on T cell fate determination.

## **Methods**

Methodology for mouse immune cell isolation, CD3<sup>+</sup> T cell and OT-1 CD8<sup>+</sup> T cell activation, flow cytometry, metabolomics, and statistical analysis is the same as in **Chapter Two**. Some critical reagents are listed previously in **Table 6**.

### **Mouse Husbandry**

OT-1 transgenic mice<sup>160</sup> and Myc-eGFP mice<sup>235</sup> were obtained from Jackson Lab. Stocks were maintained and bred at the H. Lee Moffitt Cancer Center and Research Institute under approved protocols by the Institutional Animal Care and Use Committee.

### **Isotope analysis**

Activated OT-1 T cells were washing in DMEM containing high glucose and no arginine, glutamine or lysine. Cells were then labeled with either 2 mM <sup>13</sup>C-Arginine (Cambridge Isotopes, fully labeled) and 2 mM <sup>12</sup>C-Glutamine (Gibco) or 2mM <sup>13</sup>C- Glutamine (Cambridge Isotopes, fully labeled) and 2 mM <sup>12</sup>C- Arginine (Sigma Aldrich) for 3 or 6 hours at 37°C at which time media was removed from the cells and pellets were immediately placed on ice.



For targeted isotope tracer analysis, 5  $\mu\text{L}$  of each sample was analyzed using an ultra-high performance liquid chromatograph (Vanquish, ThermoFisher Scientific, San Jose, CA) interfaced with a QExactive HF mass spectrometer (ThermoFisher Scientific, San Jose, CA) using full MS and selected ion monitoring (SIM) for five labeled and unlabeled endogenous metabolites; arginine, putrescine, ornithine, spermine and spermidine. Samples were separated using an Accucore reversed phase C18 column (27826-153030, 2.1 mm ID x 100 mm length, 2.6  $\mu\text{m}$  particle size, ThermoFisher Scientific) at 350  $\mu\text{L}/\text{min}$ . A gradient starting at 20% B was held for 2 minutes, then ramped from 20% B to 50% B from 2 to 4 minutes and from 50% B to 80% B from 4 to 6 minutes; followed by re-equilibration over 3 minutes, for a total of 9 minutes for each experiment. Solvent A was 100% HPLC grade water (LC365-4, Burdick & Jackson, Honeywell, Muskegon, MI) containing 0.05% Heptafluorobutyric acid (LC6206, HFBA, Proteomics Grade, ProteoChem, Hurricane, UT), and solvent B was 100% HPLC grade methanol (LC230-4, Burdick & Jackson, Honeywell, Muskegon, MI) containing 0.05% Heptafluorobutyric acid (LC6206, HFBA, Proteomics Grade, ProteoChem, Hurricane, UT); HFBA was used as counter-ion to enable analysis of the polyamines<sup>245</sup>. Samples were analyzed in positive ion mode using an ESI voltage of 3.5 kV. Mass spectrometry instrument parameters for SIM included the following: resolution 70,000; isolation window width 1.0 m/z ; AGC target 2e5; maximum IT 200 ms; an inclusion list containing the m/z for each labelled and unlabeled targeted metabolite and a scheduled time window for metabolite elution. Peak heights for unlabeled metabolites and <sup>13</sup>C-labeled metabolites were extracted from the chromatograms using Xcalibur Quan Browser (version 3.0.63, ThermoFisher Scientific, San Jose, CA).

### **Metabolic Analyses**

Seahorse metabolic assays were conducted using antigen-activated OT-1 CD8+ T cells plated in Seahorse base medium supplemented with 6 mM glucose and 1 mM glutamine at  $10^5$  T cells per well in a 96-well Seahorse plate. Mitochondrial stress tests (MST) and glycolytic rate assays were used as per manufacturer's protocol or 4  $\mu\text{M}$  etomoxir, 100  $\mu\text{M}$  DON, or 100 mM 2-

deoxyglucose was injected prior to running the MST. Extracellular acidification and oxygen consumption rates were analyzed using Wave Software.

### Quantitative PCR Analysis

Cell pellet storage, RNA isolation and cDNA conversion were all conducted as in **Chapter Two**. All RNA was quantified by Sybr Green. *Slc7a1*, *Slc38a1*, *Slc38a2*, *Odc1*, *Oat*, *Srm*, *Sms*, and *B2M* sequences are listed previously in **Table 5**. *Dhps*, *Dohh*, *Slc1a5*, *Slc3a2*, *Slc7a2*, *Slc7a5*, *Slc7a6*, *Slc7a11*, and *Aldh18a1* sequences are listed below in **Table 7**.

**Table 7: RT-PCR Primer Sequences**

Gene	Sequence 5'-3'
<i>Aldh18a1</i> Forward	GTCCAGCCCTCAGCTATTAGA
<i>Aldh18a1</i> Reverse	CTTCAGCTCACTTCGGTGGG
<i>Slc1a5</i> Forward	GGTCTCCTGGATTATGTGGTACG
<i>Slc1a5</i> Reverse	AGCACAGAATGTATTTGCCGAG
<i>Slc3a2</i> Forward	TGATGAATGCACCCTTGTACTTG
<i>Slc3a2</i> Reverse	TCCCCAGTGAAAGTGGG
<i>Slc7a2</i> Forward	TGTCAACAAGTCTTCTGGGCT
<i>Slc7a2</i> Reverse	CAAGCGCCTTCAGGTCAAAC
<i>Slc7a3</i> Forward	TTCTGGCCGAGTTGTCTATGTTTG
<i>Slc7a3</i> Reverse	AGTGCGGTTCTGTGGCTGTCTC
<i>Slc7a5</i> Forward	CCGGTCTTCCCCACTTGTC
<i>Slc7a5</i> Reverse	CTTGTCCCATGTCCTTCCCC
<i>Slc7a6</i> Forward	CATTCGGCATGTTCAAGTTGG
<i>Slc7a6</i> Reverse	ATGGATCATGGACAGAAGGTTTC
<i>Slc7a11</i> Forward	TGGGCTACGTA CTGACAAAC
<i>Slc7a11</i> Reverse	AAAGATCGGGACTGCTAATGAG
<i>Dhps</i> Forward	AACACAGAGGGTGTGAAGTG
<i>Dhps</i> Reverse	GCACAGGGATGTGGTTCTTA
<i>Dohh</i> Forward	GTGGTTGAGGTGGCTGAAA
<i>Dohh</i> Reverse	AGGTAGGGTCTGACACAT

### RNA-seq

Cell pellets were harvested and kept in Buffer RLT at -80°C until use. RNA was isolated using manufacturer's protocol (AllPrep DNA/RNA Mini Kit, Qiagen) with the addition of DNase. RNA-sequencing was run in the Genomics Core and data processing was done with the Bioinformatics Core, both at Moffitt Cancer Center.

For KEGG analysis, genesets were downloaded from Broad Institute's MSigDB (<http://software.broadinstitute.org/gsea/msigdb/collections.jsp>) and KEGG gene sets were

further used for the analysis. Genes were equally weighted with a coefficient of 1 in each gene set. A gene set score was calculated for each sample by taking the sum of each genes z-score if it appeared in the gene set of interest. Upon gene set scoring, a student's t-test was used to statistically determine the most significantly altered gene sets between treatment. Heat maps display the z-score of the genes within the gene set of interest on a range from -3 to 3 and are hierarchically clustered using the Ward linkage method and Euclidean distance metric.

**CHAPTER FOUR:**  
**T-REGULATORY SUBPOPULATIONS ASSOCIATED WITH RECENT ULTRAVIOLET  
RADIATION EXPOSURE IN A SKIN CANCER SCREENING COHORT**

**A note to the reader:** this chapter has been previously published in a research article in *Journal of Immunology*, Hesterberg et al 2018<sup>2</sup>.

**Introduction**

This is the first epidemiological study to investigate the association between UVR and immune response mediated by Treg cells among a cohort of individuals undergoing routine skin cancer screening exams using a quantitative, spectrophotometer-based measure of UVR. Circulating Tregs were characterized using flow cytometry of cells in the peripheral blood, as defined previously on the basis of FoxP3, CD4, and CD25 expression<sup>145,246</sup>. The percent of total circulating conventional T cells and Tregs were quantified, in addition to specific Treg cell subpopulations, defined by the expression of CD45RA and CD27 markers<sup>132,134,145</sup> and markers associated with bidirectional trafficking between lymph node and skin<sup>247,248</sup>, including cutaneous lymphocyte-associated antigen (CLA) and the chemokine receptor CCR4<sup>132,134,142,145,153,247,249</sup> and graded expression levels of FoxP3<sup>246</sup>. We hypothesized that UVR would be associated with higher levels of a circulating Treg cell population or a higher number of total Treg cells in this cohort.

**Results**

**Characterization of Tregs associated with UV exposure**

During the first year of recruitment (July 2014-July 2015), 917 individuals were approached, of whom 448 (49%) consented to participate. No significant differences were observed between study participants and individuals who declined participation with respect to

sex ( $p=0.17$ ) or age ( $p=0.16$ ). Participants were asked to complete a web-based questionnaire, including demographic and skin cancer risk factor information. In addition, blood samples and skin pigmentation measurements were obtained from each participant. Blood samples were collected from 409 patients, of which 378 samples were found to have sufficient numbers of viable cells available for flow cytometry. Individuals with a pathologically confirmed NMSC at baseline ( $n=23$ ) or missing skin pigmentation readings ( $n=5$ ) were excluded. Therefore, analyses included 350 individuals with complete information on both Tregs and UVR exposure.

Skin pigmentation readings were used as a marker of recent UVR exposure and for natural skin tone, consistent with previous epidemiologic studies<sup>150,151</sup>. Males had significantly higher spectrophotometer readings ( $14.61 \pm 3.12$ ) than females ( $9.37 \pm 2.62$ ,  $p<0.0001$ ), whereas there was no association with age ( $p=0.81$ ).

PBMC samples were analyzed by flow cytometry, as shown in **Figure 24**<sup>145</sup>. First, CD8<sup>+</sup> T cells and CD4<sup>+</sup> T cells of CD3<sup>+</sup> lymphocytes were identified followed by CD4<sup>+</sup> T cells which were further defined as CD25<sup>-</sup>FoxP3<sup>-</sup> conventional T helper cells (Th CD4) and total CD25<sup>+</sup>FoxP3<sup>+</sup> Treg cells. Reduced expression of CD127 on CD25<sup>+</sup>FoxP3<sup>+</sup>Treg cells was confirmed, as described previously, but was not included in this analysis (data not shown)<sup>145</sup>. Recent UVR exposure was plotted against each population of T cells (**Figure 25**). The proportion of CD8 ( $33 \pm 14.4$ ), Th CD4 ( $66.1 \pm 14.6$ ), and total Treg cells ( $4.29 \pm 2.15$ ) were within normal range for peripheral blood of healthy individuals<sup>145</sup>. CD8<sup>+</sup> T cells ( $r=0.03$ ,  $p=0.56$ ), Th CD4<sup>+</sup> T cells ( $r=0.09$ ,  $p=0.09$ ), and total percent of Tregs among all CD4<sup>+</sup> T cells ( $r=-0.03$ ,  $p=0.54$ ) did not correlate with UV exposure (**Figure 25A-C**).

In addition to these populations, functionally distinct Treg subpopulations were examined, as defined in **Figure 24B-F**. Four phenotypically distinct Treg cell populations were evident by flow cytometry with the vast majority ( $75.0 \% \pm 10.5$ ) displaying a CD45RA<sup>-</sup>/CD27<sup>+</sup> central memory phenotype, as described previously<sup>145</sup>. CLA<sup>+</sup> and CCR4<sup>hi</sup> Treg cells did not express CD45RA, consistent with prior antigen engagement, but consisted of both CD27<sup>+</sup> and

CD27<sup>+</sup> subpopulations (**Figure 24E-F**), similar to conventional Th CD4<sup>+</sup> T cells (**Figure 26C-D**). The CD45RA<sup>+</sup>/CD27<sup>+</sup> (activated, effector memory) Treg (**Figure 25G**), CLA<sup>+</sup> Treg (**Figure 25F**) and CCR4<sup>hi</sup> Treg cells (**Figure 25I**) were positively correlated with recent UVR exposure among all individuals ( $r=0.19$ ,  $p<0.01$ ;  $r=0.13$ ,  $p=0.01$ ;  $r=0.17$ ,  $p<0.01$ ; respectively). In contrast, CD45RA<sup>+</sup>/CD27<sup>+</sup> Tregs (i.e., naïve) showed a less pronounced, negative correlation ( $r=-0.11$ ,  $p=0.03$ ) (**Figure 25D**) indicating that these specific Treg subsets, not total Tregs or conventional T cells, correlated with recent UVR exposure. Of note, no self-reported measures of past UVR exposures or sun susceptibility factors were associated with these four Treg populations (**Table 8**).

To further explore the Treg populations and their association to UVR, CD4<sup>+</sup> T cells were also segregated into 6 populations defined previously<sup>246</sup> using CD45RA, CD25 and levels of FoxP3 (**Figure 24G-H**) with Groups I-III all expressing FoxP3 consistent with having a Treg phenotype<sup>246</sup>. Group II (CD45RA<sup>+</sup>CD25<sup>+++</sup>FoxP3<sup>hi</sup>) and Group I (CD45RA<sup>+</sup>CD25<sup>++</sup>FoxP3<sup>lo</sup>) are functionally suppressive while Group III having a CD45RA<sup>+</sup>CD25<sup>++</sup>FoxP3<sup>lo</sup> phenotype are non-suppressive, but are capable of secreting cytokines. Although the CD45RA<sup>+</sup>/CD27<sup>+</sup> FoxP3 population showed an association to UVR exposure, no association was observed with the CD45RA<sup>+</sup> Tregs defined as Group II or Group III (**Figure 24K and 24L**, respectively). Interestingly, Group I Tregs were negatively associated with recent UVR exposure ( $r=-0.16$ ,  $p<0.01$ ) (**Figure 25J**).

To further define the characteristics of the Tregs and conventional T cells through association studies, a correlation matrix was prepared for all T cell populations identified. Group I and Group II Treg populations were highly correlated with total Tregs, but were not associated with Tregs defined by other surface markers including CD27, CLA and CCR4 (**Figure 27**). Indeed, we found there is a high positive correlation between CD45RA<sup>+</sup>/CD27<sup>+</sup> Tregs “naïve Tregs” and the Group I population “resting Tregs” (**Figure 27**). These results are consistent with the negative association between both Group I and CD45RA<sup>+</sup>/CD27<sup>+</sup> Treg populations.

Moreover, overlays of the flow cytometry expression patterns revealed CD27, CLA and CCR4 are represented throughout Group II-IV populations (**Figure 24I**) indicating these markers further differentiate Tregs. Gating on such populations within Group II-III may be necessary to observe correlations between Tregs defined by this strategy and recent UVR exposure.

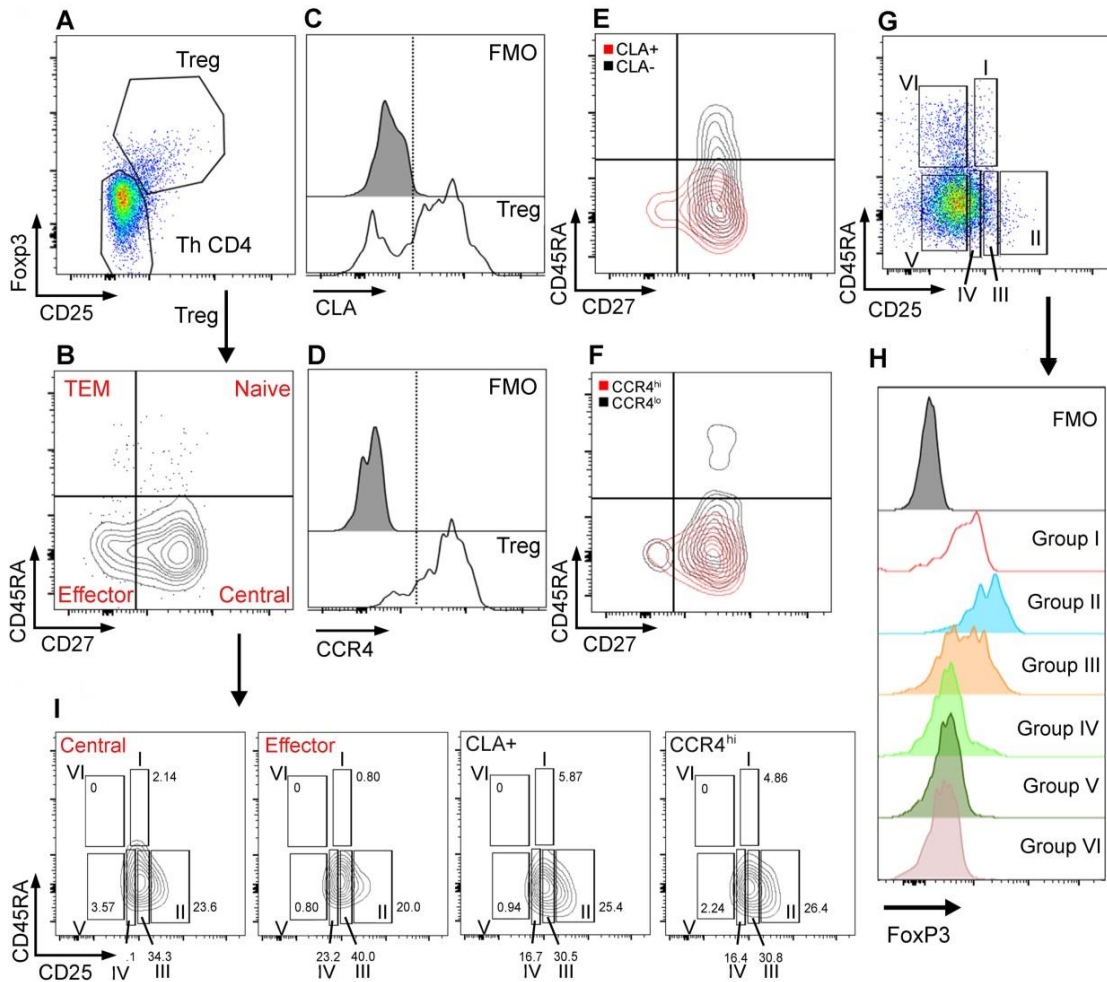


**Figure 24: Flow cytometry gating strategy for Treg cell analysis.** PBMCs were gated first on viability and on CD3 and CD4 positivity. (A-D) (A) CD4+ Treg cells were defined by high expression of CD25 and intracellular Foxp3 and conventional CD4+ T cells (Th CD4) were defined by low expression of CD25 and Foxp3. (B) Tregs were then analyzed for CD45RA and CD27 expression and populations were defined by dual or single expression. (C-F) CLA and CCR4 expression was also analyzed among Treg cells. CLA and CCR4 positive Treg cells were also confirmed to be CD45RA negative with mixed expression of CD27. (G-I) (E) Six groups of CD4+ T cells were defined by CD45RA positivity and varying CD25 expression. (H) Each population was analyzed for FoxP3 expression. (I) Distribution of these populations were analyzed in CD45RA-/CD27+ CM.Treg cells, CD45RA-/CD27- E.Treg cells, CLA+ Treg cells and CCR4<sup>hi</sup> Treg cells as defined in (B-D).

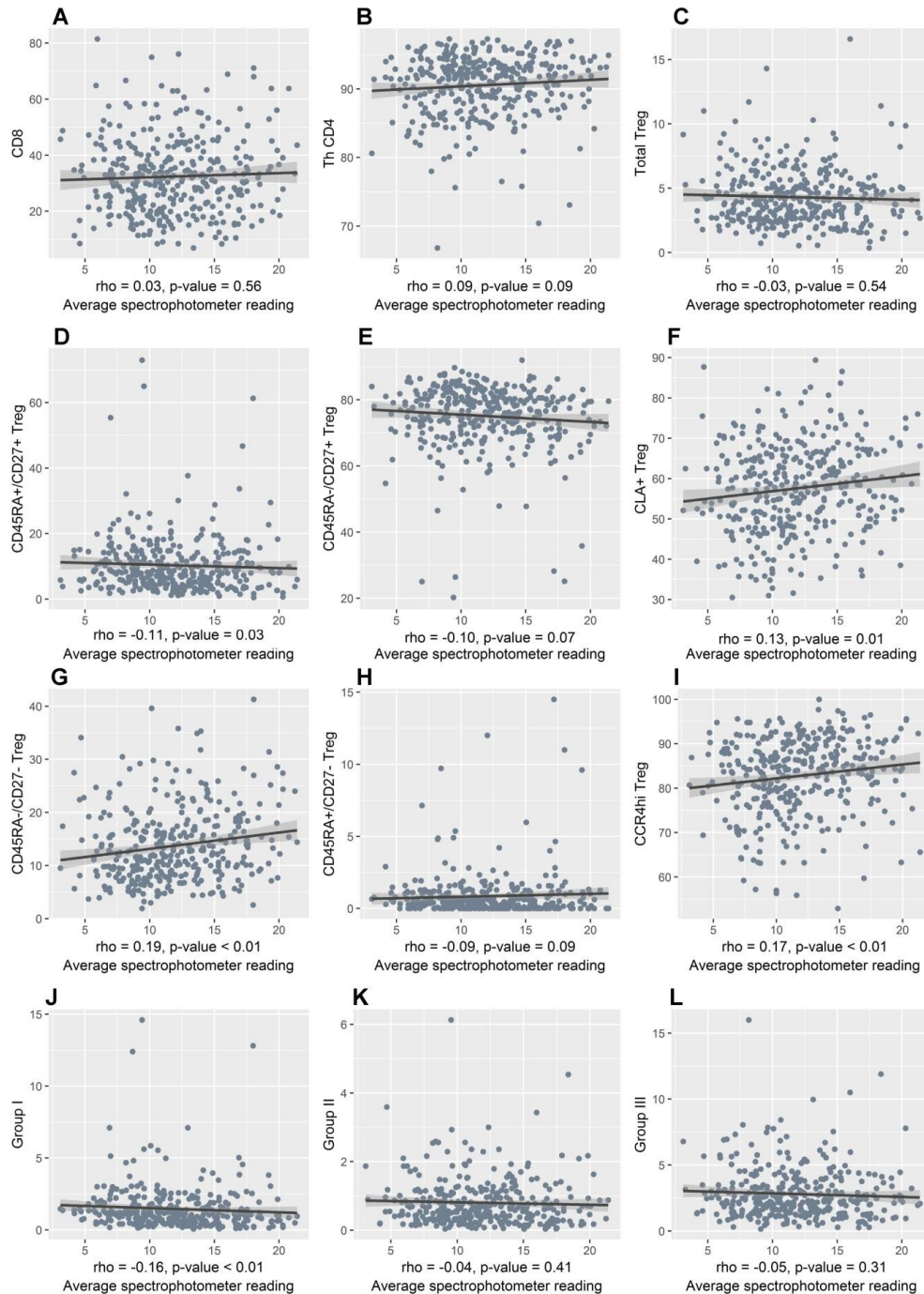


**Figure 25: T cell populations in correlation with recent UV exposure among 350 individuals undergoing skin cancer screening.** Correlations between Treg cells and UVR were calculated using Spearman's rank, and a trend line was created to visualize the associations. (A-C) Scatterplot of spectrophotometer reading and CD8, Th CD4, total Treg cells. (D-I) Scatterplot of spectrophotometer reading and phenotypes of Tregs defined in **Figure 23A**. (J-L) Scatterplot of spectrophotometer reading and Group I, II, and III T (Treg) cell phenotypes defined in **Figure 23G**.



**Table 8: Circulating regulatory T (Treg) cell phenotypes and questionnaire factors.**

		Treg cell phenotypes								
		CD45RA <sup>+</sup> /CD27 <sup>+</sup> Treg			CD45RA <sup>-</sup> /CD27 <sup>-</sup> Treg		CLA <sup>+</sup> Treg		CCR4 <sup>hi</sup> Treg	
		n (%)	Mean(SD) <sup>1</sup>	p-value <sup>2</sup>	Mean(SD) <sup>1</sup>	p-value <sup>2</sup>	Mean(SD) <sup>1</sup>	p-value <sup>2</sup>	Mean(SD) <sup>1</sup>	p-value <sup>2</sup>
<b>Reaction to 1 hour of sun exposure</b>										
	No change	11 (3.2)	15.6 (17.8)		14.9 (7.6)		53.8 (12.6)		79.1 (10.8)	
	Tans without sunburn	68 (19.7)	10.8 (9.4)	0.28	13.5 (7.9)	0.54	55.5 (12.2)	0.65	81.8 (10.1)	0.31
	Mild sunburn with tan	150 (43.4)	10.1 (6.8)	0.27	13.2 (6.6)	0.57	57.5 (9.7)	0.24	83.2 (7.8)	0.14
	Sunburn without blisters	100 (28.9)	10.0 (9.7)	0.08	13.7 (5.8)	0.99	59.3 (11.2)	0.05	83.4 (8.4)	0.05
	Blistering sunburn	17 (4.9)	8.4 (6.0)	0.06	18.3 (10.7)	0.15	56.5 (16.5)	0.27	82.0 (9.2)	0.17
<b>Ever had a job working in the sun</b>										
	No	249 (72.0)	10.5 (9.1)		13.5 (6.9)		57.7 (11.2)		82.5 (8.5)	
	Yes	97 (28.0)	9.7 (7.7)	0.90	14.2 (7.3)	0.89	57.0 (11.1)	0.07	83.6 (9.0)	0.90
<b>Years of job in the sun</b>										
	No	249 (72.4)	10.5 (9.1)		13.5 (6.9)		57.7 (11.2)		82.5 (8.5)	
	Less than 5	52 (15.1)	10.4 (9.3)	0.95	14.3 (7.5)	0.81	55.2 (11)	0.01	82.2 (9.2)	0.19
	6 to 10	10 (2.9)	10.2 (7.1)	0.62	14.7 (7.3)	0.98	61.5 (13.8)	0.73	85.2 (11.1)	0.50
	more than 10	33 (9.6)	7.9 (4.4)	0.28	14.1 (7.1)	0.89	58.9 (10)	0.92	85.5 (7.9)	0.18
<b>Ever had a blistering sunburn</b>										
	No	93 (26.9)	10.0 (8.6)		13.6 (6.4)		57.6 (11.2)		82.9 (9.5)	
	Yes	253 (73.1)	10.4 (8.8)	0.43	13.8 (7.2)	0.94	57.4 (11.2)	0.89	82.7 (8.3)	0.80
<b>Age of first blistering sunburn</b>										
	Less than or equal to 10	74 (34.7)	10.3 (11.0)		14.4 (7.5)		58.7 (11.6)		83.1 (8.1)	
	Between 11 to 20	109 (51.2)	10.1 (6.4)	0.62	13.6 (7.0)	0.66	56.7 (10.6)	0.34	82.5 (8.6)	0.86
	Above 20	30 (14.1)	10.8 (11.3)	0.85	11.7 (4.7)	0.26	58.0 (9.9)	0.91	82.6 (7.4)	0.97
<b>Blistering sunburn frequency in last year</b>										
	None	321 (93.0)	10.3 (8.3)		13.6 (6.8)		57.3 (11.1)		82.7 (8.7)	
	More than once	24 (7.0)	10.7 (13.9)	0.57	15.4 (8.9)	0.37	59.2 (12.1)	0.34	83.7 (8.3)	0.48
<b>Natural skin tone<sup>3</sup></b>										
	Lighter	175 (50.0)	10.3 (9.3)		13.5 (6.4)		58.2 (10.2)		83.3 (7.8)	
	Darker	175 (50.0)	10.4 (8.0)	0.70	13.9 (7.4)	0.55	56.9 (12.1)	0.42	82.2 (9.3)	0.82

<sup>1</sup>SD=Standard deviation

<sup>2</sup>p-values were calculated using linear regression, adjusted for age (categorical) and sex with transformed Treg data as follows: CD45RA<sup>+</sup>/CD27<sup>+</sup> Treg (8th root), CD45RA<sup>-</sup>/CD27<sup>-</sup> Treg (4th root), CLA<sup>+</sup> Treg and CCR4<sup>hi</sup> Treg (4th power).

<sup>3</sup>Natural skin tone based on median spectrophotometer readings in the axilla, as defined in **Methods**.

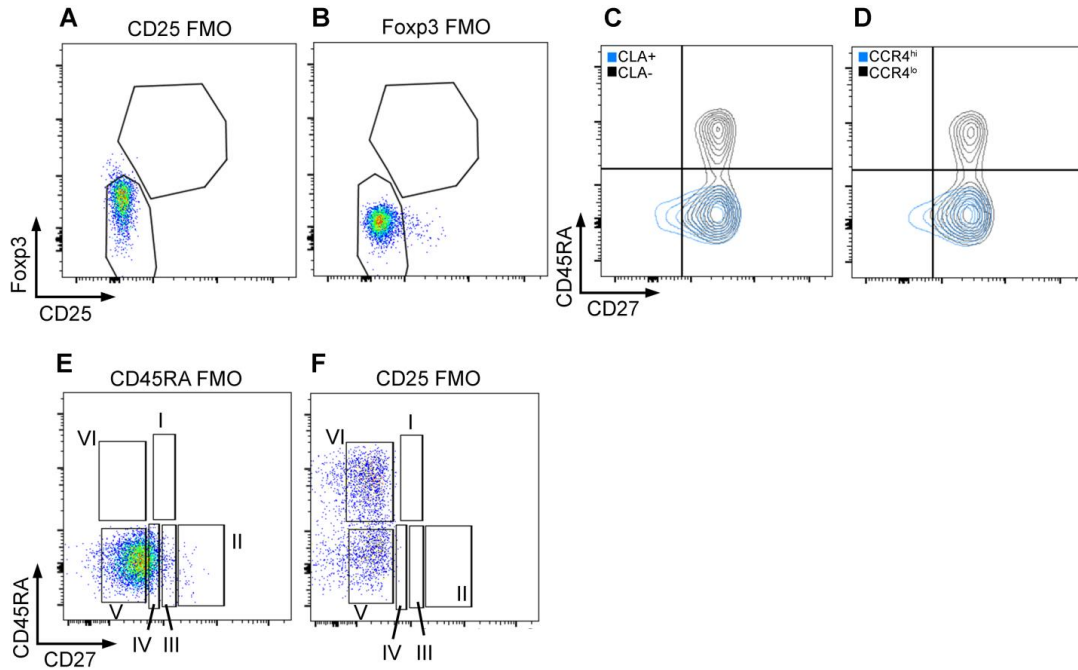


**Figure 26: Flow cytometry gating strategy controls in reference to Figure 23.** PBMCs were gated first on viability and on CD3 and CD4 positivity. (A-B) CD25 and Fxp3 fluorescence-minus-one (FMO) control samples used to define CD25<sup>+</sup> Fxp3<sup>+</sup> Treg populations, (C-D) CLA<sup>+</sup> and CCR4<sup>hi</sup> Th CD4<sup>+</sup> T cells were confirmed to be CD45RA<sup>-</sup> with mixed expression of CD27, (E-F) CD45RA and CD25 FMO control samples used to defined Group I-VI.

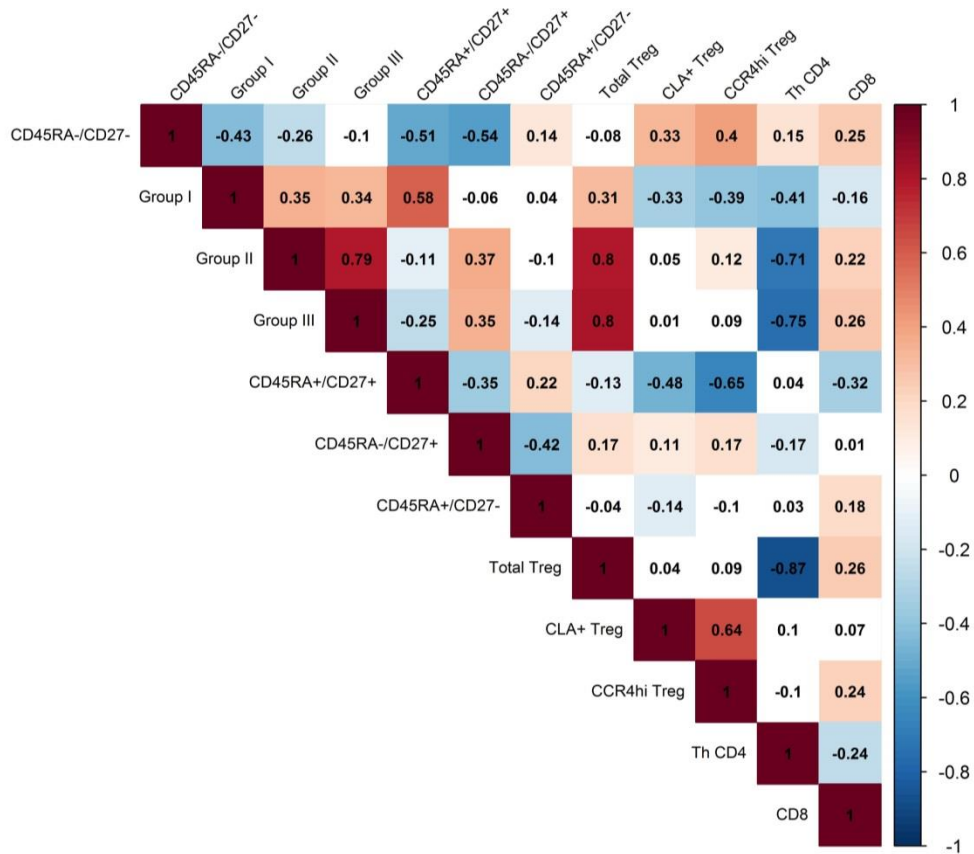


**Figure 27: Spearman rank correlation matrix for T cell populations among 350 skin cancer screening patients.** Spearman correlation coefficients ( $\rho$ ) are presented for all T cell populations. The matrix cells are shaded only if they are significantly correlated at  $p < 0.05$  level. Red shading represents a positive correlation whereas blue shading represents a negative correlation.

### Natural skin tone represents an effect modifier of the UVR and Treg association

Previous studies of nevus development in children have reported effect modification of UVR-associated physiologic effects by one's natural skin tone<sup>250,251</sup>. To test whether the associations between UVR and Treg cell phenotypes differed by natural skin tone, we stratified our analysis by lighter versus darker skin tone, based on the median value of the spectrophotometer readings of the sun-unexposed axilla. Interestingly, a significant positive correlation between recent UVR and the proportion of activated, effector memory CD45RA<sup>-</sup>/CD27<sup>-</sup> Treg cells ( $r=0.30$ ,  $p < 0.01$ ) was observed only in individuals of lighter skin (**Figure 28**). In contrast, CD45RA<sup>+</sup>/CD27<sup>+</sup> naïve Treg population negatively correlated with recent UVR exposure in lighter-skinned individuals, though the trend was not as striking as the association

with increased CD45RA<sup>+</sup>/CD27<sup>-</sup> Tregs (**Figure 28**). The positive correlation between UVR and CLA<sup>+</sup> Treg cells was also restricted to the lighter-skinned individuals ( $r=0.15$ ,  $p=0.04$ ). However, UVR and CCR4<sup>hi</sup> Tregs were positively correlated among both darker-skinned ( $r=0.18$ ,  $p=0.02$ ) and lighter-skinned individuals ( $r=0.14$ ,  $p=0.06$ ), with the former being statistically significant. These results suggest that individuals with a lighter natural skin tone may be at higher risk for UVR-induced changes in Treg cells.

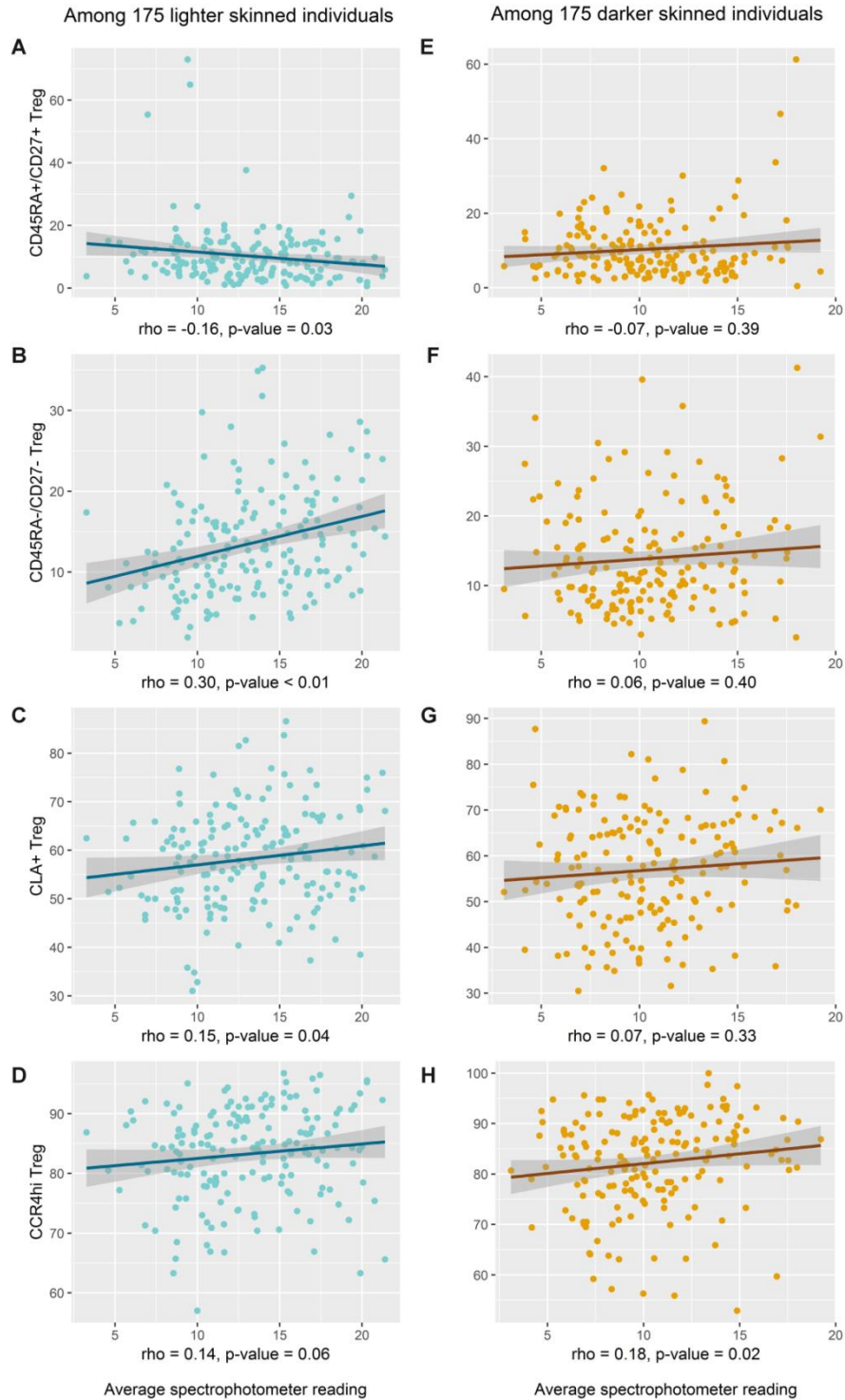


**Figure 28: Effect modification by natural skin tone.** Scatterplot of spectrophotometer readings and Treg cell subsets that were found to have significant associations with UVR after stratification by natural skin tone as defined by median spectrophotometer readings of sun-unexposed underside of the upper arm (i.e. the axilla). Correlations between Treg cells and UVR were calculated using Spearman's rank, and a trend line was created to visualize the associations.

## Demographics are associated with Tregs

Associations between demographic factors and Treg subpopulations, including naïve CD45RA<sup>+</sup>/CD27<sup>+</sup>, activated effector CD45RA<sup>-</sup>/CD27<sup>-</sup>, CLA<sup>+</sup>, and CCR4<sup>hi</sup> Tregs (based on results shown in **Figure 24**), are presented in **Table 9**. A statistically significant inverse trend was observed between age and naïve CD45RA<sup>+</sup>/CD27<sup>+</sup> Tregs ( $p$ -trend= $<0.01$ ). Conversely, CD45RA<sup>-</sup>/CD27<sup>-</sup> Treg cells were positively associated with age ( $p$ -trend=0.04). This is similar to the expected loss of conventional naïve T cells due to thymic involution and shown previously for Treg cells in mice<sup>146,252-254</sup>. Significant positive trends were also observed between age and the two skin migratory Treg cells, the CLA<sup>+</sup> ( $p$ -trend=0.02) and CCR4<sup>hi</sup> ( $p$ -trend=0.01) Treg populations (**Table 9**).

Interestingly, Treg populations differed significantly by sex after adjusting for age, including higher numbers of CD45RA<sup>-</sup>/CD27<sup>-</sup> Tregs in males ( $14.5 \pm 6.8$  in males versus mean  $13.0 \pm 7.0$  in females,  $p=0.02$ ), higher CLA<sup>+</sup> Tregs in males ( $59.3 \pm 10.7$  in males versus mean  $56.0 \pm 11.3$  in females,  $p=0.01$ ), and higher CCR4<sup>hi</sup> Tregs in males ( $84.5 \pm 8.4$  in males versus  $82.8 \pm 8.4$  in females,  $p<0.01$ ). Race was also associated with CD45RA<sup>-</sup>/CD27<sup>-</sup> Tregs (mean  $13.5 \pm 6.8$  in white versus mean  $19.9 \pm 9.6$  in others,  $p<0.01$ ). Ethnicity was not associated with Treg populations (**Table 9**). Treg cells defined as Group I-III (**Figure 24D**) were also analyzed by demographic information. No association was found among Group I-III populations with age, sex or ethnicity. Group II populations were significantly associated with race with white participants having higher numbers (**Table 10**). This finding is consistent with a the significant racial difference observed for the distinct Treg subpopulation defined by CD45RA<sup>-</sup>/CD27<sup>-</sup> expression, which was strongly negatively correlated with age, independent of Group I-III distribution (**Figure 27**).



**Table 9: Circulating regulatory T (Treg) cell phenotypes and demographic characteristics.**

		Treg cell phenotypes												
		CD45RA <sup>+</sup> /CD27 <sup>-</sup> Treg				CD45RA <sup>-</sup> /CD27 <sup>-</sup> Treg			CLA <sup>+</sup> Treg			CCR4 <sup>hi</sup> Treg		
		N (%)	Mean (SD) <sup>1</sup>	Coef. <sup>2</sup>	P-value <sup>2</sup>	Mean (SD)	Coef.	P-value	Mean (SD)	Coef.	P-value	Mean (SD)	Coef.	P-value
<b>Age<sup>3</sup></b>														
	60-64	78 (22.3)	12 (9.3)	-0.0031	<b>&lt; 0.01</b>	12.4 (6.9)	0.0042	<b>0.04</b>	55.4 (10.8)	0.2228	<b>0.02</b>	80.5 (9.1)	383549	<b>0.01</b>
	65-69	125 (35.7)	10.8 (10.3)			14.2 (7.5)			57.4 (10.6)			82.7 (8.4)		
	70-74	78 (22.3)	9.8 (6.9)			13.7 (6.4)			58.1 (11.7)			83.7 (8.1)		
	75-79	41 (11.7)	9.5 (6.3)			13.6 (6.6)			58 (11.7)			83.1 (8.5)		
	80-89	28 (8.0)	6.4 (4.3)			15.5 (6.3)			62 (11.5)			86 (8.2)		
<b>Gender<sup>4</sup></b>														
	Female	187 (53.4)	10.8 (9.1)			13.0 (7.0)			56.0 (11.3)			81.2 (8.5)		
	Male	163 (46.6)	9.8 (8.2)	-0.0187	<i>0.15</i>	14.5 (6.8)	0.0588	<b>0.02</b>	59.3 (10.7)	3.1290	<b>0.01</b>	84.5 (8.4)	7335781	<b>&lt;0.01</b>
<b>Race</b>														
	White	340 (97.1)	10.3 (8.6)			13.5 (6.8)			57.8 (11.1)			82.8 (8.4)		
	Others	10 (2.9)	10.7 (10.8)	-0.0515	<i>0.18</i>	19.9 (9.6)	0.2225	<b>&lt;0.01</b>	51.0 (11.9)	-6.1680	<i>0.09</i>	80.1 (13.4)	-1106525	<i>0.85</i>
<b>Ethnicity</b>														
	Non-Hispanic	330 (94.8)	10.4 (8.6)			13.7 (6.9)			57.5 (11.2)			82.6 (8.6)		
	Hispanic or Latino	18 (5.2)	10.2 (9.8)	-0.0166	<i>0.57</i>	14.5 (7.9)	0.0293	<i>0.61</i>	59.0 (11.3)	1.7580	<i>0.51</i>	84.2 (8.4)	4063970	<i>0.34</i>

<sup>1</sup>SD=standard deviation

<sup>2</sup>Coefficients and p-values were calculated using linear regression, adjusted for age CD45RA<sup>-</sup> (categorical) and sex with transformed Treg data as follows: CD45RA<sup>+</sup>/CD27<sup>+</sup> Treg (8th root), /CD27<sup>-</sup> Treg (4th root), CLA<sup>+</sup> Treg and CCR4<sup>hi</sup> Treg (4th power)

<sup>3</sup>Coefficient and p-trend was calculated using linear regression with continuous age, presented in years, and adjusted for sex, with transformed Treg data

<sup>4</sup>p-values were calculated using linear regression adjusted for age (categorical)

**Table 10: Circulating Group I-III regulatory T (Treg) cell phenotypes and demographic characteristics.**

	N (%)	Group I		Group II		Group III	
		Mean (SD)	P-value	Mean (SD)	P-value	Mean (SD)	P-value
<b>Age<sup>3</sup></b>							
60-64	78 (22.3)	1.6 (2)	0.10	0.7 (0.4)	0.44	2.6 (1.5)	0.62
65-69	125 (35.7)	1.5 (1.6)		0.9 (0.8)		3.1 (2.4)	
70-74	78 (22.3)	1.5 (1.4)		0.7 (0.6)		2.5 (1.4)	
75-79	41 (11.7)	1.5 (1.1)		0.9 (1)		3 (1.9)	
80-89	28 (8.0)	0.9 (0.6)		0.8 (0.8)		2.6 (1.7)	
<b>Gender<sup>4</sup></b>							
Female	187 (53.4)	1.5 (1.7)		0.7 (0.6)		2.8 (2)	
Male	163 (46.6)	1.4 (1.4)	0.06	0.9 (0.8)	0.15	2.9 (1.9)	0.46
<b>Race</b>							
White	340 (97.1)	1.5 (1.6)		0.8 (0.7)		2.8 (2)	
Others	10 (2.9)	1.3 (1.1)	0.22	0.4 (0.2)	0.04	2.4 (0.8)	0.74
<b>Ethnicity</b>							
Non-Hispanic	330 (94.8)	1.5 (1.6)		0.8 (0.7)		2.8 (1.9)	
Hispanic or Latino	18 (5.2)	1.6 (1.7)	0.76	0.8 (0.7)	0.93	3.2 (2.4)	0.51

<sup>1</sup>SD=standard deviation

<sup>2</sup>p-values were calculated using linear regression, adjusted for age (categorical) and sex with transformed Treg data: Group I (8th root), Group II (4th root), Group III (4th root)

<sup>3</sup>p-trend was calculated using linear regression with continuous age, presented in years, and adjusted for sex

<sup>4</sup>p-values were calculated using linear regression adjusted for age (categorical)

### Recent UVR and Tregs are independently associated

Associations between recent UVR and quartiles of circulating Treg cells are presented in **Table 11**. We observed a positive trend between recent UVR and quartiles of CD45RA<sup>-</sup>/CD27<sup>-</sup> Treg in all individuals ( $p$ -trend=0.02) (**Table 11**). After stratification by natural skin tone, the UVR association with CD45RA<sup>-</sup>/CD27<sup>-</sup> Treg cells was particularly pronounced among lighter-skinned individuals, with each unit increase in spectrophotometer readings associated with a 32% increase in odds of being in the uppermost versus lowermost quartile of CD45RA<sup>-</sup>/CD27<sup>-</sup> Tregs (OR=1.32, 95% CI=1.12-1.61), after adjustment for age and sex. The strength of this association supports its biological relevance. Interestingly, we observed a significant inverse trend with recent UVR exposure and quartiles of CD45RA<sup>-</sup>/CD27<sup>+</sup> Treg among all individuals ( $p$ -



trend=0.04) and lighter-skinned individuals (p-trend=0.01), but not among darker-skinned individuals (p-trend=0.22). Among darker-skinned individuals, UVR exposure was significantly lower among those in the second and third quartiles of CD45RA<sup>+</sup>/CD27<sup>+</sup> Treg compared to the first, although no clear trend was observed, taking into account the highest quartile (p-trend=0.11). No associations were observed between UVR exposure and quartiles of total Treg, CLA<sup>+</sup> Treg and CCR4<sup>hi</sup> Treg, overall or after stratification by natural skin tone (Table 12).

**Table 11: Quartiles of circulating regulatory T (Treg) cell subpopulations and UV spectrophotometer readings among all 350 patients undergoing skin cancer screening.**

		Average UV spectrophotometer reading								
		All (n=350)			Lighter skin <sup>1</sup> (n=175)			Darker skin (n=175)		
Treg cell phenotypes <sup>2</sup>	n	Mean (SD) <sup>3</sup>	OR (95%CI) <sup>4</sup>	n	Mean (SD)	OR (95%CI)	n	Mean (SD)	OR (95%CI)	
<b>CD45RA<sup>+</sup>/CD27<sup>+</sup> Treg</b>										
Q1	88	12.63 (3.96)	1.0 (ref.)	46	14.19 (3.83)	1.0 (ref.)	42	10.92 (3.36)	1.0 (ref.)	
Q2	87	11.58 (3.74)	0.91 (0.81-1.01)	41	12.67 (3.93)	0.84 (0.70-0.98)	46	10.61 (3.30)	0.99 (0.83-1.17)	
Q3	87	11.50 (3.86)	0.91 (0.81-1.01)	43	12.91 (3.91)	0.86 (0.73-1.01)	44	10.12 (3.31)	0.93 (0.77-1.12)	
Q4	88	11.53 (3.89)	0.92 (0.83-1.02)	45	12.75 (3.89)	0.88 (0.75-1.02)	43	10.25 (3.49)	0.95 (0.79-1.13)	
			P-trend: 0.24				P-trend: 0.18			
<b>CD45RA<sup>-</sup>/CD27<sup>-</sup> Treg</b>										
Q1	88	10.88 (3.40)	1.0 (ref.)	44	11.48 (3.78)	1.0 (ref.)	44	10.27 (2.89)	1.0 (ref.)	
Q2	87	11.50 (3.64)	1.00 (0.89-1.12)	42	12.96 (3.79)	1.08 (0.92-1.27)	45	10.13 (2.94)	0.92 (0.75-1.11)	
Q3	89	12.09 (3.87)	1.05 (0.94-1.17)	47	13.41 (3.81)	1.20 (1.03-1.42)	42	10.61 (3.39)	0.84 (0.67-1.04)	
Q4	86	12.80 (4.34)	1.13 (1.01-1.27)	42	14.79 (3.65)	1.32 (1.12-1.61)	44	10.89 (4.11)	0.99 (0.83-1.20)	
			P-trend: 0.02				P-trend: <0.001			
<b>CD45RA<sup>+</sup>/CD27<sup>-</sup> Treg</b>										
Q1	88	12.36 (4.15)	1.0 (ref.)	39	13.78 (3.70)	1.0 (ref.)	49	11.23 (4.18)	1.0 (ref.)	
Q2	88	11.72 (3.92)	0.94 (0.84-1.04)	43	13.30 (3.90)	0.94 (0.79-1.10)	45	10.21 (3.33)	0.88 (0.75-1.03)	
Q3	87	12.42 (3.96)	0.92 (0.82-1.02)	53	13.79 (4.04)	0.85 (0.70-1.00)	34	10.30 (2.74)	0.83 (0.69-0.99)	
Q4	87	10.73 (3.22)	0.88 (0.78-0.98)	40	11.53 (3.59)	0.77 (0.63-0.93)	47	10.05 (2.72)	0.93 (0.78-1.10)	
			P-trend: 0.04				P-trend: 0.01			
<b>CD45RA<sup>-</sup>/CD27<sup>+</sup> Treg</b>										
Q1	88	12.84 (3.75)	1.0 (ref.)	45	13.60 (4.38)	1.0 (ref.)	43	12.05 (2.80)	1.0 (ref.)	
Q2	89	11.26 (3.56)	0.91 (0.81-1.02)	41	13.33 (3.25)	1.01 (0.86-1.19)	48	9.49 (2.80)	0.72 (0.57-0.89)	
Q3	85	11.18 (3.67)	0.86 (0.77-0.96)	43	12.32 (3.76)	0.89 (0.76-1.04)	42	10.01 (3.22)	0.77 (0.63-0.93)	
Q4	88	11.95 (4.30)	0.99 (0.88-1.10)	46	13.33 (4.09)	1.05 (0.90-1.23)	42	10.43 (4.04)	0.87 (0.70-1.05)	
			P-trend: 0.41				P-trend: 0.93			

<sup>1</sup>Natural skin tone based on median spectrophotometer readings in sun-unexposed underside of the upper arm, as described in **Methods**

<sup>2</sup>Tregs were categorized into quartiles using the following cut-offs:

CD45RA<sup>+</sup>/CD27<sup>+</sup> Treg: 4.89-8.34-13.5

CD45RA<sup>-</sup>/CD27<sup>+</sup> Treg: 71.43-76.9-80.9

CD45RA<sup>-</sup>/CD27<sup>-</sup> Treg: 8.44-12.25-17.4

CD45RA<sup>+</sup>/CD27<sup>-</sup> Treg: 0.12-0.43-1.03

<sup>3</sup>SD=standard deviation

<sup>4</sup>Odds ratios (OR) and 95% confidence intervals (CI) for average spectrophotometer readings were calculated using logistic regression, comparing each risk group to the reference group Q1

<sup>5</sup>p-trend was calculated using ordinal logistic regression

**Table 12: Quartiles of total Tregs, CLA+ and CCR4hi Tregs and UV spectrophotometer readings in all individuals and stratified by natural skin tone.**

Treg cell phenotypes <sup>2</sup>	n	Average UV spectrophotometer reading								
		All (n=350)			Lighter skin <sup>1</sup> (n=175)			Darker skin (n=175)		
		Mean (SD) <sup>3</sup>	OR (95%CI) <sup>4</sup>		n	Mean (SD)	OR (95%CI)		n	Mean (SD)
<b>Total Treg</b>										
Q1	88	11.74 (3.92)	1.0 (ref.)	43	13.28 (4.05)	1.0 (ref.)		45	10.28 (3.21)	1.0 (ref.)
Q2	87	11.89 (3.86)	1.00 (0.89-1.11)	42	13.34 (4.11)	0.96 (0.81-1.12)		45	10.54 (3.09)	1.05 (0.87-1.26)
Q3	88	12.35 (4.00)	0.99 (0.89-1.10)	47	13.14 (3.98)	0.93 (0.80-1.08)		41	11.44 (3.87)	1.04 (0.88-1.23)
Q4	87	11.26 (3.69)	0.89 (0.79-0.99)	43	12.85 (3.59)	0.86 (0.72-1.02)		44	9.70 (3.11)	0.84 (0.68-1.02)
		P-trend: 0.07			P-trend: 0.11			P-trend: 0.23		
<b>CLA+ Treg</b>										
Q1	92	11.25 (3.47)	1.0 (ref.)	38	12.38 (3.75)	1.0 (ref.)		54	10.46 (3.05)	1.0 (ref.)
Q2	84	11.52 (4.15)	1.02 (0.92-1.14)	45	13.06 (4.19)	1.03 (0.87-1.21)		39	9.75 (3.38)	0.93 (0.78-1.10)
Q3	86	11.85 (3.61)	1.00 (0.89-1.12)	51	12.80 (3.63)	0.96 (0.80-1.13)		35	10.47 (3.15)	0.92 (0.76-1.12)
Q4	88	12.63 (4.15)	1.07 (0.97-1.19)	41	14.40 (3.91)	1.16 (0.99-1.37)		47	11.08 (3.76)	1.00 (0.85-1.17)
		P-trend: 0.25			P-trend: 0.13			P-trend: 0.89		
<b>CCR4<sup>hi</sup> Treg</b>										
Q1	89	11.09 (3.77)	1.0 (ref.)	40	12.93 (4.13)	1.0 (ref.)		49	9.59 (2.65)	1.0 (ref.)
Q2	89	11.57 (3.83)	1.06 (0.95-1.18)	44	12.64 (3.75)	1.00 (0.85-1.18)		45	10.51 (3.65)	1.13 (0.95-1.35)
Q3	85	11.86 (3.96)	0.99 (0.89-1.11)	47	12.77 (3.92)	0.92 (0.78-1.08)		38	10.73 (3.75)	1.05 (0.86-1.27)
Q4	87	12.75 (3.81)	1.07 (0.97-1.18)	44	14.26 (3.74)	1.08 (0.94-1.26)		43	11.21 (3.26)	1.08 (0.90-1.30)
		P-trend: 0.61			P-trend: 0.42			P-trend: 0.84		

<sup>1</sup>Natural skin tone based on median spectrophotometer readings in the axilla, as defined in *Materials and Methods*.

<sup>2</sup>Tregs were categorized into quartiles using cut-offs as the following:

Total Treg: 2.73-4.01-5.28, CLA+ Treg: 50-57.8-65.58, CCR4<sup>hi</sup> Treg: 77.9-84.2-89.2

<sup>3</sup>SD=standard deviation

<sup>4</sup>Odds ratios (OR) and 95% confidence intervals (CI) for average spectrophotometer reading were calculated using logistic regression, comparing each risk group to the reference group Q1

<sup>5</sup>p-trend was calculated using ordinal logistic regression

## Discussion

NMSC is the most common malignancy in the United States with older age (> 60 years) representing an important risk factor<sup>255</sup>. This is the first epidemiologic study of recent UVR exposure and Tregs in a population of individuals ages 60 years and older at high risk for NMSC. In 350 individuals undergoing skin cancer screening, recent UVR exposure was positively associated with activated, effector memory CD45RA<sup>+</sup>/CD27<sup>-</sup> Treg cells, whereas an inverse association was observed between recent UVR and CD45RA<sup>-</sup>/CD27<sup>+</sup> Treg cells. Furthermore, these associations were specific to lighter-skinned individuals. No associations were observed between recent UVR exposure and the total percentage of Tregs relative to conventional CD4<sup>+</sup> or CD8<sup>+</sup> T cells.

To the best of our knowledge, previous findings of UVR-related changes in Treg cells have been exclusively reported for *in vitro* studies or in mouse models *in vivo*, where subsets of T cells were not specifically studied<sup>138,247,256</sup>. Tregs are largely thought of as migratory populations both in circulation and in lymph nodes, but many are retained in cutaneous tissue where they curb autoimmune diseases of the skin, contribute to tumor progression, allergic responses, and microbial immunity<sup>257,258</sup>. In cutaneous tissues, over representation or increased suppressive functions of Treg cells may contribute to immune evasion and development of skin cancer.

We have reported previously that CD45RA<sup>-</sup>/CD27<sup>-</sup> Treg cells represent a more suppressive subset on a per cell basis in T cell suppression assays<sup>145</sup>. Due to the similarity between CD45RA<sup>-</sup>/CD27<sup>-</sup> Tregs and conventional T effector cells, these cells were termed effector memory or Treg<sup>EM</sup> cells. Down regulation of CD45RA and CD27 is aligned with acute antigen activation in the context of MHC class II, which in the case of Tregs, is largely induced by stimulatory autoantigens<sup>259-261</sup>. This precise Treg subset was also expanded in a higher risk cohort of patients with a premalignant human disease MDS characterized by a high rate of leukemia transformation<sup>145</sup>. In this disease, the total number of Tregs increases during later stages of leukemia progression suggesting that an activation-associated phenotypic change and expansion occur at different points of the disease suggesting that antigen activation may precede the accumulation of Tregs as a whole<sup>262,263</sup>. Collectively, our results show an increase in the CD45RA<sup>-</sup>/CD27<sup>-</sup> Tregs in association with UVR exposure, which may occur through local tissue damage and antigen release. This increase is in tandem to low UV exposure in individuals with higher levels of naive CD45RA<sup>+</sup>/CD27<sup>+</sup> Tregs.

Alternative gating strategies on CD4 T cells by CD25 and CD45RA to define Tregs, rather than by FoxP3 and CD25, resulted in no significant findings among this cohort (**Figure 24G-H, 25K-L, Table 9**). These populations have been previously shown to be phenotypically distinct in which CD45RA<sup>-</sup>CD25<sup>+++</sup> CD4<sup>+</sup> cells, defined as Group II, exhibit more repressive

activity on conventional T cells than other Treg populations<sup>246</sup>. Indeed, these populations expressed the highest intracellular FoxP3 expression in the cohort presented here, but no association was found with recent UVR exposure. This population correlated with populations of total Tregs defined by FoxP3 and CD25, which also showed no correlation with recent UVR exposure. Given that CD45RA<sup>-</sup>/CD27<sup>-</sup> Tregs were found to be present within groups II, III, and IV, loss of CD27 could contribute to a distinct functional attribute with clinically-relevance to UVR exposure. Analysis of this process could yield a better understanding of Treg activity in response to UVR exposure.

Two skin-homing receptors were also measured on Treg cells in the context of UVR, chemokine receptor CCR4 and CLA<sup>143,264</sup>. CLA is a carbohydrate epitope induced by the alpha 1,3-fucosyltransferase VII gene and by cytokines and antigen stimulation<sup>265-267</sup>, which is consistent with higher CD45RA<sup>-</sup>/CD27<sup>-</sup> Treg cells. In our data set, all CLA<sup>+</sup> cells lacked CD45RA expression confirming that these are activated Treg cells (**Figure 24C**). Recently, CLA expression on the Treg cell surface was shown to occur after exposure to nitric oxide, a chemical that is released into the skin upon UVR exposure<sup>264</sup>. CCR4 is another skin-associated T cell marker that has been shown to increase following UVB exposure in mice suggesting that not only are Tregs activated, but that they are stimulated to express both homing receptors significant for infiltration into cutaneous tissues<sup>143,268</sup>. Most studies suggest that Tregs can migrate from lymph nodes to skin and then re-enter the circulation<sup>268</sup>. Transcriptional signatures and phenotypes suggest that the migratory versus resident populations can be distinguished<sup>257,258</sup>. However, conjoined parabiotic surgery of two mice that share the same vasculature compartment showed that there are T cells in the skin epidermis that do not equilibrate through blood and are permanently resident in skin<sup>269-272</sup>. Since many resident Treg cells remain in the dermis and do not recirculate after activation and migration to skin, Treg cells may accumulate through repeated sun exposure; a well-defined risk factor for skin cancer<sup>273,274</sup>. While positive correlations were observed between UV exposure and CLA<sup>+</sup> and CCR4<sup>hi</sup> Tregs,

after adjusting for age and sex these associations were no longer statistically significant indicating that the strongest independent marker is the accumulation of CD45RA<sup>+</sup>/CD27<sup>-</sup> Treg cells. While it is difficult to delineate the origins of tissue resident cells, future studies are needed to define whether UVR contributes to the population of tissue resident memory Treg cells in human skin.

Although several mechanisms control the suppressive functions of Treg cells, UV promotes IL-10 secretion and reportedly exert suppressive activity largely through IL-10 production and express the glucocorticoid-induced TNF family-related receptor (GITR)<sup>275-277</sup>. In cancer studies, engagement of GITR with agonistic antibodies potentiates anti-tumor immunity by destabilizing FoxP3 expression and reducing Treg cells<sup>278</sup>. Given that studies have shown that adoptively transferred UV-activated Tregs into host mice suppress tumor-immune responses, CD4<sup>+</sup> T cell proliferation and contact hypersensitivity<sup>276,279-281</sup>, it is likely that UV exposure increases the suppressive activity of Tregs through antigen activation. This is congruent with the data reported here in that distribution of total Tregs is not associated with recent UV exposure (**Figure 25C, Table 8**). The mechanism for both Treg expansion and increased suppressive activity has often pointed to the UV-vitamin D production axis<sup>282</sup>. Vitamin D is both acquired through the diet and through activation of the first synthesis step by radiation in the UVB range<sup>282</sup>. Topical application of Vitamin D's active form increases the suppressive activity of Treg cells<sup>283</sup> and causes comparable effects to UVB radiation in mice. This method for UV-induced immune suppression is controversial given that Vitamin D receptor knockout mice are still susceptible to UV-activated Treg cells<sup>284</sup>. Furthermore, there are reports that Vitamin D receptor is not highly expressed in mouse FoxP3<sup>+</sup>CD4<sup>+</sup> Treg cells, but there is an inverse relationship between VDR-dependent signaling and FoxP3 regulation<sup>285-289</sup>. Vitamin D production by UVB exposure is particularly high in lighter-skinned individuals, potentially due to the protectiveness of melanin in individuals with natural dark skin<sup>288,290-292</sup>, which may explain the more pronounced associations between recent UVR exposure and Treg cells among lighter-

skinned individuals in our cohort. Given the controversial evidence for vitamin D and its role in UV-induced immune suppression, investigation of vitamin D or vitamin D receptors in the context of UVR exposure and Treg cells is an important future step.

The cross-sectional nature of this analysis cannot establish the presence of UVR exposure prior to measurement of Treg cells, although the UVR-associated changes in skin pigmentation had to have occurred as a result of exposure prior to the time of blood draw. The exact timing of UVR exposure is unknown, and therefore, the temporal relationship between UVR exposure and associated changes in circulating Treg cells require further investigation. In mouse studies, UVB-induced Treg cell activation in skin lasted for two weeks after exposure and then later contributed to expansion of these cells in the peripheral blood<sup>293</sup>. Some previous studies of UVR exposure and immune-related conditions have relied on self-report of sun exposures and ecologic measures, such as latitude, to estimate UVR exposure<sup>147,149,150,294</sup>. Other studies have demonstrated that Treg cell populations are altered with UVR exposure in a small cohort of patients presenting with autoimmune disorders<sup>151,154</sup>, including one such study that demonstrated that activated CD45RA<sup>+</sup> Treg cells are increased in psoriasis patients with recent UV exposure<sup>152</sup>. Our study builds upon these findings, suggesting that Treg cell activation occurs with recent UVR in this cohort.

The spectrophotometer readings used in the present study provide an objective and quantitative measure of recent UVR exposure. Future analysis of this prospective cohort will focus on the associations between baseline UVR exposure, Treg cells and subsequent development of NMSC. Here, we report the first quantitative UVR exposure study associated with subpopulations of Treg cells in peripheral blood. Future studies are necessary to understand if UVR leads to the accumulation of tissue resident Treg cell populations and whether that in turn contributes to carcinogenesis. Additionally, our study reports differences in Treg cell subpopulations by age, sex and race with potential importance in other immune-related diseases.

## **Methods**

### **Study design and population**

Cross-sectional, baseline data from participants enrolled in the first year of the Viruses and Skin Cancer (VIRUSCAN) Study, an ongoing, four-year prospective cohort study of UVR, cutaneous viral infections and skin cancer being conducted at the Moffitt Cancer Center, were used for the current analysis. Individuals undergoing routine skin cancer screening exams at the University of South Florida Dermatology Clinic (USFDC) were eligible for the study if they were at least 60 years of age and had not had both a previous SCC and BCC. At the time of study enrollment, participants underwent a total body skin examination, and suspicious lesions were biopsied as a part of routine clinical care. Study participants with a pathologically confirmed NMSC at baseline were excluded. Questionnaire data, peripheral blood samples and skin pigmentation measurements were also required at study entry. Individuals that failed to complete these study-related activities were excluded from the analysis. The study was approved by the USF Institutional Review board, and all patients provided written informed consent at the time of enrollment.

### **Spectrophotometer data collection**

Skin pigmentation readings were obtained using a spectrophotometer (CM-600D, Konica Minolta Sensing Americas, Inc.) with Spectra Magic NX Lite USB Ver. 2.5 software, using the specular component included (SCI) mode of the instrument which minimizes the influence of the gloss and texture of the skin on skin pigmentation readings, as described previously<sup>295,296</sup>. The instrument was calibrated against a white tile each morning, per manufacturer guidelines. The spectrophotometer readings were obtained by study personnel at the initial study visit when blood samples were collected. This instrument measures color on three different axes: lightness (L) on a scale of 0 (black) to 100 (white), axis “a”, indicating color within the red-green range, and axis “b”, measuring color within the yellow-blue range, with increasing values on a and b axes indicating saturation of color<sup>297</sup>. Natural skin tone was assessed using spectrophotometer



readings of the sun-unexposed underside of the upper arm (i.e. the axilla). The degree of recent tanning in response to recent UVR exposure was measured by calculating the difference between the color readings ( $\Delta E^*ab$ ) on an area of sun-exposed skin (top of the forearm or forehead) and the axilla. Three readings were obtained at each anatomic site, and the average values were recorded. A strong, intra-individual correlation was observed between spectrophotometer readings obtained at the forearm and forehead ( $r=0.6079$ ;  $p<2.2\times 10^{-16}$ ) (**Figure 29**). Therefore, the average of these two values was used as the single measurement of recent UVR exposure.

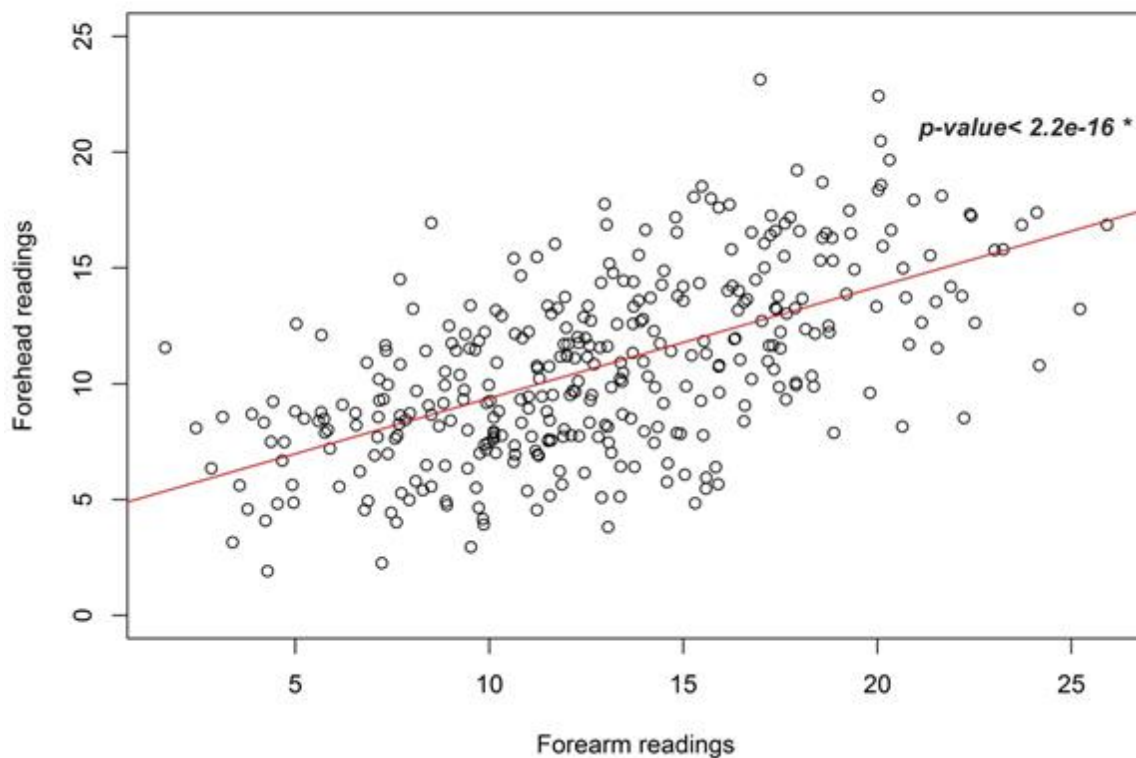


**Figure 29: Spectrophotometer readings between forearm and forehead.** Intra-Individual correlation between spectrophotometer readings obtained at the forearm and forehead among 350 skin cancer screening patients enrolled in year 1 of the VIRUSCAN study. \*The p-value was calculated using Spearman correlation, with correlation coefficient  $\rho=0.6079$ .



### **Blood collection and flow cytometry data acquisition and analysis**

Blood samples were collected in three 10 ml heparin sodium containing blood collection tubes. Samples were processed for isolation of peripheral blood mononuclear cells (PBMCs) by Ficoll-Hypaque centrifugation using 10-20 ml of Lymphocyte Separation Media (Ficoll) according to manufacturer guidelines (Amersham Pharma Biotch, Piscataway, NJ). Freezing medium (10% DMSO, 90% FBS) was used to viably freeze PBMCs in preparation of the future cytometry analysis. Frozen PBMCs stored in liquid nitrogen were thawed on ice and placed into 1 mL phosphate buffered saline (PBS). Approximately  $10^6$  PBMCs were first labeled with the viability dye Ghost Dye Red 780 ( $1\mu\text{L}$ , Tonbo Bioscience) for 20-30 minutes at room temperature to exclude dead cells from the analysis. PBMCs were then treated with  $1\mu\text{L}$  FcR receptor blocking reagent (Miltenyi) and labeled with antibodies to detect the following cell surface antigens: anti-CD3-APC, anti-CD45RA-PerCPCy5.5 (Tonbo Bioscience), anti-CD4-BV785, anti-CCR4-BV421, anti-CLA-FITC, PD-1-PE (Biolegend), anti-CD25-BUV395 (BD Horizon) and anti-CD27-BUV737 (BD Horizon) using  $1\mu\text{L}$  each and for 30 minutes at  $4^\circ\text{C}$ . Cells were fixed with a FoxP3/Transcription Factor Staining Buffer Set (ThermoFisher Scientific) according to the manufacturer's protocol and labeled with  $5\mu\text{L}$  FoxP3-PEDazzle594 (Biolegend) for 30 minutes.

After staining and fixation, cell populations were analyzed within 24 hours on a BD LSRII flow cytometry instrument (BD Biosciences) using the gating strategy defined in **Figure 24** and **Figure 26** and quantified using FlowJo v9 (FlowJo, LLC). The PBMC samples from all patients were thawed and evaluated for viability. Those with less than  $1.0 \times 10^5$  viable lymphocytes were excluded from the final data analysis ( $n=31$ ). In samples included in the analysis,  $3.1 \times 10^5 \pm 2.2 \times 10^5$  viable cells were present. Samples were evaluated for  $\text{CD8}^+$  T cells and  $\text{CD4}^+$  T cells of  $\text{CD3}^+$  lymphocytes.  $\text{CD4}^+$  T cells were further defined by  $\text{CD25}^-\text{FoxP3}^-$  conventional T helper cells (Th CD4) and total  $\text{CD25}^+\text{FoxP3}^+$  Treg and Treg cell subpopulations:  $\text{CD45RA}^+/\text{CD27}^+$  (naïve) Treg cells,  $\text{CD45RA}^-/\text{CD27}^-$  (activated, effector memory) Treg cells (ie, equivalent to

conventional T-effector cells), CD45RA<sup>+</sup>/CD27<sup>-</sup> (terminal memory) Treg cells (ie, equivalent to conventional T cells with an exhausted phenotype), CD45RA<sup>-</sup>/CD27<sup>+</sup> (central memory) Treg cells, cutaneous lymphocyte-associated antigen (CLA) CLA<sup>+</sup> (skin migratory) Treg cells, and chemokine receptor CCR4<sup>hi</sup> (skin migratory) Treg cells, as previously described<sup>132,134,142,145,153,247,249</sup>. All population data is described as a frequency of the parent population. In addition to the described gating strategy, CD4<sup>+</sup> T cells samples were also divided into six populations according to Miyara et al<sup>246</sup> (**Figure 24D**) to define CD45RA<sup>-</sup>CD25<sup>++</sup>FoxP3<sup>lo</sup> as resting Treg cells (Group I), CD45RA<sup>-</sup>CD25<sup>+++</sup>FoxP3<sup>hi</sup> (Group II) as activated Treg cells, and defined CD45RA<sup>-</sup>CD25<sup>++</sup> FoxP3<sup>lo</sup> (Group III) as nonsuppressive Treg cells.

All gating strategies were confirmed by use of fluorescence-minus-one (FMO) control samples in which cells are stained with all colors except the antibody noted (**Figure 26A-B, E-F**).

### **Statistical Methods**

Correlations between Treg cells and UVR were calculated using Spearman's rank, and a trend line was created to visualize the associations. The correlations between T cell populations were described using Spearman's rank correlation coefficient. Additionally, given that previous studies have reported effect modification of UVR-associated physiologic effects by one's natural skin tone<sup>250,251</sup> analysis by lighter versus darker skin tone was performed, based on the median value of the spectrophotometer readings of the sun-unexposed axilla, to investigate whether the associations between UVR and Treg cell phenotypes differed by natural skin tone. Linear regression was used to examine the associations between baseline characteristics and Treg cell phenotypes, adjusted for age and sex. Differences in UVR by sex and age were examined using the Wilcoxon rank sum test and Spearman correlation, respectively. Logistic regression was used to calculate odds ratios (OR's) and 95% confidence intervals (CI's) to estimate the associations between recent UVR exposure and quartiles of the Treg cell phenotypes, adjusted for age and sex. Quartiles were used to account for the possible non-linear relationship between

Treg cells and recent UVR and to avoid use of data transformation within the multivariate models. Statistical analysis was conducted using R, version 3.3.2 (R Foundation for Statistical Computing, Vienna Austria).

## CHAPTER FIVE: IMPLICATIONS AND FUTURE PERSPECTIVES

The work presented here increases the understanding of the role of glutamine metabolic pathways in CD8<sup>+</sup> T cells, a negative immune regulator, Cereblon (CRBN) of MYC, ERK, and glutamine metabolism, and suppressive regulatory T cell (Treg) populations that are susceptible to expansion with UV exposure. These findings lay the groundwork for exciting future studies.

Polyamine metabolism regulates oxidative phosphorylation, mitochondria, and asymmetric division in activated CD8<sup>+</sup> T cells, having large implications on long-term memory differentiation. Long-term memory populations of CD8<sup>+</sup> T cells exhibit higher mitochondrial biomass and higher oxidative phosphorylation<sup>298,299</sup> and blocking oxidative phosphorylation with high dose etomoxir reduces function. CD8<sup>+</sup> T cells that are forced to use glycolysis rather than oxidative phosphorylation preferentially create effector memory populations, rather than central memory<sup>300</sup>, and blocking glucose metabolism increases central memory T cells<sup>301</sup>. Blocking polyamine metabolism results in phenotypic similarities to central memory T cells, suggesting that polyamine production drives effector memory differentiation. The function of any memory cells with lower polyamine pools has yet to be determined.

Further supporting the hypothesis that blocking polyamine metabolism increases CD8<sup>+</sup> T cell long-term memory function is the skewing of normal asymmetric cell division. There are several theories explaining T cell differentiation into effector and memory T cell function. Asymmetric cell division is one such theory in which activated naive T cells asymmetrically distribute protein, organelles and RNA resulting in daughter cells with different fates<sup>14,234,302</sup>. These first generation daughter cells exhibit differing phenotypes. For example, T cells with lower levels of Myc, CD8 and mTOR have memory function characterized by elevated oxidative

phosphorylation, mitochondrial content, CD62L expression, and recall response. Following this theory, it is evident that blocking polyamines causes the accumulation of cells containing lower amounts of CD8 and Myc protein. Thus, limiting polyamine metabolism could increase long-term memory T cell function.

The hypothesis that polyamines increase effector function is especially interesting in light of the effects of Cereblon (CRBN), a regulator of the polyamine pathway in activated CD8<sup>+</sup> T cells. It is evident that CD8<sup>+</sup> T cells lacking CRBN increase short-term effector function *in vivo* and *in vitro*, as demonstrated by increased glucose metabolism, cytokine production and expression of effect function genes. Given the increase in polyamines, inhibiting CRBN could have negative consequences on long-term CD8<sup>+</sup> T cell memory responses. Some of the data presented here is in conflict with this hypothesis. For instance, homeostatic-driven memory development during the aging process in mice lacking CRBN enriches long-term CD8<sup>+</sup> T cell memory. CRBN-deficient CD8<sup>+</sup> T cells also have increased glutamine and arginine uptake, which could drive a positive anti-tumor response or general immune response, overcoming any negative consequences of increased polyamine production. High levels of arginine are beneficial to long-term T cell immunity and survival, possibly through alterations in pathways outside of polyamine production<sup>44</sup>. Several studies also indicate that Myc protein expression is essential to both viral long-term memory development<sup>303</sup> and homeostatic proliferation induced memory<sup>304</sup>. Other pathways outside of glutamine and arginine metabolism could aid in Myc-driven long-term immunity. Further, cellular machinery that turns off Myc mRNA and protein expression appears to be in tact in CRBN-deficient CD8<sup>+</sup> T cells. Therefore, detrimental effects of overexpressed Myc in CD8<sup>+</sup> T cells could also be dampened in the absence of CRBN.

Given the role of polyamine production on asymmetric division and the distribution of Myc to daughter cells, it is essential to observe any effect CRBN has on asymmetric division. Outside of the work presented here, previous studies have also demonstrated that inhibiting amino acid uptake and glutaminase disrupts T cell asymmetric cell division processes<sup>14,234</sup>. The

increased Myc expression and polyamines observed in the absence of CRBN could accumulate the inheritance of Myc protein to all daughter cells, ultimately skewing the first generation population toward Myc<sup>hi</sup> effector cells. However, adding exogenous arginine or a mix of amino acids does not have an effect on asymmetric division<sup>14</sup>. It is therefore possible that normal asymmetric division occurs in the first generation of CD8<sup>+</sup> T cells in the absence of CRBN, but more Myc<sup>hi</sup> effector cells accumulate in undivided cells and subsequent generations.

Future work on polyamine biosynthesis, CRBN and long-term memory CD8<sup>+</sup> T cells will increase the translatability of these findings. Both polyamine biosynthesis and CRBN are easily targetable through small molecules described in this work. Immunotherapy to treat cancer is rapidly expanding to different types of cancer and will require more modifications to increase the durability of responses. For example, tumor-infiltrating lymphocytes (TILs) exhibit dysfunctional mitochondrial activity<sup>305</sup>, resulting in low anti-tumor immunity. Expanding TIL ex vivo in the clinic for re-infusion to the patient is a popular immunotherapeutic technique in cancers like melanoma<sup>306</sup>. During this process, a patient's TIL are removed from tumor fragments and rapidly expanded in the effector molecule, IL-2. Different T cell memory populations can increase the response to TIL therapy<sup>307,308</sup>, and it has been proposed that increasing memory T cells during the TIL rapid expansion process by adding cytokines other than IL-2 or genetic modification can enhance patient response<sup>306</sup>. Adding DFMO or immunomodulatory drugs during the expansion process to increase the function, metabolism and memory of TIL would be a safe and easy way to increase patient responses.

Another immunotherapeutic strategy to treat hematological malignancies is the addition of chimeric antigen receptor (CAR) to a patient's T cells. Similar to tumor-infiltrating lymphocytes in solid tumors, T cells from patients with hematological malignancies have impaired metabolism, including decreased glucose metabolism<sup>33</sup>. Increasing metabolic potential of CAR T has been shown to be more successful for patients receiving CAR T cells<sup>309</sup> and using CAR constructs with higher metabolic potential is desirable<sup>239</sup>. Production of CAR T cells is similar to

the process of TIL therapy in that there is an activation of patients' T cells ex vivo to introduce the CAR construct. There is therefore a window to target pathways that regulate metabolism, such as polyamine production or CRBN.

The Treg population enriched with recent UV exposure warrants more investigation. Several studies have demonstrated that overall numbers of Tregs are expanded with chronic long-term UV exposure<sup>153,281</sup>, but more investigation into why acute UV has such an effect on Tregs could be interesting in the future. These could aid in understanding the role of the immune system during UV-induced or UV-related carcinogenesis. Further, following this same cohort of patients could aid in understanding changes in Treg populations and skin cancer development.

Ultimately, these studies serve as the basis for work that will be directly translatable to the clinic, from immunotherapy, cancer prevention, and basic immunology.

## REFERENCES

- 1 Hesterberg, R. S., Cleveland, J. L. & Epling-Burnette, P. K. Role of Polyamines in Immune Cell Functions. *Medical sciences (Basel, Switzerland)* **6**, doi:10.3390/medsci6010022 (2018).
- 2 Hesterberg, R. S. *et al.* T Regulatory Cell Subpopulations Associated with Recent Ultraviolet Radiation Exposure in a Skin Cancer Screening Cohort. *J Immunol* **201**, 3269-3281, doi:10.4049/jimmunol.1800940 (2018).
- 3 Germain, R. N. T-cell development and the CD4-CD8 lineage decision. *Nat Rev Immunol* **2**, 309-322, doi:10.1038/nri798 (2002).
- 4 Gao, G. F. *et al.* Crystal structure of the complex between human CD8alpha(alpha) and HLA-A2. *Nature* **387**, 630-634, doi:10.1038/42523 (1997).
- 5 Nagaraj, S. *et al.* Altered recognition of antigen is a mechanism of CD8+ T cell tolerance in cancer. *Nat Med* **13**, 828-835, doi:10.1038/nm1609 (2007).
- 6 Chen, L. & Flies, D. B. Molecular mechanisms of T cell co-stimulation and co-inhibition. *Nat Rev Immunol* **13**, 227-242, doi:10.1038/nri3405 (2013).
- 7 Boomer, J. S. & Green, J. M. An enigmatic tail of CD28 signaling. *Cold Spring Harb Perspect Biol* **2**, a002436, doi:10.1101/cshperspect.a002436 (2010).
- 8 (!!! INVALID CITATION !!! [150, 151]).
- 9 Balagopalan, L. *et al.* c-Cbl-mediated regulation of LAT-nucleated signaling complexes. *Mol Cell Biol* **27**, 8622-8636, doi:10.1128/MCB.00467-07 (2007).
- 10 Park, S. G. *et al.* The kinase PDK1 integrates T cell antigen receptor and CD28 coreceptor signaling to induce NF-kappaB and activate T cells. *Nat Immunol* **10**, 158-166, doi:10.1038/ni.1687 (2009).
- 11 Guertin, D. A. *et al.* Ablation in mice of the mTORC components raptor, rictor, or mLST8 reveals that mTORC2 is required for signaling to Akt-FOXO and PKCalpha, but not S6K1. *Dev Cell* **11**, 859-871, doi:10.1016/j.devcel.2006.10.007 (2006).
- 12 Iwata, T. N. *et al.* Conditional Disruption of Raptor Reveals an Essential Role for mTORC1 in B Cell Development, Survival, and Metabolism. *J Immunol* **197**, 2250-2260, doi:10.4049/jimmunol.1600492 (2016).
- 13 Wang, R. *et al.* The transcription factor Myc controls metabolic reprogramming upon T lymphocyte activation. *Immunity* **35**, 871-882, doi:10.1016/j.immuni.2011.09.021 (2011).
- 14 Verbist, K. C. *et al.* Metabolic maintenance of cell asymmetry following division in activated T lymphocytes. *Nature* **532**, 389-393, doi:10.1038/nature17442 (2016).
- 15 Ho, P. C. *et al.* Phosphoenolpyruvate Is a Metabolic Checkpoint of Anti-tumor T Cell Responses. *Cell* **162**, 1217-1228, doi:10.1016/j.cell.2015.08.012 (2015).
- 16 Higgins, J. J., Pucilowska, J., Lombardi, R. Q. & Rooney, J. P. A mutation in a novel ATP-dependent Lon protease gene in a kindred with mild mental retardation. *Neurology* **63**, 1927-1931 (2004).
- 17 Hendriks, J. *et al.* CD27 is required for generation and long-term maintenance of T cell immunity. *Nat Immunol* **1**, 433-440, doi:10.1038/80877 (2000).
- 18 Agematsu, K., Hokibara, S., Nagumo, H. & Komiyama, A. CD27: a memory B-cell marker. *Immunol Today* **21**, 204-206 (2000).
- 19 Takeda, K. *et al.* CD27-mediated activation of murine NK cells. *J Immunol* **164**, 1741-1745 (2000).



- 20 Croft, M. Costimulation of T cells by OX40, 4-1BB, and CD27. *Cytokine Growth Factor Rev* **14**, 265-273 (2003).
- 21 Gramaglia, I., Weinberg, A. D., Lemon, M. & Croft, M. Ox-40 ligand: a potent costimulatory molecule for sustaining primary CD4 T cell responses. *J Immunol* **161**, 6510-6517 (1998).
- 22 Rogers, P. R. & Croft, M. CD28, Ox-40, LFA-1, and CD4 modulation of Th1/Th2 differentiation is directly dependent on the dose of antigen. *J Immunol* **164**, 2955-2963 (2000).
- 23 Smith, A. *et al.* The role of the integrin LFA-1 in T-lymphocyte migration. *Immunol Rev* **218**, 135-146, doi:10.1111/j.1600-065X.2007.00537.x (2007).
- 24 Nocentini, G. *et al.* A new member of the tumor necrosis factor/nerve growth factor receptor family inhibits T cell receptor-induced apoptosis. *Proc Natl Acad Sci U S A* **94**, 6216-6221 (1997).
- 25 Khayyamian, S. *et al.* ICOS-ligand, expressed on human endothelial cells, costimulates Th1 and Th2 cytokine secretion by memory CD4+ T cells. *Proc Natl Acad Sci U S A* **99**, 6198-6203, doi:10.1073/pnas.092576699 (2002).
- 26 Cai, G. & Freeman, G. J. The CD160, BTLA, LIGHT/HVEM pathway: a bidirectional switch regulating T-cell activation. *Immunol Rev* **229**, 244-258, doi:10.1111/j.1600-065X.2009.00783.x (2009).
- 27 Anderson, A. C., Joller, N. & Kuchroo, V. K. Lag-3, Tim-3, and TIGIT: Co-inhibitory Receptors with Specialized Functions in Immune Regulation. *Immunity* **44**, 989-1004, doi:10.1016/j.immuni.2016.05.001 (2016).
- 28 Buck, M. D. *et al.* Mitochondrial Dynamics Controls T Cell Fate through Metabolic Programming. *Cell* **166**, 63-76, doi:10.1016/j.cell.2016.05.035 (2016).
- 29 Michalek, R. D. & Rathmell, J. C. The metabolic life and times of a T-cell. *Immunol Rev* **236**, 190-202, doi:10.1111/j.1600-065X.2010.00911.x (2010).
- 30 Palmer, C. S. *et al.* Regulators of Glucose Metabolism in CD4(+) and CD8(+) T Cells. *Int Rev Immunol* **35**, 477-488, doi:10.3109/08830185.2015.1082178 (2016).
- 31 Parry, R. V. *et al.* CTLA-4 and PD-1 receptors inhibit T-cell activation by distinct mechanisms. *Mol Cell Biol* **25**, 9543-9553, doi:10.1128/MCB.25.21.9543-9553.2005 (2005).
- 32 Wing, K. *et al.* CTLA-4 control over Foxp3+ regulatory T cell function. *Science* **322**, 271-275, doi:10.1126/science.1160062 (2008).
- 33 Siska, P. J. *et al.* Suppression of Glut1 and Glucose Metabolism by Decreased Akt/mTORC1 Signaling Drives T Cell Impairment in B Cell Leukemia. *J Immunol* **197**, 2532-2540, doi:10.4049/jimmunol.1502464 (2016).
- 34 Andrews, L. P., Marciscano, A. E., Drake, C. G. & Vignali, D. A. LAG3 (CD223) as a cancer immunotherapy target. *Immunol Rev* **276**, 80-96, doi:10.1111/imr.12519 (2017).
- 35 Chang, C. H. & Pearce, E. L. Emerging concepts of T cell metabolism as a target of immunotherapy. *Nat Immunol* **17**, 364-368, doi:10.1038/ni.3415 (2016).
- 36 Motz, G. T. & Coukos, G. Deciphering and reversing tumor immune suppression. *Immunity* **39**, 61-73, doi:10.1016/j.immuni.2013.07.005 (2013).
- 37 Hernandez, C., Huebener, P. & Schwabe, R. F. Damage-associated molecular patterns in cancer: a double-edged sword. *Oncogene* **35**, 5931-5941, doi:10.1038/onc.2016.104 (2016).
- 38 Garrido, F., Aptsiauri, N., Doorduijn, E. M., Garcia Lora, A. M. & van Hall, T. The urgent need to recover MHC class I in cancers for effective immunotherapy. *Current opinion in immunology* **39**, 44-51, doi:10.1016/j.coi.2015.12.007 (2016).
- 39 Houghton, A. N. & Guevara-Patino, J. A. Immune recognition of self in immunity against cancer. *J Clin Invest* **114**, 468-471, doi:10.1172/jci22685 (2004).

- 40 Hwang, I. & Nguyen, N. Mechanisms of tumor-induced T cell immune suppression and therapeutics to counter those effects. *Archives of pharmacal research* **38**, 1415-1433, doi:10.1007/s12272-015-0566-y (2015).
- 41 Francisco, L. M. *et al.* PD-L1 regulates the development, maintenance, and function of induced regulatory T cells. *The Journal of experimental medicine* **206**, 3015-3029, doi:10.1084/jem.20090847 (2009).
- 42 Nagaraj, S., Schrum, A. G., Cho, H. I., Celis, E. & Gabrilovich, D. I. Mechanism of T cell tolerance induced by myeloid-derived suppressor cells. *J Immunol* **184**, 3106-3116, doi:10.4049/jimmunol.0902661 (2010).
- 43 Gabrilovich, D. I. & Nagaraj, S. Myeloid-derived suppressor cells as regulators of the immune system. *Nature reviews. Immunology* **9**, 162-174, doi:10.1038/nri2506 (2009).
- 44 Geiger, R. *et al.* L-Arginine Modulates T Cell Metabolism and Enhances Survival and Anti-tumor Activity. *Cell* **167**, 829-842 e813, doi:10.1016/j.cell.2016.09.031 (2016).
- 45 Fischer, K. *et al.* Inhibitory effect of tumor cell-derived lactic acid on human T cells. *Blood* **109**, 3812-3819, doi:10.1182/blood-2006-07-035972 (2007).
- 46 Wegiel, B., Vuerich, M., Daneshmandi, S. & Seth, P. Metabolic Switch in the Tumor Microenvironment Determines Immune Responses to Anti-cancer Therapy. *Frontiers in oncology* **8**, 284, doi:10.3389/fonc.2018.00284 (2018).
- 47 Chang, C. H. *et al.* Metabolic Competition in the Tumor Microenvironment Is a Driver of Cancer Progression. *Cell* **162**, 1229-1241, doi:10.1016/j.cell.2015.08.016 (2015).
- 48 Ito, T. *et al.* Identification of a primary target of thalidomide teratogenicity. *Science* **327**, 1345-1350, doi:10.1126/science.1177319 (2010).
- 49 Dimopoulos, M. *et al.* Lenalidomide plus dexamethasone for relapsed or refractory multiple myeloma. *N Engl J Med* **357**, 2123-2132, doi:10.1056/NEJMoa070594 (2007).
- 50 Weber, D. M. *et al.* Lenalidomide plus dexamethasone for relapsed multiple myeloma in North America. *N Engl J Med* **357**, 2133-2142, doi:10.1056/NEJMoa070596 (2007).
- 51 Chanan-Khan, A. *et al.* Clinical efficacy of lenalidomide in patients with relapsed or refractory chronic lymphocytic leukemia: results of a phase II study. *J Clin Oncol* **24**, 5343-5349, doi:10.1200/JCO.2005.05.0401 (2006).
- 52 Yang, Y. *et al.* Exploiting synthetic lethality for the therapy of ABC diffuse large B cell lymphoma. *Cancer Cell* **21**, 723-737, doi:10.1016/j.ccr.2012.05.024 (2012).
- 53 Hagner, P. R. *et al.* CC-122, a pleiotropic pathway modifier, mimics an interferon response and has antitumor activity in DLBCL. *Blood* **126**, 779-789, doi:10.1182/blood-2015-02-628669 (2015).
- 54 List, A. *et al.* Efficacy of lenalidomide in myelodysplastic syndromes. *N Engl J Med* **352**, 549-557, doi:10.1056/NEJMoa041668 (2005).
- 55 Talati, C., Sallman, D. & List, A. Lenalidomide: Myelodysplastic syndromes with del(5q) and beyond. *Semin Hematol* **54**, 159-166, doi:10.1053/j.seminhematol.2017.06.003 (2017).
- 56 Fischer, E. S. *et al.* Structure of the DDB1-CRBN E3 ubiquitin ligase in complex with thalidomide. *Nature* **512**, 49-53, doi:10.1038/nature13527 (2014).
- 57 Petzold, G., Fischer, E. S. & Thoma, N. H. Structural basis of lenalidomide-induced CK1alpha degradation by the CRL4(CRBN) ubiquitin ligase. *Nature* **532**, 127-130, doi:10.1038/nature16979 (2016).
- 58 Chamberlain, P. P. *et al.* Structure of the human Cereblon-DDB1-lenalidomide complex reveals basis for responsiveness to thalidomide analogs. *Nat Struct Mol Biol* **21**, 803-809, doi:10.1038/nsmb.2874 (2014).
- 59 Gopalakrishnan, R., Matta, H., Tolani, B., Triche, T., Jr. & Chaudhary, P. M. Immunomodulatory drugs target IKZF1-IRF4-MYC axis in primary effusion lymphoma in a cereblon-dependent manner and display synergistic cytotoxicity with BRD4 inhibitors. *Oncogene* **35**, 1797-1810, doi:10.1038/onc.2015.245 (2016).

- 60 Lu, G. *et al.* The myeloma drug lenalidomide promotes the cereblon-dependent destruction of Ikaros proteins. *Science* **343**, 305-309, doi:10.1126/science.1244917 (2014).
- 61 Winter, G. E. *et al.* DRUG DEVELOPMENT. Phthalimide conjugation as a strategy for in vivo target protein degradation. *Science* **348**, 1376-1381, doi:10.1126/science.aab1433 (2015).
- 62 O'Brien, S. *et al.* Ikaros imposes a barrier to CD8+ T cell differentiation by restricting autocrine IL-2 production. *J Immunol* **192**, 5118-5129, doi:10.4049/jimmunol.1301992 (2014).
- 63 Harker, N. *et al.* The CD8alpha gene locus is regulated by the Ikaros family of proteins. *Mol Cell* **10**, 1403-1415 (2002).
- 64 Kronke, J. *et al.* Lenalidomide causes selective degradation of IKZF1 and IKZF3 in multiple myeloma cells. *Science* **343**, 301-305, doi:10.1126/science.1244851 (2014).
- 65 Eichner, R. *et al.* Immunomodulatory drugs disrupt the cereblon-CD147-MCT1 axis to exert antitumor activity and teratogenicity. *Nat Med* **22**, 735-743, doi:10.1038/nm.4128 (2016).
- 66 Higgins, J. J., Hao, J., Kosofsky, B. E. & Rajadhyaksha, A. M. Dysregulation of large-conductance Ca<sup>2+</sup>-activated K<sup>+</sup> channel expression in nonsyndromal mental retardation due to a cereblon p.R419X mutation. *Neurogenetics* **9**, 219-223, doi:10.1007/s10048-008-0128-2 (2008).
- 67 Nguyen, T. V. *et al.* Glutamine Triggers Acetylation-Dependent Degradation of Glutamine Synthetase via the Thalidomide Receptor Cereblon. *Mol Cell* **61**, 809-820, doi:10.1016/j.molcel.2016.02.032 (2016).
- 68 Lee, K. M., Jo, S., Kim, H., Lee, J. & Park, C. S. Functional modulation of AMP-activated protein kinase by cereblon. *Biochim Biophys Acta* **1813**, 448-455, doi:10.1016/j.bbamcr.2011.01.005 (2011).
- 69 Kang, J. A. *et al.* Epigenetic regulation of Kcna3-encoding Kv1.3 potassium channel by cereblon contributes to regulation of CD4+ T-cell activation. *Proc Natl Acad Sci U S A* **113**, 8771-8776, doi:10.1073/pnas.1502166113 (2016).
- 70 Choi, B. S. *et al.* Differential impact of L-arginine deprivation on the activation and effector functions of T cells and macrophages. *J Leukoc Biol* **85**, 268-277, doi:10.1189/jlb.0508310 (2009).
- 71 Carr, E. L. *et al.* Glutamine uptake and metabolism are coordinately regulated by ERK/MAPK during T lymphocyte activation. *J Immunol* **185**, 1037-1044, doi:10.4049/jimmunol.0903586 (2010).
- 72 Johnson, M. O. *et al.* Distinct Regulation of Th17 and Th1 Cell Differentiation by Glutaminase-Dependent Metabolism. *Cell* **175**, 1780-1795.e1719, doi:10.1016/j.cell.2018.10.001 (2018).
- 73 Glick, G. D. *et al.* Anaplerotic metabolism of alloreactive T cells provides a metabolic approach to treat graft-versus-host disease. *J Pharmacol Exp Ther* **351**, 298-307, doi:10.1124/jpet.114.218099 (2014).
- 74 Nguyen, H. D., Kuril, S., Bastian, D. & Yu, X. Z. T-Cell Metabolism in Hematopoietic Cell Transplantation. *Front Immunol* **9**, 176, doi:10.3389/fimmu.2018.00176 (2018).
- 75 Gatza, E. *et al.* Manipulating the bioenergetics of alloreactive T cells causes their selective apoptosis and arrests graft-versus-host disease. *Science translational medicine* **3**, 67ra68, doi:10.1126/scitranslmed.3001975 (2011).
- 76 Macintyre, A. N. *et al.* The glucose transporter Glut1 is selectively essential for CD4 T cell activation and effector function. *Cell metabolism* **20**, 61-72, doi:10.1016/j.cmet.2014.05.004 (2014).
- 77 Hunt, N. H. & Fragonas, J. C. Effects of anti-oxidants on ornithine decarboxylase in mitogenically-activated T lymphocytes. *Biochim Biophys Acta* **1133**, 261-267 (1992).

- 78 Widjaja, C. E. *et al.* Proteasome activity regulates CD8+ T lymphocyte metabolism and fate specification. *J Clin Invest* **127**, 3609-3623, doi:10.1172/JCI90895 (2017).
- 79 Klein Geltink, R. I. *et al.* Mitochondrial Priming by CD28. *Cell* **171**, 385-397 e311, doi:10.1016/j.cell.2017.08.018 (2017).
- 80 Pearce, E. L., Poffenberger, M. C., Chang, C. H. & Jones, R. G. Fueling immunity: insights into metabolism and lymphocyte function. *Science* **342**, 1242454, doi:10.1126/science.1242454 (2013).
- 81 Sullivan, B. M., Juedes, A., Szabo, S. J., von Herrath, M. & Glimcher, L. H. Antigen-driven effector CD8 T cell function regulated by T-bet. *Proc Natl Acad Sci U S A* **100**, 15818-15823, doi:10.1073/pnas.2636938100 (2003).
- 82 Cobb, D. *et al.* T-bet-dependent regulation of CD8+ T-cell expansion during experimental *Trypanosoma cruzi* infection. *Immunology* **128**, 589-599, doi:10.1111/j.1365-2567.2009.03169.x (2009).
- 83 Gnanaprakasam, J. N. & Wang, R. MYC in Regulating Immunity: Metabolism and Beyond. *Genes (Basel)* **8**, doi:10.3390/genes8030088 (2017).
- 84 Ehrke, M. J., Porter, C. W., Eppolito, C. & Mihich, E. Selective modulation by alpha-difluoromethylornithine of T-lymphocyte and antibody-mediated cytotoxic responses to mouse tumor allografts. *Cancer Res* **46**, 2798-2803 (1986).
- 85 Bowlin, T. L., McKown, B. J. & Sunkara, P. S. Increased ornithine decarboxylase activity and polyamine biosynthesis are required for optimal cytolytic T lymphocyte induction. *Cellular immunology* **105**, 110-117 (1987).
- 86 Bowlin, T. L., McKown, B. J. & Schroeder, K. K. Methyl-acetylenicputrescine (MAP), an inhibitor of polyamine biosynthesis, reduces the frequency and cytolytic activity of alloantigen-induced LyT 2.2 positive lymphocytes in vivo. *Int J Immunopharmacol* **11**, 259-265 (1989).
- 87 Bowlin, T. L., Rosenberger, A. L. & McKown, B. J. Alpha-difluoromethylornithine, an inhibitor of polyamine biosynthesis, augments cyclosporin A inhibition of cytolytic T lymphocyte induction. *Clinical and experimental immunology* **77**, 151-156 (1989).
- 88 Schall, R. P., Sekar, J., Tandon, P. M. & Susskind, B. M. Difluoromethylornithine (DFMO) arrests murine CTL development in the late, pre-effector stage. *Immunopharmacology* **21**, 129-143 (1991).
- 89 Bowlin, T. L., Davis, G. F. & McKown, B. J. Inhibition of alloantigen-induced cytolytic T lymphocytes in vitro with (2R,5R)-6-heptyne-2,5-diamine, an irreversible inhibitor of ornithine decarboxylase. *Cell Immunol* **111**, 443-450 (1988).
- 90 Bronte, V. & Zanovello, P. Regulation of immune responses by L-arginine metabolism. *Nat Rev Immunol* **5**, 641-654, doi:10.1038/nri1668 (2005).
- 91 Ye, C. *et al.* Targeting Ornithine Decarboxylase by alpha-Difluoromethylornithine Inhibits Tumor Growth by Impairing Myeloid-Derived Suppressor Cells. *J Immunol* **196**, 915-923, doi:10.4049/jimmunol.1500729 (2016).
- 92 Ziv, Y. *et al.* Effect of tamoxifen on 1,2-dimethylhydrazine-HCl-induced colon carcinogenesis in rats. *Anticancer Res* **17**, 803-810 (1997).
- 93 Bowlin, T. L., Hoeper, B. J., Rosenberger, A. L., Davis, G. F. & Sunkara, P. S. Effects of three irreversible inhibitors of ornithine decarboxylase on macrophage-mediated tumoricidal activity and antitumor activity in B16F1 tumor-bearing mice. *Cancer Res* **50**, 4510-4514 (1990).
- 94 Hayes, C. S. *et al.* Polyamine-blocking therapy reverses immunosuppression in the tumor microenvironment. *Cancer immunology research* **2**, 274-285, doi:10.1158/2326-6066.cir-13-0120-t (2014).
- 95 Alexander, E. T., Minton, A., Peters, M. C., Phanstiel, O. t. & Gilmour, S. K. A novel polyamine blockade therapy activates an anti-tumor immune response. *Oncotarget* **8**, 84140-84152, doi:10.18632/oncotarget.20493 (2017).

- 96 Sunderkotter, C. *et al.* Subpopulations of mouse blood monocytes differ in maturation stage and inflammatory response. *J Immunol* **172**, 4410-4417 (2004).
- 97 Voisin, M. B., Buzoni-Gatel, D., Bout, D. & Velge-Roussel, F. Both expansion of regulatory GR1+ CD11b+ myeloid cells and anergy of T lymphocytes participate in hyporesponsiveness of the lung-associated immune system during acute toxoplasmosis. *Infect Immun* **72**, 5487-5492, doi:10.1128/IAI.72.9.5487-5492.2004 (2004).
- 98 Mencacci, A. *et al.* CD80+Gr-1+ myeloid cells inhibit development of antifungal Th1 immunity in mice with candidiasis. *J Immunol* **169**, 3180-3190 (2002).
- 99 Garg, A. & Spector, S. A. HIV type 1 gp120-induced expansion of myeloid derived suppressor cells is dependent on interleukin 6 and suppresses immunity. *J Infect Dis* **209**, 441-451, doi:10.1093/infdis/jit469 (2014).
- 100 Kumar, V., Patel, S., Tcyganov, E. & Gabrilovich, D. I. The Nature of Myeloid-Derived Suppressor Cells in the Tumor Microenvironment. *Trends Immunol* **37**, 208-220, doi:10.1016/j.it.2016.01.004 (2016).
- 101 Nagaraj, S., Youn, J. I. & Gabrilovich, D. I. Reciprocal relationship between myeloid-derived suppressor cells and T cells. *J Immunol* **191**, 17-23, doi:10.4049/jimmunol.1300654 (2013).
- 102 Raber, P., Ochoa, A. C. & Rodriguez, P. C. Metabolism of L-arginine by myeloid-derived suppressor cells in cancer: mechanisms of T cell suppression and therapeutic perspectives. *Immunological investigations* **41**, 614-634, doi:10.3109/08820139.2012.680634 (2012).
- 103 Niino, D. *et al.* Ratio of M2 macrophage expression is closely associated with poor prognosis for Angioimmunoblastic T-cell lymphoma (AITL). *Pathol Int* **60**, 278-283, doi:10.1111/j.1440-1827.2010.02514.x (2010).
- 104 Wang, Y. C. *et al.* Notch signaling determines the M1 versus M2 polarization of macrophages in antitumor immune responses. *Cancer Res* **70**, 4840-4849, doi:10.1158/0008-5472.CAN-10-0269 (2010).
- 105 Nagaraj, S. *et al.* Antigen-specific CD4(+) T cells regulate function of myeloid-derived suppressor cells in cancer via retrograde MHC class II signaling. *Cancer Res* **72**, 928-938, doi:10.1158/0008-5472.CAN-11-2863 (2012).
- 106 Youn, J. I., Collazo, M., Shalova, I. N., Biswas, S. K. & Gabrilovich, D. I. Characterization of the nature of granulocytic myeloid-derived suppressor cells in tumor-bearing mice. *J Leukoc Biol* **91**, 167-181, doi:10.1189/jlb.0311177 (2012).
- 107 Mills, E. L. *et al.* Succinate Dehydrogenase Supports Metabolic Repurposing of Mitochondria to Drive Inflammatory Macrophages. *Cell* **167**, 457-470 e413, doi:10.1016/j.cell.2016.08.064 (2016).
- 108 Cao, Y. *et al.* L-arginine and docetaxel synergistically enhance anti-tumor immunity by modifying the immune status of tumor-bearing mice. *Int Immunopharmacol* **35**, 7-14, doi:10.1016/j.intimp.2016.03.002 (2016).
- 109 He, X., Lin, H., Yuan, L. & Li, B. Combination therapy with L-arginine and alpha-PD-L1 antibody boosts immune response against osteosarcoma in immunocompetent mice. *Cancer Biol Ther* **18**, 94-100, doi:10.1080/15384047.2016.1276136 (2017).
- 110 Gerriets, V. A. & Rathmell, J. C. Metabolic pathways in T cell fate and function. *Trends Immunol* **33**, 168-173, doi:10.1016/j.it.2012.01.010 (2012).
- 111 Rubin, R. L. & Burlingame, R. W. Drug-induced autoimmunity: a disorder at the interface between metabolism and immunity. *Biochem Soc Trans* **19**, 153-159 (1991).
- 112 Rathmell, J. C. Apoptosis and B cell tolerance. *Curr Dir Autoimmun* **6**, 38-60 (2003).
- 113 Teti, D., Visalli, M. & McNair, H. Analysis of polyamines as markers of (patho)physiological conditions. *J Chromatogr B Analyt Technol Biomed Life Sci* **781**, 107-149 (2002).

- 114 Karouzakis, E., Gay, R. E., Gay, S. & Neidhart, M. Increased recycling of polyamines is associated with global DNA hypomethylation in rheumatoid arthritis synovial fibroblasts. *Arthritis Rheum* **64**, 1809-1817, doi:10.1002/art.34340 (2012).
- 115 Pignata, S., Di Luccia, A., Lamanda, R., Menchise, A. & D'Agostino, L. Interaction of putrescine with nuclear oligopeptides in the enterocyte-like Caco-2 cells. *Digestion* **60**, 255-261, doi:10.1159/000007666 (1999).
- 116 D'Agostino, L. & Di Luccia, A. Polyamines interact with DNA as molecular aggregates. *Eur J Biochem* **269**, 4317-4325 (2002).
- 117 D'Agostino, L., di Pietro, M. & Di Luccia, A. Nuclear aggregates of polyamines are supramolecular structures that play a crucial role in genomic DNA protection and conformation. *FEBS J* **272**, 3777-3787, doi:10.1111/j.1742-4658.2005.04782.x (2005).
- 118 Riboldi, P. *et al.* Anti-DNA antibodies: a diagnostic and prognostic tool for systemic lupus erythematosus? *Autoimmunity* **38**, 39-45, doi:10.1080/08916930400022616 (2005).
- 119 Fineschi, S. *et al.* Prevalence of autoantibodies against structure specific recognition protein 1 in systemic lupus erythematosus. *Lupus* **13**, 463-468, doi:10.1191/0961203304lu1049oa (2004).
- 120 Kim, H. A. *et al.* Polyamine patterns in plasma of patients with systemic lupus erythematosus and fever. *Lupus* **27**, 930-938, doi:10.1177/0961203317751860 (2018).
- 121 Yukioka, K. *et al.* Polyamine levels in synovial tissues and synovial fluids of patients with rheumatoid arthritis. *The Journal of rheumatology* **19**, 689-692 (1992).
- 122 Didona, D., Paolino, G., Bottoni, U. & Cantisani, C. Non Melanoma Skin Cancer Pathogenesis Overview. *Biomedicines* **6**, 6 (2018).
- 123 Leiter, U., Eigentler, T. & Garbe, C. Epidemiology of skin cancer. *Adv Exp Med Biol* **810**, 120-140 (2014).
- 124 Raasch, B. A., Buettner, P. G. & Garbe, C. Basal cell carcinoma: histological classification and body-site distribution. *Br J Dermatol* **155**, 401-407, doi:10.1111/j.1365-2133.2006.07234.x (2006).
- 125 Rana, S., Byrne, S. N., MacDonald, L. J., Chan, C. Y. & Halliday, G. M. Ultraviolet B suppresses immunity by inhibiting effector and memory T cells. *Am J Pathol* **172**, 993-1004, doi:10.2353/ajpath.2008.070517 (2008).
- 126 Li-Weber, M. *et al.* Ultraviolet irradiation suppresses T cell activation via blocking TCR-mediated ERK and NF-kappa B signaling pathways. *J Immunol* **175**, 2132-2143 (2005).
- 127 Schwarz, T. 25 years of UV-induced immunosuppression mediated by T cells-from disregarded T suppressor cells to highly respected regulatory T cells. *Photochem Photobiol* **84**, 10-18, doi:10.1111/j.1751-1097.2007.00223.x (2008).
- 128 Dunn, G. P., Old, L. J. & Schreiber, R. D. The immunobiology of cancer immunosurveillance and immunoediting. *Immunity* **21**, 137-148, doi:10.1016/j.immuni.2004.07.017 (2004).
- 129 Woo, E. Y. *et al.* Regulatory CD4(+)CD25(+) T cells in tumors from patients with early-stage non-small cell lung cancer and late-stage ovarian cancer. *Cancer Res* **61**, 4766-4772 (2001).
- 130 Liyanage, U. K. *et al.* Prevalence of regulatory T cells is increased in peripheral blood and tumor microenvironment of patients with pancreas or breast adenocarcinoma. *J Immunol* **169**, 2756-2761 (2002).
- 131 Maldonado, A. *et al.* Decreased effector memory CD45RA+ CD62L- CD8+ T cells and increased central memory CD45RA- CD62L+ CD8+ T cells in peripheral blood of rheumatoid arthritis patients. *Arthritis Res Ther* **5**, R91-96 (2003).
- 132 Schaier, M. *et al.* DR(high+)CD45RA(-)-Tregs potentially affect the suppressive activity of the total Treg pool in renal transplant patients. *PLoS One* **7**, e34208, doi:10.1371/journal.pone.0034208 (2012).

- 133 Ponchel, F. *et al.* Dysregulated lymphocyte proliferation and differentiation in patients with rheumatoid arthritis. *Blood* **100**, 4550-4556, doi:10.1182/blood-2002-03-0671 (2002).
- 134 Hartling, H. J. *et al.* CD4(+) and CD8(+) regulatory T cells (Tregs) are elevated and display an active phenotype in patients with chronic HCV mono-infection and HIV/HCV co-infection. *Scand J Immunol* **76**, 294-305, doi:10.1111/j.1365-3083.2012.02725.x (2012).
- 135 Rosenblum, M. D., Way, S. S. & Abbas, A. K. Regulatory T cell memory. *Nat Rev Immunol* **16**, 90-101, doi:10.1038/nri.2015.1 (2016).
- 136 Hendriks, J., Xiao, Y. & Borst, J. CD27 promotes survival of activated T cells and complements CD28 in generation and establishment of the effector T cell pool. *J Exp Med* **198**, 1369-1380, doi:10.1084/jem.20030916 (2003).
- 137 Hendriks, J. *et al.* During viral infection of the respiratory tract, CD27, 4-1BB, and OX40 collectively determine formation of CD8+ memory T cells and their capacity for secondary expansion. *J Immunol* **175**, 1665-1676 (2005).
- 138 Schenkel, J. M. & Masopust, D. Tissue-resident memory T cells. *Immunity* **41**, 886-897, doi:10.1016/j.immuni.2014.12.007 (2014).
- 139 Duhon, T., Duhon, R., Lanzavecchia, A., Sallusto, F. & Campbell, D. J. Functionally distinct subsets of human FOXP3+ Treg cells that phenotypically mirror effector Th cells. *Blood* **119**, 4430-4440, doi:10.1182/blood-2011-11-392324 (2012).
- 140 Holick, M. F. Sunlight, ultraviolet radiation, vitamin D and skin cancer: how much sunlight do we need? *Adv Exp Med Biol* **810**, 1-16 (2014).
- 141 Maeda, A., Beissert, S., Schwarz, T. & Schwarz, A. Phenotypic and functional characterization of ultraviolet radiation-induced regulatory T cells. *J Immunol* **180**, 3065-3071 (2008).
- 142 Schwarz, A., Navid, F., Sparwasser, T., Clausen, B. E. & Schwarz, T. In vivo reprogramming of UV radiation-induced regulatory T-cell migration to inhibit the elicitation of contact hypersensitivity. *J Allergy Clin Immunol* **128**, 826-833, doi:10.1016/j.jaci.2011.06.005 (2011).
- 143 Yamazaki, S. *et al.* Homeostasis of thymus-derived Foxp3+ regulatory T cells is controlled by ultraviolet B exposure in the skin. *The Journal of Immunology* **193**, 5488-5497 (2014).
- 144 Ben Ya'acov, A., Lichtenstein, Y., Zolotarov, L. & Ilan, Y. The gut microbiome as a target for regulatory T cell-based immunotherapy: induction of regulatory lymphocytes by oral administration of anti-LPS enriched colostrum alleviates immune mediated colitis. *BMC Gastroenterol* **15**, 154, doi:10.1186/s12876-015-0388-x (2015).
- 145 Mailloux, A. W. *et al.* Expansion of effector memory regulatory T cells represents a novel prognostic factor in lower risk myelodysplastic syndrome. *J Immunol* **189**, 3198-3208, doi:10.4049/jimmunol.1200602 (2012).
- 146 Kozłowska, E., Biernacka, M., Ciechomska, M. & Drela, N. Age-related changes in the occurrence and characteristics of thymic CD4(+) CD25(+) T cells in mice. *Immunology* **122**, 445-453, doi:10.1111/j.1365-2567.2007.02667.x (2007).
- 147 Simpson, S., Jr., Blizzard, L., Otahal, P., Van der Mei, I. & Taylor, B. Latitude is significantly associated with the prevalence of multiple sclerosis: a meta-analysis. *J Neurol Neurosurg Psychiatry* **82**, 1132-1141, doi:10.1136/jnnp.2011.240432 (2011).
- 148 Ravanat, J. L., Douki, T. & Cadet, J. Direct and indirect effects of UV radiation on DNA and its components. *J Photochem Photobiol B* **63**, 88-102 (2001).
- 149 Vieira, V. M. *et al.* Association between residences in U.S. northern latitudes and rheumatoid arthritis: A spatial analysis of the Nurses' Health Study. *Environ Health Perspect* **118**, 957-961, doi:10.1289/ehp.0901861 (2010).

- 150 Ponsonby, A. L., Lucas, R. M. & van der Mei, I. A. UVR, vitamin D and three autoimmune diseases--multiple sclerosis, type 1 diabetes, rheumatoid arthritis. *Photochem Photobiol* **81**, 1267-1275, doi:10.1562/2005-02-15-IR-441 (2005).
- 151 Breuer, J. *et al.* Ultraviolet B light attenuates the systemic immune response in central nervous system autoimmunity. *Ann Neurol* **75**, 739-758, doi:10.1002/ana.24165 (2014).
- 152 Saito, C., Maeda, A. & Morita, A. Bath-PUVA therapy induces circulating regulatory T cells in patients with psoriasis. *J Dermatol Sci* **53**, 231-233, doi:10.1016/j.jdermsci.2008.09.011 (2009).
- 153 Schwarz, A., Maeda, A. & Schwarz, T. Alteration of the migratory behavior of UV-induced regulatory T cells by tissue-specific dendritic cells. *J Immunol* **178**, 877-886 (2007).
- 154 Furuhashi, T. *et al.* Photo(chemo)therapy reduces circulating Th17 cells and restores circulating regulatory T cells in psoriasis. *PLoS One* **8**, e54895, doi:10.1371/journal.pone.0054895 (2013).
- 155 Rajadhyaksha, A. M. *et al.* Behavioral characterization of cereblon forebrain-specific conditional null mice: a model for human non-syndromic intellectual disability. *Behav Brain Res* **226**, 428-434, doi:10.1016/j.bbr.2011.09.039 (2012).
- 156 Cheung, K. P., Yang, E. & Goldrath, A. W. Memory-like CD8+ T cells generated during homeostatic proliferation defer to antigen-experienced memory cells. *J Immunol* **183**, 3364-3372, doi:10.4049/jimmunol.0900641 (2009).
- 157 Messaoudi, I., Warner, J., Nikolich-Zugich, D., Fischer, M. & Nikolich-Zugich, J. Molecular, cellular, and antigen requirements for development of age-associated T cell clonal expansions in vivo. *J Immunol* **176**, 301-308 (2006).
- 158 Messaoudi, I., Warner, J. & Nikolich-Zugich, J. Age-related CD8+ T cell clonal expansions express elevated levels of CD122 and CD127 and display defects in perceiving homeostatic signals. *J Immunol* **177**, 2784-2792 (2006).
- 159 Cahalan, M. D. & Chandy, K. G. The functional network of ion channels in T lymphocytes. *Immunol Rev* **231**, 59-87, doi:10.1111/j.1600-065X.2009.00816.x (2009).
- 160 Hogquist, K. A. *et al.* T cell receptor antagonist peptides induce positive selection. *Cell* **76**, 17-27 (1994).
- 161 Mareeva, T., Lebedeva, T., Anikeeva, N., Manser, T. & Sykulev, Y. Antibody specific for the peptide-major histocompatibility complex. Is it T cell receptor-like? *J Biol Chem* **279**, 44243-44249, doi:10.1074/jbc.M407021200 (2004).
- 162 Zhang, L. H. *et al.* Lenalidomide efficacy in activated B-cell-like subtype diffuse large B-cell lymphoma is dependent upon IRF4 and cereblon expression. *Br J Haematol* **160**, 487-502, doi:10.1111/bjh.12172 (2013).
- 163 Zheng, Y., Delgoffe, G. M., Meyer, C. F., Chan, W. & Powell, J. D. Anergic T cells are metabolically anergic. *J Immunol* **183**, 6095-6101, doi:10.4049/jimmunol.0803510 (2009).
- 164 Stein, L. R. & Imai, S. The dynamic regulation of NAD metabolism in mitochondria. *Trends Endocrinol Metab* **23**, 420-428, doi:10.1016/j.tem.2012.06.005 (2012).
- 165 Nakanishi, S. & Cleveland, J. L. Targeting the polyamine-hypusine circuit for the prevention and treatment of cancer. *Amino Acids* **48**, 2353-2362, doi:10.1007/s00726-016-2275-3 (2016).
- 166 Cui, Z. *et al.* Molecular cloning, characterization, and chromosomal assignment of porcine cationic amino acid transporter-1. *Genomics* **85**, 352-359, doi:10.1016/j.ygeno.2004.11.006 (2005).
- 167 Broer, A., Rahimi, F. & Broer, S. Deletion of Amino Acid Transporter ASCT2 (SLC1A5) Reveals an Essential Role for Transporters SNAT1 (SLC38A1) and SNAT2 (SLC38A2) to Sustain Glutaminolysis in Cancer Cells. *J Biol Chem* **291**, 13194-13205, doi:10.1074/jbc.M115.700534 (2016).



- 168 Maeda, T. *et al.* Role of polyamines derived from arginine in differentiation and proliferation of human blood cells. *Biol Pharm Bull* **29**, 234-239 (2006).
- 169 Stine, Z. E., Walton, Z. E., Altman, B. J., Hsieh, A. L. & Dang, C. V. MYC, Metabolism, and Cancer. *Cancer discovery* **5**, 1024-1039, doi:10.1158/2159-8290.Cd-15-0507 (2015).
- 170 Nilsson, J. A. *et al.* Targeting ornithine decarboxylase in Myc-induced lymphomagenesis prevents tumor formation. *Cancer Cell* **7**, 433-444, doi:10.1016/j.ccr.2005.03.036 (2005).
- 171 Nishio, Y. *et al.* Impaired CD98 signaling protects against graft-versus-host disease by increasing regulatory T cells. *Transpl Immunol* **35**, 34-39, doi:10.1016/j.trim.2016.01.005 (2016).
- 172 Clausen, D. M. *et al.* In vitro cytotoxicity and in vivo efficacy, pharmacokinetics, and metabolism of 10074-G5, a novel small-molecule inhibitor of c-Myc/Max dimerization. *J Pharmacol Exp Ther* **335**, 715-727, doi:10.1124/jpet.110.170555 (2010).
- 173 Castell, A. *et al.* A selective high affinity MYC-binding compound inhibits MYC:MAX interaction and MYC-dependent tumor cell proliferation. *Sci Rep* **8**, 10064, doi:10.1038/s41598-018-28107-4 (2018).
- 174 Bjorklund, C. C. *et al.* Rate of CRL4(CRBN) substrate Ikaros and Aiolos degradation underlies differential activity of lenalidomide and pomalidomide in multiple myeloma cells by regulation of c-Myc and IRF4. *Blood Cancer J* **5**, e354, doi:10.1038/bcj.2015.66 (2015).
- 175 Lindsten, T., June, C. H. & Thompson, C. B. Multiple mechanisms regulate c-myc gene expression during normal T cell activation. *EMBO J* **7**, 2787-2794 (1988).
- 176 Grausz, J. D., Fradelizi, D., Dautry, F., Monier, R. & Lehn, P. Modulation of c-fos and c-myc mRNA levels in normal human lymphocytes by calcium ionophore A23187 and phorbol ester. *Eur J Immunol* **16**, 1217-1221, doi:10.1002/eji.1830161006 (1986).
- 177 Zweifach, A. & Lewis, R. S. Mitogen-regulated Ca<sup>2+</sup> current of T lymphocytes is activated by depletion of intracellular Ca<sup>2+</sup> stores. *Proc Natl Acad Sci U S A* **90**, 6295-6299 (1993).
- 178 Youn, H. D. & Liu, J. O. Cabin1 represses MEF2-dependent Nur77 expression and T cell apoptosis by controlling association of histone deacetylases and acetylases with MEF2. *Immunity* **13**, 85-94 (2000).
- 179 Valenzuela, J. O. *et al.* PKC $\theta$  is required for alloreactivity and GVHD but not for immune responses toward leukemia and infection in mice. *J Clin Invest* **119**, 3774-3786, doi:10.1172/JCI39692 (2009).
- 180 Alsina, M. *et al.* Lenalidomide maintenance for high-risk multiple myeloma after allogeneic hematopoietic cell transplantation. *Biol Blood Marrow Transplant* **20**, 1183-1189, doi:10.1016/j.bbmt.2014.04.014 (2014).
- 181 Trop-Steinberg, S., Azar, Y., Bringer, R. & Or, R. Myc and AP-1 expression in T cells and T-cell activation in patients after hematopoietic stem cell transplantation. *Clin Exp Med* **15**, 189-203, doi:10.1007/s10238-014-0285-6 (2015).
- 182 Medina, M. A. Glutamine and cancer. *J Nutr* **131**, 2539S-2542S; discussion 2550S-2531S (2001).
- 183 Rodrigues, M. F. *et al.* Enhanced OXPHOS, glutaminolysis and beta-oxidation constitute the metastatic phenotype of melanoma cells. *Biochem J* **473**, 703-715, doi:10.1042/BJ20150645 (2016).
- 184 Azzaoui, I. *et al.* T-cell defect in diffuse large B-cell lymphomas involves expansion of myeloid-derived suppressor cells. *Blood* **128**, 1081-1092, doi:10.1182/blood-2015-08-662783 (2016).
- 185 Rodriguez, P. C., Ochoa, A. C. & Al-Khami, A. A. Arginine Metabolism in Myeloid Cells Shapes Innate and Adaptive Immunity. *Front Immunol* **8**, 93, doi:10.3389/fimmu.2017.00093 (2017).

- 186 Woo, S. R. *et al.* Immune inhibitory molecules LAG-3 and PD-1 synergistically regulate T-cell function to promote tumoral immune escape. *Cancer Res* **72**, 917-927, doi:10.1158/0008-5472.CAN-11-1620 (2012).
- 187 Harada, M. *et al.* Characterization of B16 melanoma-specific cytotoxic T lymphocytes. *Cancer Immunol Immunother* **47**, 198-204 (1998).
- 188 Sinha, P., Clements, V. K., Miller, S. & Ostrand-Rosenberg, S. Tumor immunity: a balancing act between T cell activation, macrophage activation and tumor-induced immune suppression. *Cancer Immunol Immunother* **54**, 1137-1142, doi:10.1007/s00262-005-0703-4 (2005).
- 189 Fu, H., Yang, H., Zhang, X. & Xu, W. The emerging roles of exosomes in tumor-stroma interaction. *J Cancer Res Clin Oncol* **142**, 1897-1907, doi:10.1007/s00432-016-2145-0 (2016).
- 190 Nagaraj, S. & Gabrilovich, D. I. Tumor escape mechanism governed by myeloid-derived suppressor cells. *Cancer Res* **68**, 2561-2563, doi:10.1158/0008-5472.CAN-07-6229 (2008).
- 191 Rodriguez, P. C. *et al.* Regulation of T cell receptor CD3zeta chain expression by L-arginine. *J Biol Chem* **277**, 21123-21129, doi:10.1074/jbc.M110675200 (2002).
- 192 Friberg, M. *et al.* Indoleamine 2,3-dioxygenase contributes to tumor cell evasion of T cell-mediated rejection. *Int J Cancer* **101**, 151-155, doi:10.1002/ijc.10645 (2002).
- 193 Munn, D. H. *et al.* Potential regulatory function of human dendritic cells expressing indoleamine 2,3-dioxygenase. *Science* **297**, 1867-1870, doi:10.1126/science.1073514 (2002).
- 194 Sharma, M. D. *et al.* Indoleamine 2,3-dioxygenase controls conversion of Foxp3+ Tregs to TH17-like cells in tumor-draining lymph nodes. *Blood* **113**, 6102-6111, doi:10.1182/blood-2008-12-195354 (2009).
- 195 Bernstein, P. L., Herrick, D. J., Prokipcak, R. D. & Ross, J. Control of c-myc mRNA half-life in vitro by a protein capable of binding to a coding region stability determinant. *Genes Dev* **6**, 642-654 (1992).
- 196 De Melo, J., Kim, S. S., Lourenco, C. & Penn, L. Z. Lysine-52 stabilizes the MYC oncoprotein through an SCF(Fbxw7)-independent mechanism. *Oncogene* **36**, 6815-6822, doi:10.1038/onc.2017.268 (2017).
- 197 Amy, C. M. & Bartholomew, J. C. Regulation of N-myc transcript stability in human neuroblastoma and retinoblastoma cells. *Cancer Res* **47**, 6310-6314 (1987).
- 198 Clement, J. Q. & Wilkinson, M. F. Rapid induction of nuclear transcripts and inhibition of intron decay in response to the polymerase II inhibitor DRB. *J Mol Biol* **299**, 1179-1191, doi:10.1006/jmbi.2000.3745 (2000).
- 199 Dorsett, Y. *et al.* MicroRNA-155 suppresses activation-induced cytidine deaminase-mediated Myc-Igh translocation. *Immunity* **28**, 630-638, doi:10.1016/j.immuni.2008.04.002 (2008).
- 200 Liu, J. & Levens, D. Making myc. *Current topics in microbiology and immunology* **302**, 1-32 (2006).
- 201 Grzmil, M. & Hemmings, B. A. Translation regulation as a therapeutic target in cancer. *Cancer Res* **72**, 3891-3900, doi:10.1158/0008-5472.Can-12-0026 (2012).
- 202 Liu, L. *et al.* Polyamines regulate c-Myc translation through Chk2-dependent HuR phosphorylation. *Mol Biol Cell* **20**, 4885-4898, doi:10.1091/mbc.E09-07-0550 (2009).
- 203 Cantrell, D. A. T cell antigen receptor signal transduction pathways. *Cancer Surv* **27**, 165-175 (1996).
- 204 Joseph, N., Reicher, B. & Barda-Saad, M. The calcium feedback loop and T cell activation: how cytoskeleton networks control intracellular calcium flux. *Biochim Biophys Acta* **1838**, 557-568, doi:10.1016/j.bbamem.2013.07.009 (2014).

- 205 Jo, S., Lee, K. H., Song, S., Jung, Y. K. & Park, C. S. Identification and functional characterization of cereblon as a binding protein for large-conductance calcium-activated potassium channel in rat brain. *J Neurochem* **94**, 1212-1224, doi:10.1111/j.1471-4159.2005.03344.x (2005).
- 206 Szabo, S. J. *et al.* Distinct effects of T-bet in TH1 lineage commitment and IFN-gamma production in CD4 and CD8 T cells. *Science* **295**, 338-342, doi:10.1126/science.1065543 (2002).
- 207 Mullen, A. C. *et al.* Role of T-bet in commitment of TH1 cells before IL-12-dependent selection. *Science* **292**, 1907-1910, doi:10.1126/science.1059835 (2001).
- 208 Paley, M. A. *et al.* Progenitor and terminal subsets of CD8+ T cells cooperate to contain chronic viral infection. *Science* **338**, 1220-1225, doi:10.1126/science.1229620 (2012).
- 209 Li, J. *et al.* Phosphatidylinositol 3-kinase-independent signaling pathways contribute to ICOS-mediated T cell costimulation in acute graft-versus-host disease in mice. *J Immunol* **191**, 200-207, doi:10.4049/jimmunol.1203485 (2013).
- 210 Saha, A. *et al.* Programmed death ligand-1 expression on donor T cells drives graft-versus-host disease lethality. *J Clin Invest* **126**, 2642-2660, doi:10.1172/JCI85796 (2016).
- 211 Beckermann, K. E., Dudzinski, S. O. & Rathmell, J. C. Dysfunctional T cell metabolism in the tumor microenvironment. *Cytokine Growth Factor Rev* **35**, 7-14, doi:10.1016/j.cytogfr.2017.04.003 (2017).
- 212 Takahashi, K. & Yamanaka, S. Induction of pluripotent stem cells from mouse embryonic and adult fibroblast cultures by defined factors. *Cell* **126**, 663-676, doi:10.1016/j.cell.2006.07.024 (2006).
- 213 Vizcardo, R. *et al.* Regeneration of human tumor antigen-specific T cells from iPSCs derived from mature CD8(+) T cells. *Cell Stem Cell* **12**, 31-36, doi:10.1016/j.stem.2012.12.006 (2013).
- 214 Flynn, J. K. & Gorry, P. R. Stem memory T cells (TSCM)-their role in cancer and HIV immunotherapies. *Clin Transl Immunology* **3**, e20, doi:10.1038/cti.2014.16 (2014).
- 215 McDaniel, J. M. *et al.* Reversal of T-cell tolerance in myelodysplastic syndrome through lenalidomide immune modulation. *Leukemia* **26**, 1425-1429, doi:10.1038/leu.2011.359 (2012).
- 216 Otahal, P. *et al.* Lenalidomide enhances antitumor functions of chimeric antigen receptor modified T cells. *Oncoimmunology* **5**, e1115940, doi:10.1080/2162402X.2015.1115940 (2016).
- 217 Lopez-Girona, A. *et al.* Cereblon is a direct protein target for immunomodulatory and antiproliferative activities of lenalidomide and pomalidomide. *Leukemia* **26**, 2326-2335, doi:10.1038/leu.2012.119 (2012).
- 218 Zhu, Y. X., Kortuem, K. M. & Stewart, A. K. Molecular mechanism of action of immunomodulatory drugs thalidomide, lenalidomide and pomalidomide in multiple myeloma. *Leuk Lymphoma* **54**, 683-687, doi:10.3109/10428194.2012.728597 (2013).
- 219 Hagner, P. R. *et al.* Activity of lenalidomide in mantle cell lymphoma can be explained by NK cell-mediated cytotoxicity. *Br J Haematol* **179**, 399-409, doi:10.1111/bjh.14866 (2017).
- 220 Chen, X. *et al.* Induction of myelodysplasia by myeloid-derived suppressor cells. *J Clin Invest* **123**, 4595-4611, doi:10.1172/JCI67580 (2013).
- 221 Van Valckenborgh, E. *et al.* Multiple myeloma induces the immunosuppressive capacity of distinct myeloid-derived suppressor cell subpopulations in the bone marrow. *Leukemia* **26**, 2424-2428, doi:10.1038/leu.2012.113 (2012).
- 222 Hanna, B. S., Ozturk, S. & Seiffert, M. Beyond bystanders: Myeloid cells in chronic lymphocytic leukemia. *Mol Immunol*, doi:10.1016/j.molimm.2017.11.014 (2017).

- 223 Yang, L. *et al.* Naive T-cells in myelodysplastic syndrome display intrinsic human telomerase reverse transcriptase (hTERT) deficiency. *Leukemia* **27**, 897-906, doi:10.1038/leu.2012.300 (2013).
- 224 Van Gelder, R. N. *et al.* Amplified RNA synthesized from limited quantities of heterogeneous cDNA. *Proc Natl Acad Sci U S A* **87**, 1663-1667 (1990).
- 225 Warrington, J. A., Nair, A., Mahadevappa, M. & Tsyganskaya, M. Comparison of human adult and fetal expression and identification of 535 housekeeping/maintenance genes. *Physiological genomics* **2**, 143-147, doi:10.1152/physiolgenomics.2000.2.3.143 (2000).
- 226 Pluskal, T., Castillo, S., Villar-Briones, A. & Oresic, M. MZmine 2: modular framework for processing, visualizing, and analyzing mass spectrometry-based molecular profile data. *BMC Bioinformatics* **11**, 395, doi:10.1186/1471-2105-11-395 (2010).
- 227 Xia, J. & Wishart, D. S. Using MetaboAnalyst 3.0 for Comprehensive Metabolomics Data Analysis. *Current protocols in bioinformatics* **55**, 14.10.11-14.10.91, doi:10.1002/cpbi.11 (2016).
- 228 Pearce, E. L. *et al.* Control of effector CD8+ T cell function by the transcription factor Eomesodermin. *Science* **302**, 1041-1043, doi:10.1126/science.1090148 (2003).
- 229 Olson, J. A., McDonald-Hyman, C., Jameson, S. C. & Hamilton, S. E. Effector-like CD8(+) T cells in the memory population mediate potent protective immunity. *Immunity* **38**, 1250-1260, doi:10.1016/j.immuni.2013.05.009 (2013).
- 230 Hamilton, S. E. & Jameson, S. C. CD8(+) T cell differentiation: choosing a path through T-bet. *Immunity* **27**, 180-182, doi:10.1016/j.immuni.2007.08.003 (2007).
- 231 Intlekofer, A. M. *et al.* Effector and memory CD8+ T cell fate coupled by T-bet and eomesodermin. *Nat Immunol* **6**, 1236-1244, doi:10.1038/ni1268 (2005).
- 232 Simonetta, F. *et al.* High eomesodermin expression among CD57+ CD8+ T cells identifies a CD8+ T cell subset associated with viral control during chronic human immunodeficiency virus infection. *Journal of virology* **88**, 11861-11871, doi:10.1128/jvi.02013-14 (2014).
- 233 Berrien-Elliott, M. M. *et al.* Checkpoint blockade immunotherapy relies on T-bet but not Eomes to induce effector function in tumor-infiltrating CD8+ T cells. *Cancer immunology research* **3**, 116-124, doi:10.1158/2326-6066.Cir-14-0159 (2015).
- 234 Pollizzi, K. N. *et al.* Asymmetric inheritance of mTORC1 kinase activity during division dictates CD8(+) T cell differentiation. *Nat Immunol* **17**, 704-711, doi:10.1038/ni.3438 (2016).
- 235 Huang, C. Y., Bredemeyer, A. L., Walker, L. M., Bassing, C. H. & Sleckman, B. P. Dynamic regulation of c-Myc proto-oncogene expression during lymphocyte development revealed by a GFP-c-Myc knock-in mouse. *Eur J Immunol* **38**, 342-349, doi:10.1002/eji.200737972 (2008).
- 236 Bello-Fernandez, C., Packham, G. & Cleveland, J. L. The ornithine decarboxylase gene is a transcriptional target of c-Myc. *Proc Natl Acad Sci U S A* **90**, 7804-7808 (1993).
- 237 Liu, L. *et al.* Polyamine-modulated expression of c-myc plays a critical role in stimulation of normal intestinal epithelial cell proliferation. *American journal of physiology. Cell physiology* **288**, C89-99, doi:10.1152/ajpcell.00326.2004 (2005).
- 238 Blaeschke, F. *et al.* Induction of a central memory and stem cell memory phenotype in functionally active CD4(+) and CD8(+) CAR T cells produced in an automated good manufacturing practice system for the treatment of CD19(+) acute lymphoblastic leukemia. *Cancer Immunol Immunother* **67**, 1053-1066, doi:10.1007/s00262-018-2155-7 (2018).
- 239 Guedan, S. *et al.* Enhancing CAR T cell persistence through ICOS and 4-1BB costimulation. *JCI insight* **3**, doi:10.1172/jci.insight.96976 (2018).

- 240 Soda, K. The mechanisms by which polyamines accelerate tumor spread. *Journal of experimental & clinical cancer research : CR* **30**, 95, doi:10.1186/1756-9966-30-95 (2011).
- 241 Wahl, D. R., Byersdorfer, C. A., Ferrara, J. L., Opipari, A. W., Jr. & Glick, G. D. Distinct metabolic programs in activated T cells: opportunities for selective immunomodulation. *Immunol Rev* **249**, 104-115, doi:10.1111/j.1600-065X.2012.01148.x (2012).
- 242 Brand, K. A. & Hermfisse, U. Aerobic glycolysis by proliferating cells: a protective strategy against reactive oxygen species. *FASEB journal : official publication of the Federation of American Societies for Experimental Biology* **11**, 388-395 (1997).
- 243 MacIver, N. J., Michalek, R. D. & Rathmell, J. C. Metabolic regulation of T lymphocytes. *Annual review of immunology* **31**, 259-283, doi:10.1146/annurev-immunol-032712-095956 (2013).
- 244 Cluntun, A. A. *et al.* The rate of glycolysis quantitatively mediates specific histone acetylation sites. *Cancer & metabolism* **3**, 10, doi:10.1186/s40170-015-0135-3 (2015).
- 245 Liu, R. *et al.* Determination of polyamine metabolome in plasma and urine by ultrahigh performance liquid chromatography-tandem mass spectrometry method: application to identify potential markers for human hepatic cancer. *Analytica chimica acta* **791**, 36-45, doi:10.1016/j.aca.2013.06.044 (2013).
- 246 Miyara, M. *et al.* Functional delineation and differentiation dynamics of human CD4+ T cells expressing the FoxP3 transcription factor. *Immunity* **30**, 899-911, doi:10.1016/j.immuni.2009.03.019 (2009).
- 247 Matsushima, H. & Takashima, A. Bidirectional homing of Tregs between the skin and lymph nodes. *J Clin Invest* **120**, 653-656, doi:10.1172/JCI42280 (2010).
- 248 Ding, Y., Xu, J. & Bromberg, J. S. Regulatory T cell migration during an immune response. *Trends Immunol* **33**, 174-180, doi:10.1016/j.it.2012.01.002 (2012).
- 249 Rallon, N. I. *et al.* Level, phenotype and activation status of CD4+FoxP3+ regulatory T cells in patients chronically infected with human immunodeficiency virus and/or hepatitis C virus. *Clin Exp Immunol* **155**, 35-43, doi:10.1111/j.1365-2249.2008.03797.x (2009).
- 250 Gallagher, R. P. *et al.* Suntan, sunburn, and pigmentation factors and the frequency of acquired melanocytic nevi in children. Similarities to melanoma: the Vancouver Mole Study. *Arch Dermatol* **126**, 770-776 (1990).
- 251 Aalborg, J. *et al.* Tanning and increased nevus development in very-light-skinned children without red hair. *Arch Dermatol* **145**, 989-996, doi:10.1001/archdermatol.2009.193 (2009).
- 252 Goronzy, J. J. & Weyand, C. M. Aging, autoimmunity and arthritis: T-cell senescence and contraction of T-cell repertoire diversity - catalysts of autoimmunity and chronic inflammation. *Arthritis Res Ther* **5**, 225-234, doi:10.1186/ar974 (2003).
- 253 Goronzy, J. J. & Weyand, C. M. T cell development and receptor diversity during aging. *Curr Opin Immunol* **17**, 468-475, doi:10.1016/j.coi.2005.07.020 (2005).
- 254 Naylor, K. *et al.* The influence of age on T cell generation and TCR diversity. *J Immunol* **174**, 7446-7452 (2005).
- 255 Rogers, H. W., Weinstock, M. A., Feldman, S. R. & Coldiron, B. M. Incidence Estimate of Nonmelanoma Skin Cancer (Keratinocyte Carcinomas) in the U.S. Population, 2012. *JAMA Dermatol* **151**, 1081-1086, doi:10.1001/jamadermatol.2015.1187 (2015).
- 256 Malchow, S. *et al.* Aire-dependent thymic development of tumor-associated regulatory T cells. *Science* **339**, 1219-1224, doi:10.1126/science.1233913 (2013).
- 257 Ali, N. & Rosenblum, M. D. Regulatory T cells in skin. *Immunology* **152**, 372-381, doi:10.1111/imm.12791 (2017).
- 258 Sanchez Rodriguez, R. *et al.* Memory regulatory T cells reside in human skin. *J Clin Invest* **124**, 1027-1036, doi:10.1172/JCI72932 (2014).

- 259 Bensinger, S. J., Bandeira, A., Jordan, M. S., Caton, A. J. & Laufer, T. M. Major histocompatibility complex class II-positive cortical epithelium mediates the selection of CD4(+)-25(+) immunoregulatory T cells. *J Exp Med* **194**, 427-438 (2001).
- 260 Jordan, M. S. *et al.* Thymic selection of CD4+CD25+ regulatory T cells induced by an agonist self-peptide. *Nat Immunol* **2**, 301-306, doi:10.1038/86302 (2001).
- 261 van Santen, H. M., Benoist, C. & Mathis, D. Number of T reg cells that differentiate does not increase upon encounter of agonist ligand on thymic epithelial cells. *J Exp Med* **200**, 1221-1230, doi:10.1084/jem.20041022 (2004).
- 262 Hamdi, W. *et al.* Clinical significance of regulatory T cells in patients with myelodysplastic syndrome. *Eur J Haematol* **82**, 201-207, doi:10.1111/j.1600-0609.2008.01182.x (2009).
- 263 Kordasti, S. Y. *et al.* CD4+CD25<sup>high</sup> Foxp3<sup>+</sup> regulatory T cells in myelodysplastic syndrome (MDS). *Blood* **110**, 847-850, doi:10.1182/blood-2007-01-067546 (2007).
- 264 Yu, C. *et al.* Nitric oxide induces human CLA(+)-CD25(+)-Foxp3(+) regulatory T cells with skin-homing potential. *J Allergy Clin Immunol* **140**, 1441-1444 e1446, doi:10.1016/j.jaci.2017.05.023 (2017).
- 265 Maly, P. *et al.* The alpha(1,3)fucosyltransferase Fuc-TVII controls leukocyte trafficking through an essential role in L-, E-, and P-selectin ligand biosynthesis. *Cell* **86**, 643-653 (1996).
- 266 Nakayama, F. *et al.* Expression of cutaneous lymphocyte-associated antigen regulated by a set of glycosyltransferases in human T cells: involvement of alpha1, 3-fucosyltransferase VII and beta1,4-galactosyltransferase I. *J Invest Dermatol* **115**, 299-306, doi:10.1046/j.1523-1747.2000.00032.x (2000).
- 267 Yamaguchi, T. *et al.* The comparison of expression of cutaneous lymphocyte-associated antigen (CLA), and Th1- and Th2-associated antigens in mycosis fungoides and cutaneous lesions of adult T-cell leukemia/lymphoma. *Eur J Dermatol* **13**, 553-559 (2003).
- 268 Ferran, M. *et al.* Circulating CLA+ T lymphocytes as peripheral cell biomarkers in T-cell-mediated skin diseases. *Exp Dermatol* **22**, 439-442, doi:10.1111/exd.12154 (2013).
- 269 Iijima, N. & Iwasaki, A. T cell memory. A local macrophage chemokine network sustains protective tissue-resident memory CD4 T cells. *Science* **346**, 93-98, doi:10.1126/science.1257530 (2014).
- 270 Jiang, X. *et al.* Skin infection generates non-migratory memory CD8+ T(RM) cells providing global skin immunity. *Nature* **483**, 227-231, doi:10.1038/nature10851 (2012).
- 271 Schenkel, J. M., Fraser, K. A., Vezys, V. & Masopust, D. Sensing and alarm function of resident memory CD8(+) T cells. *Nat Immunol* **14**, 509-513, doi:10.1038/ni.2568 (2013).
- 272 Park, C. O. & Kupper, T. S. The emerging role of resident memory T cells in protective immunity and inflammatory disease. *Nat Med* **21**, 688-697, doi:10.1038/nm.3883 (2015).
- 273 Wu, S., Han, J., Laden, F. & Qureshi, A. A. Long-term ultraviolet flux, other potential risk factors, and skin cancer risk: a cohort study. *Cancer Epidemiol Biomarkers Prev* **23**, 1080-1089, doi:10.1158/1055-9965.EPI-13-0821 (2014).
- 274 Wu, S., Han, J., Li, W. Q., Li, T. & Qureshi, A. A. Basal-cell carcinoma incidence and associated risk factors in U.S. women and men. *Am J Epidemiol* **178**, 890-897, doi:10.1093/aje/kwt073 (2013).
- 275 Ghoreishi, M. & Dutz, J. P. Tolerance induction by transcutaneous immunization through ultraviolet-irradiated skin is transferable through CD4+CD25+ T regulatory cells and is dependent on host-derived IL-10. *J Immunol* **176**, 2635-2644 (2006).
- 276 Wang, L. *et al.* Post-immune UV irradiation induces Tr1-like regulatory T cells that suppress humoral immune responses. *International immunology* **20**, 57-70, doi:10.1093/intimm/dxm124 (2008).

- 277 Imabun, S. *et al.* Recurrent valvular pneumoperitoneum caused by a minute gastric ulcer--a case report. *Jpn J Surg* **21**, 571-575 (1991).
- 278 Schaer, D. A. *et al.* GITR pathway activation abrogates tumor immune suppression through loss of regulatory T cell lineage stability. *Cancer Immunol Res* **1**, 320-331, doi:10.1158/2326-6066.CIR-13-0086 (2013).
- 279 Schwarz, A. *et al.* Evidence for functional relevance of CTLA-4 in ultraviolet-radiation-induced tolerance. *J Immunol* **165**, 1824-1831 (2000).
- 280 Toda, M. *et al.* UV irradiation of immunized mice induces type 1 regulatory T cells that suppress tumor antigen specific cytotoxic T lymphocyte responses. *Int J Cancer* **129**, 1126-1136, doi:10.1002/ijc.25775 (2011).
- 281 Schwarz, A. *et al.* Ultraviolet radiation-induced regulatory T cells not only inhibit the induction but can suppress the effector phase of contact hypersensitivity. *J Immunol* **172**, 1036-1043 (2004).
- 282 Mora, J. R., Iwata, M. & von Andrian, U. H. Vitamin effects on the immune system: vitamins A and D take centre stage. *Nat Rev Immunol* **8**, 685-698, doi:10.1038/nri2378 (2008).
- 283 Gorman, S. *et al.* Topically applied 1,25-dihydroxyvitamin D3 enhances the suppressive activity of CD4+CD25+ cells in the draining lymph nodes. *J Immunol* **179**, 6273-6283 (2007).
- 284 Schwarz, A., Navid, F., Sparwasser, T., Clausen, B. E. & Schwarz, T. 1,25-dihydroxyvitamin D exerts similar immunosuppressive effects as UVR but is dispensable for local UVR-induced immunosuppression. *J Invest Dermatol* **132**, 2762-2769, doi:10.1038/jid.2012.238 (2012).
- 285 Mayne, C. G., Spanier, J. A., Relland, L. M., Williams, C. B. & Hayes, C. E. 1,25-Dihydroxyvitamin D3 acts directly on the T lymphocyte vitamin D receptor to inhibit experimental autoimmune encephalomyelitis. *Eur J Immunol* **41**, 822-832, doi:10.1002/eji.201040632 (2011).
- 286 Joshi, S. *et al.* 1,25-dihydroxyvitamin D(3) ameliorates Th17 autoimmunity via transcriptional modulation of interleukin-17A. *Mol Cell Biol* **31**, 3653-3669, doi:10.1128/MCB.05020-11 (2011).
- 287 Chang, J. H., Cha, H. R., Lee, D. S., Seo, K. Y. & Kweon, M. N. 1,25-Dihydroxyvitamin D3 inhibits the differentiation and migration of T(H)17 cells to protect against experimental autoimmune encephalomyelitis. *PLoS One* **5**, e12925, doi:10.1371/journal.pone.0012925 (2010).
- 288 Bonilla, C. *et al.* Skin pigmentation, sun exposure and vitamin D levels in children of the Avon Longitudinal Study of Parents and Children. *BMC public health* **14**, 597, doi:10.1186/1471-2458-14-597 (2014).
- 289 Hayes, C. E. *et al.* Vitamin D Actions on CD4(+) T Cells in Autoimmune Disease. *Front Immunol* **6**, 100, doi:10.3389/fimmu.2015.00100 (2015).
- 290 Armas, L. A. *et al.* Ultraviolet-B radiation increases serum 25-hydroxyvitamin D levels: the effect of UVB dose and skin color. *Journal of the American Academy of Dermatology* **57**, 588-593, doi:10.1016/j.jaad.2007.03.004 (2007).
- 291 Libon, F., Cavalier, E. & Nikkels, A. F. Skin color is relevant to vitamin D synthesis. *Dermatology (Basel, Switzerland)* **227**, 250-254, doi:10.1159/000354750 (2013).
- 292 D'Orazio, J., Jarrett, S., Amaro-Ortiz, A. & Scott, T. UV radiation and the skin. *International journal of molecular sciences* **14**, 12222-12248, doi:10.3390/ijms140612222 (2013).
- 293 Yamazaki, S. *et al.* Homeostasis of thymus-derived Foxp3+ regulatory T cells is controlled by ultraviolet B exposure in the skin. *J Immunol* **193**, 5488-5497, doi:10.4049/jimmunol.1400985 (2014).

- 294 Hollingworth, S., Walker, K., Page, A. & Eadie, M. Pharmacoepidemiology and the Australian regional prevalence of multiple sclerosis. *Mult Scler* **19**, 1712-1716, doi:10.1177/1352458513482371 (2013).
- 295 John, E. M., Schwartz, G. G., Koo, J., Van Den Berg, D. & Ingles, S. A. Sun exposure, vitamin D receptor gene polymorphisms, and risk of advanced prostate cancer. *Cancer Res* **65**, 5470-5479, doi:10.1158/0008-5472.CAN-04-3134 (2005).
- 296 John, E. M., Schwartz, G. G., Koo, J., Wang, W. & Ingles, S. A. Sun exposure, vitamin D receptor gene polymorphisms, and breast cancer risk in a multiethnic population. *Am J Epidemiol* **166**, 1409-1419, doi:10.1093/aje/kwm259 (2007).
- 297 Clarys, P., Alewaeters, K., Lambrecht, R. & Barel, A. O. Skin color measurements: comparison between three instruments: the Chromameter(R), the DermaSpectrometer(R) and the Mexameter(R). *Skin research and technology : official journal of International Society for Bioengineering and the Skin (ISBS) [and] International Society for Digital Imaging of Skin (ISDIS) [and] International Society for Skin Imaging (ISSI)* **6**, 230-238 (2000).
- 298 van der Windt, G. J. *et al.* CD8 memory T cells have a bioenergetic advantage that underlies their rapid recall ability. *Proc Natl Acad Sci U S A* **110**, 14336-14341, doi:10.1073/pnas.1221740110 (2013).
- 299 Martin, M. D. *et al.* Phenotypic and Functional Alterations in Circulating Memory CD8 T Cells with Time after Primary Infection. *PLoS pathogens* **11**, e1005219, doi:10.1371/journal.ppat.1005219 (2015).
- 300 Phan, A. T. *et al.* Constitutive Glycolytic Metabolism Supports CD8(+) T Cell Effector Memory Differentiation during Viral Infection. *Immunity* **45**, 1024-1037, doi:10.1016/j.immuni.2016.10.017 (2016).
- 301 Sukumar, M. *et al.* Inhibiting glycolytic metabolism enhances CD8+ T cell memory and antitumor function. *J Clin Invest* **123**, 4479-4488, doi:10.1172/jci69589 (2013).
- 302 Oliaro, J. *et al.* Asymmetric cell division of T cells upon antigen presentation uses multiple conserved mechanisms. *J Immunol* **185**, 367-375, doi:10.4049/jimmunol.0903627 (2010).
- 303 Haque, M. *et al.* C-Myc regulation by costimulatory signals modulates the generation of CD8+ memory T cells during viral infection. *Open biology* **6**, 150208, doi:10.1098/rsob.150208 (2016).
- 304 Bianchi, T., Gasser, S., Trumpp, A. & MacDonald, H. R. c-Myc acts downstream of IL-15 in the regulation of memory CD8 T-cell homeostasis. *Blood* **107**, 3992-3999, doi:10.1182/blood-2005-09-3851 (2006).
- 305 Scharping, N. E. *et al.* The Tumor Microenvironment Represses T Cell Mitochondrial Biogenesis to Drive Intratumoral T Cell Metabolic Insufficiency and Dysfunction. *Immunity* **45**, 374-388, doi:10.1016/j.immuni.2016.07.009 (2016).
- 306 Rohaan, M. W., van den Berg, J. H., Kvistborg, P. & Haanen, J. Adoptive transfer of tumor-infiltrating lymphocytes in melanoma: a viable treatment option. *Journal for immunotherapy of cancer* **6**, 102, doi:10.1186/s40425-018-0391-1 (2018).
- 307 Powell, D. J., Jr., Dudley, M. E., Robbins, P. F. & Rosenberg, S. A. Transition of late-stage effector T cells to CD27+ CD28+ tumor-reactive effector memory T cells in humans after adoptive cell transfer therapy. *Blood* **105**, 241-250, doi:10.1182/blood-2004-06-2482 (2005).
- 308 Busch, D. H., Frassle, S. P., Sommermeyer, D., Buchholz, V. R. & Riddell, S. R. Role of memory T cell subsets for adoptive immunotherapy. *Seminars in immunology* **28**, 28-34, doi:10.1016/j.smim.2016.02.001 (2016).
- 309 Menk, A. V. *et al.* 4-1BB costimulation induces T cell mitochondrial function and biogenesis enabling cancer immunotherapeutic responses. *The Journal of experimental medicine* **215**, 1091-1100, doi:10.1084/jem.20171068 (2018).



## APPENDIX A: INSTITUTIONAL REVIEW BOARD APPROVAL



RESEARCH INTEGRITY AND COMPLIANCE  
Institutional Review Boards, FWA No. 00001669  
12901 Bruce B. Downs Blvd., MDC035 • Tampa, FL 33612-4199  
(813) 974-5638 • FAX (813) 974-7091

3/12/2014

Dana Rollison, Ph.D.  
H Lee Moffitt Cancer Center  
12902 Magnolia Drive  
Tampa, FL 33612

RE: **Expedited Approval for Initial Review**  
IRB#: Pro00016372  
Title: Prospective Study of Cutaneous Viral Infections and Non-Melanoma Skin Cancer -  
MCC# 17755

Study Approval Period: 3/10/2014 to 3/10/2015

Dear Dr. Rollison:

On 3/10/2014, the Institutional Review Board (IRB) reviewed and **APPROVED** the above application and all documents outlined below.

Approved Item(s):  
Protocol Document(s):  
[Protocol \(version 1, 01/31/2014\)](#)

Consent/Assent Document(s)\*:  
[Informed Consent \(version 1, 02/26/2014\) - clean pdf](#)

\*Please use only the official IRB stamped informed consent/assent document(s) found under the "Attachments" tab. Please note, these consent/assent document(s) are only valid during the approval period indicated at the top of the form(s).

It was the determination of the IRB that your study qualified for expedited review which includes activities that (1) present no more than minimal risk to human subjects, and (2) involve only procedures listed in one or more of the categories outlined below. The IRB may review research through the expedited review procedure authorized by 45CFR46.110 and 21 CFR 56.110. The research proposed in this study is categorized under the following expedited review category:

(2) Collection of blood samples by finger stick, heel stick, ear stick, or venipuncture as follows:  
(a) from healthy, nonpregnant adults who weigh at least 110 pounds. For these subjects, the amounts drawn may not exceed 550 ml in an 8 week period and collection may not occur more frequently than 2 times per week; or (b) from other adults and children, considering the age, weight, and health of the subjects, the collection procedure, the amount of blood to be collected, and the frequency with which it will be collected. For these subjects, the amount drawn may not exceed the lesser of 50 ml or 3 ml per kg in an 8 week period and collection may not occur more frequently than 2 times per week.

(3) Prospective collection of biological specimens for research purposes by noninvasive means.

(7) Research on individual or group characteristics or behavior (including, but not limited to, research on perception, cognition, motivation, identity, language, communication, cultural beliefs or practices, and social behavior) or research employing survey, interview, oral history, focus group, program evaluation, human factors evaluation, or quality assurance methodologies.

As the principal investigator of this study, it is your responsibility to conduct this study in accordance with IRB policies and procedures and as approved by the IRB. Any changes to the approved research must be submitted to the IRB for review and approval by an amendment.

We appreciate your dedication to the ethical conduct of human subject research at the University of South Florida and your continued commitment to human research protections. If you have any questions regarding this matter, please call 813-974-5638.

Sincerely,

A handwritten signature in blue ink that reads "V. Jorgensen MD". The signature is written in a cursive style.

E. Verena Jorgensen, M.D., Chairperson  
USF Institutional Review Board

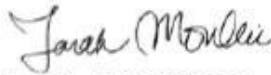
## APPENDIX B: INSTITUTIONAL ANIMAL CARE & USE COMMITTEE APPROVALS



**RESEARCH INTEGRITY AND COMPLIANCE  
INSTITUTIONAL ANIMAL CARE & USE COMMITTEE**

**MEMORANDUM**

TO: Pearlle Epling-Burnette, PharmD, PhD

FROM:   
Farah Moulvi, MSPH, IACUC Coordinator  
Institutional Animal Care & Use Committee  
Research Integrity & Compliance

DATE: 3/30/2018

PROJECT TITLE: Immunological modulation through cereblon suppression-Breeding Protocol  
Preclinical development of HDAC8 inhibitor therapy for myelofibrosis  
Cereblon suppression offers novel approach for anti-tumor immunity

FUNDING SOURCE: Celgene Corporation

IACUC PROTOCOL #: M IS00004986

PROTOCOL STATUS: **APPROVED**

The Institutional Animal Care and Use Committee (IACUC) reviewed your application requesting the use of animals in research for the above-entitled study. The IACUC **APPROVED** your request to use the following animals in your protocol for a one-year period beginning 3/30/2018:

C57BL/6 ERT2-Cre	500
C57BL/6 B6.Cg-Tg(Lck-cre)1540Jxm/J (Lck-Cre)	500
C57BL/6 cereblon (Crbn) -/-	1000
C57BL/6 HDAC11 -/-	500
C57BL/6 ERT2-Cre x Cereblon (Crbn) floxed/floxed	500
C57BL/6 B6.Cg-Thy1a/Cy Tg(ToraTorb)8Rest/J (PMEL)	500
C57BL/6 Tg (ToraTorb) 1100Mjb/J (OT1) x Crbn -/-	500
C57BL/6 CD28 -/-	500
C57BL/6 cereblon (Crbn) -/- CD28 -/-	500
C57BL/6 cereblon (Crbn -/-) x B6.Cg-Thy1a/Cy Tg(ToraTorb)8Rest/J (PMEL)	500
C57BL/6 cereblon (Crbn) -/- x B6;129-Myctm1Slek/J (c-MycGfp)	500
C57BL/6 ToraTorb (OT2)	500
C57BL/6 CD45.1 congenic	500
C57BL/6 Tg (ToraTorb) 1100Mjb/J (OT1)	500

C57BL6 ToraTorb (OT2) x cereblon (Crbn) -/-	500
C57BL6 cereblon (Crbn) floxed/floxed	500
C57BL/6 HDAC6 -/-	500
BALB/c CByJ.SJL(B6)-Ptprca/J (BALB/c Ly-5.1 congenic)	500
C57BL/6 B6;129-Myctm1Slek/J (c-MycGfp)	500
C57BL/6 Cereblon floxed/floxed x B6.Cg-Tg (Lck-cre)1540Jxm/J (Lck-Cre)	500

Please take note of the following:

- **IACUC approval is granted for a one-year period at the end of which, an annual renewal form must be submitted for years two (2) and three (3) of the protocol through the eIACUC system.** After three years all continuing studies must be completely re-described in a new electronic application and submitted to IACUC for review.

- **All modifications to the IACUC-Approved Protocol must be approved by the IACUC prior to initiating the modification.** Modifications can be submitted to the IACUC for review and approval as an Amendment or Procedural Change through the eIACUC system. These changes must be within the scope of the original research hypothesis, involve the original species and justified in writing. Any change in the IACUC-approved protocol that does not meet the latter definition is considered a major protocol change and requires the submission of a new application.

- **All costs invoiced to a grant account must be allocable to the purpose of the grant.** Costs allocable to one protocol may not be shifted to another in order to meet deficiencies caused by overruns, or for other reasons convenience. Rotation of charges among protocols by month without establishing that the rotation schedule credibly reflects the relative benefit to each protocol is unacceptable.

---

RESEARCH & INNOVATION • RESEARCH INTEGRITY AND COMPLIANCE  
 INSTITUTIONAL ANIMAL CARE AND USE COMMITTEE  
 PHS No. A4100-01, AAALAC No. 000434, USDA No. 59-R-0015  
 University of South Florida • 12901 Bruce B. Downs Blvd., MDC35 • Tampa, FL 33612-4799  
 (813) 974-7106 • FAX (813) 974-7091

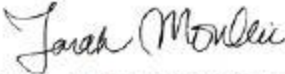




RESEARCH INTEGRITY AND COMPLIANCE  
INSTITUTIONAL ANIMAL CARE & USE COMMITTEE

## MEMORANDUM

TO: Pearlie Epling-Burnette, PharmD, PhD

FROM:   
Farah Moulvi, MSPH, IACUC Coordinator  
Institutional Animal Care & Use Committee  
Research Integrity & Compliance

DATE: 12/2/2015

PROJECT TITLE: Targeting CRBN for Tumor Immunity  
Immunological modulation through cereblon suppression

FUNDING SOURCE: Celgene Corporation

IACUC PROTOCOL #: R IS00001690

PROTOCOL STATUS: APPROVED

The Institutional Animal Care and Use Committee (IACUC) reviewed your application requesting the use of animals in research for the above-entitled study. The IACUC **APPROVED** your request to use the following animals in your protocol for a **one-year period beginning 12/2/2015**:

Mouse: C57BL/6 (6-8 weeks/25g/M or F)	485
Mouse: C57BL/6 crbn <sup>-/-</sup> (6-8 weeks/25g/M or F)	485
Mouse: C57BL/6 crbn <sup>-/-</sup> OT-1 (6-8 weeks/25g/M or F)	30
Mouse: C57BL/6 OT-1 (6-8 weeks/25g/M or F)	30
Mouse: C57BL/6 crbn <sup>-/-</sup> Pmel (6-8 weeks/25g/M or F)	15
Mouse: C7BL/6 Pmel (6-8 weeks/25g/M or F)	15
Mouse: C57BL/6 LCK-cre (6-8 weeks/25g/M or F)	320
Mouse: C57BL/6 LCK-cre crbn <sup>fl/fl</sup> (6-8	320

12/2/2015

weeks/25g/M or F)	
Mouse: C57Bl/6 rag1 -/- (6-8 weeks/25g/M or F)	180
Mouse: C57Bl/6 Ly5.1 (6-8 weeks/25g/M or F)	330
Mouse: C57Bl/6 MYC-GFP (6-8 weeks/25g/M or F)	230
Mouse: C57Bl/6 crbn -/- MYC-GFP (6-8 weeks/25g/M or F)	230

Please take note of the following:

- IACUC approval is granted for a one-year period at the end of which, an annual renewal form must be submitted for years two (2) and three (3) of the protocol through the eIACUC system. After three years all continuing studies must be completely re-described in a new electronic application and submitted to IACUC for review.
- All modifications to the IACUC-Approved Protocol must be approved by the IACUC prior to initiating the modification. Modifications can be submitted to the IACUC for review and approval as an Amendment or Procedural Change through the eIACUC system. These changes must be within the scope of the original research hypothesis, involve the original species and justified in writing. Any change in the IACUC-approved protocol that does not meet the latter definition is considered a major protocol change and requires the submission of a new application.
- All costs invoiced to a grant account must be allocable to the purpose of the grant. Costs allocable to one protocol may not be shifted to another in order to meet deficiencies caused by overruns, or for other reasons convenience. Rotation of charges among protocols by month without establishing that the rotation schedule credibly reflects the relative benefit to each protocol is unacceptable.


---

RESEARCH & INNOVATION • RESEARCH INTEGRITY AND COMPLIANCE  
 INSTITUTIONAL ANIMAL CARE AND USE COMMITTEE  
 PHS No. A4100-01, AAALAC No. 000434, USDA No. 58-R-0015  
 University of South Florida • 12901 Bruce B. Downs Blvd., MDC35 • Tampa, FL 33612-4799  
 (813) 974-7106 • FAX (813) 974-7091

12/2/2015

## APPENDIX C: COPYRIGHT PERMISSIONS OF PREVIOUSLY PUBLISHED MATERIAL

MDPI Journals A–Z Information & Guidelines Initiatives About

 OPEN ACCESS

Title / Keyword  Journal

Author / Affiliation  Article Type

---

### MDPI Contact

MDPI  
St. Alban-Anlage 66,  
4052 Basel, Switzerland  
Support contact [✉](#)  
Tel. +41 61 683 77 34  
Fax: +41 61 302 89 18

For more contact information, see [here](#).

[in](#) [f](#) [t](#) [g+](#)

### MDPI Open Access Information and Policy

All articles published by MDPI are made immediately available worldwide under an open access license. This means:

- everyone has free and unlimited access to the full-text of *all* articles published in MDPI journals;
- everyone is free to re-use the published material if proper accreditation/citation of the original publication is given;
- open access publication is supported by the authors' institutes or research funding agencies by payment of a comparatively low [Article Processing Charge \(APC\)](#) for accepted articles.

---

### External Open Access Resources

MDPI is a RoMEO [green publisher](#) — RoMEO is a database of Publishers' copyright and self-archiving policies hosted by the [University of Nottingham](#)

Those who are new to the concept of open access might find the following websites or 'Open Access 101' video informative:

[Wikipedia article on 'Open Access'](#)

[Peter Suber's 'Open Access Overview'](#)

[Information Platform Open Access \[in English, in German\]](#)

[SHERPA's 'Authors and Open Access'](#)

## COPYRIGHT TRANSFER

All manuscripts are considered to be the property of AAI from the time of submission. Should AAI not publish the paper, AAI releases its rights therein at the time the manuscript is returned to the corresponding author.

Manuscripts published in *The Journal of Immunology* become the sole property of, with all rights in copyright reserved to, The American Association of Immunologists, Inc. (AAI).

The corresponding author, on behalf of all authors, signs a copyright transfer form. When all authors of an article have written it as part of their official duties as employees of the U.S. government, the article is exempt from this requirement for transfer of copyright.

Authors retain the following permissions as long as proper attribution (Originally published in *The Journal of Immunology*; Author(s). Year. Title. *J. Immunol.* Vol: pp-pp. Copyright © [year] The American Association of Immunologists, Inc.) is included:

1. If mandated by the funder of the research, authors may deposit the accepted, uncopyedited version of the manuscript into PubMed Central, with an embargo period (time at which the manuscript is available to the public) of 12 months after publication. This right applies solely to deposition into PubMed Central; the authors agree not to deposit the manuscript to any other repository (except a thesis repository if required - see item 3), agency, or entity. Authors whose funder mandates a PubMed Central embargo of 6 months have permission to make the manuscript available at 6 months after publication. This right applies only to articles under a funder mandate to submit to PubMed Central (for research funded by NIH, this means articles accepted for publication on or after April 7, 2008).
2. To reuse original figures or tables in the author's own work. This permission extends to the author only, not to the institution. The author may not permit others to reproduce their figures or tables in works not written by the author.
3. To include the final, published version of the article in a thesis and/or dissertation in print. If required by the degree-conferring institution, an electronic version of the final, published version may be deposited into a thesis repository as long as a link to the article on *The Journal of Immunology* Web site is included.
4. To reprint the article in print collections composed solely of the author's own writings. Permission must be obtained from AAI to reprint the article in any publication that includes the work of others.
5. To post a copy of the accepted, uncopyedited version on the author's personal website with a notice that "This is the accepted, uncopyedited version of the manuscript. The definitive version was published in *The Journal of Immunology* Vol: pp-pp. DOI." A hyperlink to the published article on *The Journal of Immunology* website must be included; the published PDF may not be displayed. For posting on any other website, including any social media, corporate or government (other than PubMed Central according to the terms in item 1 above) website, permission must be requested from AAI. POSTING TO INSTITUTIONAL REPOSITORIES IS NOT PERMITTED.
6. To present the work orally in part or in its entirety.
7. If the work was prepared as a work-for-hire, the author's employer may print out PDFs or make photocopies for internal use only. Distribution of the article by the author's employer in other formats or for any other purpose requires permission from AAI.

Authors reusing their own material as described in items 1-7 do not need to contact AAI for permission, except where noted. For all other reuse, the authors should contact AAI.